A RECONSTRUCTION OF THE RESPONSE OF THE WATER BALANCE IN WESTERN UNITED STATES LAKE BASINS TO CLIMATIC CHANGE

Volume 1

by

Fred M. Phillips and Andrew R. Campbell
Co-Principal Investigators
Department of Geoscience
New Mexico Institute of Mining and Technology

and

Cynthia Kruger, Peggy Johnson, Randall Roberts and Eric Keyes
Graduate Research Assistants
Department of Geoscience
New Mexico Institute of Mining and Technology

TECHNICAL COMPLETION REPORT

Project Numbers 1345662, 1423687

August 1992

New Mexico Water Resources Research Institute

in cooperation with

Department of Geoscience
New Mexico Institute of Mining and Technology

The Research on which this report is based was financed in part by the U.S. Department of the Interior, Geological Survey, through the New Mexico Water Resources Research Institute.

DISCLAMER

The purpose of Water Resources Research Institute technical reports is to provide a timely outlet for research results obtained on projects supported in whole or in part by the institute. Through these reports, we are promoting the free exchange of information and ideas and hope to stimulate thoughtful discussion and actions that may lead to resolution of water problems. The WRRI, through peer review of draft reports, attempts to substantiate the accuracy of information contained in its reports, but the views expressed are those of the authors and do not necessarily reflect those of the WRRI or its reviewers. Contents of this publication do not necessarily reflect the views and policies of the U.S. Department of the Interior, nor does mention of trade names or commercial products constitute their endorsement by the United States government.

ABSTRACT

Changes in the water balance are among the most serious potential consequences of global climate change. Predicting future water balance fluctuations is dependent on understanding the causes of past fluctuations. In arid, hydrologically closed basins, the water balance can be quantified as the ratio of water surface area in the terminal sink or sinks to the basin drainage area. In this study, we have used the oxygen isotope content of carbonate minerals precipitated from lake waters to reconstruct lake surface-area history. We have developed a numerical water-balance and isotope-balance model to simulate the lake's isotopic evolution and thus produced a lake surface-area history.

We have reconstructed the surface-area history of two basins in the southwestern United States. At the Plains of San Agustin, New Mexico, we used the oxygen isotope content of ostracode valves to achieve a high-resolution reconstruction of the interval 36 to 15 ka (thousand years before present). At Searles Lake, California, we used oxygen isotopes in inorganic carbonate minerals to produce a water-balance history for the period 1,180 to 10 ka. Comparing the Searles record with the marine oxygen isotope chronology shows the single strongest influence on the water balance is global glacial/interglacial cycles. Thus water-balance changes can be linked directly to global climatic change.

However, we also see patterns that differ from those of the global glacial cycles. We detect unexplained long-term trends of humid and arid water balance with an apparent periodicity of about 400 kyr. We also observe that the water balance seems to be characterized by relatively stable humid and arid modes, with rapid, unstable transitions between these modes.

Key words: Climate, isotopes, lakes, arid climates, time-series analysis.

PREFACE

This report describes the methods, results, and interpretations for paleohydrological studies on two closed-basin lakes in the western United States. The purpose of the report is to thoroughly document all aspects of the study so that it can be carefully evaluated and, if desired, replicated. Due to this objective, all aspects of the study are treated in much greater detail than the casual reader might find desirable. The authors intend to publish the results in summary form in the periodical literature, and they suggest that the reader interested primarily in a concise description of the results start with those articles.

This report consists of two volumes. The first volume contains a description of the study and graphical presentation of the data and results. It also presents fairly thorough bibliographic studies of previous research in the two lake basins studied and of related experimental studies. These are intended to provide a starting point for other researchers intending to perform additional studies in the same areas, or using similar methods. We suggest that careful consideration of the table of contents will aid the reader in focusing on the aspects of the study that are of interest. The second volume contains appendices which are mostly listings of computer programs, tables of data, and tables of computer inputs and outputs. These are largely presented in graphical form in the first volume, and are intended primarily as documentation and as a data source for future numerical analyses.

The authors offer their sincere thanks to George I. Smith of the U.S. Geological Survey in Menlo Park, California. This study would not have been possible without his active participation and advice. They also thank Kerr-McGee Corporation, and particularly Gail Moulton, for permission to sample the KM-3 core at Trona, California. They gratefully acknowledge "Cato" Lee for permission to drill on his ranch in the San Agustine Basin. They thank Vera Markgraf of the University of Colorado for her advice and participation in the drilling. Other individuals who contributed include Stewart S. Smith, who assisted the sampling at Trona, John Hawley and Robert Weber, who helped locate the San Agustine drilling site, Richard Forester (U.S. Geological Survey, Denver), who shared techniques for isolating ostracodes and assisted with specimen identification, and Annette Schafer-Perini, who gave much useful advice on numerical methods.

TABLE OF CONTENTS

Volume 1

Volume 2

LIST OF FIGURES

LIST OF TABLES

INTRODUCTION

During the past decade there has been steadily increasing recognition that anthropogenic changes in the atmosphere's composition and vegetation distribution (among other anthropogenic changes) have the potential to alter substantially the earth's climate. Human-induced climate change could also alter the environment to which humans are accustomed. One critical change could occur in the water cycle. Water availability depends on the water balance, of which one measure is the ratio of precipitation on a drainage basin to potential evaporation. The water balance largely determines runoff from rivers, recharge to groundwater, and water available for plant growth. Understanding how climate change affects water balance is necessary to predict the effects of anthropogenic climate disturbances.

One approach to understanding the links between climate change and changes in the water balance is to reconstruct past water-balance fluctuations and to relate them to reconstructed climates. In recent years great advances have been made in reconstructing the history of some Quaternary climatic parameters, largely through investigations on marine sediment cores (Shackleton and Opdyke 1973; Hays et al. 1976). Unfortunately, corresponding data on changes in the continental water balance are lacking. Previous studies have focused on high temporal resolution reconstructions for the latest Quaternary (Street and Grove 1979; Spencer et al. 1984 and 1985; Benson et al. 1990) or low-resolution reconstructions for longer periods (Abell 1982). The goal of this study is to produce a high-resolution reconstruction of the water balance in the western United States spanning most of the Quaternary.

The fragmentary and qualitative nature of the continental paleohydrological record is due to the scarcity of suitable investigation sites. To yield complete, high resolution records, one must use sites with essentially continuous deposition of materials from which paleoclimatic information can be extracted. The material must be subject to absolute dating. Finally, inferences from the data concerning the water balance should be possible.

This study uses sediments from closed-basin lakes in the western United States. Lacustrine basins can provide environments for nearly continuous sedimentation. Sedimentation rates are high enough to give high temporal resolution. Recent advances in geochronology have made absolute dating of many lacustrine sediments possible. Some component of the lacustrine sediment is usually precipitated out of the lake waters, and thus can contain a record of the environmental conditions at the time of precipitation. Finally, closed-basin lake fluctuations can be used to measure lake water-balance changes.

Halley (1715) first observed that the surface area of closed-basin lakes is a function of the balance of precipitation and evaporation. Because there is no other outlet for water flowing into the lake, the evaporation rate times the surface area must equal the lake's inflow. More recently, Russell (1885) and Meinzer (1922) noted that lake size in the Basin and Range Province of the western U.S. had varied greatly over the latest Quaternary, and analysis of these variations could provide information on water-balance changes. Smith and Street-Perrott (1983) and Benson et al. (1990) have provided up-to-date reviews of late Quaternary lake fluctuations in the western U.S. and Street-Perrott and Harrison (1985) and Benson and Paillet (1989) have provided reviews of the theory of lake-level response to climate change.

The classical method for reconstructing ancient lake levels is by observing shorelines and shallow sediments exposed around the margins of lake basins (e.g., Russell 1885; Morrison 1964). However, these studies are limited by the discontinuous nature of shoreline formation and the tendency of younger lake transgressions to obliterate the evidence of older ones. In contrast, sediment cores from the bottoms of lake basins can provide long, relatively continuous records, but are difficult to analyze quantitatively (e.g., Smith 1984). To overcome this problem we use geochemical information stored in the minerals precipitated out of the lake water.

Water molecules containing the heavy stable isotope of oxygen, oxygen-18 (^{18}O), are less volatile than those containing the light isotope, ^{16}O. Oxygen-18 is concentrated in the lake water during evaporation. The oxygen isotope composition of the carbonate (CO_3) ion dissolved in the lake water is controlled by the water's isotopic composition. Minerals containing the carbonate ion that have precipitated out of the lake water will have an oxygen isotopic composition determined by the original lake water. In this study we have used the ^{18}O content of both biologically and inorganically precipitated carbonate minerals to reconstruct the isotopic history of the lake water.

In addition to the balance of inflow to evaporation, the lake water's isotopic composition also depends on the isotopic composition of the water flowing into the lake, the temperature, the atmospheric humidity, and other factors. Along with the water balance, these factors have fluctuated with time. To "back out" the effect of the changing water balance (the dominant variable), we have designed a computer program that solves the equations describing the isotopic evolution of the lake water as a function of time. The program follows the approach outlined in Phillips et al. (1986a), and is described later in the Numerical Modeling section.

STUDY AREAS

Searles Valley in southeastern California and the Plains of San Agustin in west-central New Mexico were chosen as study sites because they have continuous sedimentation since the early Quaternary, geochronological control was available, and long sediment cores have been extracted from both basins.

For much of the Pleistocene, Searles Valley contained a lake that was one of a chain of lakes fed by the ancient Owens River, with its headwaters in the Sierra Nevada's eastern slopes. As the climate became more humid, each lake successively overflowed into the next, eventually terminating in Death Valley during the wettest episodes. In 1968, a 930 m exploration core hole was drilled to bedrock by Kerr-McGee Corporation at Searles playa. The KM-3 core has been investigated thoroughly by Kerr-McGee and the U.S. Geological Survey (USGS) and the results have been reported by Smith et al. (1983). Kerr-McGee allowed us access to the core for sampling at Trona, California. These samples have served as the basis for our reconstruction of the lake-level history of Searles over the past 1.5 Myr[1].

The Plains of San Agustin form a closed tectonic depression in west-central New Mexico. Abandoned shorelines provide abundant evidence that the Plains were once occupied by a large lake (Powers 1939). In the mid-1950s two long cores were drilled at San Agustin. Clisby and Sears (1956) presented evidence that these cores spanned the entire Quaternary. Unfortunately, due to core preservation methods employed after drilling, most of the lacustrine carbonates were destroyed, and those remaining could not be relied upon to represent the original isotopic composition. We therefore limited our investigation to a relatively short core recoverable by drilling with a hollow-stem auger. Samples from this core yielded a high-resolution isotopic record of 36 ka to 15 ka.

ISSUES ADDRESSED

Beginning in the 1960s, oceanographers were able to obtain long sediment cores from deep ocean basins, which through geochemical and paleoecological analysis provided paleooceanographic change records covering the entire Quaternary. The most important records were the fluctuation in ^{18}O content, which constitutes a proxy for the volume of glacial ice on the continents. These records showed that Quaternary climate was characterized by distinctive, clearly cyclic fluctuations in ice volume, temperature, and other parameters (Ruddiman and Wright 1987). Various hypotheses on Quaternary climate changes were tested, from these longterm records. In 1976, Hays et al. presented evidence to support the hypothesis that the theory of astronomical controls on the seasonal distribution of solar insolation,

1. In this report we follow the convention of designating ages by Ma (million years before present) or ka (thousand years before present) and periods of time by Myr (million years) or kyr (thousand years).

proposed by Milankovitch (1941), could explain much of the observed climatic variation. The most notable connections between the astronomical cycles and the marine ^{18}O cycles were common periodicities of 21 kyr, 40 kyr, and 100 kyr.

When recovery of these long climate records began, the chronological approach to continental glaciation was dominated by the "classical" four-fold Quaternary glaciation theory. The marine ^{18}O record clearly demonstrated that there were more than four Quaternary glacial cycles. How the glacial cycles apparent in the marine record correlated with the evidence adduced for the four-fold glacial chronology was not then clear, nor is it today. Recently, it has become obvious that one major barrier to successful marine/continental correlation in North America has been the miscorrelation between continental glacial deposits in the "type" Midwestern area (Hallberg 1986). Fullerton and Richmond (1986) have summarized the current status of Quaternary glacial correlations. From their summary, it is clear that continental glaciations and the marine oxygen isotope glacial stages are correlated, but the questions of relative magnitude and temporal extent of glaciations in the continental record (prior to the Illinoian) are still not resolved.

Given the vagueness of the proxy continental climatic record, any relatively continuous, high-resolution continental record of climate change spanning most of the Quaternary should contribute substantially to our understanding the nature and causes of Quaternary "ice ages." It is worthwhile to examine some issues involved in relating a continental water-balance record with a marine oxygen isotope record prior to actually attempting a comparison. We therefore pose the following four questions:

Question: Can we expect a direct correlation between lake surface area in the southwestern U.S. and the oceans' oxygen isotope composition?

Variations in the marine carbonate's ^{18}O content are largely a function of changes in continental ice volume, with ocean water temperature being a secondary factor (Shackleton 1987). Continental ice volume changes are controlled by the balance between the snowfall rate on glaciers and their melting rate; in other words, by a type of water balance. The surface area of closed basin lakes also depends on the balance of climatic parameters: precipitation and evaporation. Given this underlying connection between the climatic parameters controlling the surface area of closed-basin lakes and the volume of glacial ice, it is not unreasonable to expect some relation between the marine ^{18}O record and the lake surface-area record. However, the factors directly controlling the two mass balances are not identical, and thus it would be naive to expect identical responses. The most critical difference is in temperature. Reduced temperature is a necessity for significant glacial

expansion in mid-latitude areas but not for lake expansion. For example, it is possible that under a regime of increased temperature, precipitation, and summer cloudiness, glacial extent might decrease but lake area increase (e.g., Benson 1986). The most recent data from the Great Basin indicate that during the terminal Pleistocene event, maximum lake area lagged maximum Sierra Nevada glacial extent by 3,000 to 5,000 years (Benson et al. 1990; Dorn et al. 1987). This might be attributed to an effect as described above. However, this timing discrepancy should be considered quasi-synchronous given the actual chronological resolution of both the marine cores and the KM-3 core. In addition to temperature, the locations also differ. The marine ^{18}O record reflects most strongly the volume of continental ice at mid-to-high latitudes, whereas the lake records we are studying are at lower mid-latitudes. Thus, while we do expect a general correlation between North American ice volume and lake surface area in southwestern lake basins, it is also reasonable to expect significant and possibly systematic differences.

Question: Is it possible to establish one-to-one temporal correlations between fluctuations in the lake-level records and those in the marine oxygen isotope record?

The answer to this question will have important implications for testing the Milankovitch astronomical-control theory of Quaternary climate change. Strong statistical correlations have already been established between the marine oxygen isotope fluctuations and those predicted by the Milankovitch theory (Hays et al. 1976). Winograd et al. (1988) have shown very similar patterns shared by the $\delta^{18}O$ of calcite precipitated from Great Basin groundwater and the marine $\delta^{18}O$ record. If the lake-level fluctuations can be correlated on a one-to-one basis, then this causual connection to the Milankovitch forcing can plausibly be extended to explain the lake-level history. Given the absolute chronology already determined for the KM-3 core at Searles Lake (see Jannik et al. 1991; and the next section of this report, for summaries), we believe it is feasible to test whether such a correlation exists.

Question: Are there systematic differences between the lacustrine and marine records?

As discussed earlier, our current perception of the North American history of glacial timing and extent is in many ways less secure than it was twenty years ago. One possible response would be to adopt the marine oxygen isotope record as a satisfactory proxy for continental data. From this viewpoint, the task remaining for Quaternary geologists would be to "fit" their particular continental deposits into the marine chronology. This hypothesis can be at least partially tested by examining a long, continuous

continental record, such as the lake-level reconstruction, for systematic deviations from the marine oxygen isotope record.

Paleoclimatic proxy records contain a good deal of "noise." It is unrealistic to expect perfect correlation even if the original signals of two different records were identical. However, systematic differences between our lake-level reconstructions and the marine oxygen isotope stratigraphy would constitute a strong indication of some bias being inserted between the continental climate "signal" and the oxygen isotope "response." Applying the marine oxygen isotope record as a satisfactory proxy for continental climate would have to be reevaluated.

Question: Can explanations be offered for any systematic differences?

Systematic differences between the two records would indicate our understanding of the processes governing climate forcing and response are not adequate. The discrepancy might, however, provide clues to processes that should be incorporated.

The sections that follow lay the foundation for answering the above questions. The Searles Lake investigations are described next, and subsequently those at the Plains of San Agustin. The numerical tools used for interpreting the data are then described. Finally, the above questions are addressed.

SEARLES LAKE STUDIES

STUDY PLAN

Problem Addressed

Searles Lake, a currently dry, closed-basin lake in southeastern California (Figure 1), has been the subject of many mineralogic, geochemical and paleohydrologic studies over the past one-hundred years (e.g., Russell 1885, Flint and Gale 1958). Elevated shorelines and bars in Searles Valley and related basins were recognized by nineteenth-century geologists as evidence of past deep lakes. Early twentieth-century studies revealed the relationship between Searles Lake and four other lakes in the area (Bailey 1902). Runoff from the eastern Sierra Nevada into the paleo-Owens River created a chain of five paleolakes. Searles was the third and, for most of the Pleistocene, the terminal lake in the chain. Consequently, large amounts of solutes were concentrated and precipitated as chemical sediments. Exploration cores drilled by mining companies and the USGS to define the mineral deposits at Searles revealed thick sequences of alternating muds and evaporite minerals (e.g., Smith and Pratt 1957).

Of particular interest is the 930-meter Kerr-McGee core KM-3, of which 693 meters are lacustrine deposits dating from the Holocene to the early Pliocene. An absolute chronology for KM-3 and other cores has been

established by carbon-14 (Stuiver and Smith 1979) uranium-thorium (Peng et al. 1978, Bischoff et al. 1985), chlorine-36 (Phillips et al. 1983; Jannik 1989, Jannik et al. 1991) and paleomagnetic (Liddicoat et al. 1980) dates. Therefore, core KM-3 has the potential to provide a long sensitive record of mid-latitude continental climatic change.

Objective and Approach

This section provides an overview of the methods described in more detail below. This study's primary objective was to construct a record of stable isotope variation in Searles Lake sediments for the past 1.6 Myr and to interpret that record in terms of a lake surface-area history. Our approach was as follows:

- Sample Searles Lake core KM-3 with enough frequency to determine degree and duration of climatic cycles
- Examine composite chronology proposed by Jannik (1989)
- Evaluate sources of error for each dating technique
- Assign ages to all KM-3 samples using composite chronology

The chronology proposed by Jannik is a composite of selected ^{14}C, U/Th, ^{36}Cl, and paleomagnetic dates, interpolated based on the accumulation of acid-insoluble residue. An examination of the dating methods, dates selected, and relative error is necessary before time-series analysis, comparison with other paleoclimate records, or numerical modeling of the lake begins.

- Develop methodologies to separate primary carbonate minerals from diagenetic carbonates, and to separate primary carbonates from each other

Searles Lake sediments contain a variety of primary and diagenetic carbonate minerals (Smith and Haines 1964; Smith 1979; Smith et al. 1987). Carbonates termed "primary" include gaylussite dolomite, calcite, and argonite. Northupite is also probably primary. These minerals are presumed to have precipitated in isotopic equilibrium with the lake water. Diagenetic carbonates are formed when infiltrating concentrated brines react with primary carbonates to form new minerals. Therefore, diagenetic carbonates may not reflect the original lake water's isotopic composition.

- Perform mass spectrometric analysis of primary carbonates to determine oxygen-18 (^{18}O) and carbon-13C) content
- Compile Searles Lake isotope record

Interpreting the ^{13}C and $^{13}0$ content of CO_2 extracted from primary lake carbonates assumes the CO_2 incorporated into the mineral at the time of precipitation was in isotopic equilibrium with the dissolved lake CO_2. A second assumption is that the dissolved lake CO_2 was in isotopic equilibrium

with lake water. If these assumptions are born out, ^{13}C and ^{18}O content analysis of carbonates would determine the paleolake waters isotopic content.

- Estimate paleometerological parameters such as relative humidity, temperature, and net evaporation
- Use analytical model to predict range of expected ^{18}O and ^{13}C during infill, overflow and desiccation episodes. Compare value range to mass spectrometer results

Comparing the isotopic content of Searles Lake carbonates with the isotopic content predicted by an analytical solution allows evaluation of the methodologies used to separate and extract the carbonates from the lake mud, and the validity of the assumptions of the carbonates' primary origin. The analytical results were also used in validating the numerical model.

- Interpret Searles Lake isotope chronology
- Model preliminary water-balance reconstruction from lake levels inferred by lake isotope chronology

The stable isotope content record of the lake water through time was used to interpret changes in lake-water balance. From the water balance, climate changes were inferred, and the response of the Searles Lake water balance to changes in climate was inferred.

- Compare Searles Lake isotope chronology to other paleoclimate records, and deep-sea isotope records

RELATED STUDIES

Closed-Basin Lakes.

One of the earliest reports on Great Basin lakes is found in Russell (1885). Russell recognized that the Quaternary closed-basin lake levels were climate-dependent and hypothesized the changes in humidity and temperature that would have been required to produce the large saline lakes. Meinzer (1922) took a broader approach to paleoclimate reconstructions of closed-basin lakes. He discussed the relationships between the water balance of all closed-basin lakes in the western U.S., these lakes and their respective locations, geology, bathymetry, and climate.

An extensive quantitative reconstruction of paleoclimates using closed-basin lake records is found in Mifflin and Wheat (1979). Paleotemperatures were assumed in order to calculate the changes in evaporation, precipitation and runoff necessary to produce the paleolake levels indicated by geomorphic evidence in Lake Lahontan, Nevada.

Smith and Street-Perrott (1983) calculated the required inflow from the Owens River necessary to produce the Owens River system closed-basin paleolakes, including Searles Lake. Assumed paleotemperatures were used to calculate paleo-evaporation and precipitation. Street-Perrott and Harrison (1985) summarized the factors affecting the sensitivity of closed-basin lakes to climatic change, the various approaches to reconstructing lake levels, and

evidence used by investigators to accomplish the reconstruction. Other investigations that used stable isotopes to determine lake water balance are summarized in Pearson and Coplen (1978).

A numerical approach to isotopic evolution in closed-basin lakes was taken by Phillips et al. (1986). A lumped-parameter numerical model was created to simulate the isotopic evolution of a lake through time, given specified fluxes, meteorological and chemical parameters. The model was validated by simulating the isotopic evolution of Owens Lake during a desiccation episode. The numerical model used in this study to reconstruct the paleo-water balances of Searles and San Agustin is based on the Phillips et al. (1986) model.

The causes of lake-level fluctuations have been discussed by several investigators. Kutzbach and Street-Perrott (1985) correlated fluctuations in tropical lake levels with fluctuations in solar insolation calculated from the Milankovitch theory. Changes in sedimentation in Searles Lake due to orbital forcing also have been suggested by Smith (1984), Bischoff et al. (1985), and Jannik et al.(1991). Lake-level fluctuations caused by changing atmospheric circulation patterns have been suggested by Street-Perrott and Roberts (1983).

Several long paleoclimate records from the Great Basin have been developed in the past few years. Winograd et al. (1985) measured the deuterium content in calcite fluid inclusions from eastern Nevada calcite veins. The calcite was precipitated from calcite-saturated groundwater, and therefore, the deuterium content of the fluid inclusions should reflect that of the groundwater. A systematic depletion in the deuterium values during the past 2.0 Myr was theorized to be due to the uplift of the Coastal Ranges and the Sierra Nevada during the Quaternary. A 50 ka to 310 ka ^{18}O record from a southwestern Nevada calcite vein was reported by Winograd et al. (1988). The stable isotope record mimicked ocean and ice core ^{18}O records presented by Martinson et al. (1987) and Lorius et al. (1985), respectively. However, the timing of the ^{18}O fluctuations in the Nevada calcite did not correspond to that of the ocean records. Rather, the isotopic events identified in the Nevada ^{18}O record occurred earlier than the marine record suggests. A mechanism for a systematically decreasing time-lag of climatic events among the three study areas is not apparent. It would appear that some systematic error occurred in the development of the absolutely dated chronology for at least one of the ^{18}O records. The discrepancy in the timing of climatic events suggested by the ocean ^{18}O record and the Nevada ^{18}O record is of great interest regarding previously inferred dependence of climatic fluctuations upon orbited forcing (Hays et al. 1976). If the Nevada ^{18}O chronology is assumed to be correct, the time difference of events between the Nevada ^{18}O chronology and the Martinson et al. chronology, which was "obritally tuned," has been suggested to imply that solar insolation fluctuations predicted by

the Milankovitach theory are not the primary forces contributing to climatic change (Winograd et al. 1988).

A detailed discussion and comparison of the lake-level histories in four Great Basin closed-basin lakes is provided in Benson et al. (1990). Geomorphic, sedimentological and geochemical evidence of lake-level fluctuations for Lake Bonneville, Lake Lahontan, Lake Russell and Searles Lake were discussed, and the most recent major lake decline in the four lake systems were concluded to be penecontemporaneous.

Searles Lake

An impressive volume of work has been published on the geology, chemistry, and chronology of tectonic and climatic events in Searles Valley. Russell (1885) included the paleolake occupying Searles Valley on Plate 1 of his section on Great Basin paleolakes. Bailey (1902) recognized the relationship between Searles Lake and other Owens River paleolakes. In the early twentieth century, the discovery of large potash deposits in Searles Lake drew investigators to the area to define and exploit the mineral deposits. Gale (1914) reviewed the known available mineral assemblages at Searles and drew remarkably insightful conclusions as to Searles' sedimentation history and related paleolakes.

Investigations at Searles were resumed during the late 1950s with the advent of suitable radiometric dating techniques and a drive by the USGS to document more precisely the lacustrine mineral deposits beneath Searles Valley. Hundreds of sediment cores were drilled by mining companies and the USGS. Stratigraphic studies based on several cores can be found in Smith and Pratt (1957), Flint and Gale (1958), Haines (1959), Smith (1962; 1979) and Smith et al. (1983).

Detailed discussions of Searles Lake mineralogy include Droste (1961), Hay and Moiola (1964), Smith and Haines (1964), and Smith (1976, 1979). Studies of the geochemistry of Searles Lake deposits and brines include reports by Eugster and Smith (1965), Eugster and Hardie (1978), Smith (1979), Guldman (1984), and Hay and Guldman (1987). The hydrology of Searles Lake is reported in Hardt et al. (1972).

The unusually favorable opportunity to obtain a detailed record of continental climatic change prompted numerous studies employing isotopic and paleomagnetic techniques to date Searles Lake sediments. Investigators used new developments in radiocarbon techniques to establish a chronology for the shallow sediments beneath Searles Lake. These include Flint and Gale (1958), Stuiver (1964) and Stuiver and Smith (1979). Reasonable agreement of ^{230}Th ages of upper stratigraphic units with radiocarbon dates (Peng et al. 1978) allowed a continuation of the ^{230}Th chronology to units at the top of the Mixed Layer (Bischoff et al. 1985). Identification of paleomagnetic boundaries in Searles Lake core KM-3 extended the absolute chronology to 3.15

Ma (Liddicoat et al. 1980). Several halite units were dated by the ^{36}Cl method (Phillips et al. 1983, Jannik 1989, Jannik et al. 1991). A tephra layer in core KM-3 was tentatively correlated with the Lava Creek B ash (Hay and Guldman 1987). Radiocarbon dates on rock varnish from high-stand shorelines are presented in Dorn et al. (1990).

Paleoclimatic interpretations of Searles Lake based on stable isotope information have been presented in Oana and Deevey (1960), Stuiver (1964), and Horita (1987; 1990). Paleoclimatic interpretations based on sedimentological and outcrop evidence have been presented in Smith (1968; 1976; 1979; 1985; 1987), and Smith et al. (1983).

Stable Isotope Systematics

The stable isotope data for this study come from the evaporitic carbonate minerals sampled from the sediments in Searles Lake. Through a series of calculations, the carbonate's stable isotopic composition can be used to determine the isotopic composition of the paleolake water. The isotopic composition of the lake water then can be used to calculate the lake's water balance.

Fractionation Between Minerals and Water.

The stable isotopic composition of primary carbonates deposited from the lake is a function of the isotopic composition of the lake water, temperature, water salinity and the isotopic fractionation factor for that carbonate mineral.

In this study we measured the oxygen ($\delta^{18}O$) and carbon ($\delta^{13}O$) isotopic compositions and calculated the lake-water isotopic composition from which that carbonate was deposited. Dolomite was present in some parts of the core and its isotopic composition could be determined directly . For those parts of the core where dolomite was absent, other carbonate minerals (principally gaylussite) were used instead. We have established a correlation between dolomite and other carbonate species from study samples in which both minerals coexist. Details are given in a later section.

Once samples were normalized to dolomite, the data could be used with the computer model which calculated the $\delta^{18}O$ of the lake water. This calculation is based on the fractionation factor for dolomite/water, water temperature and water salinity.

Fractionation at the Air-Water Interface.

Paleolake levels can be reconstructed from oxygen isotopes because vapor evaporated from a water body is isotopically lighter than the composition of the water body itself. Thus, during evaporation the water body's isotopic composition becomes enriched. The fundamental explanation for this phenomenon is that the water molecules containing lighter isotopes of oxygen (or hydrogen) are less massive than those with heavier isotopes, and consequently are more volatile and more mobile. Two separate kinds of isotopic

fractionation occur during evaporation. The first, equilibrium liquid-vapor fractionation, occurs when liquid water and water vapor equilibrate isotopically in a closed system. This equilibrium fractionation is relatively easy to determine experimentally and is a function only of temperature. We have used the equilibrium fractionation factor determined by Bottinga and Craig (1968).

The second kind of fractionation is caused when evaporating water molecules must diffuse through a thin layer of relatively still air over the water surface. The water molecules containing lighter isotopes of oxygen and hydrogen diffuse more readily, due to their smaller mass, and thus the final evaporate is lighter than it would be from equilibrium fractionation. This phenomena was first described by Craig and Gordon (1965). Besides the temperature, the two main factors affecting this "kinetic" fractionation are the relative humidity of the atmosphere over the lake and the wind speed. We have used the formulation by Merlivat and Jouzel (1979) to describe the kinetic fractionation because it is simple, physically based, and relatively easy to parameterize.

Covariation of $\delta^{13}C$ and $\delta^{18}O$.

Talbot (1990) has shown that usually the ^{13}C content and ^{18}O content of closed-basin lacustrine carbonates are strongly correlated. McKenzie (1984) hypothesized a biological control of the ^{13}C. Photosynthetic organisms consume dissolved CO_2 and respire it. In general, the respired CO_2 is heavier isotopically than that consumed because the organisms preferentially incorporate the isotopically lighter carbon in their tissues. When they die, the organisms sink to the lake sediment. The sediment thus serves as a sink for light carbon and the dissolved carbon in the lake tends to grow heavier.

The main control on organic productivity of many lakes is nutrient availability. According to McKenzie (1984), when the lake's water balance becomes less favorable, two things happen. First, the lake volume shrinks and the nutrients dissolved in the lake water become more concentrated causing the organic productivity to increase. As the productivity increases, more isotopically light carbon is sequestered in the sediments and the dissolved carbonate species become heavier in $\delta^{13}C$. Second, as larger amounts of water are evaporated during the lake contraction, the remaining lake water becomes enriched in $\delta^{18}O$. The dissolved carbonate in isotopic equilibrium with the lake water is also enriched in ^{18}O. Shrinking or expanding lake volume tends to force changes in both ^{13}C and ^{18}O in the same direction, and thus they exhibit a strong convariance.

In Searles Lake there is also another, probably more important, cause for this covariance. It can be a result of the increase in the partial pressure

of CO_2 in the highly alkaline waters of the Searles system as the lake volume decreases. Large amounts of CO_2 with light $\delta^{13}C$ will be preferentially degassed to the atmosphere. Thus in addition to loss of light carbon to the sediments, it will also be lost to the atmosphere, tending to force covariance of $\delta^{18}O$ with $\delta^{13}C$.

STUDY AREA

Location

Searles Lake is located in the southwestern corner of the Basin and Range physiographic province along the boundaries of Inyo and San Bernadino counties, California (35^0 45'N, 117^0 20'W). Currently, Searles Lake is a dry (playa) lake, with standing water only after intense rainfall.

During pluvial periods, Searles Lake was the third in a chain of five paleolakes created by runoff from the eastern Sierra Nevada into the ancestral Owens River. As flow in the Owens River increased, Owens Lake filled up to approximately 64 m in lake depth, then overflowed into Indian Wells Valley to form China Lake. Upon reaching 8 m, China Lake, in turn, overflowed into Searles Valley to form Searles Lake. When Searles Lake deepened to about 180 m, China Lake and Searles Lake coalesced to form one large lake (Searles Lake), which at 200 m overflowed into Panamint Valley, creating Panamint Lake. For most of its history, Searles Lake was the usual terminus of the Owens River paleolake system. During extreme pluvial periods, Panamint Lake overflowed into Death Valley. Lake Manly (Death Valley) was the ultimate sink for the Armagosa and Mojave River paleolake systems. Also, Mono Lake and Adobe Lake may have overflowed during extreme pluvial periods, contributing to the flow in the ancestral Owens River system. Figure 1 shows the relationship among all the paleolakes. Figure 2 is a schematic cross-sectional representation of the Owens River paleolakes.

Hydrology

Currently, Searles Lake has a surface area of approximately 100 km^2 in the bottom of Searles Valley. According to Smith (1979), Searles Valley floor is 60 km long and 15 km wide; approximately 66 percent of the playa is silt covered, and the remaining third is hard salt pan.

Searles Valley has a drainage area of approximately 1600 km^2 (Smith 1979). Owens River has a drainage area of approximately 3300 mi^2(~8550 km^2), of which 536 mi^2 (1390 km^2) in the high altitude area of the eastern Sierra Nevada contributes most of the runoff reaching Owens River (Lee 1912). The remaining drainage area is predominantly desert or transition slopes. From Lee's work, Jannik (1989) calculated that even during intense pluvial periods, the Sierra Nevada created such a strong rain shadow that most of Searles Lake water still originated from the high-altitude section of the eastern Sierra Nevada. Any precipitation falling within Searles Lake's drainage area would

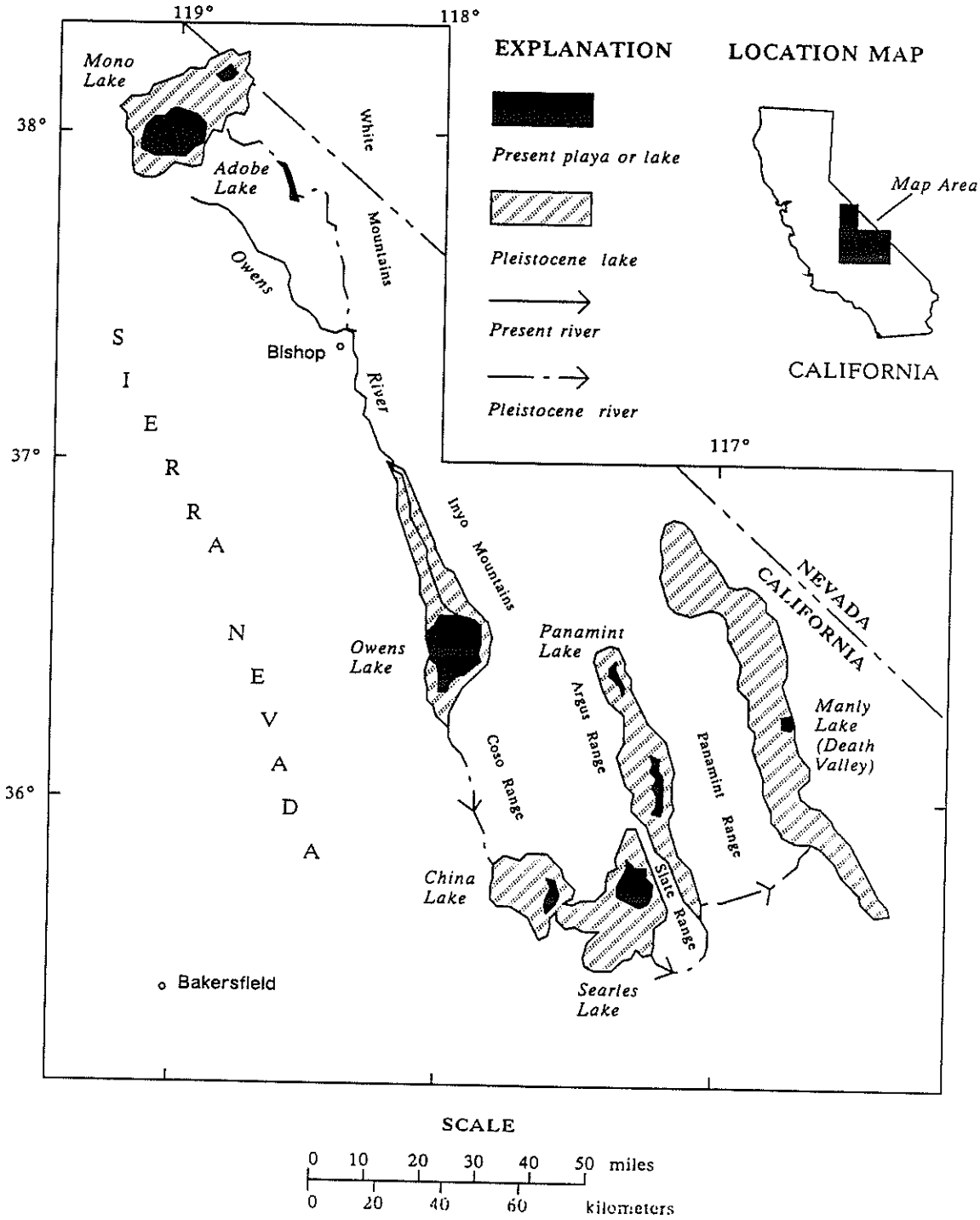

FIGURE 1. Location of Searles Lake and related Pleistocene lakes (Smith et al. 1983)

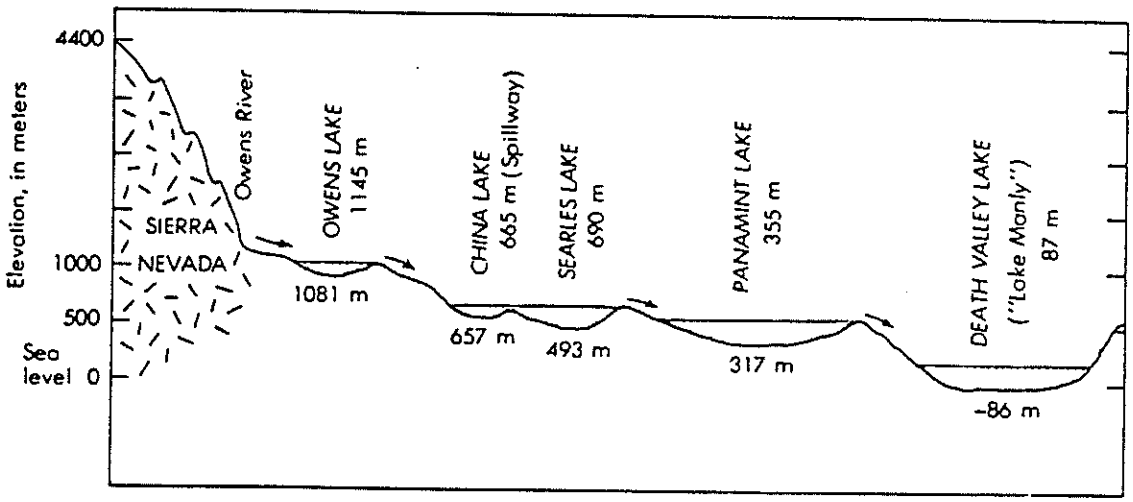

FIGURE 2. Schematic cross-section of lake basins in the paleo-Owens River chain

have been negligible compared to the inflow into Searles via Owens and China Lakes.

Climate.

Most of the following climate information was reported by Smith (1979). The climate at Searles Lake is hot and arid. Temperature extremes range from -12.2^{0}C to 47.8^{0}C, with an average annual temperature of 19.1^{0}C (for a 36-year period ending 1973). Annual precipitation during this period averaged 96.3 mm, with extremes ranging from 23 mm to 291 mm per year. Most precipitation occurs during the winter. A linear regression of relative humidity in the surrounding area gave an approximate annual average relative humidity for Searles Valley of 22 percent (Appendix I).

Searles Valley playa supports no vegetation. Smith (1979) reported vegetation on the surrounding mountains and alluvial fans as typical of the Mojave Desert: desert holly (Atriplex hymenlytra), creosote bush (Larrea tridentate), burro-bush (Franseria dumosa), and hop sage (Grayia spinosa). Pinyon pine and joshua trees are reported in the surrounding mountain ranges.

Geologic Environment

Searles Valley is a Cenozoic tectonic closed depression (Smith 1979). The valley floor is surrounded by several mountain ranges: the Argus Range and Spangler Hills to the west, the Slate Range on the north and east, and the Lava Mountains to the south. The Argus Range consists primarily of Mesozoic granites. The Slate Range contains Precambrian metamorphic units, small amounts of Palezoic limestone, Mesozoic granites and metavolcanics and Cenozoic volcanics (Jennings et al. 1962; Jannik 1989). The Lava Mountains consist primarily of late Tertiary volcanics and sandstone (Smith 1968). The surrounding mountains contain little limestone or dolomite to serve as a source of detrital carbonate in the Searles Lake sediments.

Core KM-3

Numerous sediment cores have been recovered from the lake bed in Searles Valley. A detailed examination of sediment chemistry and mineralogy from several cores in Searles Lake is provided in Smith (1979). In 1968, a 930 m exploration core designated KM-3 was drilled to bedrock by Kerr-McGee Corporation. In 1976, the USGS was allowed to examine company data on the core, and the core itself, and to publish the results of their investigation, including internal Kerr-McGee data. Results are reported by Smith et al. (1983).

Detailed geochemical analyses were performed on the KM-3 sediments by Kerr-McGee Corporation. The core was divided into 254 units based on lithology. Analyses were conducted to determine percent acid-insoluble residue, and ten elements in the acid-soluble fraction. In addition, the percent by weight of important evaporite minerals were calculated, including halite and several carbonate, sulfate, and borate minerals. Analyses (Smith

et al. 1983, Plates 2-4) were used as a general guide in selecting samples from core KM-3 for stable isotope study.

The following core descriptions, stratigraphic and mineralogic information were obtained from Smith (1979) and Smith et al. (1983). Core KM-3 was drilled near the center of Searles Valley (figure 1). The ~8 cm diameter core consisted of three distinct sections: 15 m of quartz monzonite bedrock of which only ~3 m of core was actually recovered; 212 m of alluvial arkosic sand and gravel; and 693 m of lacustrine sediments. The lacustrine sediments were divided into fourteen informal stratigraphic units based on lithology and mineralogy. The informal stratigraphic units are those used by the mining companies at Searles Lake and have been adopted by investigators. A copy of the core log summary presented in Smith et al. (1983) is shown in table 1, and graphically in figure 3.

In the broadest sense, Searles Lake sediments have been divided into two categories: "muds" and "salts." These are not sedimentologically exact terms, but they are useful in delineating sediments deposited in different environments and have been applied to Searles sediments in the past. The "muds" consist of marl, silt, or clay mixtures, and are plastic when wet. The muds vary in origin from deep lake marls and oozes to playa sediments, tephra, and possibly paleosols. The muds contain clays as well as alkaline earth carbonates (calcite, dolomite, aragonite), clastics, and mixed carbonate minerals such as gaylussite and pirssonite. The saline units can be thin seams of single or multiple evaporite minerals, such as hanksite, borax, tincalconite, thenardite, northupite, nahcolite, and halite, or thick coarsely crystalline units of halite or trona. Many saline minerals can also be found disseminated within the mud units.

Mineralogy

Solute buildup in Searles Lake water provided an unusual environment for the accumulating thick sequences of evaporite minerals. These minerals, and the accompanying brines, have been the target of mining companies at Searles Lake for the last 100 years. A list of evaporite minerals and the diagenetic products of some of the minerals (Smith 1979) is shown in table 2. Of greatest interest to our study are primary and diagenetic carbonates. Those carbonates considered to be of primary origin are dolomite, calcite, aragonite, and northupite. Gaylussite and pirssonite have sometimes thought to be of diagenetic origin, but more recent evidence indicates that fine-grained gaylussite is probably primary.

Assumptions of diagenetic or primary origin of these carbonates are crucial in attempting to reconstruct lake history by stable isotope records. If isotopic exchange had occurred with interstitial brines, or by any other mechanism, paleohydrologic information from the isotopic record may be lost. Therefore, a brief discussion of the evidence leading to conclusions of

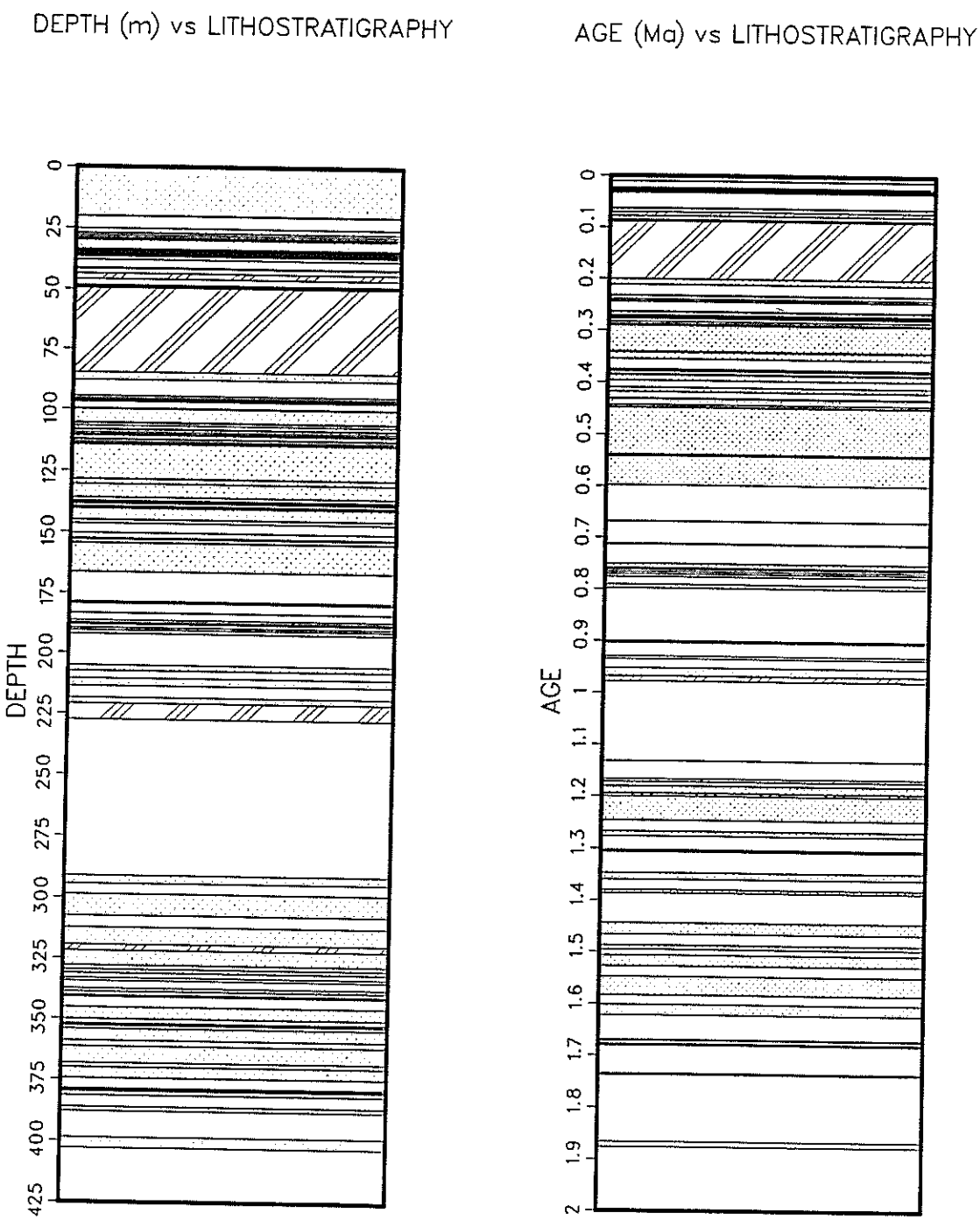

FIGURE 3. A comparison of core KM-3 stratigraphy with depth and with age. Cross-hatching indicates poor core recovery; stippling, intervals of predominately evaporite minerals; and absence of pattern, predominately lacustrine marls ("muds")

TABLE 1. Generalized description of the KM-3 core, Searles Lake, CA (from Smith et al. 1983)

Depth to base of unit (m)	Thickness of unit (m)	Description
5.8	5.8	Not cored. Overburden Mud is included in this zone.
19.9	14.1	*Upper Salt.*—Salines, mostly trona and halite; abundant hanksite near top, borax at base; light- to medium-gray (N6–8) and yellowish-gray (5Y8/1), with some thin interbeds of olive-gray (5Y4/1) mud; mostly indistinctly bedded to massive, locally vuggy.
25.0	5.1	*Parting Mud.*—Megascopic crystals of gaylussite and pirssonite in soft mud composed of microscopic crystals of dolomite, halite, aragonite, other evaporite minerals, and clastic silicates; light- to moderate-olive-gray (5Y3–5/1–4); upper part finely laminated, lower part massive.
37.9	12.9	*Lower Salt.*—Seven saline layers interbedded with six mud layers; salines are mostly halite and trona in upper two layers, trona, halite, and burkeite in underlying two layers, and trona in lower three layers; interbedded mud layers contain megascopic crystals of gaylussite and pirssonite; salines range in color from white through dark gray to yellowish orange (N5–8, 10YR6/6), mud from dark olive gray to brown (5Y4–6/1–4); salts poorly bedded to massive; some mud layers have thin laminar bedding.
69.0	31.1	*Bottom Mud.*—Mud containing megascopic gaylussite crystals; mud is composed of microscopic crystals of dolomite, aragonite, calcite, and other carbonate minerals, and about 30 percent acid-insoluble silicates and organic residues; thin-bedded to massive, with some laminar bedding; medium- to dark-brown, brownish-gray, and olive (5YR4/4 to 5Y3–4/1–2). Discontinuous saline layers at 41.4 m (0.5 m thick), 48.5 m (0.4 m thick), and 54.4 m (0.8 m thick).
90.8	21.8	Interval of poor core recovery; recovered core (3.4 m) is composed of mud containing megascopic gaylussite crystals, massive, medium- to dark-brown and olive (5YR5/2 to 5Y3/2). Top of interval probably represents top of Mixed Layer. This and following three units probably represent Units A and B of Mixed Layer, of which most of the saline layers were lost during drilling (see text).
95.4	4.6	Salines, mostly trona, containing mud; faintly bedded to massive; moderate-brown to olive (5YR4/4 to 5Y5/1).
99.8	4.4	Mud, mostly acid-insoluble material, some dolomite; light-olive-gray (5Y5–6/1–2), thin-bedded.
114.0	14.2	Salines, mostly trona, with small amounts of other minerals and extensive mud impurities; light- to dark-green and brown (5GY5/1, 5Y4–6/1, 5YR3/4); faint bedding in lighter colored salines, with interbeds of mud common near base. Contact between Units B and C of Mixed Layer is at base of this interval.
124.0	10.0	Salines, with some interbedded mud; saline minerals are mostly halite, with smaller amounts of trona and other evaporite minerals; indistinct bedding, beds mostly 1 to 2 cm thick; salines light- to dark-olive-gray (5Y4–7/1–2) and moderate-brown (10YR4–6/2–4).
130.4	6.4	Salines and some mud; salines are about two-thirds halite and one-third trona, with some thenardite; yellowish-gray (5Y5–7/2); upper part of unit contains largest percentage of mud impurities.
135.6	5.2	Salines, mostly halite, with minor trona and thenardite; dark- to medium-gray (N3–5); upper part of unit contains mud impurities.
151.2	15.6	Interbedded mud and salines; salines are mostly halite, with some trona; salines olive-gray (5Y4/1 to 5Y6/1), mud brownish-black (5YR2/1); saline layers, 0.3 to 0.6 m thick, constitute about one-third of zone.
166.4	15.2	Salines, mostly halite, with smaller amounts of trona and thenardite, nearly pure in lower part; mostly gray to yellowish-gray (N4–7 to 5Y4–6/1); bedding 1 to 2 cm thick, some zones porous but most nonporous. Contact between Units C and D+E of Mixed Layer is at base of this interval.
178.6	12.2	Mud containing megascopic crystals of gaylussite and pirssonite, microscopic crystals of

TABLE 1. (cont.)

Depth to base of unit (m)	Thickness of unit (m)	Description
		dolomite, halite, and probably other acid-soluble minerals; brownish-black (5YR2/1) in upper and lower part, moderate-brown (5YR3/4) in middle.
186.5	7.9	Mud, with interbedded salts at 179 and 184 m; salts, in beds 0.1 and 0.6 m thick, are mostly halite and trona, with some thenardite and northupite; mud is composed largely of microscopic crystals of dolomite and other carbonates; olive to brownish-black (5Y2/1 to 5YR2/1).
192.0	5.5	Salines interbedded with mud containing scattered saline crystals; salines are mostly halite, with subordinate trona, thenardite, and other minerals; salines olive-gray and medium- to dark-gray (5Y6/1 to N4-6), mud dark-olive-black (5Y1-2/1).
196.1	4.1	Mud, dark-olive-black (5Y1-2/1).
196.6	0.5	Salines, mostly halite; olive-gray (5Y4/1).
204.5	7.9	Mostly mud, with some disseminated saline crystals; brown (5YR3/4) in upper part, olive-gray (5Y4/1) in lower.
207.4	2.9	Salines, with interbedded mud; salines are mostly halite, distinctly bedded, averaging 1 cm in thickness; salines yellowish-gray (5Y7/2), mud olive-gray (5Y4/1).
210.9	3.5	Mud, moderate-brown (5YR4/4) in upper half, olive-black (5Y2/1) in lower part.
213.6	2.7	Salines, mostly halite, with mud impurities; olive-black (5Y2/1) to light-olive-gray (5Y6/1); upper part faintly bedded, lower part massive to mottled.
218.4	4.7	Mud, massive, olive-black (5Y3/1).
218.5	0.1	Salines, trona and halite.
227.4	8.9	Mud, massive, olive-black (5Y2/1).
227.7	0.3	Salines, trona and halite. Contact between Units D+E and F of Mixed Layer is at base of this interval.
248.1	20.4	Mud, mostly grayish-olive (5GY4/1), with a grayish-brown (5YR3/2) zone at 236-238 m and a greenish-gray (5GY6/2) zone at 244-245 m.
249.5	1.4	Mud, dark-greenish-gray (5GY4/1), mottled to faintly bedded; lower half extremely hard (limestone).
271.4	21.9	Mud, with irregular concentrations of a few mottled areas caused by light-colored dolomite or salts; mostly pale- to grayish-green (10G4-6/2), upper 3 m grayish-olive-green (5GY3/2); massive except near 260 and 268 m, where thin to laminar bedding is defined by pale-orange (10YR6-8/2-4) layers (dolomite?).
276.9	5.5	Mud, similar to interval above but containing searlesite.
291.1	14.2	Mud, similar to that at 249.5 m. Contact between Units F and G (new) of Mixed Layer is at base of this interval.
294.4	3.3	Impure salines with mud impurities similar to interval above; salines, mostly halite and thenardite, are mottled aggregates surrounded by mud.
299.3	4.9	Mud, dusky-yellow-green (5GY5/2); upper part mottled, lower part has buff laminae and thin beds.
306.3	7.0	Salines and some mud; salines are chiefly halite and thenardite, white to light-gray (N5-8); mud pale-green (10G6/2); upper part faintly bedded, lower part mottled.
324.3	18.0	Two saltbeds separated by mudbeds (see pl. 1); salts, largely halite, massive, light-greenish-gray (5GY6-8/1); muds massive, greenish-gray (5G6/1).
333.1	8.8	Three mud and two impure salt layers (pl. 1); mud pale-green (10G6/2), massive, with dispersed salts; saline layers, consisting of mottled zones of lighter colored secondary crystals oriented randomly in mud matrix, are halite, with some thenardite, glauberite, and anhydrite.
334.7	1.6	Impure salts, halite; dark-greenish-gray (5GY4/1).
337.3	2.6	Mud containing some halite; brownish-gray (5YR4/1).
341.1	3.8	Muddy salt grading downward into impure mud; salts largely halite and anhydrite; mud dark-greenish-gray (5GY4/1).
345.3	4.2	Mud with some dispersed salts; massive, faint mottled coloring; olive-gray (5Y4/1).
405.7	60.4	Nine alternating salt and mud layers in nearly equal volumes, with individual layers generally 4 to 6 m thick (see pl. 1); salts are halite and other saline minerals, mostly light- through medium-gray (N5-7) to light-olive-gray (5Y6/1) and grayish-orange-pink (5YR7/2); mud greenish-gray (5G4-6/1) to dark-greenish-gray (5GY4/1); mud is massive except in 0.5-m-thick zone below saltbeds, where it is thin bedded; salts are faintly bedded to massive.
413.3	7.6	Mud; inadvertently not photographed, but reported by field log as green to brown.
422.5	19.3	Core not recovered.
425.5	22.3	Mud, soft and plastic, olive-black (5Y2/1). Contact between Units G and H (new) of Mixed Layer is at base of this interval.
437.7	12.2	Mud, with small crystals of thenardite dispersed randomly; more coherent than interval above; average moderate-brown (5YR3/4).
444.6	6.9	Mud, soft and plastic, olive-black (5Y2/1).

TABLE 1. (cont.)

Depth to base of unit (m)	Thickness of unit (m)	Description
449.6	5.0	Mud, more coherent than interval above; moderate-brown (5YR3/4).
451.4	1.8	Salts and mud; salts in thin beds and mottled areas, yellowish-gray (5Y8/1), chiefly glauberite and anhydrite, with some halite; mud massive, olive-gray (5Y4/1).
482.5	31.1	Mud, moderate-brown (5YR3/4), with some zones of light-olive-gray (5Y5-6/1-2); salts largely halite and anhydrite, both dispersed and concentrated in mottled zones.
483.4	0.9	Mud and some salts; mud olive-gray (5Y4/1), thin bedded; salts are chiefly anhydrite and halite.
494.4	11.0	Mud, moderate-yellowish- to pale-brown (10YR5/2-4), massive.
507.5	13.1	Mud, light-olive-gray (5Y5/2) to pale-yellowish-brown(10YR/2), 2-m-thick zone at 502 m is pale brown (5YR5/2).
507.8	0.3	Mud and salt; mud light-olive-gray (5Y5/2); salts are mostly glauberite.
516.6	8.8	Mud and disseminated salts; light-olive-gray (5Y6/1) to pale-yellowish-brown (10YR6/2).
524.0	7.4	Mud; moderate-brown (5YR4/4) in upper part, yellowish-brown (10YR6/2) to pale-brown (5YR5/2) in lower part.
530.1	6.1	Mud; upper part greenish-gray (5GY6/1), mottled, thin-bedded to massive; lower part yellowish-brown (10YR6/2), thin-bedded.
541.6	11.5	Mud, mottled, pale-brown (5YR5/2) to pale-yellowish-brown (10YR6/2). Contact between Units H and I (new) of Mixed Layer is at base of this interval.
582.2	40.6	Mud, olive-gray (5Y4/1) down to 558 m, light-olive-gray (5Y6/1) below that depth, with 2-m-thick pale-brown (5YR5/2) zone at base.
634.0	51.8	Mud, light-olive-gray (5Y5-6/1-2).
640.1	6.1	Mud, brownish- black (5YR2/1) to olive-black (5Y2/1).
649.2	9.1	Mud, light-olive-gray (5Y5-6/1-2) and pale-olive (10Y6/2).
658.7	9.5	Mud; grayish-olive (10Y4/2) in upper part, yellowish-gray (5Y6/2) in lower part.
681.5	22.8	Mud, mostly pale-olive (10Y6/2) to yellowish-gray (5Y7/2), with zones near-olive-gray (5Y4/1) at 662, 665, and 669 m.
684.0	2.4	Tuff mixed with mud, grading down into pure tuff; impure tuff is olive-gray (5Y4/1), pure tuff yellowish-gray (5Y7/2); well indurated in basal 40 cm.
690.4	6.4	Mud, silt- to sand-size; mottled, ranging in color from olive gray (5Y4/1) to dark yellowish brown (10YR4/2)
690.9	0.5	Tuff, yellowish-gray (5Y6-8/1), well-indurated, crossbedded.
693.4	2.5	Mud and sand; faint to conspicuous thin beds, light-olive-gray (5Y5/2), with streaks of pale-brown (5YR5/2). Contact between Unit I of Mixed Layer and alluvial sand and gravel is at base of this interval.
915.3	211.9	Pebbly arkosic sand and gravel, most commonly moderate brown (5YR3-4/4), with zones that average light brown (5YR6/4) in color between 726-740 and 748-798 m; mostly coarse to very coarse sand, poorly sorted, containing quartz monzonite and volcanic-rock fragments, as large as 15 cm in diameter; faintly bedded to massive; not cored between 748.3-793.4, 804.7-826.3, and 839.1-903.1 m.
929.6	14.3	Quartz monzonite, light- to medium-gray (N5-7), with pale-brown (5YR5/2) stains along fractures extending through cored interval; rock bit was used from 915.3 to 926.3 m, and so no core was recovered.

TABLE 2. Names and composition of the non-clastic minerals found in the KM-3 core (Smith et al. 1983)

Mineral	*Composition*
Analcime	$NaAlSi_2O_6 \cdot H_2O$
Anhydrite	$CaSO_4$
Aragonite	$CaCO_3$
Borax	$Na_2B_4O_7 \cdot 10H_2O$
Burkeite	$2Na_2SO_4 \cdot Na_2CO_3$
Calcite	$CaCO_3$
Celestite	$(Sr, Ba)\ SO_4$
Dolomite	$CaMg\ (CO_3)_2$
Gaylussite	$CaCO_3 \cdot Na_2CO_3 \cdot 5H_2O$
Glauberite	$Na_2SO_4 \cdot CaSO_4$
Gypsum	$CaSO_4 \cdot 2H_2O$
Halite	$NaCl$
Hanksite	$9Na_2SO_4 \cdot 2Na_2CO_3 \cdot KCl$
Heulandite	$CaO \cdot Al_2O_3 \cdot 6SiO_2 \cdot 5H_2O$
Magnesite	$MgCO_3$
Nahcolite	$NaHCO_3$
Northupite	$Na_2CO_3 \cdot MgCO_3 \cdot NaCl$
Pirssonite	$CaCO_3 \cdot Na_2CO_3 \cdot 2H_2O$
Searlesite	$NaBSi_2O_6 \cdot H_2O$
Thenardite	Na_2SO_4
Tincalconite	$Na_2B_4O_7 \cdot 5H_2O$
Trona	$Na_2CO_3 \cdot NaHCO_3 \cdot 2H_2O$

primary or diagenetic origin is warranted. In this study we use the term "primary" for those minerals that form in contact with the lake water. It would include minerals that form by conversion from some other proto-phase and minerals that form by incongruent dissolution from another mineral, as long as the mineralogic change happened while still in contact with the lake waters. This definition is used because such minerals should be in isotopic equilibrium with the lake water and thus preserve the isotopic composition of the lake at the time that the mineral was deposited.

Smith (1979) suggested a primary origin for dolomite based on several factors: 1) the mineral occurs only in microscopic form; 2) it is found in lake-bed outcrops surrounding the valley floor, where other minerals of diagenetic origin are missing; 3) dolomite occurs in distinct zones, suggesting it occurred only when the lake chemistry was conducive to dolomite formation; 4) the magnesium content of interstitial brines is very low, and other minerals occurring with dolomite contain very small amounts of magnesium; and 5) dolomite does not occur in areas where minerals present could react diagenetically to form dolomite.

The occurrence of dolomite as a primary evaporite mineral in many lakes has been indicated by numerous investigators (Clayton et al. 1968; De Decker and Last 1988; Muller 1970). Last (1990) has reviewed a large number of Quaternary lacustrine dolomites and the majority of these were evaluated as being primary. These occurrences satisfy the definition of an isotopically primary mineral used in the present study regardless of whether stoichiometric dolomite was the original phase to be precipitated or not. Clayton et al. (1968), following Jones (1965), presented evidence of modern dolomite formation in Deep Springs Lake, California. Smith (1979) suggested that current dolomite formation in Deep Springs Lake may be a modern analog of dolomite formation in Searles Lake, as the two lakes are presumed to be very similar chemically .

Calcite in core KM-3 is also assumed to be of primary origin. Although it occurs less frequently than dolomite in core KM-3, it is predominant in a few sections of the core, most notably very deep in the core (Units G through I). Calcite is a well known primary precipitate from lake waters, and no compelling evidence suggests a diagenetic origin. It is likely that calcite has another primary origin in addition to being a direct precipitate from lake water. Evidence for this comes from modern sediments at Mono Lake CA, in which calcite has been found forming on the lake bottom by incongruent dissolution of primary gaylussite (Bischoff et al. 1991). Smith (1979) also suggests that some of the calcite in KM-3 is recrystallized from aragonite.

Aragonite occurs only in the upper stratigraphic units, mainly the Parting Mud and the Bottom Mud. Aragonite is thermodynamically metastable

near the earth's surface. Any aragonite that may have been precipitated earlier in the lake's history has probably been altered to calcite, or reacted with the interstitial brines to form gaylussite or pirssonite. No evidence suggests that the aragonite present in KM-3 is of other than primary origin.

Gaylussite and pirssonite have a more complex origin. Both gaylussite and pirssonite exhibit two grain sizes; large single crystals and finely disseminated small crystals. Textural evidence such as the large macrocrystals of gaylussite cross-cutting mud laminae with deformation of the laminae suggests that the macrocrystals formed after compaction of the sediment. Whether these macrocrystals formed as a new diagenetic phase or as a result of isochemical recrystallization of the fine-grained gaylussite is not known. All macrocrystals of gaylussite and pirssonite were therefore hand-picked prior to isotopic analysis of the sample. The fine-grained disseminated gaylussite is likely to be a primary mineral. It has been reported as a primary mineral in both Owens Lake (Smith et al. 1987), and Mono Lake (Bischoff et al. 1991).

Megascopic and microscopic northupite occurs in discrete intervals throughout most units of the Mixed Layer. Primary northupite is thought to have originated by the mixture of magnesium-bearing waters with concentrated sodium carbonate and chloride brines (Smith and Haines 1964). However, Smith (1979) suggested that microcrystalline northupite may be diagenetic in some core sections. As no northupite/water fractionation factor was available, northupite was not used in the core KM-3 stable isotope analysis.

Brines

The interstitial brines have been classified by Eugster and Hardie (1978) as being the Na-CO_3SO_4Cl type. The brines origin is discussed at length in Eugster and Hardie (1978). Figure 4 displays graphically the chemical evolution of the Searles brines.

Hardt et al. (1972) described the relationship of the relatively fresh water in the alluvial fans to the brines. The hydrostatic head of the brines is, and perhaps generally has been, higher than the head in the surrounding freshwater aquifers. Brine movement is therefore down, through the lake sediments, and possibly eventually moving out laterally from the basin (Friedman et al. 1982).

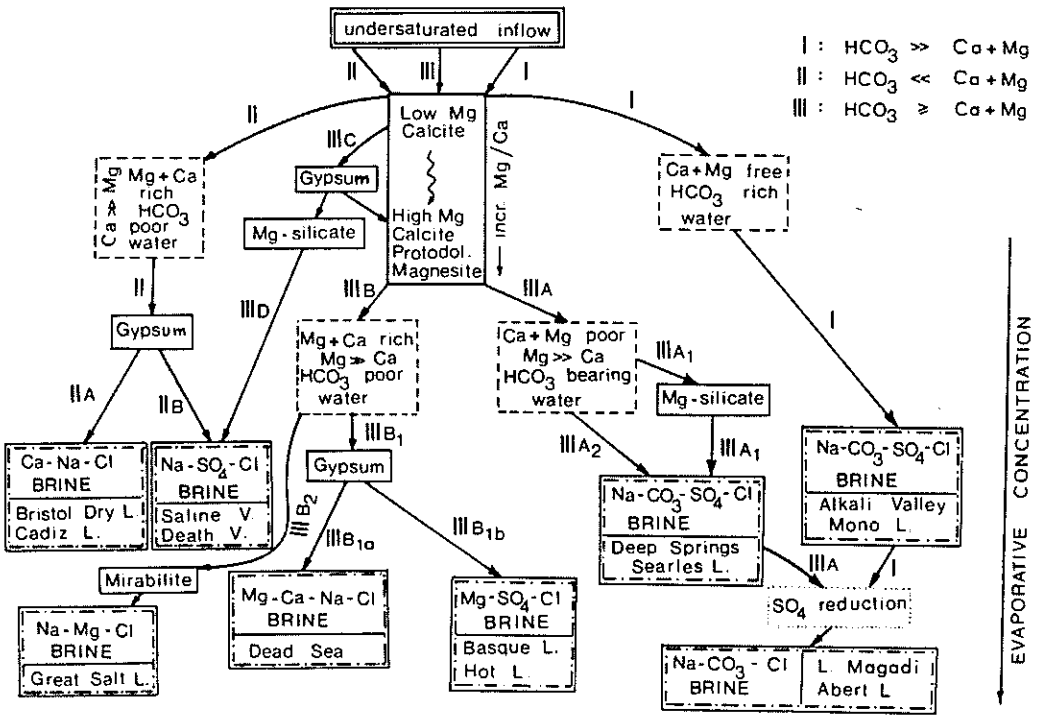

FIGURE 4. Water quality path of Searles Lake brines during evaporative concentration (Eugster and Hardie 1978)

CHRONOLOGY DEVELOPMENT

Carbon-14

During the late 1950s and 1960s, numerous investigators used radiocarbon techniques to obtain age estimates of lake sediments at Searles Lake (Flint and Gale 1958; Stuiver 1964; Stuiver and Smith 1979). Eighty-eight radiocarbon dates for sediment in the Overburden Mud, Upper Salt, Parting Mud, Lower Salt and the Bottom Mud have been published. A summary of these dates can be found in Benson et al. (1990). Materials used for radiocarbon age estimates include wood, disseminated organic carbon, and primary and diagenetic carbonate minerals.

The reliability of the materials for radiocarbon dating at Searles has been debated at length (Benson et al. 1990; Stuiver and Smith 1979). Potentially diagenetic carbonate minerals are not considered to be useful except as a supplement to more suitable materials. Briefly, the likely contamination of diagenetic carbonates with carbon from interstitial brines casts considerable doubt on minerals' reliability for radiocarbon dating.

Debate over the reliability of radiocarbon dates from primary carbonates is due to several factors. Non-equilibrium of the $^{14}C/^{12}C$ ratio between the lake water and atmosphere, the "reservoir effect," can cause the lake water to have an apparent age hundreds to thousands of years too old (Broecker and Walton 1965; Peng et al. 1978; Stuiver and Smith 1979). Therefore, radiocarbon age estimates of carbonates precipitated in isotopic equilibrium with lake water will be too "old." Another possible source of error in the radiocarbon age estimates of inorganic carbonates could be the assumption that the carbonate minerals were precipitated in isotopic equilibrium with the lake water. This problem is most likely to occur at low-lake levels where kinetic effects due to supersatuation of carbonates can produce non-equilibrium precipitates (Stiller et al. 1985). However, resulting errors in radiocarbon ages are likely to be small in comparison with other sources of error. Finally, Stuiver and Smith (1979) list substantially evidence that possible reworking of older sediments has occurred, especially in the Overburden Mud and the Upper Salt. Redeposition of older sediments could lead to ^{14}C dates that are too "old." Further, the dissolution of dead carbon into the lake would also cause precipitating carbonates to appear too "old."

Disseminated organic radiocarbon dates would be affected by many of the same processes as inorganic carbonates. The $^{14}C/^{12}C$ ratio of organisms utilizing dissolved carbon in the lake water will reflect the water's "apparent age. Similarly, isotopic exchange with interstitial fluids will produce errors in the radiocarbon age estimates of organic sediments. Finally, bacterial contamination of wet-sediment cores may produce radiocarbon age estimates of organic sediments that are too "young" (Geyh et al. 1974 in Benson et al. 1990).

Radiocarbon age estimates on wood are probably the most reliable (Stuiver and Smith 1979). Only two wood dates are available at Searles Lake: one in the Overburden Mud and one in a lower mud unit in the Lower Salt. No evidence has cast doubt on the reliability of these dates.

Inorganic carbonate minerals are least reliable for radiocarbon dating due to "reservoir effects," possible isotopic exchange with interstitial fluids, and redeposition of older sediments. Stuiver and Smith (1979) estimate errors associated with the ^{14}C dates of carbonate minerals range from 500 to 2500 years, in addition to reported counting errors. Estimated errors for disseminated organic dates range from 500-2500 years too "old," in addition to counting errors. As there are sufficient disseminated organic carbon and wood dates available, the inorganic dates will not be considered further in this paper.

Uranium/Thorium.

To expand the absolute-age chronology of Searles Lake sediments, Peng et al. (1978) compared radiocarbon dates of Lower Salt muds (Stuiver and Smith 1979) with ^{230}Th dates on the surrounding salt beds. Nineteen ^{230}Th dates were published on halite and trona samples from two cores. The uranium-thorium dates were in general agreement with the radiocarbon dates. This fact encouraged further uranium-series dating of the Bottom Mud and Mixed Layer Unit A+B by Bischoff et al. (1985). An additional nineteen ^{230}Th dates on trona, gaylussite and dolomite were published, extending the absolute-age chronology to approximately 230 ka.

The reliability of the ^{230}Th age estimates depends upon how well the technique satisfies two basic assumptions: 1) all ^{230}Th present in the sample resulted from post depositional in situ decay of uranium (it is assumed that there is no non-radiogenic ^{230}Th present), and 2) the sediment has remained a geochemically closed system; there has been no gain/loss or exchange of uranium or thorium (Ku and Liang 1984). In Peng et al. (1978), several additional assumptions were made in calculating the ^{230}Th age. First an estimated correlation factor for non-radiogenic ^{230}Th was derived by assuming that the initial $^{230}Th/^{232}Th$ ratio was the same for all salt units in the Lower Salt. Second, it was assumed that the salt units had been precipitated in an extremely short time.

Varying degrees of error are introduced by the above assumptions. Fluctuations in initial $^{230}Th/^{232}Th$ ratios are expected. Isotopic exchange with interstitial brines is possible, though difficult to determine. Age estimates of the Lower Salt based on the accumulation of acid-insoluble residue (Jannik 1989) support the assumption that the salt units were deposited in less than 1000 years and possibly less than 100 years.

A potential problem of post-depositional contamination also exists with the age estimates presented by Bischoff et al. (1985). Finally, because

intervals of core loss were not always noted during drilling, there may be uncertainly concerning the sample depth. With all possible errors in mind, the counting errors associated with the ^{230}Th dates for Searles Lake salts represent only a minimum error estimate.

Magnetostratigraphy.

Interpretation of paleomagnetic polarities from Searles Lake core KM-3 allowed development of a magnetostratigraphy for the paleolake sediments (Liddicoat et al. 1980). Using the revised time scale of Mankinen and Dalrymple (1979), the deepest lacustrine sediments were correlated with the base of the Mammoth subchron of the Gauss chron. (3.15 Ma). The youngest boundary defined was the Brunhes-Matuyama (~70 Ka). A total of twenty-four polarity boundaries were described, including five zones that were not included in the Mankinen and Dalrymple time scale. Reevaluation of the paleomagnetic data has led to the correlation of one of the previously unidentified magnetic zones (at 281.1 to 287.7 m) with the Cobb Mountain event at 1.10 Ma (Maniken and Gromme' 1982). This event had not been adequately dated at the time Liddicoat et al. (1980) was published.

Possible interpretation errors due to core sections reversed in the core boxes were discussed by the investigators. Reported errors associated with zone definition ranged from 0.4 m to 10.6 m. Using an average core sedimentation rate of 45 yr/cm, a minimum age error of 1.8 kyr to 45.5 kyr may be assumed for these paleomagnetic age-estimates.

Tephrochronology

A series of ash units was deposited in Searles Lake sediments as result of widespread Cenzoic volcanic activity. Fourteen tephra layers were identified in core KM-3 (Hay and Guldman 1987). One ash unit, at ~168.6 m, has been tentatively identified. It was correlated with the Lava Creek B (formerly 'Pearlette Type O') ash. The most recent age estimate for the Lava Creek B ash is 610 ka (J.D. Obradovich, written communication in Izett 1981). The age is based on a mean of several K-Ar dates. No error associated with this date has been published. Fission-track ages of zircons within the Lava Creek B ash from several localities are 0.6 ± 0.07 Ma (Naeser et al. 1973) and 0.6 ± 0.15 Ma (Christiansen and Blank, 1972 in Naeser et al 1973). These ages closely agree with the K-Ar date of 0.610 Ma.

The correlation of the tephra unit in core KM-3 with the Lava Creek B ash was made partially due to its stratigraphic position relative to the Brunhes-Matuyama paleomagnetic boundary. There appears to be some circular reasoning with this correlation, as the paleomagnetic boundary was originally identified partially based on its proximity to this tephra unit, then assumed to be the Bishop Tuff (Liddicoat et al. 1980). However, additional mineralogic information supports the identification of this ash unit as the Lava Creek B. The identification is also supported by the very similar stratigraphic

position of the Lava Creek B ash in Lake Lahontan sediments (Morrison and Davis 1984).

Chlorine-36.

Absolute age estimates based on the decay of ^{36}Cl in halite have extended the chronology of sediments at Searles Lake. Six ^{36}Cl dates on halite units from 14.2 m to 401.3 m in depth ranged from 10 ka to 1.95 Ma (Phillips et al. 1983). The ^{36}Cl dates were in general agreement with radiocarbon, uranium-series, and paleomagnetic age estimates of the same units. Based on the success of Phillips et al. (1983), Jannik (1989) determined an additional fourteen ^{36}Cl age estimates on halite units in core KM-3 from 3.0 m to 401.3 m in depth. ^{36}Cl dates on these new samples ranges from 6.7 ka to 1.27 Ma. The deepest sample at 401.3 m (1.95 Ma) had been suspected of contamination by Phillips et al. (1983), and the new date (1.25 Ma) of this depth confirmed earlier suspicions. Summaries of all ^{36}Cl age estimates are reported by Jannik (1989) and Jannik et al (1991).

As the ^{36}Cl method is somewhat new, a brief discussion of ^{36}Cl theory as it applies to the Searles Lake sediments is warranted. The hydrophilic nature of chlorine allows the chloride ion to travel through a hydrologic system with minimal chemical interaction. As Searles Lake was the frequent terminus of the Owens River paleolake system, chloride accumulated in the lake water and eventually precipitated out in evaporite minerals during arid periods. Upon deposition, the decay of ^{36}Cl began.

The various ^{36}Cl sources of in the evaporite minerals are discussed in great detail in Jannik (1989). Briefly, there are three main sources of ^{36}Cl. First, the initial ^{36}Cl input to a hydrologic system is through the inclusion of atmospheric-produced ^{36}Cl in precipitation. Second, surface production of ^{36}Cl in rocks is caused by cosmic-ray spallation of calcium and potassium and neutron activation of ^{35}Cl. The weathering of these rocks will add ^{36}Cl to surface or groundwater systems. Third, post-deposition production of ^{36}Cl due to activation of ^{35}Cl by cosmic-ray neutrons in addition to neutron activation by the decay of uranium and thorium in the sediments, can occur, increasing the $^{36}Cl/Cl$ ratio in the evaporite minerals. Phillips et al. (1983) estimated the $^{36}Cl/Cl$ input from the three different sources for the halite units in the Upper Salt. Approximately 30 percent of the ^{36}Cl in the halite is derived from atmospheric sources, about 17 percent from subsurface production, and apparently more than 50 percent from surface production.

In light of all the possible contributions of ^{36}Cl to the eventual $^{36}Cl/Cl$ ratio of the Searles Lake halite units, the determination of age estimates based on the ^{36}Cl method depends upon several conditions: 1) the $^{36}Cl/Cl$ ratio of inflow waters at Searles Lake was constant or known; 2)

subsurface production of ^{36}Cl is assumed to be negligible; and 3) no post-deposition transfer of chloride to or from the halite crystal has occurred. The general agreement of the ^{36}Cl age estimates with other radiocarbon, uranium-series, and paleomagnetic age estimates support these assumptions. However, a few ^{36}Cl measurements from Searles Lake showed abnormally high $^{36}Cl/Cl$ ratios. Jannik (1989) suggested laboratory contamination had taken place, yet she did not rule out other sources of error.

Analytical errors on the Searles Lake ^{36}Cl dates ranged from ±10.0 kyr in shallow samples to ± 176 kyr for deep samples. As with all other methods described previously, these analytical errors represent only a minimum error.

AIR-Interpolated Ages.

With a detailed absolute chronology established, assigning ages to samples between absolutely dated points usually involves a linear interpolation of ages based on an assumption of constant sedimentation rates. However, large variations have been found in sedimentation rates at Searles Lake due to the extreme fluctuations between slowly deposited deep-water muds and rapidly precipitated shallow-water evaporite sequences. Therefore, Jannik (1989) developed a technique to minimize the errors associated with interpolation. This technique is based on evidence for a relatively constant accumulation of acid-insoluble residue (AIR) in lake sediments (Jannik et al. 1991) The AIR in Searles sediments consists of fine-grained clastic detritius and apparently originates largely from local basin runoff.

The sedimentation rate variability in Searles is due largely to solute accumulation in the lake water during non-overflow periods of the lake's history. During low lake level or desiccation episodes, accumulated solutes precipitated out of the water rapidly as thick sequences of evaporite minerals. Conversely, the AIR component of inflow waters has a relatively short residence time in the lake water, and therefore accumulates at a relatively constant rate through time.

Results from detailed geochemical analyses of core KM-3 were presented by Smith et al. (1983). The core was divided into 254 intervals according to lithology. Geochemical analysis, including determination of AIR, was performed on each interval. Jannik (1989) calculated cumulative AIR versus time and concluded that the accumulation of the AIR component of the sediments varied smoothly through time. A plot of "AIR vs. Depth" displayed a "stair-step" pattern reflecting the change in sedimentation rates from pluvial (low sedimentation) to more arid (high sedimentation) periods. AIR data were assigned ages by linearly interpolating between absolutely dated points. The AIR ages were then correlated with AIR depths to create "AIR-interpolated ages" for the lithologic intervals. Analyses of some intervals were combined due to similar geochemical characteristics. A total of 144 intervals were assigned AIR-interpolated ages.

The AIR values are merely a method for interpolating ages between absolute radiometric and paleomagnetic dates. The purpose of using the AIR-interpolation procedure (instead of depth interpolation) is to compensate for drastic fluctuations in sedimentation rate caused by alternating evaporite and marl-depositing conditions. A very high deposition rate for the Upper Salt can be demonstrated by ^{14}C dating (discussed above). It seems reasonable to infer that similar evaporites deeper in the core were deposited under similar conditions. The AIR interpolation avoids unrealistically long deposition times for these evaporites. Errors assumed for this technique are difficult to quantify. The AIR technique has, however, substantially decreased errors that would have resulted had a simple linear depth interpolation between absolutely dated points been used.

Composite Chronology.

With all possible errors in mind using absolute dating techniques, the chronology for Searles Lake is remarkably detailed, especially in the upper units. Following Jannik (1989), a composite chronology of core KM-3 is presented below according to the informal (but generally accepted) stratigraphic unit names. Slight revisions of the Jannik chronology have been made, and a discussion of these revisions follows.

Overburden Mud. Evidence presented by Stuiver and Smith (1979) indicates most of the mud in this unit is reworked older sediment. Therefore, no dates on carbonate minerals or organic sediments are thought to be reliable. A ^{36}Cl date of 67 ka ± 10 kyr is clearly much too old and unreliable. The only reliable date available is a ^{14}C date on wood at 2.4 m in depth with an age of 3.52 ka ± 0.19 kyr. One AIR-interpolated age at the Overburden Mud/Upper Salt boundary implies an age of 6 ka.

Upper Salt. Twelve radiocarbon dates (Stuiver and Smith 1979) for this unit are from inorganic carbonates and are considered unreliable. Four radiocarbon dates on disseminated organic carbon ranged from 11.4 ka ± 0.6 kyr near the top of the unit to 9.72 ka ± 0.2 kyr at the base of the unit. All other dates fell within the 10 ka to 11 ka range for the bottom 80 percent of the unit.

As discussed by previous investigators (Stuiver 1964; Benson et al. 1990) the reversals in age and the small range of ages throughout the bottom 80 percent of the Lower Salt indicate rapid precipitation of this salt unit. The AIR data also support this conclusion.

Two U-Th age estimates (Peng et al. 1978) near the top and base of the Lower Salt zone gave "corrected" ^{230}Th ages of 5.3 ka ± 1.2 kyr and 8.7 ka ± 0.2 kyr, respectively. The age estimates are in general agreement with AIR and ^{14}C dates.

Again, as stable isotope analysis was not made on samples above the Parting Mud, age estimates for the Upper Salt are not crucial to this report. We have used an approximate average of the ^{14}C values for the Parting

Mud/Upper Salt boundary, of 10 ka, which is in general agreement with all other age estimates. AIR dates for locations within the unit have been used as they are stratigraphically consistent while the radiocarbon dates are not.

Parting Mud. Thirty-nine ^{14}C dates for the Parting mud are summarized in Stuiver and Smith (1979); fourteen radiocarbon dates were from inorganic carbonates and, therefore, unreliable. Twenty-five radiocarbon dates from disseminated organic carbon were presented; the radiocarbon age estimates on these samples range from 10.06 ka ± 90 yr to 10.9 ka ± 90 yr at the top of the unit, and 22.4 ka ± 1.0 kyr to 24.69 ka 1.07 kyr at the base. Following Stuiver and Smith (1979), an age estimate of 23 ka for the base of the Parting Mud is chosen here, although the age could range from ~21 ka to 24 ka.

Lower Salt. Twenty-seven radiocarbon dates for this unit are summarized in Stuiver and Smith (1979): seven from inorganic carbon, nineteen from disseminated organic carbon, and one radiocarbon date on wood is available. As before, radiocarbon dates on inorganic carbonates are probably unreliable and will not be considered further. The uppermost radiocarbon date is on sub-unit M-7, with an age estimate of 23.75 ka ± 0.4 kyr. The deepest reliable date is from sub-unit M-2, with an age-estimate of 32.6 ka 0.5 Kyr. Sub-unit M-3 is the most uncertain, with two disseminated organic radiocarbon dates of 32.0 ka ± 1 kyr and 29.5 ka ± 2 kyr. The wood radiocarbon date for M-3 is 26.7 ka ± 2 kyr. Between M-6 and M-2, several radiocarbon dates are stratigraphically inconsistent. Detailed AIR dates are available in the Lower Salt units. These data again support conclusions by previous authors that most of the salt sub-units were deposited in a very short time.

Eighteen U-Th age estimates are available for the salt sub-units of the Lower Salt; sixteen "corrected" ^{230}Th dates were published in Peng et al. (1978) and one ^{230}Th age estimate for the S-1 sub-unit was presented in Bischoff and others (1985). A few ^{230}Th age-estimates were stratigraphically inconsistent. Thorium-230 dates ranged from 23.8 ka ± 1.4 kyr for sub-unit S-7, to 33.0 ka ± 1.5 kyr for sub-unit S-1 (Peng et al. 1978). The ^{230}Th age-estimate for S-1 in Bischoff et al. (1985) was 35.3 ka + 2.7 -2.4 kyr.

Selecting a chronology for the Lower Salt was problematic. Overall, both ^{14}C and ^{230}Th dates were in general agreement. However, data that were stratigraphically reversed, in addition to doubts concerning "reservoir effects" and Peng's ^{232}Th corrections, made choosing the best dates difficult. Therefore, we have chosen to assign a "probable" age to the Lower Salt/Bottom Mud boundary of 33.0 ka. This age is within the reported confidence intervals of all ^{14}C and ^{230}Th age estimates. Using the "probable age" of the LS/BM boundary of 33 ka, the "probable age" of the PM/LS boundary of 23 ka, and AIR data, we interpolated a chronology for the sub-units of the Lower Salt. In general, the new AIR interpolated-ages for the sub-units are in agreement with

^{14}C and ^{230}Th age estimates. A problem immediately apparent with this AIR-interpolated chronology is that the AIR ages for the sub-unit M-3 boundaries are not within the confidence interval of the radiocarbon age estimate on the wood from sub-unit M-3, presumably the most reliable date in the Lower Salt. Therefore, the confidence intervals for assigned sample ages within this unit should probably be as large as ± 5 kyr.

Bottom Mud. Four ^{14}C age estimates are available for the Bottom Mud; three of the four dates are on disseminated organic carbon. Two the the three organic dates are near the top of the Bottom Mud, and the previously assigned "probable age" of the LS/BM boundary is within the confidence interval of both dates.

Five ^{230}Th age estimates for the Bottom Mud were presented in Bischoff et al. (1985). Ages ranged from 58.4 ka + 1.5 -1.1 kyr near the top of the Bottom Mud, to 122.3 ka + 3.6 -3.0 kyr approximately 30 percent above the base of the unit.

AIR data are available for the Bottom Mud. Of greatest interest is one point at the base of the unit. If the first ^{230}Th date of 58.4 ka is incorporated into the chronology, a sedimentation rate of less than 1 cm/100 yr is inferred from the LS/BM boundary to this sample. This sedimentation rate is more than an order of magnitude less than the rates in the intervals above and below. Therefore, only the lower four ^{230}Th age estimates are used. AIR data are also incorporated into the Bottom Mud chronology. An age estimate of 153.8 ka is interpolated for the BM/Mixed Layer boundary.

Mixed Layer A & B. Four ^{230}Th age-estimates for the A&B unit were presented by Bischoff et al. (1985). The A&B/C boundary was dated by the ^{36}Cl method to yield an age of 286 ka ± 47 ka (Jannik 1989). Seven AIR intervals are also available for this unit.

We have chosen not to use two of the four ^{230}Th age estimates available for the A & B unit. The uppermost sample (Bischoff sample 7) yields an extremely low calculated sedimentation rate. The deepest ^{230}Th date (Bischoff sample 11) also yields a low sedimentation rate, and has a very large analytical uncertainty. Two ^{230}Th ages were available for Bischoff sample 8, and, following Jannik (1989), we have averaged the two dates for an age-estimate of 160.5 ka at 70.86 m in KM-3. ALL AIR data were used.

Unit C. Four ^{36}Cl age estimates and twenty six AIR-interpolated ages are available for Unit C (Jannik 1989). All available data were incorporated into the unit C chronology. The AIR interpolated age at the Unit C/D+E boundary is 598 ka.

Units D & E. Four ^{36}Cl age estimates are available for unit D+E (Phillips et al. 1983; Jannik 1989). One of the four (SLC-6) represented a reversal, and therefore, was not included in this chronology. An ash layer at 168.6 m was correlated with the Lava Creek B ash (610 ka) (Hay and Guldman 1986). The

first three paleomagnetic boundaries in KM-3 were defined in the D+E unit (Liddicoat et al. 1980): the Brunhes-Matuyama (730 ka) at 185 m, the Matuyama-Jaramillo (900 ka) at 204.9, and the Jaramillo-Matuyama (970 ka) at 221.2 m. Thirteen AIR ages are also available in D+E (Jannik 1989). All available age estimates, with the exception of the one ^{36}Cl date previously mentioned, are incorporated into the chronology presented in this paper.

Unit F. Only seven AIR-interpolated ages (Jannik 1989) are available for Unit F. The deepest AIR interval, located at the F/G boundary, gives an approximate age of 1.268 Ma for the stratigraphic boundary. Two anomalous (normal) paleomagnetic zones were identified in Unit F by Liddicoat et al. (1980). At that time they could not be correlated with any well-dated magnetic events, but more recent publications have determined an age of 1.10 Ma ± 0.02 Myr for the Cobb Mountain event, the first, brief, normal event below the base of the Jaramillo (Mankinen et al. 1978; Mankinen and Gromme' 1982). We have therefore assigned an age of 1.10 Ma to the top of this normal zone at 281.1 m. Below the Cobb Mountain normal event there is another short normal interval between 322.3 and 330.2 m depth. We tentatively identify this interval with a poorly defined magnetic event dated at 1.22 Ma ± 0.04 Myr on Tenerife (Abdel-Monem et al. 1972) and c.a. 1.18 Ma in the Lesser Antilles (Briden et al. 1979). We therefore assign an age of 1.20 Ma at 322.3 m. The evidence for a global magnetic event at this time is weak and the validity of the event in the KM-3 core is somewhat suspect (Liddicoat et al. 1980). Thus this datum should be viewed cautiously. However, it is consistent with age interpolation on the basis of sedimentation rate and does not cause significant deviation of the chronology from the case in which it is not included. If the event is ever better dated, the chronology can be revised to reflect the new age.

Unit G. This is the deepest stratigraphic unit presented in this report that was sampled for stable isotope analysis. One ^{36}Cl date and thirty-four AIR-interpolated ages are available for this unit (Jannik 1989). Six paleomagnetic ages are also available (Liddicoat et al. 1980). Two of the six paleomagnetic ages represent undefined boundaries and will not be used in this chronology. The four defined paleomagnetic boundaries that are used are: 1) the Matuyama-Olduvai (1.67 Ma) at 378.6 m; 2) the Olduvai-Matuyama (1.87 Ma) at 403.25 m; 3) The Matuyama-Reunion (2.01 Ma) at 408.3 m; 4) and the Reunion-Matuyama (2.04 Ma) at 424.7 m near the G/H stratigraphic boundary. The ^{36}Cl date, all paleomagnetic dates and all AIR ages are used in this chronology. An approximate age of the G/H stratigraphic boundary is 2.04 Ma.

Combined Chronology.

All ^{14}C, ^{230}Th, ^{36}Cl, AIR-interpolated and paleomagnetic ages used in this chronology are listed in Appendix A. Graphical representations of KM-3 core depth vs. age are shown in figures 5 and 6. KM-3 mud samples prepared for stable isotope analysis were assigned ages using linear depth interpolation between absolutely dated isotope and paleomagnetic points and AIR interpolations.

LDW-6 Chronology.

Due to poor recovery in the A & B section of the KM-3 core, additional samples were collected from the LDW-6 core to fill in this interval. Although recovery in LDW-6 generally was quite good, there are some 10-meter intervals with up to 4 meters missing. Usually there are no records with 4 meters missing. During sampling it was always assumed that the missing core was at the bottom interval. This has created data gaps which may or may not be real.

The age-depth relationship for the LDW-6 samples was determined using the ^{230}Th date at 60b meters (data point 8 from Bischoff et al. 1985) and the ^{36}Cl date at 114 meters (Jannik 1989). Although the Bischoff et al. data point 9 was located in the sample interval, it was not used in establishing the chronology due to a discrepancy in published depth and the depth we determined for this sample location during our sampling for stable-isotope studies.

Once ages were determined for each sample, the data were inserted directly into the KM-3 data set. A very good correlation was found between the LDW-6 isotope values and the few isotope values determined for that interval in KM-3.

METHODS AND PROCEDURES

Introduction

A detailed sampling scheme was developed to achieve a high time-resolution record of stable isotope variation in Searles Lake paleowaters. Care was taken in sampling the core to minimize location errors. Once the core was sampled, the relative amounts and types of minerals were determined. Any substances interfering with mass spectrometer analysis of primary carbonates were removed from the samples. Following this, a methodology was developed to separate primary carbonates from each other, as each mineral has its own water-carbonate fractionation factor and phosphoric-acid fractionation factor.

Sampling

Two-hundred and fifteen samples were collected from core KM-3 mud units during October 1986. The desired sampling frequency was approximately one sample every one to two thousand years. Using Smith et al. (1983) core log and calculated sedimentation rates as a guide, approximately 20 grams of sample were taken every one to two feet in most intervals from the Parting Mud through Unit G of the Mixed Layer. Sample descriptions and field notes are

CORE KM-3 CHRONOLOGY: UPPER UNITS

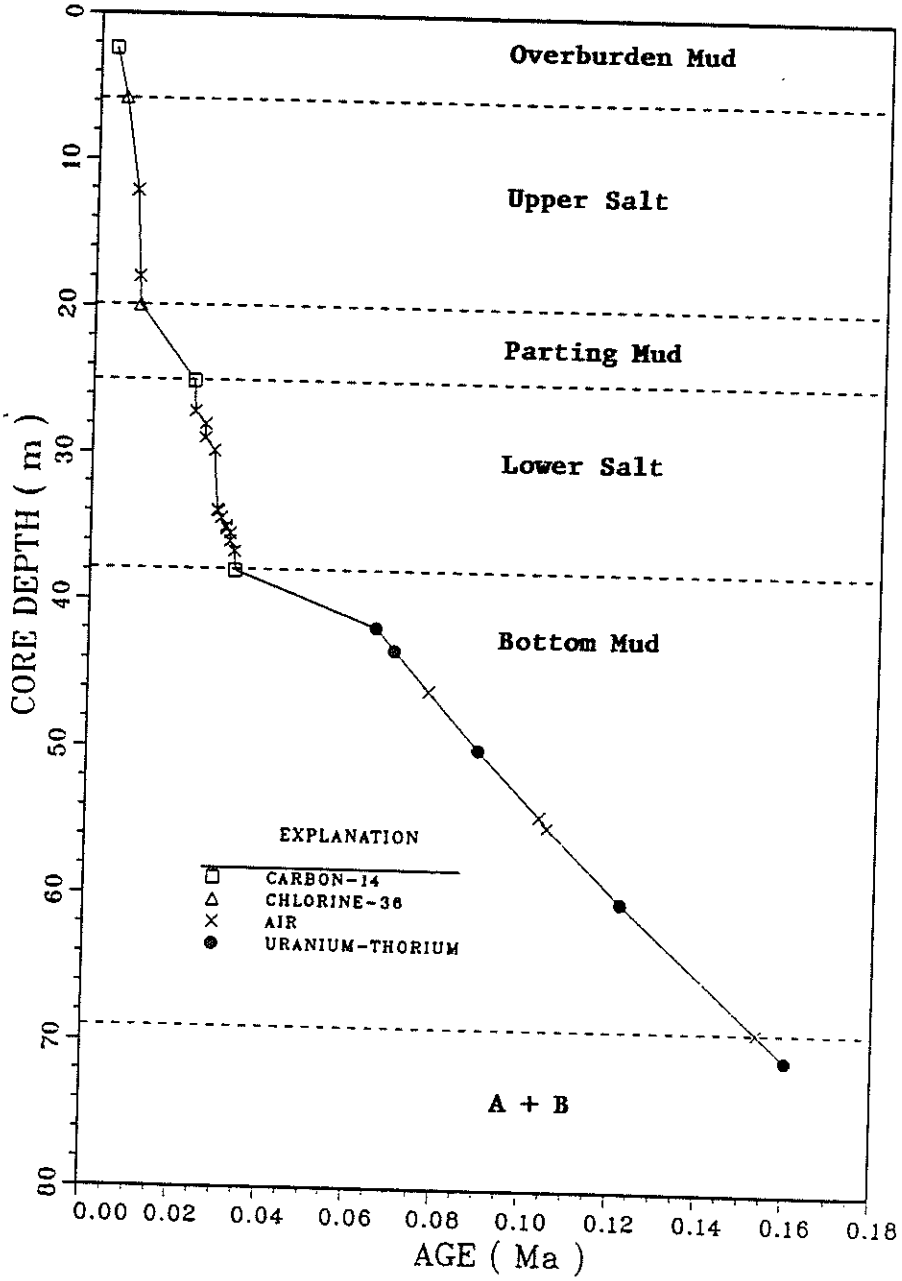

FIGURE 5. Age versus depth relationship for upper portion (0-80 m depth) of core KM-3, using ^{14}C, U/Th, and ^{36}Cl dates and acid-insoluble residue (AIR) interpolation (revised from Jannik 1989)

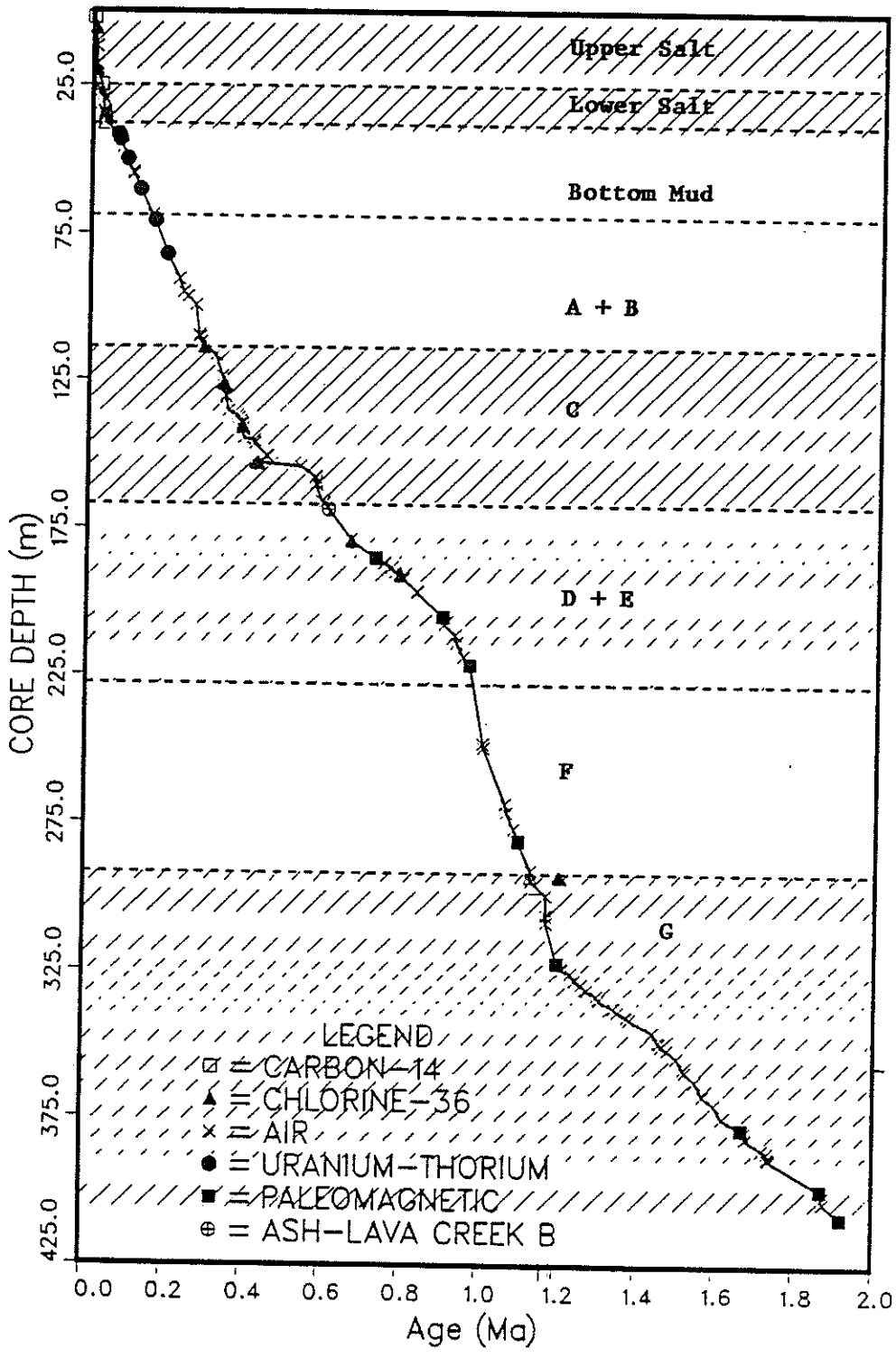

FIGURE 6. Age versus depth relationship for the upper 425 m of core KM-3, using ^{14}C, U/Th, ^{36}Cl, and paleomagnetic dates and acid insoluble residue (AIR) interpolation (revised from Jannik 1989) Hatchuring indicates saline-dominated intervals

listed in Appendix B. Care was taken to remove large macroscopic salt crystals and to scrape off the outside of the core to minimize contamination. Severe "telescoping" (slumping to one end of a partially filled core box) had occurred in several core boxes; the core boxes with this problem are noted in Appendix B. Sample depths are listed to the tenth of a foot, but this should not be interpreted to imply confidence in the depths to this degree, especially in intervals with severe telescoping problems.

Sampling Preparation

Core samples contain a variety of primary and secondary authigenic minerals as described in an earlier section. To obtain a good stable isotopic analysis of the primary carbonate (principally gaylussite) the other minerals were removed using physical and chemical methods. The samples also contain detrital silicates, which were not removed because only the carbonate minerals react with the phosphoric acid to release CO_2.

First, macroscopic crystals of salt were removed from the sample by hand-picking. This included crystals of halite and possibly secondary gaylussite and pirssonite. It is important to remove all halite because it reacts with the phosphoric acid to produce HCl. The HCl stays with the CO_2 and creates severe problems during the mass spectrometry analysis. Second, due to the much greater solubility of the halite minerals, water leaching was used to dissolve the remaining unwanted minerals. This procedure is described in Appendix C. X-ray diffraction (XRD) techniques were used to determine the success of the leaching procedure. Scanning parameters and XRD results are listed in Appendix B.

An unexpected problem with the leaching procedure was raised by the XRD results. Although the double carbonate salts identified by XRD in bulk samples dissolved, calcite appeared to have precipitated during the leaching process. An experiment was conducted to determine the origin of this calcite, which we referred to as "mongrel" calcite due to its uncertain parentage. Clean gaylussite and pirssonite crystals were placed in water to dissolve overnight. The solid collected by filtration was identified by XRD as calcite and confirmed that calcite had resulted from the dissolution of the two double carbonates. This phenomenon was previously observed by G.I. Smith (pers. comm).

A second problem with the leaching process was the occasional persistence of pirssonite and, more often, northupite. Repeated leachings would not remove all of these minerals. These samples eventually were analyzed for ^{18}O and ^{13}C but were not included in the final stable isotope chronology, and are noted so in Appendix F.

Once the samples had been leached and carbonate mineralogy identified by XRD, they were prepared for stable isotopic analysis by the standard

phosphoric acid procedure (McCrea 1950). The CO_2 samples were run on a Finnegan MAT model Delta E mass spectrometer at New Mexico Institute of Mining and Technology. All ^{18}O values are reported in per mil relative to the SMOW standard, and all ^{13}C values are reported in per mil relative to the PDB standard.

Isotopic Systematics of Searles Lake Carbonates

Due to the problem of mongrel calcite and the persistence of diagenetic carbonates and northupite, examining isotopic relationship between these minerals and primary carbonates was required. Six representative samples were selected to isolate the sample's various carbonate components and to analyze each for its stable isotopic composition. Two samples contained gaylussite; one sample contained only gaylussite and no other carbonates, and one sample contained both gaylussite and dolomite. Four samples contained pirssonite: three contained pirssonite and dolomite, and one contained pirssonite, dolomite and northupite. No sample containing only pirssonite could be found. Each sample (including bulk sample, water-leached bulk sample, double carbonate and water-leached double carbonate) was analyzed for $\delta^{18}O$ and $\delta^{13}C$ values. For these samples the mineralogy had been determined by XRD and qualitative assigned an abundance as major (M), intermediate (I) and trace (TR). The results for representative samples are shown in Figure 7. Included are $\delta^{18}O$ and $\delta^{13}C$ results for dolomite (in this figure) for comparison. The dolomite values are obtained by timed extraction as described below.

In all samples except 605.0, where northupite is present, a linear mixing between the various components is evident. Both the bulk samples and the carbonate salt are enriched in ^{18}O with respect to the water-leached sample. The carbon isotope content of the diagenetic salts seems to be somewhat depleted in comparison with the calcite and dolomite values.

Carbonate Separation

Several techniques were used to chemically separate the mongrel and primary calcite from dolomite. The first technique was based on the relative solubilities of calcite and dolomite. An aqueous solution of EDTA was used to complex the Ca^{2+}cation of the more soluble calcite, hopefully preventing the creation of the mongrel calcite and removing primary calcite. The approach was not successful due to the dolomite's excessive EDTA complexation. Technique details and results are given in Appendix D.

The second (and successful) technique used is based on the reaction rates of the various carbonates with phosphoric acid and is termed the "timed extraction technique." Approximately 50 milligrams of bulk leached sample (passing 200 mesh) were reacted with five ml of 100 percent phosphoric acid following McCrea (1950). The carbon dioxide evolved was collected after 1/4, 3/4, 3, 19 (or 24), 43 (or 48) and 67 hours and each gas aliquot was analyzed

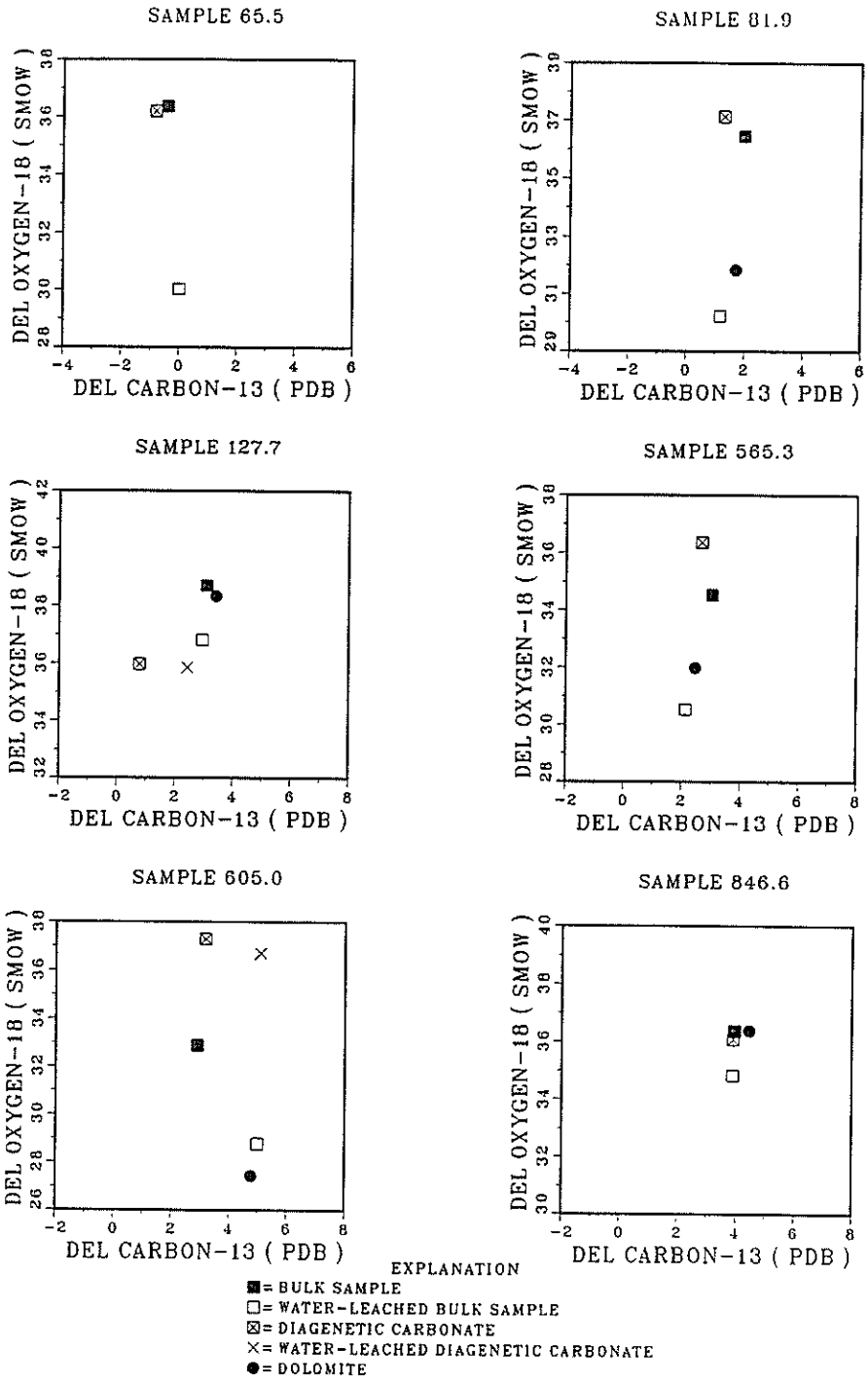

FIGURE 7. $\delta^{18}O$ versus $\delta^{13}C$ for bulk, water-leached bulk, diagenetic carbonate, water-leached diagenetic carbonate, and dolomite fractions of six samples from core KM-3

for stable isotope content. This technique has been used successfully by other investigators (Clayton et al. 1968; Degens and Epstein 1964; Epstein et al. 1963).

Representative samples were selected to test this technique. Mixtures of mongrel calcite and dolomite (sample 127.7), primary calcite and dolomite (1130.5), aragonite and dolomite (142.8) and mongrel calcite, dolomite and pirsonnite (81.9) were selected. The results are shown in figures 8 and 9. The mongrel calcite endpoint for sample 127.7 was known (35.7 per mil), and the first aliquot of carbon dioxide reflects this calcite isotopic content. After approximately three days, the $\delta^{18}O$ leveled off at 40.4 per mil. This value is assumed to represent the dolomite's isotopic composition. A similar pattern occurred in the deep primary calcite/dolomite mixture (1130.5). Although the calcite endpoint was not known, the isotopically light early endpoint is similar to other "calcite only" values for surrounding samples. Further, if the two carbonates are co-precipitates, calcite-dolomite fractionation factors should lie in the range +1 to +7 per mil (Land 1980). Both the mongrel calcite/dolomite and primary calcite/dolomite mixtures displayed an approximately five per mil difference in the calcite/dolomite values of $\delta^{18}O$, with dolomite more enriched than calcite. The change in $\delta^{13}C$ was quite different in the two samples. In the mongrel calcite/dolomite mixture, the $\delta^{13}C$ content was enriched approximately 3.5 per mil. The $\delta^{13}C$ in the primary calcite/dolomite mixture was ultimately enriched ~0.5 per mil; yet a gradual trend from endpoint (calcite) to endpoint (dolomite) is not observed. It appears that there may be more than one type of calcite or dolomite in the mixture.

Results from the timed extraction procedure for the mongrel calcite/dolomite/pirsonnite mixture were also successful. Both the mongrel calcite and pirsonnite values were already known (30.0 per mil and 37.2 per mil, respectively). Early carbon dioxide isotopic content reflects the ^{18}O and ^{13}C content of the mongrel calcite. By the fourth CO_2 aliquot at 3 hours, the $\delta^{18}O$ and $\delta^{13}C$ values of the gas clearly reflected the enriched pirsonnite values. The late samples were depleted with respect to the pirssonite in ^{18}O, yet are enriched in ^{13}C, and are enriched in both ^{18}O and ^{13}C with respect to the mongrel calcite. These late values are assumed to be an approximation of the dolomite's isotope composition. The delta calcite-dolomite for this sample was ~3.2 per mil. The aragonite/dolomite mixture reflected the same trend as the mongrel calcite/dolomite mixture yet the enrichment in ^{18}O was only ~3 per mil, and 0.9 per mil for ^{13}C.

With some confidence that the carbonates could be separated with the timed-extraction technique, time and money became the next obstacle. The cost to run over 200 samples would be extreme. Knowing the mineralogy and

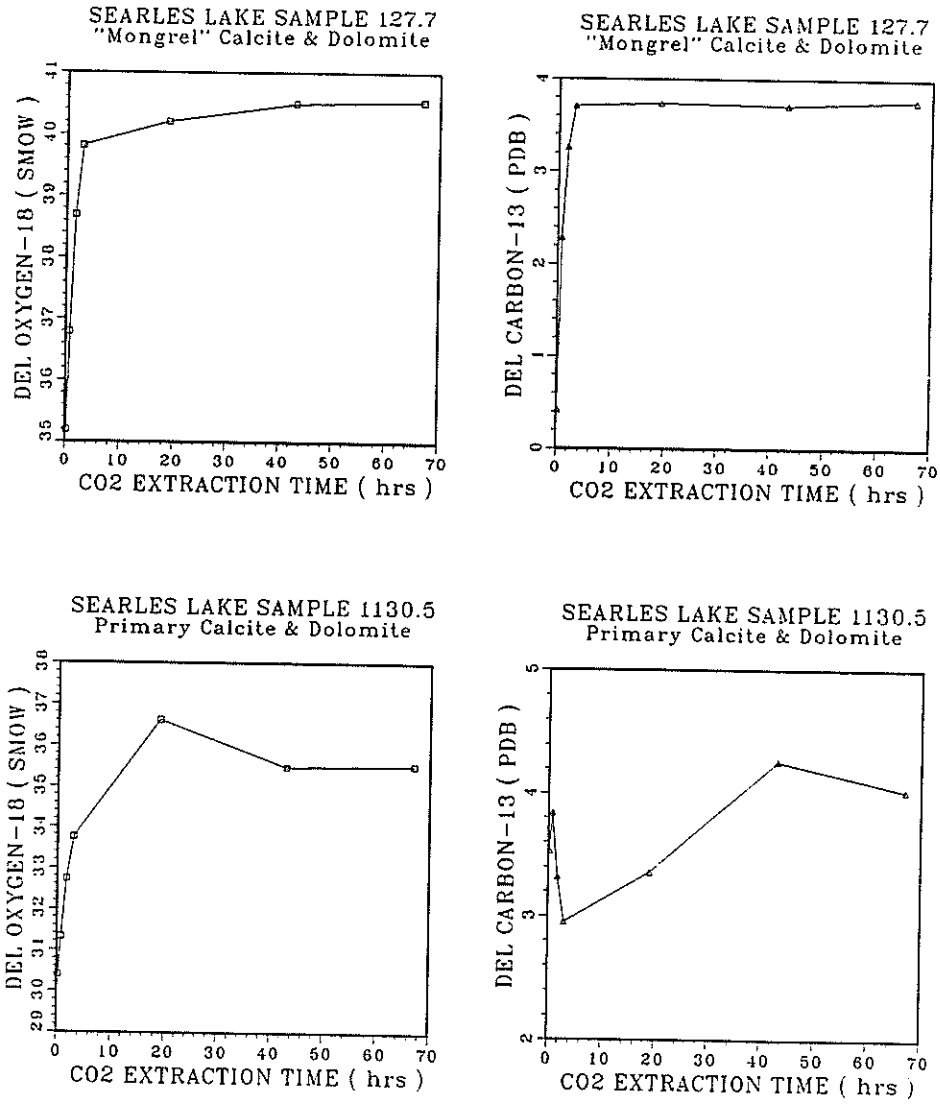

FIGURE 8. $\delta^{18}O$ and $\delta^{13}C$ as a function of time during timed extraction analysis of samples from 127.7 and 1130.5 m from KM-3

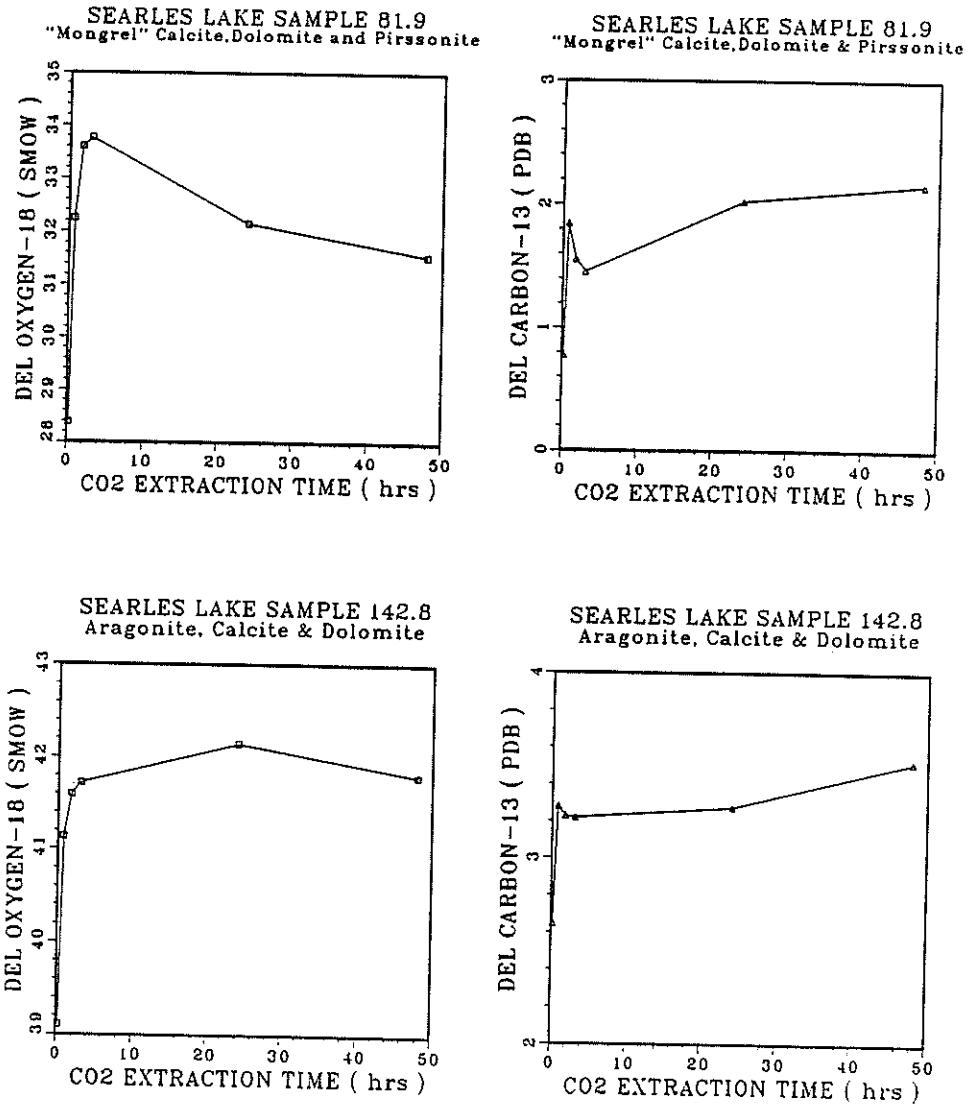

FIGURE 9. $\delta^{18}O$ and $\delta^{13}C$ as a function of this time during timed extraction analysis of samples from 81.9 and 142.8 m from KM-3

approximate relative amounts of the various minerals, a modified timed-extraction technique was devised to reduce the number of gas samples. Instead of collecting several aliquots of carbon dioxide over several days, one sample would be collected which would be representative of the final dolomite value. Upon adding phosphoric acid to the sample, the vacuum extraction line was brought back to a high vacuum, and the reaction vessel was opened. All carbon dioxide evolved was then pumped away from the vessel. After some time had elapsed, the reaction vessel was closed and the remaining carbonate (presumably dolomite) was allowed to react. All carbon dioxide evolved from the remaining carbonate was collected and analyzed for $\delta^{18}O$ and $\delta^{13}C$.

The first concern was that fractionation would take place due to kinetic effects. To test this, a pure calcite (NMIMT lab standard "MEXICAN CALCITE") was tested to see if any fractionation would occur. Results are shown in Figure 10. No appreciable fractionation of the calcite was observed. Second, the samples that had been run using the long timed-extraction technique were rerun using the open-vessel modification. Bulk sample aliquots for each sample were reacted with acid using the open-vessel technique. The vessel was left open for 5, 10, 30 and 60 minutes. The results of these extractions are compared to the closed-vessel extractions in figures 11 and 12.

Sample 127.7 had large nitrogen contamination due to leaking sample bottles. This probably accounts for the slightly enriched values. Otherwise, the dolomite value was arrived at quickly. Samples 1130.5 and 142.8 reached the dolomite value in approximately one hour. Sample 81.9 was still slightly enriched, reflecting the pirssonite content, yet the one-hour value is within the range of analytical uncertainty for this technique (discussed later in this section). Therefore, it appeared that the timed-extraction technique could be modified so that only one CO_2 aliquot need be analyzed, and this sample could be obtained within one hour. No appreciable fractionation was observed.

The reaction time for each sample was estimated during sample preparation. The observed reaction rates slowed significantly as the dolomite became the dominant mineral. Therefore, reactions were monitored until the rate of phosphoralysis had decreased to the point that it was apparent dolomite was the only mineral remaining. The reaction times ranged from a approximately twenty to ninety minutes. Admittedly, this approach requires uniform procedure by the analyst. Only one analyst (C.V. Kruger) ran these samples. Therefore, at least the interpretations of the reaction rates were consistent. Statistical analysis of repeated samples treated by this method (described below) indicates that $\delta^{18}O$ values produced by this method are reproducible to within $\pm$ 0.7 per mil, or better.

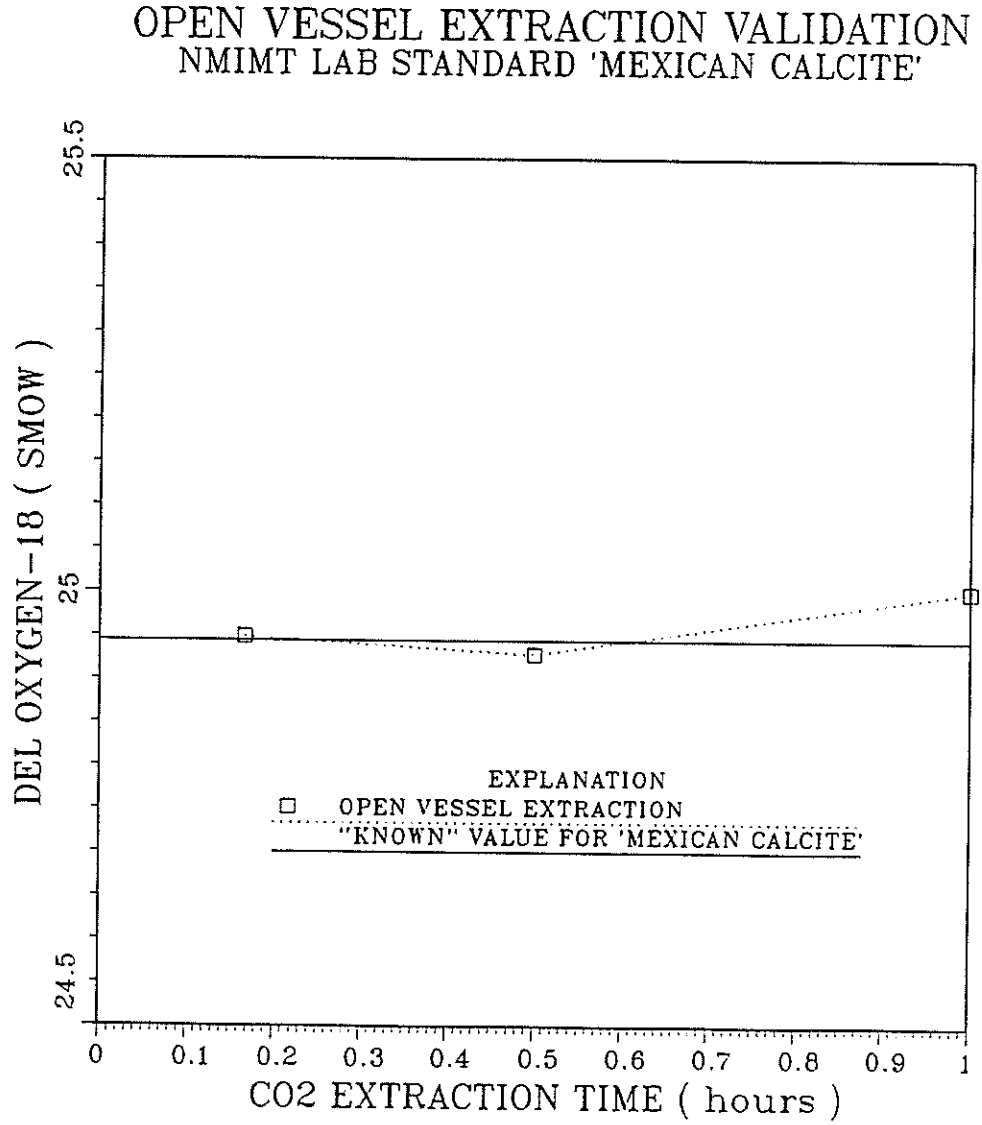

FIGURE 10. Variation in $\delta^{18}O$ as a function of extraction time during vacuum extraction for NMIMT Isotope Laboratory standard "Mexican Calcite"

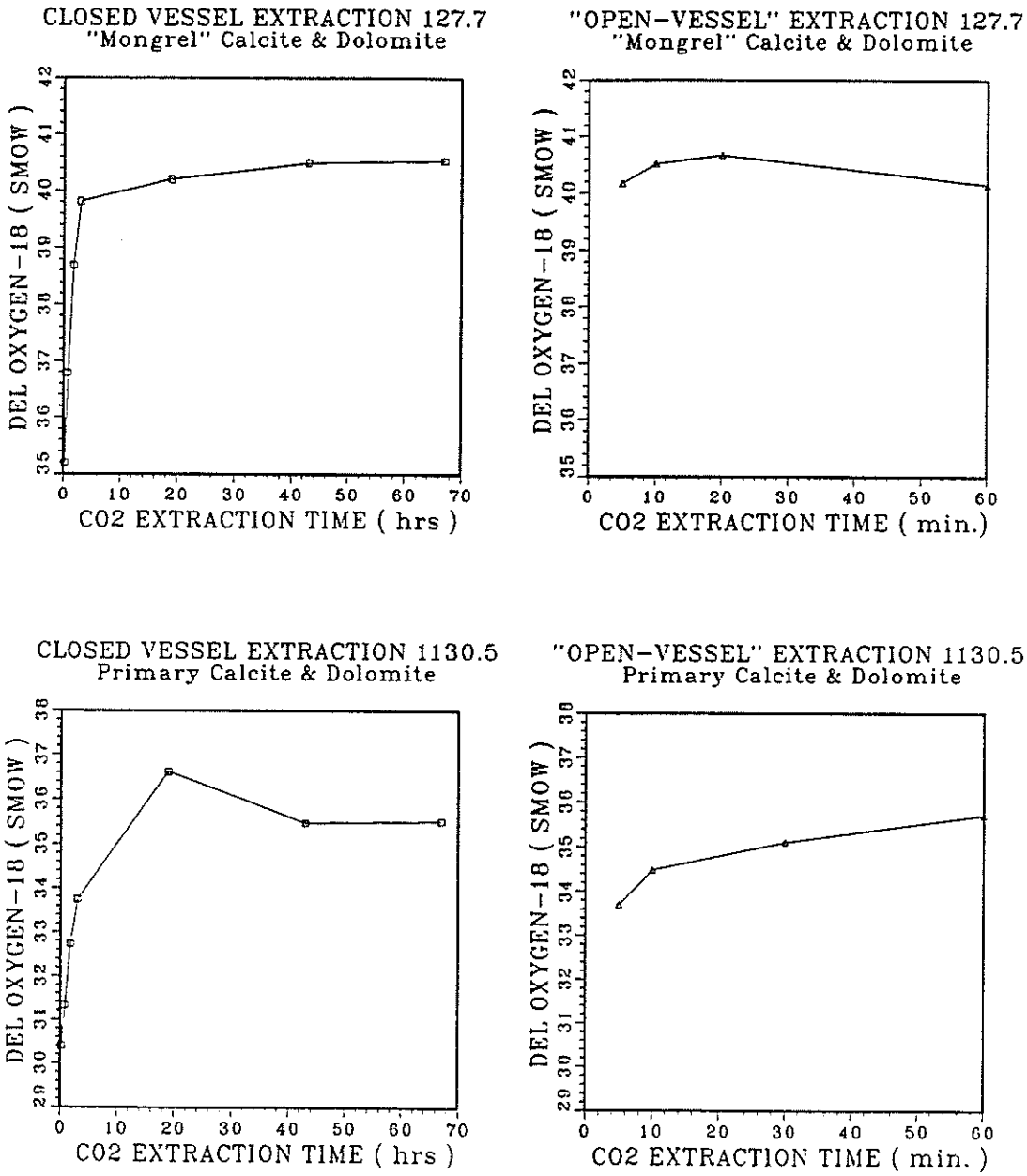

FIGURE 11. A comparison of $\delta^{18}O$ as a function of time for "closed vessel" and "open-vessel" (vacuum) extractions of samples from 127.7 and 1130.5 m in KM-3

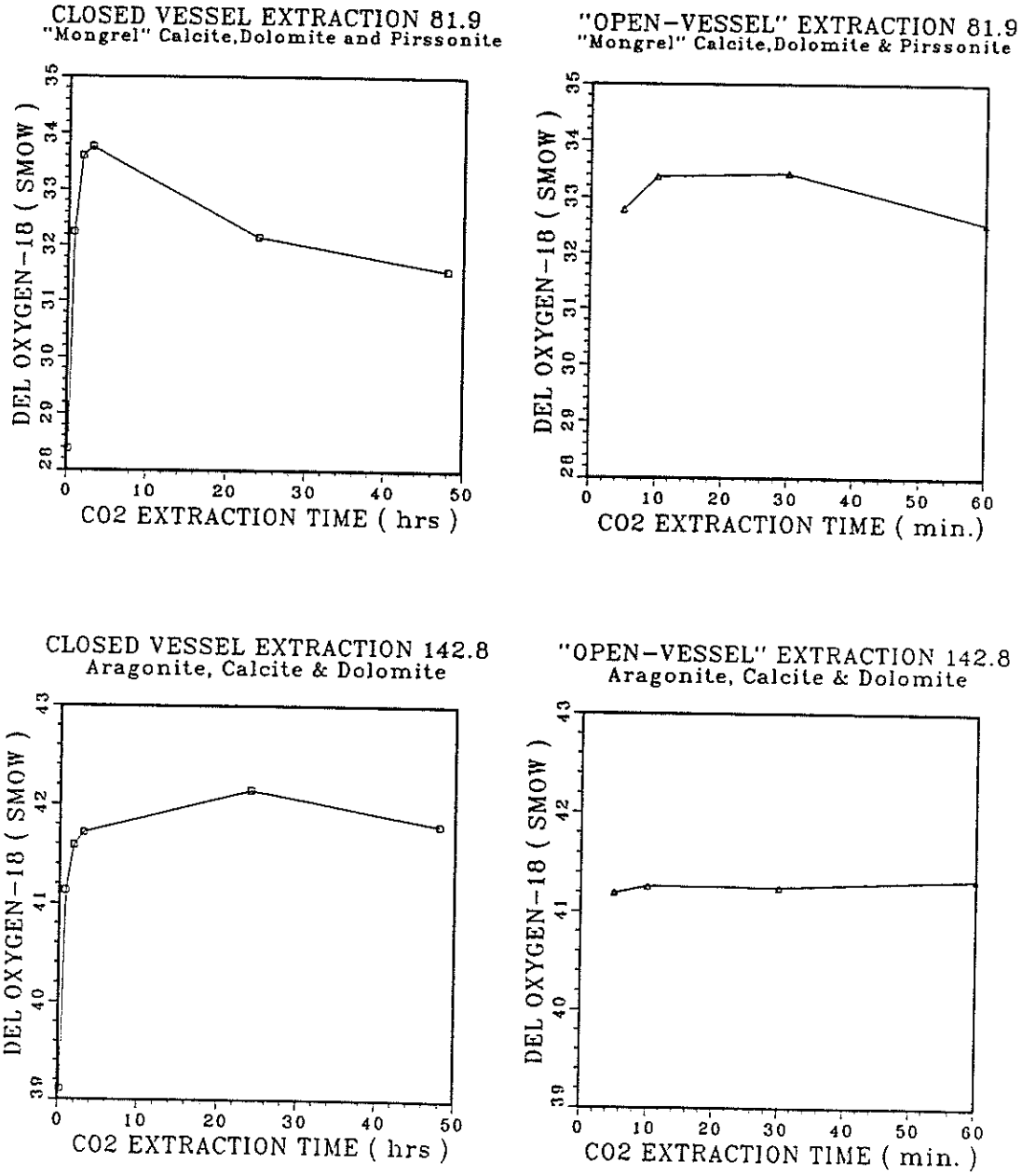

FIGURE 12. Comparison of $\delta^{18}O$ as a function of time for "closed vessel" and "open-vessel" (vacuum) extractions for samples from 81.9 and 142.8 m in KM-3

The open-vessel technique allowed over 200 samples to be analyzed quickly (with at least half of these samples analyzed more than once) relative to the closed-vessel technique.

Reproducibility

As mentioned previously, at least half the samples were run more than once. Randomly selected samples were re-run to ensure reproducibility. If a randomly re-run sample did not agree with the first analysis, (~ 1.5 per mil) the sample was run a third time. If the third sample was not in agreement with one of the first two sample analyses, the sample was considered "non-reproducible" and was not included in the isotopic chronology. Samples were also re-run if 1) there was any indication of extraction line, reaction vessel or sample bottle leaks, and 2) if the standard deviation of the mass spectrometer gas analysis was greater than 0.1 per mil.

The expected range of source of errors for typical samples were estimated statistically . Hierarchical statistics, also known as Analysis of Variance (ANOVA), were employed to separate open-vessel technique uncertainties and those uncertainties associated with the inhomogeneity of samples from mass spectrometer operator machine variability. Hierarchical statistics have been described in Li (1964). The procedure was as follows. First, three samples were selected with varying mineralogic compositions: 1) a mongrel calcite/dolomite mixture with at least intermediate amounts of both minerals (127.7); 2) a mongrel calcite/dolomite mixture with trace amounts of both minerals (690.3); and 3) a sample with calcite only and traces of northupite (375.0). Five aliquots of sediment from each sample were reacted with 100 percent phosphoric acid using the open-vessel technique, producing five CO_2 gas aliquots. Five aliquots of each gas were then run on the mass spectrometer for stable isotope content. The mass spectrometer then analyzed each gas aliquot six times during a given analysis. For each of the three samples (127.7, 375.0 690.3), 150 measurements of $\delta^{18}O$ and $\delta^{13}C$ were generated. The 150 values were entered into the ANOVA equations. The ANOVA FORTRAN program, along with input files and results are included in Appendix E.

The results are summarized in Table 3. Total standard deviations reflecting the confidence interval about the calculated mean that would occur if every sample were run according to the scheme described above (a total of 150 mass spectrometer cycles) ranges from approximately 0.15 to 0.34 per mil $\delta^{18}O$ and 0.04 to 0.08 per mil $\delta^{13}C$. The uncertainty ($\pm 1\sigma$) for one typical sample (e.g., one "open-vessel" extraction run for six cycles on the mass spectrometer) is given by (Allan Gutjahr, New Mexico Tech Mathematics Dept., pers. comm.):

TABLE 3

Quantification of sources of analytical uncertainty for $\delta^{18}O$ and $\delta^{13}C$ analyses, using hierarchial statistics

Sample and Species	Variance			Total Analytical Uncertainty	
	Between subsamples[1] σ_1^2	Between gas aliquots[2] σ_2^2	Between m.s. cycles[3] σ_3^2	For these samples[4] σ_{T_1}	For normal sample[5] σ_{T_2}
690.3 m					
$\delta^{18}O$	0.4831	0.0072	0.0067	0.3114	0.7010
$\delta^{13}C$	0.0247	0.0008	0.0033	0.0707	0.1614
375.0 m					
$\delta^{18}O$	0.1515	0.0030	0.0344	0.1751	0.4003
$\delta^{13}C$	0.0312	-0.0011	0.0162	0.0740	0.1811
127.7 m					
$\delta^{18}O$	0.1076	0.0005	0.0046	0.1469	0.3299
$\delta^{13}C$	0.0090	0.0007	0.0008	0.0428	0.0992

1. Five subsamples of unhomogenized sediment were separated from each sample vial.
2. The CO_2 gas generated from each subsample was divided into five aliquots.
3. Each gas aliquot was analyzed for six cycles on the mass spectrometer.
4. Calculated according to: $\sigma_{T_1}=((6)(5)\sigma_1^2+(6)\sigma_2^2+\sigma_3^2)/150$ for 5 subsamples.
5. Calculated according to: $\sigma_{T_2}=(\sigma_1^2+\sigma_2^2+\sigma_3^2 6)^{\frac{1}{2}}$ for one sample, one gas aliquot per sample, and six machine cycles per aliquot. σ_{T_2} is larger than σ_{T_1} because of the smaller number of repititions performed.

$$\sigma_T = (\sigma_1^2 + \sigma_2^2 + \sigma_3^2/6)^{1/2}$$

σ_T for the three samples ranges from 0.330 to 0.701 per mil for $\delta^{18}O$ and 0.099 to 0.184 per mil for $\delta^{13}C$.

Several conclusions can be drawn from the ANOVA results: 1) 70 to 85 percent of the stable isotope analyses uncertainty is due to the combined effect of sample inhomogeneity and the open-vessel extraction technique. Operator and machine reproducibility errors are relatively small (the CO_2 purification procedure contribution to the analytical standard deviation for $\delta^{18}O$ is 0.054 per mil and mass spectrometer cycle variability contribution is 0.046 per mil); 2) as was suspected, the types and relative amounts of minerals in a sample affect the ability to reproduce the isotopic measurements. Where only trace amounts of the desired carbonates are present, large errors in determining the final value will occur. Where trace amounts of interfering minerals appear, combined with small amounts of one carbonate, larger errors may also result. Therefore, the confidence intervals associated with the stable isotope analyses presented here are assumed to be greater than +0.33 per mil but less than + 0.701 per mil for $\delta^{18}O$ and greater than +0.1 but less than 0.184 per mil for $\delta^{13}C$.

Isotope Corrections for Mineralogic Composition

Although dolomite appeared in many samples, there were many core areas where it is absent. The isotopic record is still preserved in these sections in calcite but a relationship between the stable isotopic composition of calcite and dolomite needs to be established.

An additional complication in some of the Searles Lake samples is that they contain both calcite that was present when the sample was collected ("primary calcite") and calcite formed by incongruent dissolution during the laboratory leaching procedure ("mongrel calcite"). If the argument presented above is correct that the primary calcite is formed from gaylussite concurrent with sedimentation, then both primary and mongrel calcite have the same origin based on the incongruent dissolution of gaylussite but at different times, the first taking place in the natural environment and the second in the laboratory. We tested samples which contained only mongrel calcite with dolomite and only primary calcite with dolomite. The isotopic relationship of the two types of calcite to dolomite was the same (as expected from the fractionation factor). This supports a common "primary" origin for both the primary and mongrel calcite.

According to Land (1980), who presented a through discussion of this problem, no real proof of calcite-dolomite co-precipitation has ever been

presented. Further, even if co-precipitation did occur, a simple temperature-dependent isotope fraction factor between calcite and dolomite may not exist due to compositional and crystallographic variations. Published values of a α calcite-dolomite (25^{0}C) vary from +1 to +7 per mil, with Land (1980) suggesting that 3 ± 1 per mil is the most likely range. Much of this uncertainty results from the process of dolomitization of pre-existing calcite, in which case the calcite and dolomite are not coeval and an external fluid (another source of oxygen) must have been involved. This concern does not apply to the samples from Searles Lake in which calcite and dolomite are thought to be isotopically primary precipitates from the lake water. Therefore, it should be possible to determine an average α calcite-dolomite for the Searles Lake precipitates. In order to accomplish this, seventy-two stable isotope analyses were run with the normal closed vessel procedure without any sort of timed extraction. As the CO_2 partial pressure increased within the reaction vessel, phosphoralysis would slow down and most of the dolomite would remain unreacted. The isotope composition of these samples would therefore primarily reflect the earliest reacting carbonate, presumably calcite. We have compared the stable isotope content of the closed-vessel to the open-vessel results (which presumably reflect the dolomite isotopic content) to determine an average α calcite-dolomite for the Searles Lake carbonates. The closed vessel experiments were conducted at the beginning of the study before the isotope lab at New Mexico Institute of Mining and Technology (NMIMT) was operational. These samples were run at the University of Missouri-Columbia. The open vessel experiments were run at NMIMT.

Three categories of comparison were selected. First, samples run by both methods which contain only one carbonate were compared to determine if any measurable discrepancies existed between the two labs. The results are shown in Figures 13 and 14. A few points were markedly different. Because the discrepancies are random, the explanation for this probably relates more to inhomogeneity of the samples than to laboratory bias. Overall, the open vessel samples tended to be slightly (~0.8 per mil) heavier than the closed vessel analyses for ^{18}O. No constant trends were noted in the ^{13}C values.

The remaining two categories of comparison were selected to determine the efficiency of the timed-extraction technique, and were based on the relative phases of the co-existing carbonates. Category Two included samples where dolomite and calcite were in equal abundance or the abundance of the dolomite was greater than the calcite. Category Three contained samples in which the calcite was much greater than the dolomite, usually major calcite and trace dolomite. Category Two carbonates would presumably reflect the greatest range of isotopic values as the closed vessel samples would primarily reflect the isotopic values as the closed vessel samples would primarily reflect the

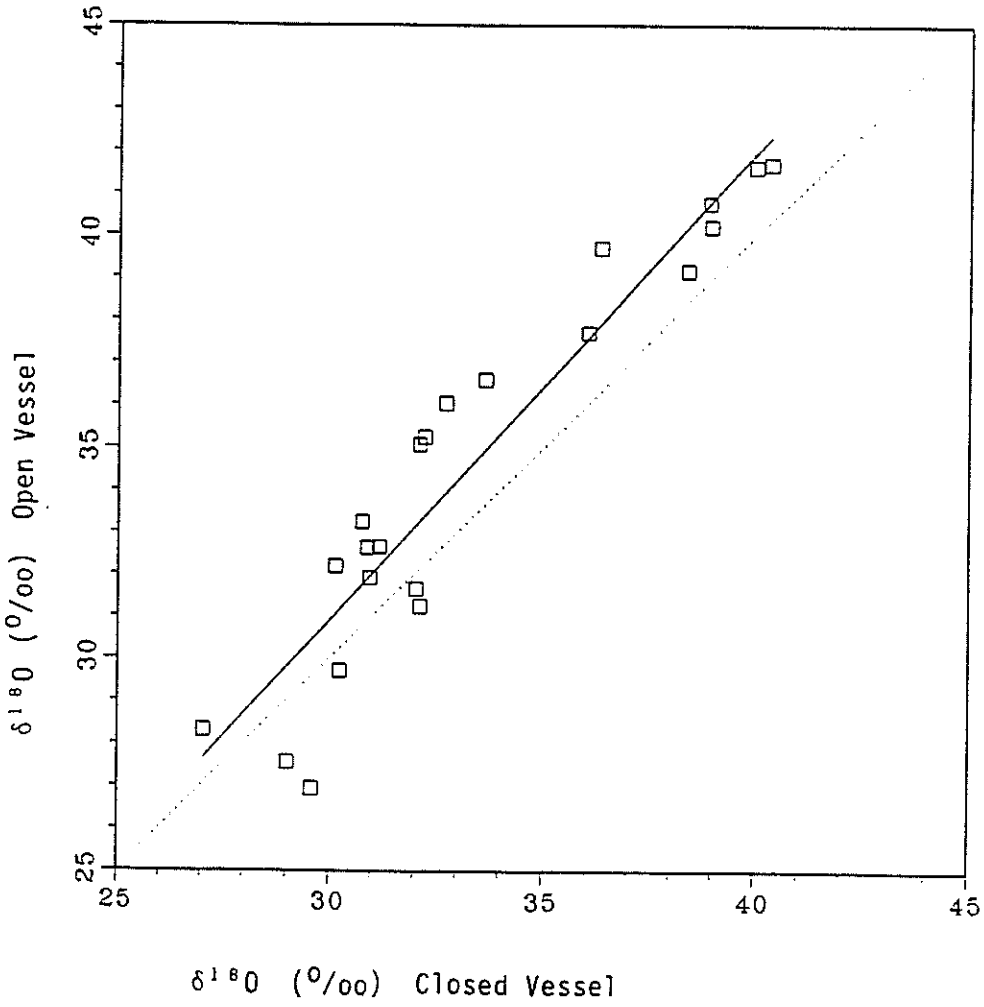

FIGURE 13. A comparison of $\delta^{18}O$ values measured at University of Missouri-Columbia by closed vessel extraction and at NMIMT by open-vessel extraction, on samples composed of a single carbonate mineral. The solid line is from regression on the data, the dotted line is one-to-one correspondence

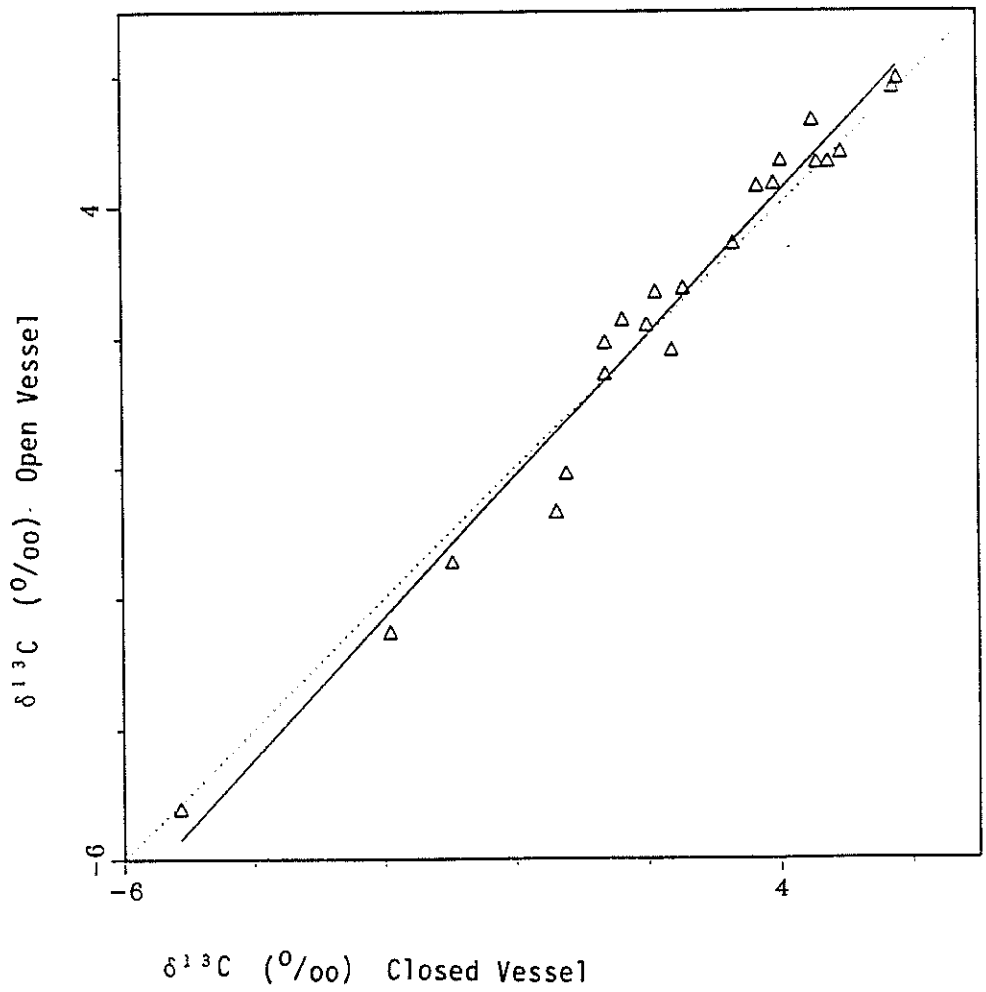

FIGURE 14. A comparison of $\delta^{13}C$ values measured at University of Missouri-Columbia by closed-vessel extraction and at NMIMT by open-vessel extraction, on samples composed of a single carbonate mineral. The solid line is from linear regression on the data, the dotted line is one-to-one correspondence

isotopic content of calcite, and the open vessel samples would best represent the isotopic composition of the co-existing dolomite. Category Three carbonates would verify the ability of the open-vessel timed extraction technique to reach the "dolomite endpoint." If large amounts of calcite were present relative to dolomite, then much of the dolomite may be consumed with the calcite, especially if the calcite's grain size was similar or larger than the dolomite. Category Two and Three comparisons are shown in figures 15 through 18 and the data are tabulated in Appendix G.

Linear regressions for each category were plotted along with a one-to-one line to help estimate differences in the samples. As predicted, the isotopic range is greater for Category Two than for Category Three. An average enrichment in the open vessel isotopic content over the closed vessel values was ~2.8 per mil ^{18}O and 0.8 per mil ^{13}C for the Category Two carbonates. The average change of isotopic composition for Category Three carbonates was ~1.0 per mil ^{18}O; the change for ^{13}C was quite variable and no definite trend observed.

Based on these comparisons, "average correction factors" for Searles Lake samples were assigned. The corrections assigned were based on mineralogy; those samples that contain "calcite only" were assigned a correction factor of +2.8 per mil ^{18}O and + 0.8 per mil ^{13}C. Samples with major phase calcite and trace phase dolomite were assigned a correction factor of +1.0 per mil ^{18}O; no ^{13}C correction factor was assigned. Given the large range of $\delta^{18}O$ and $\delta^{13}C$ values measured in the Searles sediments (approximately 25 per mil and 14 per mil, respectively), these corrections are not major. The correction factors assigned, the final ^{18}O and ^{13}C values used in the stable isotopic chronology, and the ages assigned to each sample are listed in Appendix F.

ANALYTICAL MODEL

Introduction

To help interpret stable isotope data from Searles Lake, and to validate our numerical model (described below), we have derived analytical solutions for the isotope evolution in Searles Lake. The governing equations have been developed following the approach originally presented by Gonfiantini (1965).

The lumped-parameter model presented here calculates the isotopic content and volume of Searles Lake assuming: 1) Searles Lake is either a closed basin or overflowing, 2) all climatological parameters are constant--only the inflow rate of the lake varies; and 3) the changes in inflow are instantaneous.

Terminal Lake Without Overflow

The mass balance of water in the lake is:

$$\frac{-dV}{dt} = Q_C + Q_I - Q_E \quad Q_G \qquad (1)$$

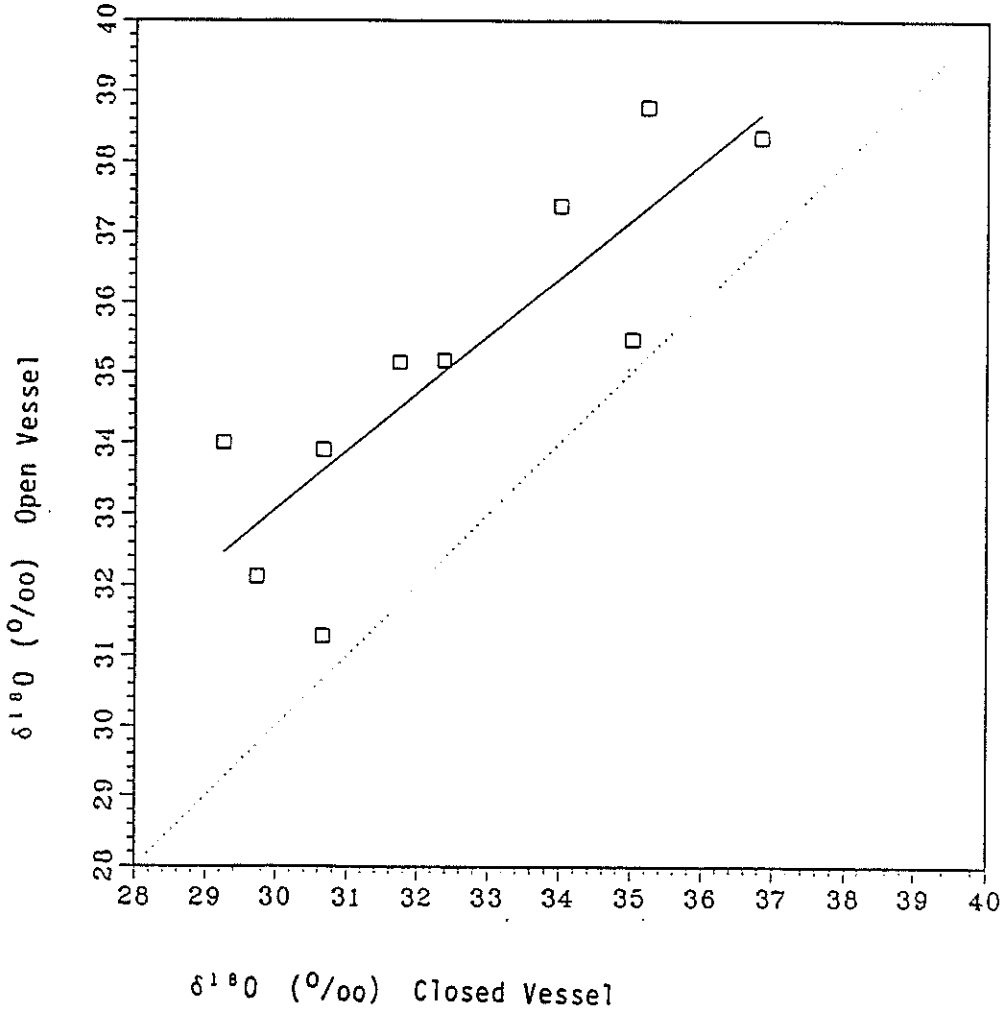

FIGURE 15. A comparison of $\delta^{18}O$ from closed-vessel extraction (yielding CO_2 predominantly from calcite) and open-vessel extraction (yielding CO_2 predominantly from dolomite) on samples with dolomite abundance equal to or larger than calcite abundance (Category Two). The solid line is from linear regression on the data, the dotted line is one-to-one correspondence

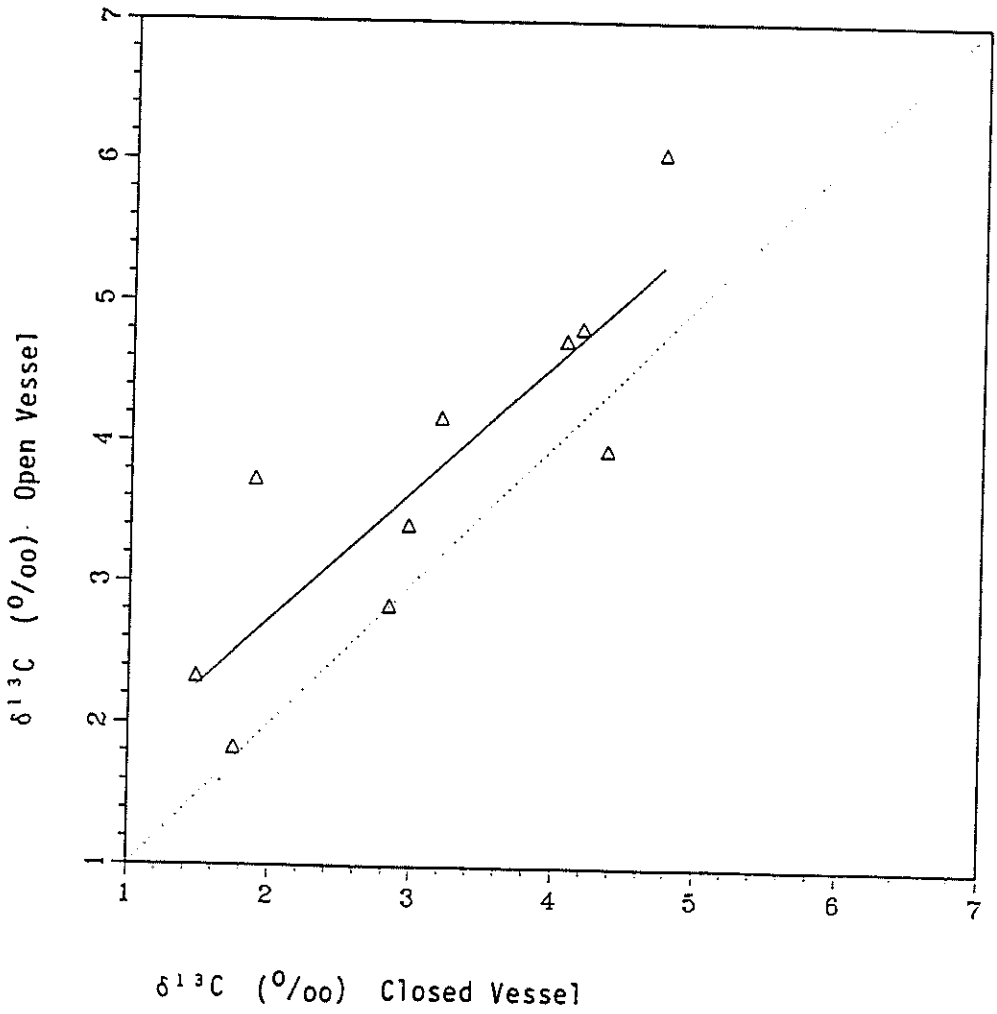

FIGURE 16. A comparison of $\delta^{13}C$ from closed-vessel extraction (yielding CO_2 predominantly from calcite) and open-vessel extraction (yielding CO_2 predominantly from dolomite) on samples with dolomite abundance equal to or larger than calcite abundance (Category Two). The solid line is from linear regression on the data, the dotted line is one-to-one correspondence

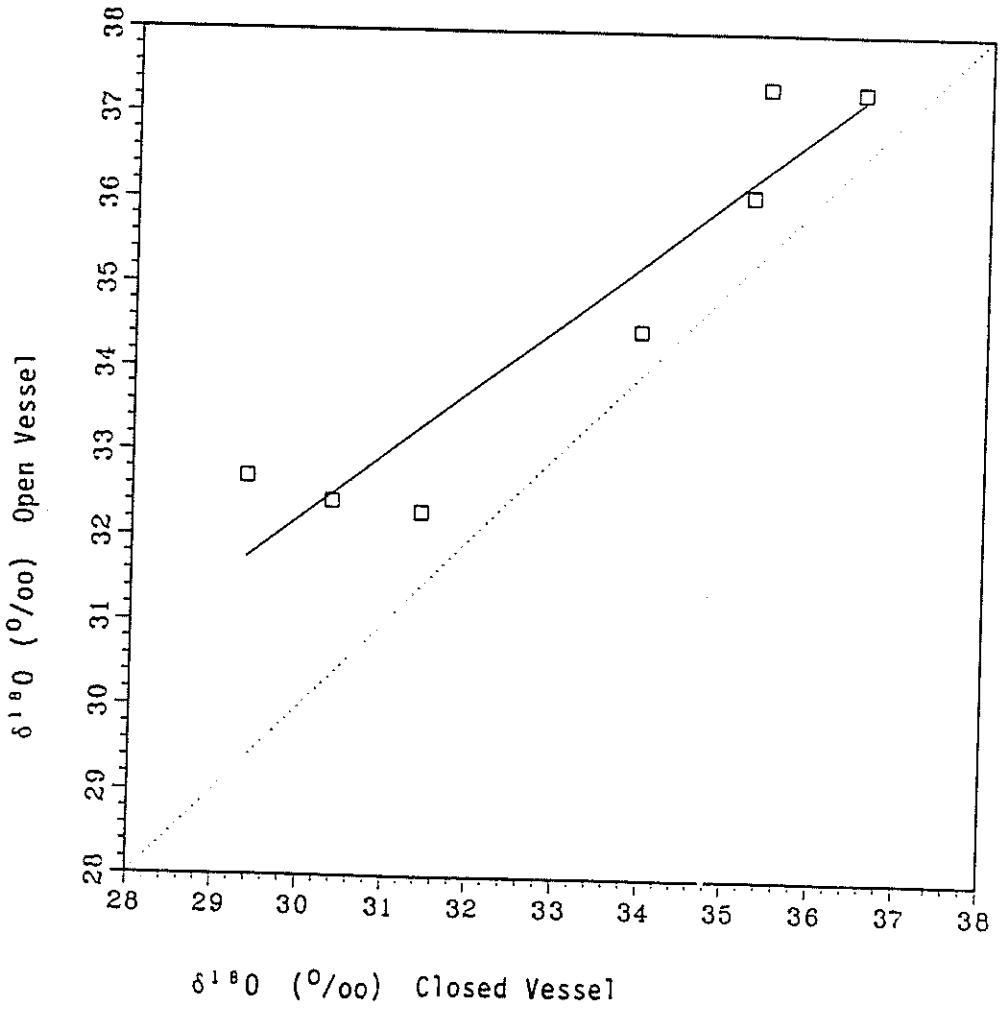

FIGURE 17. A comparison of $\delta^{18}O$ from closed-vessel extraction (yielding CO_2 predominantly from calcite) and open-vessel extraction (yielding CO_2 predominantly from dolomite) on samples with dolomite abundance much less than calcite abundance (Category Three). The solid line is from linear regression on the data, the dotted line is one-to-one correspondence

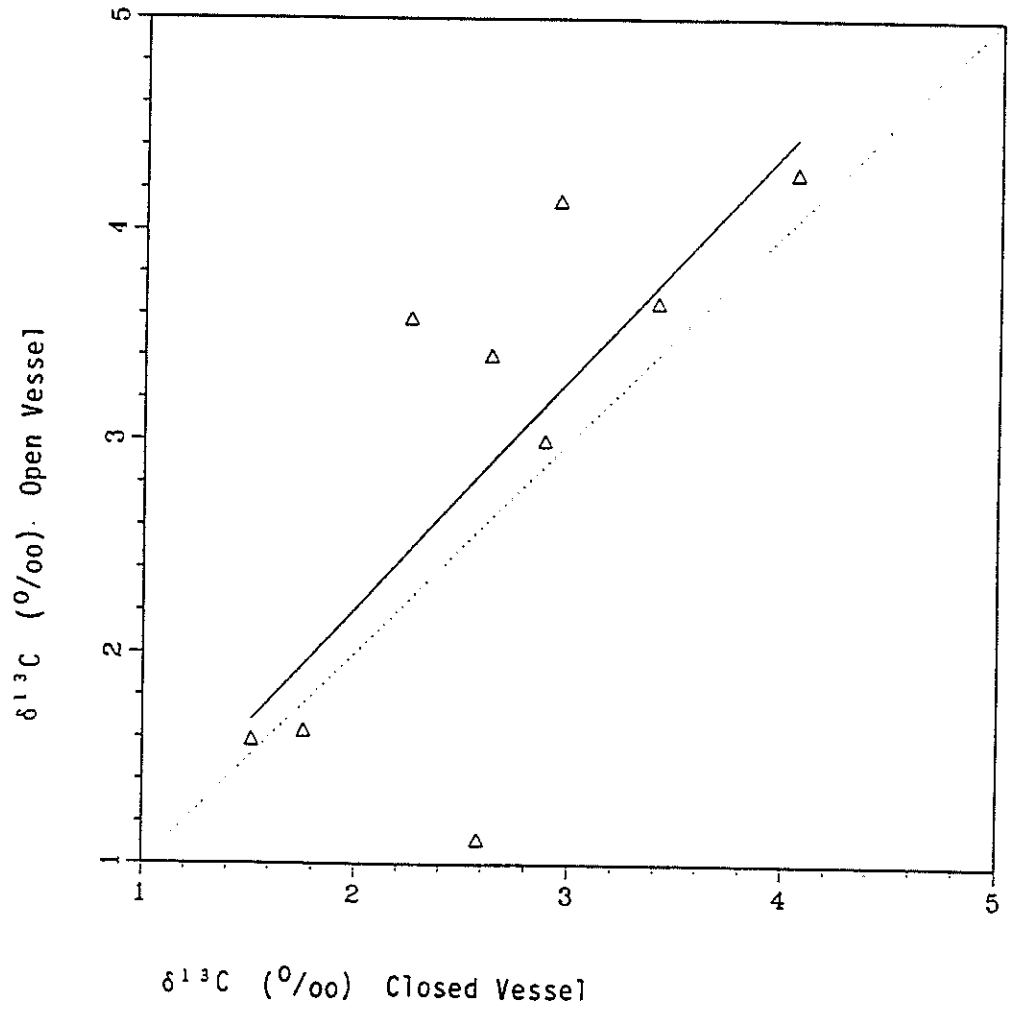

FIGURE 18. A comparison of $\delta^{13}C$ from closed-vessel extraction (yielding CO_2 predominantly from calcite) and open-vessel extraction (yielding CO_2 predominantly from dolomite) on samples with dolomite abundance much less than calcite abundance (Category Three). The solid line is from linear regression on the data, the dotted line is one-to-one correspondence

Where:

V=lake volume [L^3]

t=time [T]

Q_C=back condensation flux [L^3/T]

Q_I=inflow [L^3/T]

Q_E=evaporation flux [L^3/T]

Q_G=groundwater flux [L^3/T]

At Searles Lake, groundwater outflow/inflow is assumed to be negligible, therefore, Q_G=0. This is assumed because the Searles basin is arid and inflow was dominated by runoff from the Sierra Nevada.

Substituting:

(1) Q_E= EA

(2) A = kV

(3) K = kE

(4) therefore Q_E = KV

Where:

E = net evaporation rate [L/T]

A = surface area of the lake [L^2]

k = routing constant=surface area/volume [1/L]

E = evaporation rate per unit volume of lake water [1/T]

Q_C= hQ_E = hKV

Where:

h = relative humidity

Making substitution, and integrating equation (1)

Initial conditions:

$V(t=o) = V^0$

Yields:

$$V = \left\{V^0 - \frac{Q_I}{(1-h)k}\right\} \exp\left(-(1-h)Kt\right) + \frac{Q_I}{(1-h)k} \qquad (2)$$

The isotopic mass balance of the lake is

$$\frac{d(V\delta_L)}{dt} = Q_I\delta_I - Q_E\delta_E + Q_C\delta_C \qquad (3)$$

Where δ_L = isotopic content of the lake

δ_I = isotopic content of the inflow

δ_E = isotopic content of the evaporated water

δ_C = isotopic content of the back-condensation onto the water surface

Substituting:

$$\delta_E = \frac{\delta_L - \epsilon_v^*}{\epsilon_v^* + 1} \qquad \epsilon_v^* = \epsilon_v + \epsilon_k$$

Where:

ϵ_v = equilibrium isotopic enrichment factor for the liquid/vapor phase change

ϵ_k = kinetic enrichment factor (due to diffusion)

Solving equation (3) with initial condition:

$\delta_L(t=0) = \delta_L^0$ yields:

$$\delta_L = \frac{1}{V}\left(\frac{Q_I(\epsilon_v^* + 1)}{K}\left(\delta_I - P\right) + \left[V^0(\delta_L^0 - P) - \frac{Q_I(\epsilon_v^* + 1)}{K}\left(\delta_I - P\right)\right]\exp\left[\frac{-Kt}{\epsilon_v^* + 1}\right]\right) + P \qquad (4)$$

Where:
$$P = \frac{\epsilon_v^* + \delta_C h(\epsilon_v^* + 1)}{1 - (\epsilon_v^* + 1)(1-h)}$$

Overflow

$$\frac{V_0(d\delta_L)}{dt} = Q_I\delta_I - Q_E\delta_E + Q_C\delta_C - Q_O\delta_O \qquad (5)$$

Where:

V_O= overflow volume of the lake [L^3]

Q_O= outflow (spill) flux [L^3/T]

δ_O= isotopic composition of the outflow (spill) flux

In a well-mixed lake, $\delta_O = \delta_L$.

Integrating (5) and solving for δ_L at $\delta_L(t=0) = \delta^0_L$

$$\delta_L = \frac{B}{C} + [\delta^0_L - \frac{B}{C} \exp(-Ct)] \qquad (6)$$

Where:

$$B = \frac{Q_I \delta_I}{V_O} + K\left(\frac{e^*_v}{e^*_v + 1} + h\delta_c\right)$$

$$C = \frac{K}{e^*_v + 1} + \frac{Q_O}{V_O}$$

Desiccation

Desiccation refers here to drying of the lake caused by a cutoff of inflow. The mass balance of the lake is expressed by:

$$\frac{dV}{dt} = Q_C - Q_E \qquad (7)$$

Substituting as before and integrating equation (7) with $V(t=0)=V^0$ yields

$$V = V^0 \exp(-(1-h)Kt)$$

The isotopic mass balance is:

$$\frac{d(V\delta_L)}{dt} = Q_C\delta_C - Q_E\delta_C$$

substituting as before and integrating with $\delta_L(t=0) = \delta_L^0$

$$\delta_L = \frac{\delta_L^0 V^0}{V} \exp\left(\frac{-kt}{e_v^* + 1}\right) \qquad (8)$$

Searles Lake-Conceptual Model

Extreme conditions are modeled using the analytical solutions: 1) assuming meteorological parameters of today and 2) assuming estimated meteorological parameters during the last Wisconsin pluvial episode ~13.6 ka.

Modern meteorological parameters were obtained from Smith (1979), Smith and Street-Perrott (1983), Ruffner (1985), NOAA (1982), and Meyers (1962). Meteorological parameters for the Wisconsin glacial maximum were estimated using the deep-sea core V19-30 (Shackleton et al. 1983) using the oxygen-18 chronology as a proxy record of temperature. Linear regressions as a function of elevation were calculated for temperature, gross evaporation, relative humidity, and precipitation data from regional weather stations, assuming a linear change in the parameters with elevation. The calculations and regression results can be found in Appendix I. Once the meteorological parameters were calculated as functions of elevation, each parameter was inserted into the elevation versus temperature regression equation to obtain that parameter as a function of temperature.

Temperatures at 13.6 ka were assumed to be 7^0C cooler than present temperatures. Using the deep sea ^{18}O record, an interpolation scheme was created to calculate temperatures at each ^{18}O data point to create a record of temperature as a function of age. Using the new temperature proxy record, and the equations giving the meteorological parameters as a function of temperature, the meteorological parameters at 13.6 ka were calculated. A more detailed justification of this approach to specification of parameters is given below in the section "Model Parameterization" under "Numerical Modeling."

The volume and area of Searles Lake as a function of depth are found in Smith (1979) and shown graphically in figures 19 and 20. Figure 20 illustrates that the area/volume ratio is relatively constant for all but the shallowest water levels. Therefore, the k (area/volume) parameter was assumed to be constant, using the maximum (overflow) volume and area calculated by Smith (1979).

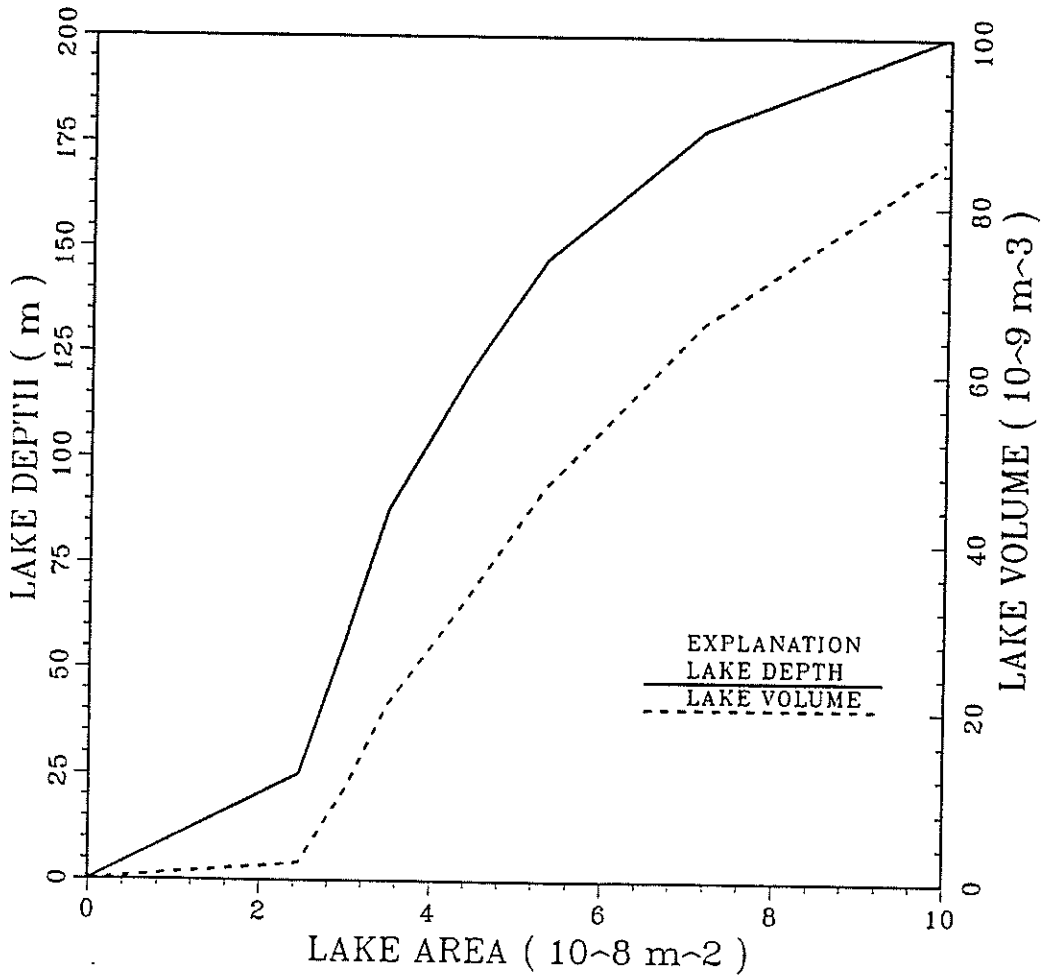

FIGURE 19. Searles Lake area as a function of lake depth and lake volume

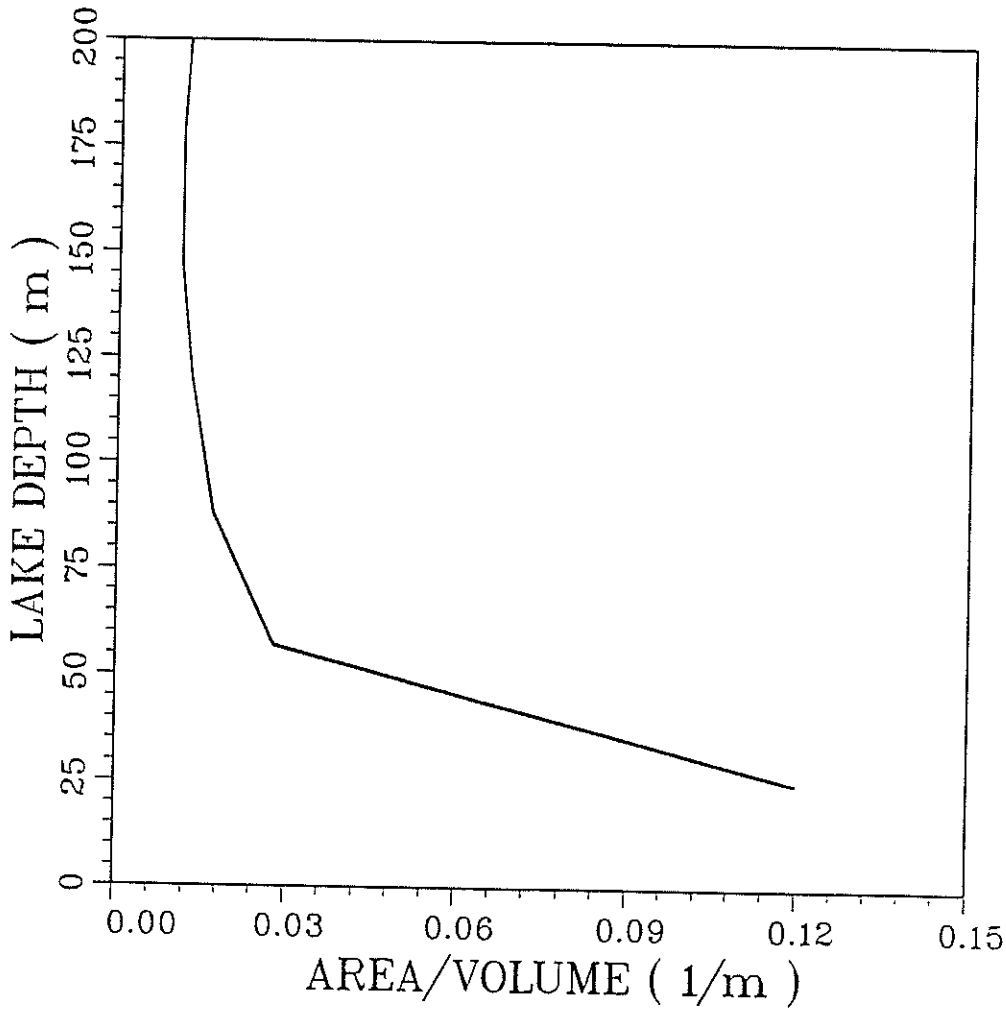

FIGURE 20. Searles Lake area/volume ratio as a function of lake depth

The initial rate of inflow to Owens Lake was calculated using a simple mass balance equation such that enough water was flowing in the Owens River to produce an overflow from Panamint Lake into Death Valley, simulating an extreme event. The isotopic values for the inflow composition were obtained from Smith et al. (1987). The isotopic composition of the back condensation flux was obtained from the atmospheric composition of deuterium in Death Valley (Ehhalt 1974). The isotopic fractionation factors for liquid water/vapor were found in Bottinga and Craig (1968), for the kinetic enrichment factor in Mevlivat and Jouzel (1979), and for dolomite/water in Northrup and Clayton (1966).

Calculations

Four simulations were run. These were run to evaluate the typical isotopic response of the lake system and are not intended to simulate any particular events. Simulation of the actual lake history was performed using a numerical model, described in another chapter below. Two simulations were run for modern parameters assuming: 1) the isotopic content of the back condensation flux was in equilibrium with the isotopic content of the inflow water; and 2) the isotopic content of the two fluxes were not in equilibrium, rather, the back condensation flux was substantially lighter than inflow waters (e.g., Phillips et al. 1986a). The simulations using the 13.6 ka parameters were run similarly.

The inflow from Owens River was modeled flowing through both Owens Lake and China Lake using meteorological and bathymetric parameters specific to those lakes, and were calculated as were those of Searles.

The simulations encompassed inflow, overflow, decreasing inflow and desiccation events. The results are listed in Appendix H, and are shown graphically in figure 21 and 22.

Discussion

The range of ^{18}O content predicted by the analytical solution is 20 to 70 per mil SMOW until desiccation, at which point extreme enrichment occurs. For the modern parameters, a steady-state value of ~+38 is observed, and ~+35 for 13.6 ka parameters. Overflow values range from +32 for modern parameters to ~+23 for 13.6 ka simulations. Overflow events may be interpreted from Searles Lake isotope record by the extremely light values predicted in these simulations.

The simulations calculate extreme events, so extreme, in fact, that the range of values actually occurring would certainly be much less. The chemical activity of water in these simulations was assumed to be unity, except in the calculations where the activity was assumed to be at halite

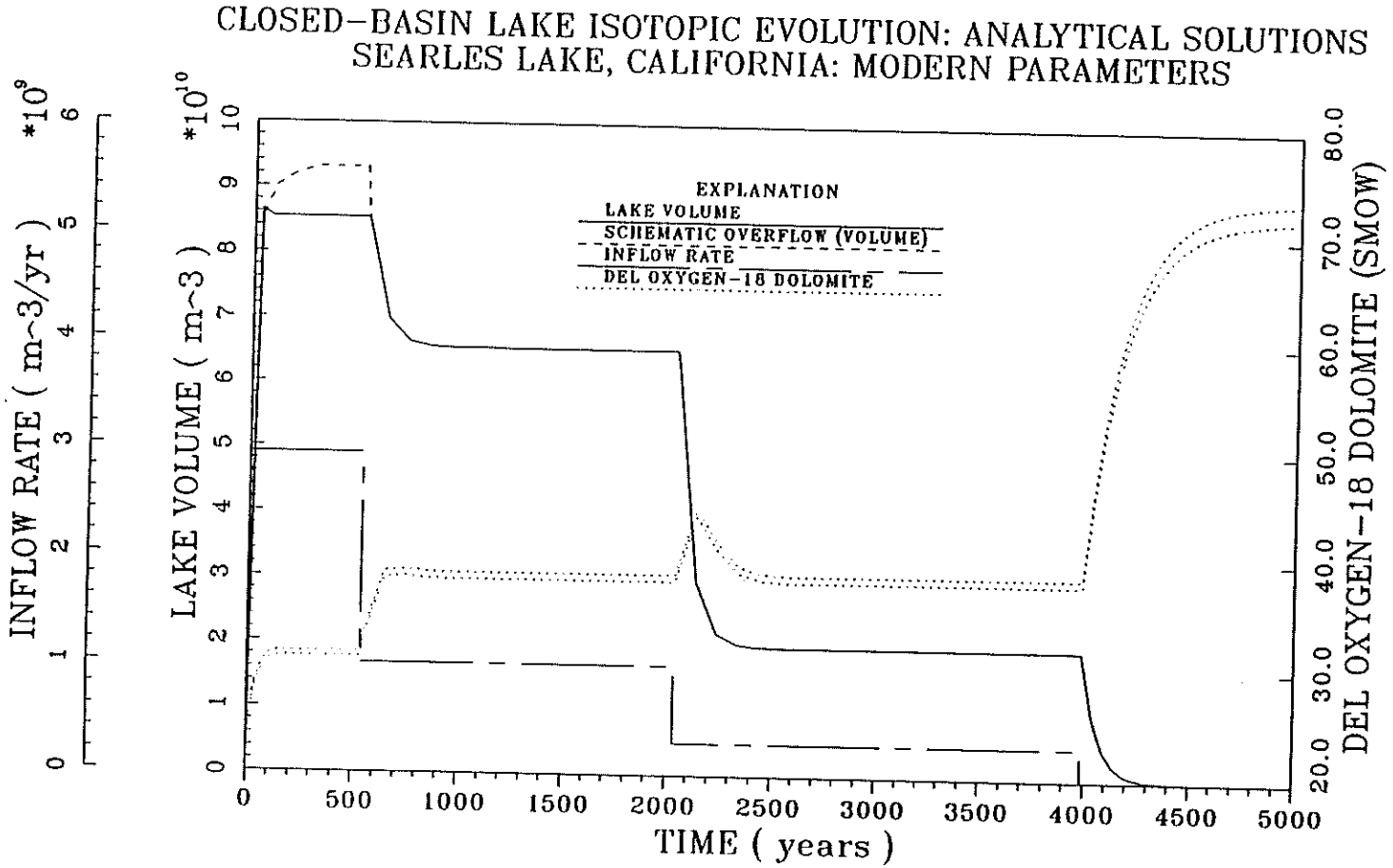

FIGURE 21. Analytical modeling of Searles Lake volume and $\delta^{18}O$ for a hypothetical inflow history, under modern climatic conditions. Atmospheric water vapor is assumed to be lighter in ^{18}O than equilibrium with lake inflow

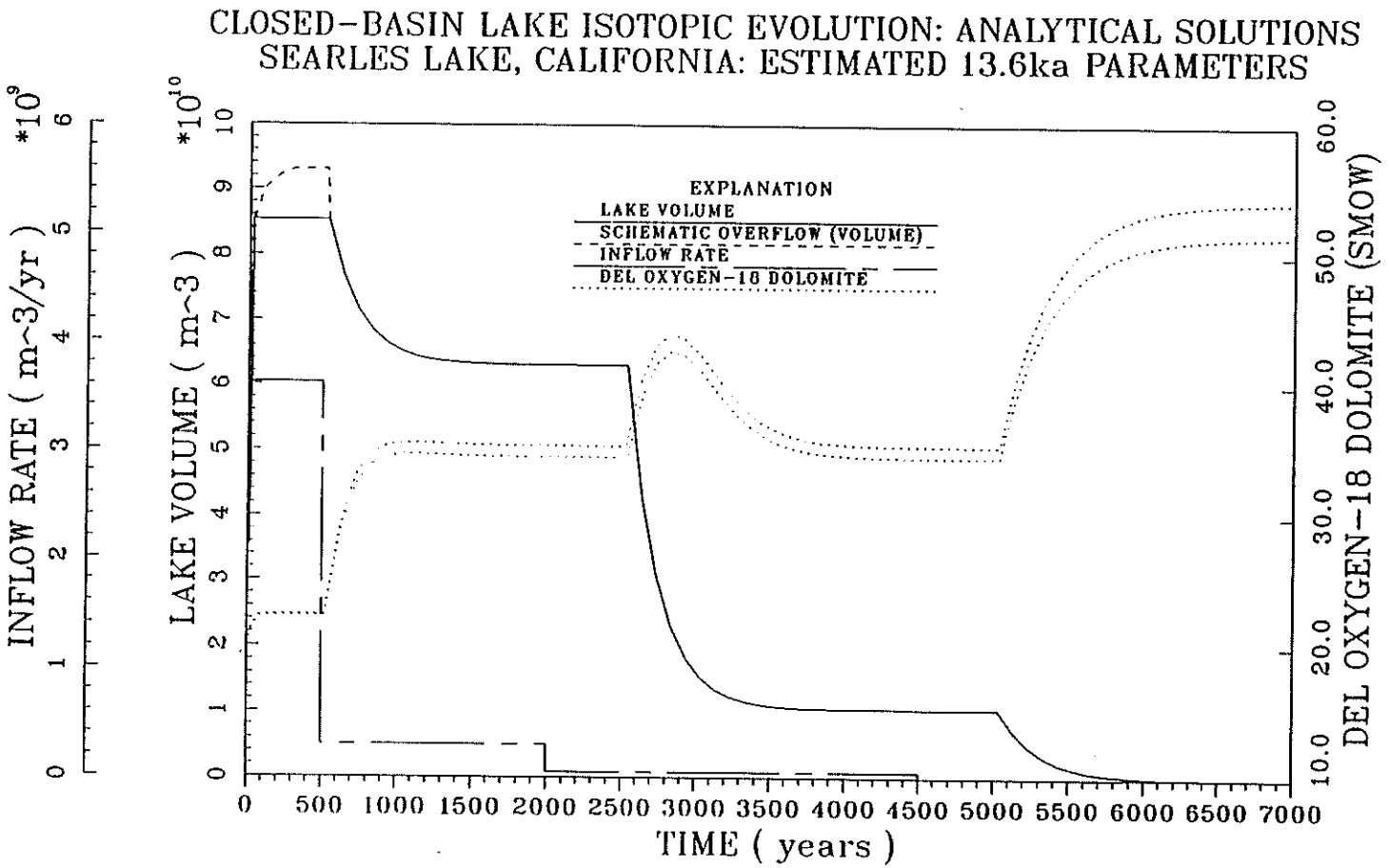

FIGURE 22. Analytical modeling of Searles Lake volume and $\delta^{18}O$ for a hypothetical inflow history, under reconstructed 13.6 ka climatic conditions. Atmospheric water vapor is assumed to be lighter in ^{18}O than equilibrium with lake inflow

saturation (H_2O activity ~0.75). Enrichment during non-desiccation episodes would possibly have been slightly less had lower values of water activity been used.

ISOTOPIC RESULTS

The corrected $\delta^{18}O$ and $\delta^{13}C$ values of 312 Searles Lake core KM-3 and LDW-6 samples can be found in Appendix F. Of the 312 samples analyzed for stable isotope content, only 291 were used in the Searles Lake chronology. The remaining 21 samples were eliminated due to unsuitable mineralogy or non-reproducibility.

The stable isotope content of Searles Lake samples used to construct a stable isotope chronology is shown graphically in Figure 23. Both $\delta^{18}O$ and $\delta^{13}C$ are plotted versus age, and superimposed on the lithology provided in Smith et al. (1983). Figures 24 through 29 subdivide the chronology

The $\delta^{18}O$ value of KM-3 samples ranges from 23.0 to 43.0 per mil SMOW. $\delta^{13}C$ value ranged from -9.3 to +7.2 per mil PDB. The range of $\delta^{18}O$ values are within the range predicted by the analytical model described above. The stable isotope contents of Searles sediments are similar, though perhaps somewhat heavier than those values reported at Deep Springs Lake (Clayton et al. 1968) of ~33.0 per mil SMOW $\delta^{18}O$ and ~4.0 per mil PDB $\delta^{13}C$, and the Coorong area in Australia (DeDecker and Last 1988) of 37-38 per mil SMOW $\delta^{18}O$ and 0-3.5 per mil PDB $\delta^{13}C$.

No overall trend in isotopic composition through time is observed, although the carbon-13 content of unit G samples are markedly lighter than those higher in the core. Statistically, the mean isotope content of KM-3 samples is ~35.1 per mil $\delta^{18}O \pm 3.8$ (1σ) and ~3.8 per mil $\delta^{13}C \pm 2.2$ (1σ). The maximum range of uncertainty for individual samples suggested by the ANOVA results was $\pm$ 0.705 per mil $\delta^{18}O$ (1σ) and $\pm$ 0.215 per mil $\delta^{13}C$ (1σ). Therefore the uncertainty associated with the $\delta^{18}O$ and $\delta^{13}C$ values of individual samples reported in this paper is 19% and 9.6%, respectively, of the standard deviation of all the stable isotope values reported for core KM-3, and 3.5 percent and 1.3 percent, respectively, of the complete range of values. The isotopic data are quantitatively interpreted in a following chapter on numerical modeling.

SAN AGUSTIN STUDIES

GEOLOGIC AND HYDROLOGIC ENVIRONMENT

Site Characteristics

The Plains of San Agustin are located in Catron and Socorro counties, west central New Mexico (33°45'- 34°15'N; 107°25'-108°20'W) (Fig. 30). The region is a high altitude, topographically closed basin which held a large,

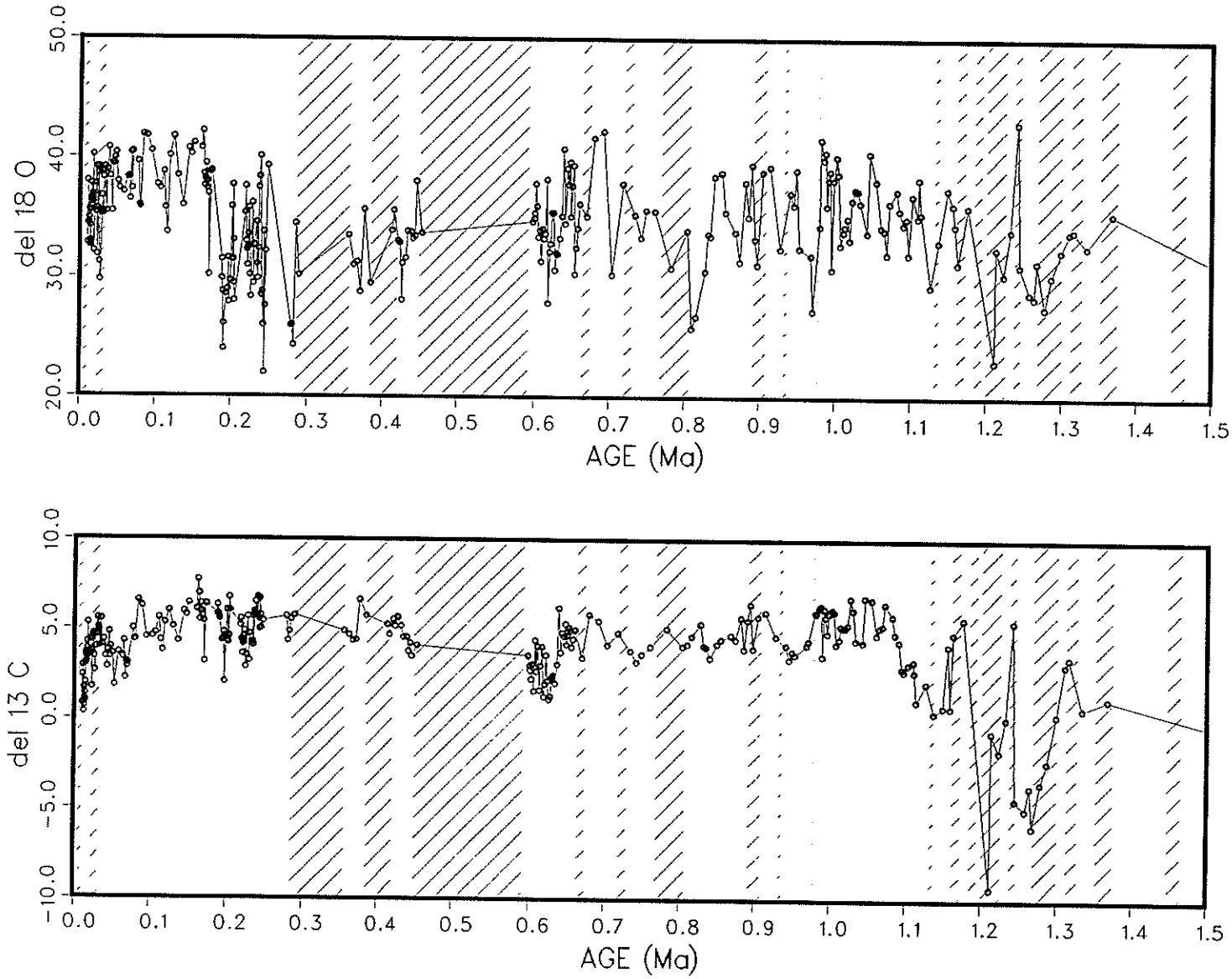

FIGURE 23. Compilation of $\delta^{18}O$ and $\delta^{13}C$ data for Searles Lake carbonates (non-dolomite samples corrected to dolomite isotopic fractionation) as a function of time, for the past 1.5 Myr. Wide cross-hatching indicates poor core recovery in KM-3, narrow cross-hatching indicates "salt" intervals, no pattern indicates "mud" intervals

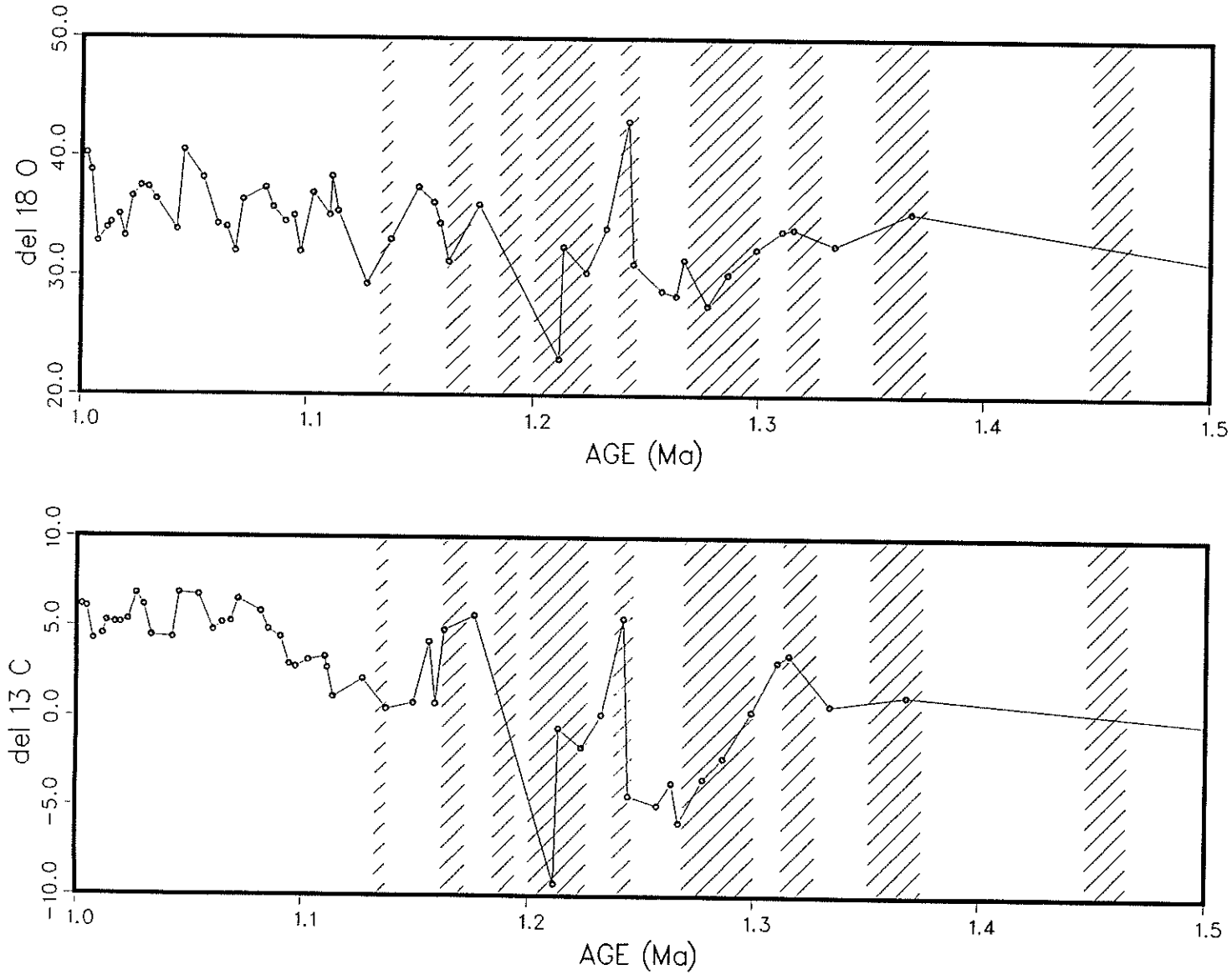

FIGURE 24. $\delta^{18}O$ and $\delta^{13}C$ data for Searles Lake carbonates as a function of time, for the interval 1.00 Ma to 1.50 Ma. Symbols as in Figure 23

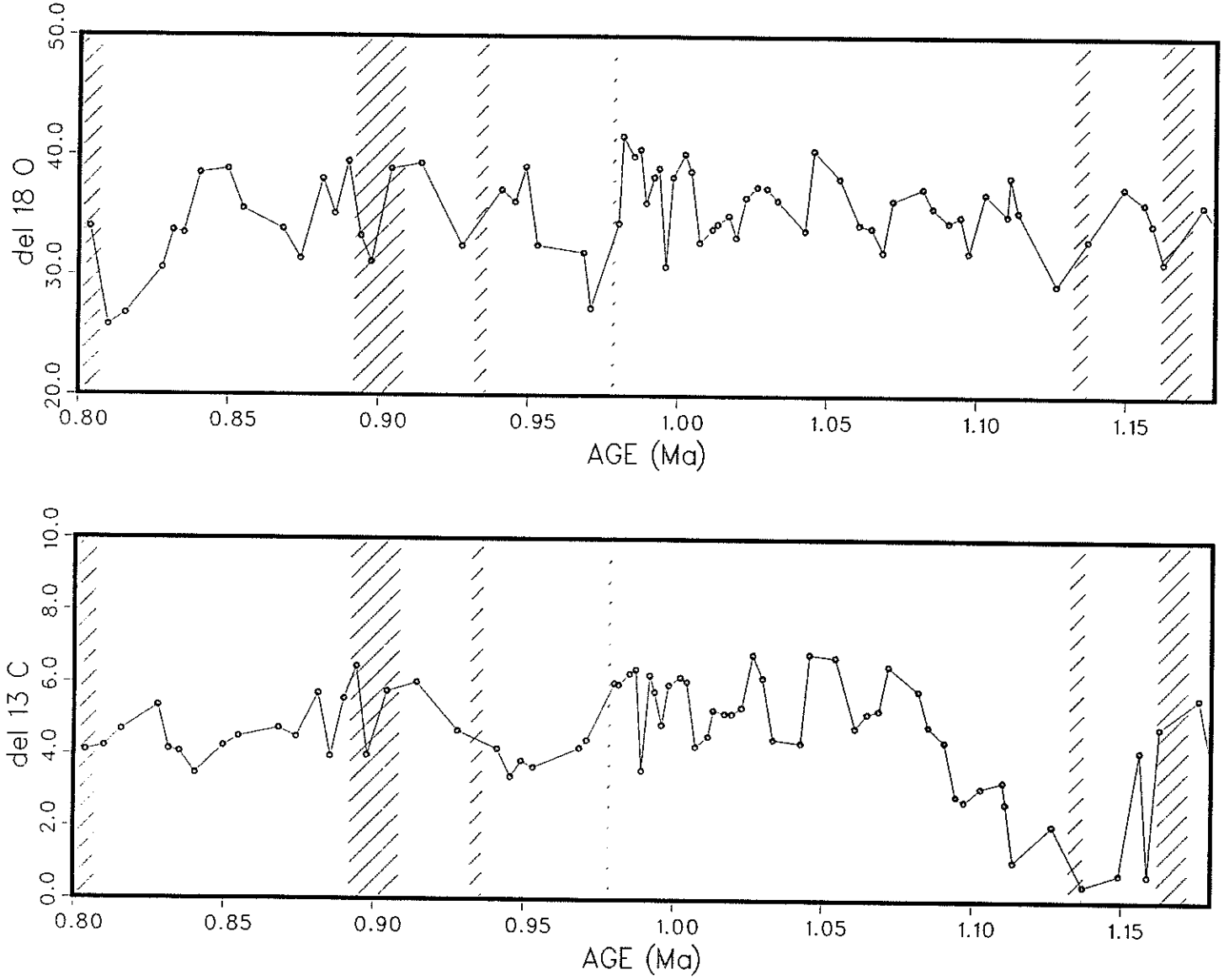

FIGURE 25. $\delta^{18}O$ and $\delta^{13}C$ data for Searles Lake carbonates as a function of time, for the interval 800 ka to 1.18 Ma. Symbols as in Figure 23

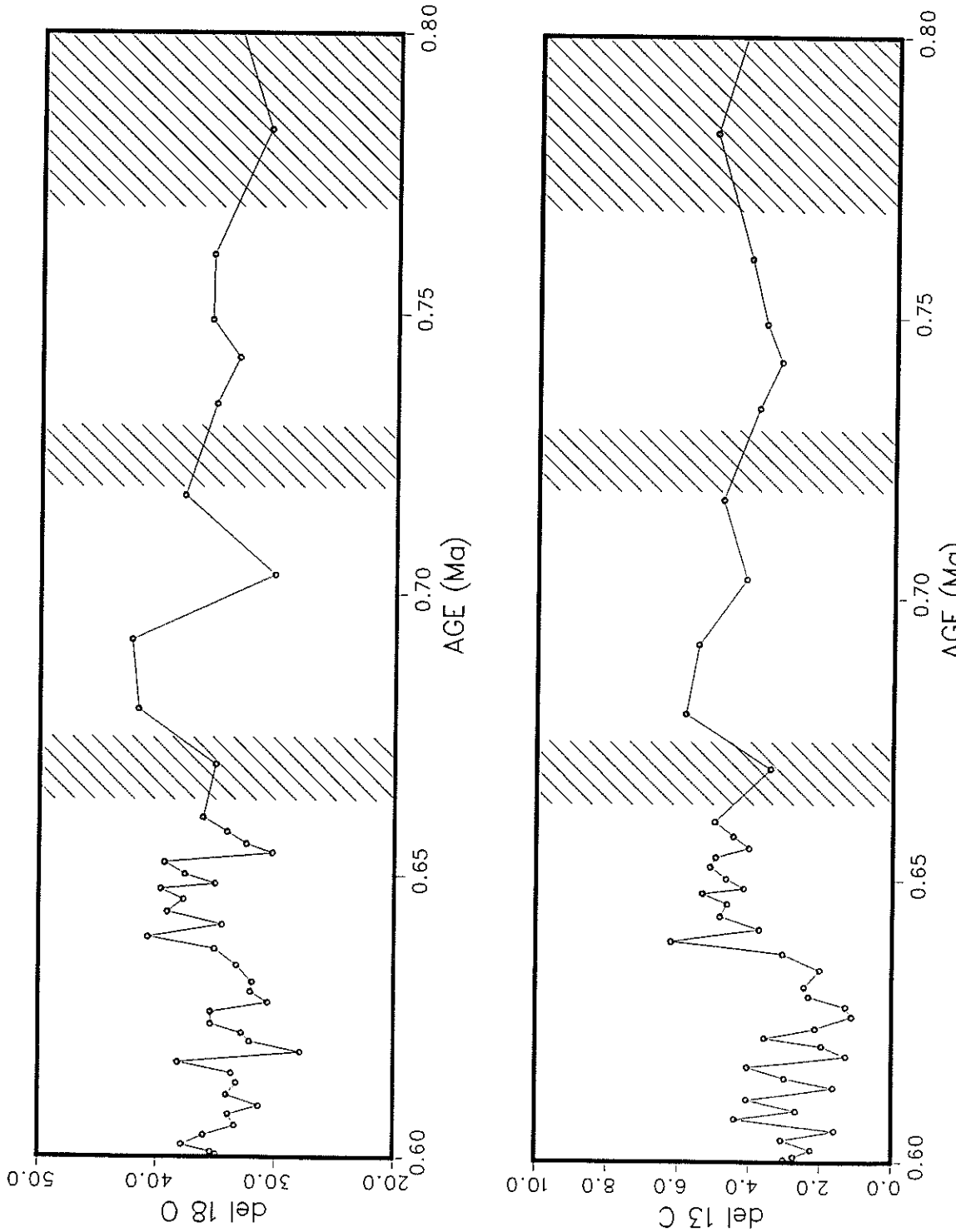

FIGURE 26. $\delta^{18}O$ and $\delta^{13}C$ data for Searles Lake carbonates as a function of time, for the interval 600 ka to 800 ka. Symbol as in Figure 23

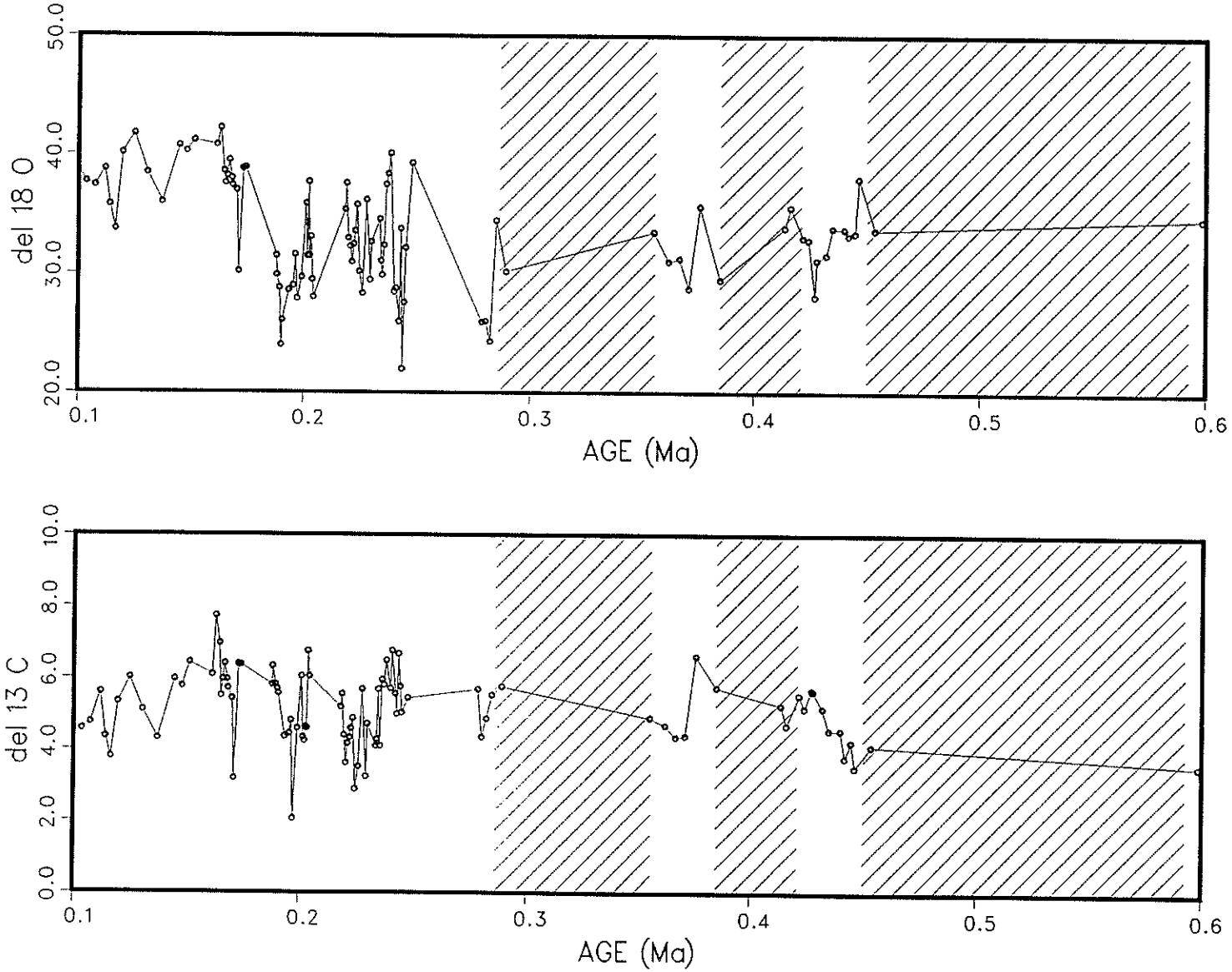

FIGURE 27. **$\delta^{18}O$ and $\delta^{13}C$ data for Searles Lake carbonates as a function of time, for the interval 100 ka to 600 ka. Symbols as in Figure 23**

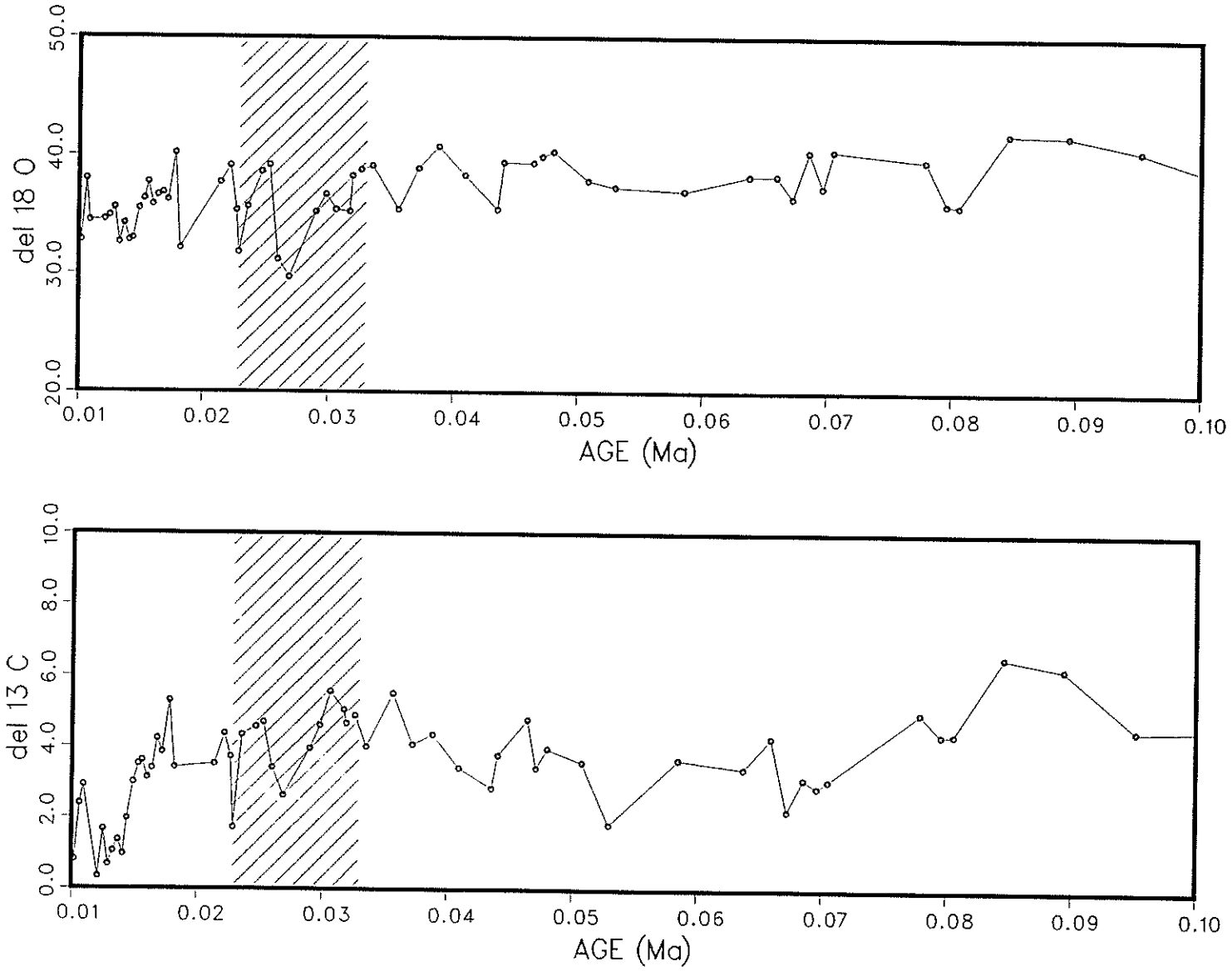

FIGURE 28. $\delta^{18}O$ and $\delta^{13}C$ data for Searles Lake carbonates as a function of time, for the interval 10 ka to 100 ka. Symbols as in Figure 23

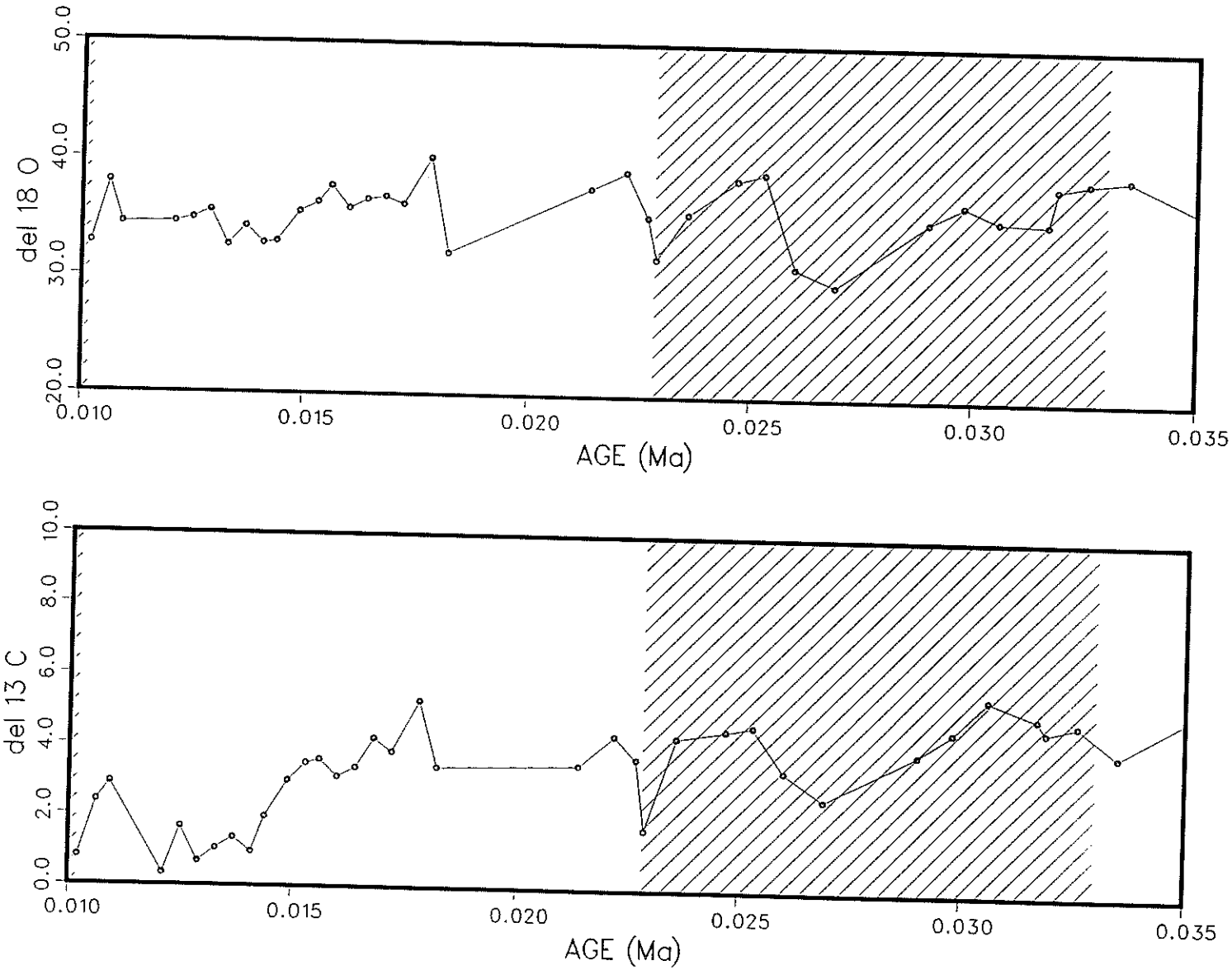

FIGURE 29. $\delta^{18}O$ and $\delta^{13}C$ data for Searles Lake carbonates as a function of time, for the interval 10 ka to 35 ka. Symbols as in Figure 23

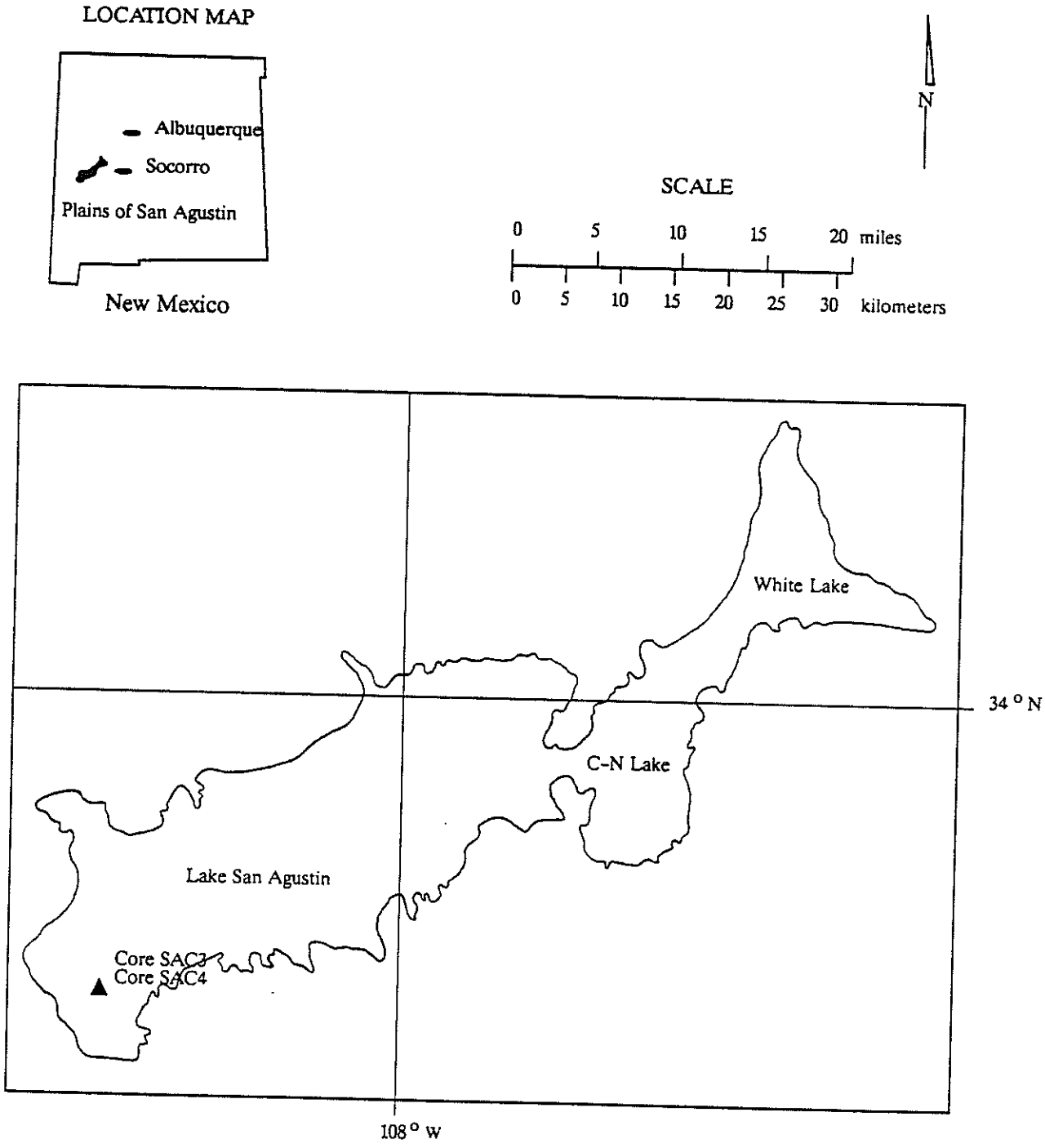

FIGURE 30. Location and configuration of Lake San Agustin at the 2,135-meter level (after Weber 1980), and location of sediment cores

perennial lake during much of the Holocene and Pleistocene. The San Agustin catchment area, which covers approximately 5,180 square kilometers (2,000 square miles), is bounded on the south and west by the Continental Divide. The boundary to the south is formed by the Luera Mountains, Pelona Mountain and O-Bar-O Mountain; to the northeast by the Gallinas Mountains; to the northwest by the Datil Mountains and Mangas Mountains; to the west by the Tularosa Mountains; and on the east by the San Mateo Mountains. Elevations range from 2,065 meters (6,775 feet) on the southwest portion of the basin floor to 3,083 meters (10,115 feet) on Mt. Withington in the San Mateo Mountains.

Today the region's climate is semiarid. Annual precipitation ranges from 250-380 millimeters (10-15 inches) in lower elevations to 760 millimeters (30 inches) in the highlands. Modern vegetation (Potter 1957) consists of saltbrush and greasewood grasslands on the lower elevation flats, pinon-juniper and ponderosa pine forests on the lower mountain slopes, and douglas fir forest at higher elevations.

Geologic Environment

Structure. The Plains of San Agustin lie within the Datil-Mogollon volcanic plateau on the boundary between the Basin and Range and Colorado Plateau physiographic provinces. The basin is a graben structure associated with the latest Miocene and/or Pliocene phase of spreading along the Rio Grande rift (Chapin and Seager 1975), and is bound by faults along the northwest, southeast and southwest margins (Stearns 1962). Minimum structural relief along these margin-bounding faults is at least 4,000 feet. However, the surface expression of this offset has been reduced more than half by Quaternary sedimentation. There is no geologic evidence of tectonic deformation in the basin during post-Wisconsin.

Lithology. Lithology in the highlands surrounding the basin consists predominantly of mid-Tertiary (Oligocene-Miocene) volcanics interbedded with sedimentary and volcaniclastic units (Stearns 1962; Weber 1980). Pliocene-Pleistocene littoral and lacustrine deposits of extinct Lake San Agustin fill the basin to significant depths. Late Pleistocene to Holocene surficial deposits cover the lower mountain slopes and valleys tributary to the Plains.

Geomorphology. Extensive geomorphic evidence of Lake San Agustin exists along the basin margins. Shoreline features in the form of well-developed beaches, spits and bars have been mapped in detail by Powers (1939). This mapping has been refined and modified recently by Weber (1980; pers. commun. 1989). The features imply a history of fluctuating lake levels with relatively few stable stages. The highest lake level recognized by Powers occurs at 2,115 meters (6,940 feet). Recent work by Weber has further defined traces of pre-Wisconsin shore deposits as high as 2,149 meters (7,050 feet), and a possible Wisconsin shore maximum at 2,135 meters(7,005 feet). Lower lake levels,

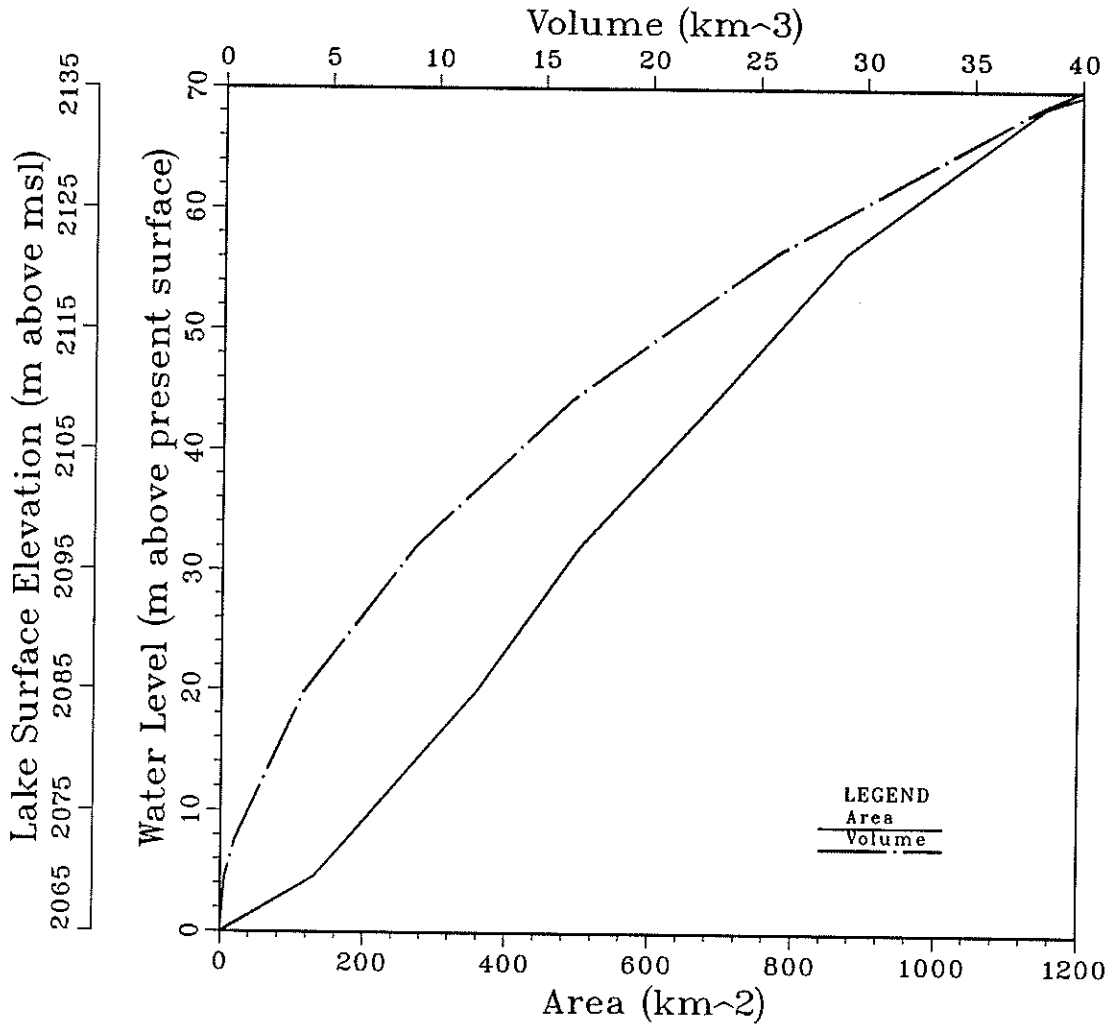

FIGURE 31. **Area/volume/depth relationships for San Agustin basin obtained by computerized digitization of USGS topographic maps**

represented by a series of wave-cut shorelines and beach deposits, extend to the modern playa boundary at approximately 2,070 meters (6,790 feet).

Three major subbasins occur within the main structural valley of the San Agustin Plains and include, from southwest to northeast, San Agustin Lake, C Bar N Lake and White Lake. The subbasins are situated at elevations of 2,065 meters (6,775 feet), 2,101 meters (6,894 feet), and 2,119 meters (6,952 feet), respectively. San Agustin Lake is connected hydrologically to C Bar N Lake via a channel way at 2,111 meters (6,925 feet). The C Bar N Lake and White Lake subbasins are separated by a sill at 2,128 meters (6,980 feet). At higher lake levels (above 2,128 meters), the subbasins were interconnected to form one large reservoir. At its 2,149-meter high stage, the lake was 70 meters (230 feet) deep with a surface area of approximately 1,226 square kilometers (473 square miles) (Weber 1980). At low lake levels (below 2,111 meters) each subbasin was isolated hydrologically, with C Bar N and White Lake existing in a playa environment. True lacustrine conditions were maintained most consistently in the San Agustin Lake subbasin. Bathymetry of the San Agustin subbasin is shown in figure 31.

The current semiarid environment and internal drainage cause playa conditions to dominate the modern basin. No perennial streams discharge into the basin and most precipitation is brief and intense during the late summer months. Wet playa conditions are therefore maintained intermittently by runoff during the wet season. Dry playa conditions prevail otherwise.

Hydrologic Environment

The modern regional hydrologic regime of the San Agustin basin is poorly understood. The regional groundwater gradient in the basin subsurface is approximately 0.0054 to the south-southeast, toward the San Francisco River. The water table ranges from 14 to 24 meters below the floor of the San Agustin subbasin (Blodgett & Titus 1973). The basin fill sediments have not been evaluated for hydraulic properties. Values previously used for hydraulic conductivity and specific storage are unfortunately rough estimates at best. Absence of evaporite minerals in subsurface sediments has been interpreted by previous investigators (Blodgett and Titus 1973) as evidence of groundwater seepage from the lake basin. This position is further supported by estimates of high hydraulic conductivities for the fractured volcanic bedrock and interbedded fluvial-lacustrine sediments underlying the basin floor. In this study, the paleohydrologic environment is conceptualized as involving transient interactions between the lake and a contiguous regional groundwater aquifer. Accordingly, fluctuations in lake level are viewed as producing a time-lagged, buffered response in the adjacent aquifer.

Lake level fluctuations are controlled by complex interactions between a variety of factors, both intrinsic and extrinsic to the basin. These include climate, hydrologic factors and vegetation change. The role played by any one

factor has been unclear. Identifying synchronous changes in lake level at San Agustin, Searles Lake, and other sites in the western and southwestern United States, may clarify the effects of regional climatic changes. However, climatic change produces corresponding local responses in vegetation, runoff, and groundwater which in turn produce interactive feedback responses. Further difficulty is encountered with attempts to distinguish the responses induced by changes in various climatic parameters. Whereas most investigators agree that changes in lake volume are most likely produced by a combined change in temperature and precipitation, with their accompanying effects on evaporation rate and humidity, there is little accord on each parameter's relative contribution.

A brief evaluation of the catchment and lake-water balance at San Agustin will provide a qualitative sense of the relative significance of the various parameters controlling lake level fluctuations. San Agustin Lake has a rather small catchment (lake area: catchment area ratios range from 1:4 for high stages to 1:30 for low stages), and it is unlikely that a high lake stage could be sustained. Contribution to lake inflow was probably provided by groundwater or interflow, particularly during higher lake stands. Changes in lake level provide estimates of lake volume changes (dV/dt) which may be assumed to represent a balance between catchment runoff (Q_R), precipitation on the lake surface (Q_P), net evaporation from the lake surface (Q_E), and the net exchange with groundwater (Q_{GW}). The water balance for the basin may then be represented by the equation:

$$dV/dt = Q_R + Q_P - Q_E - Q_{GW}$$

In this study, both qualitative interpretations and quantitative numerical modeling of the data group the inflow parameters (runoff, precipitation and groundwater inflow/interflow) into one inflow flux. The outflow parameters (net evaporation and groundwater seepage) are evaluated independently.

STRATIGRAPHIC RECORD

Sediments

Subsurface lacustrine sediments from the Plains of San Agustin have previously been described by Clisby and Sears (1956), Foreman et al. (1959), and Markgraf et al. (1983). This sediment record, established from a 600-meter core recovered from the basin's center, is dominated by silty clay, with alternating layers of sand from 14 to 65 meters and below 290 meters.

The sediment record which forms the basis of this study is a composite of two cores, SAC-4 and SAC-3. The cores were recovered at the same site, approximately 45 meters west of Boss Well in the SW 1/4 of the SE 1/4 of

section 21, T6S, R14W, Real Spring Quadrangle, Catron County, New Mexico, at a surface elevation of 2,071 meters (6,794 feet). The drill site is located along the depositional boundary separating playa and lacustrine conditions, and is situated sufficiently inward from the basin margin to avoid thick sequences of littoral and fluvial gravels, and far from regions within the basin center where deflation has removed Holocene sediments. Core SAC-4 was retrieved in one-foot sections with three-inch diameter shelby tubes. This core covers a depth interval from the present surface to 27.4 feet (8.35 meters) with 91 percent recovery. (The original units of measurement for core SA4 and SA3 were English units of length. Because field logs and notes were completed in units of feet, direct references in the text to depth within the core are in these units and parenthetical references are in metric units.) Core SAC-3 was retrieved with a split-spoon sampler and extends from 26.0 to 63.9 feet (7.92 to 19.48 meters) with 86 percent recovery.

Cores SA4 and SA3 are correlated along an abrupt contact between two distinctive sand units. This contact occurs at a depth of 26.3 feet (8.02 meters) in SAC-3 and at 26.0 feet (7.92 meters) in SAC-4 (8.02 meters) in SAC-3 and at 26.0 feet (7.92 meters) in SAC-4. Further paleontologic support for correlation is provided by a six-inch interval within the lower sand unit which contains similar and unique specimens of the ostracode *Limnocythere ceriotuberosa*. In both cores, mature ostracodes from this interval were abnormally small and retrieved with articulate valves. Similar ostracode specimens were not observed elsewhere in either core. Such lithologic and paleontologic evidence collectively provide a firm basis for correlation between the 26.0-foot (7.92-meter) level of SAC-4 and the 26.3-foot (8.02-meter) level of SAC-3.

A detailed lithologic log of the composite sediment core, SAC-3/4, is attached as Appendix J. The general nature of the sediment record is briefly described here. Deposition in the basin is dominated by clastic sedimentation; no significant intervals of chemical sediments occur in the record. The upper 25 feet (7.62 meters) of sediment consists of massive and laminated clays and clayey silts rich in organic material. The uniform nature of these shallow sediments suggests stable deep water conditions prevailed throughout the deposition interval. X-ray diffraction of laminated clay sequences indicates the presence of illite, smectite and mixed-layer clays. This clay assemblage may be suggestive of a variable weathering environment, produced in response to changing climatic conditions, or it may be a result of multiple source areas for the sediments. Sediments recovered from the interval between 25 feet (7.62 meters) and 64 feet (19.51 meters) are dominated by alternating sands and gravels. Field logs of core cuttings from sediment intervals not recovered indicate these sections are dominated by clays and clayey silts. The alternating coarse-fine sediment sequences below

25 feet (7.62 meters) indicate that continually fluctuating lake levels dominated this deposition interval.

Ostracodes

Ostracodes occur continuously and in large numbers throughout the sediment's upper 27 feet (8.23 meters). The valves are well preserved typically and always identifiable to species. Only two intervals in the lower section of core 33.7 to 34.2 feet (10.27 to 10.42 meters) and 40.4 to 41.6 feet (12.31 to 12.68 meters) contain significant numbers of ostracode valves. Five species of ostracode occur in core SAC-3/4: 1) *Limnocythere bradburyi* (Fig. 32a,b); 2) *L. ceriotuberosa* (Fig. 32c,d); 3) *L. platyforma* (Fig. 32e,f); 4) *Candona patzcuaro*; and 5) *Heterocypris* spA. Ostracode stratigraphy and isotopic data from shell carbonate provide the framework for the paleoenvironmental interpretations presented later in this report.

METHODS

Lacustrine Ostracodas as a Tool in Paleoenvironmental Reconstruction

Lacustrine Ostracode have found wide application in reconstructing continental paleoclimates (Forester 1985; De Deckker 1988) and paleohydrochemistry (Forester 1983; 1986; Chivas et al. 1985; 1986a; 1986b) since Delorme (1969) first recognized that particular ostracode species were so habitat-specific that they could be used as very sensitive indicators of temperature, water depth, salinity and hydrochemistry. When the temporal distribution of these variables is known, they can be used as a proxy record of past climatic conditions. For reviews see Forester (1987), Carbonel et al. (1988), and DeDeckker and Forester (1988).

Use of stable isotope data from lacustrine ostracode shell carbonate to make quantitative paleoenvironmental interpretations has yet to receive such broad application despite its high potential. Ostracodes are typically the most ubiquitous and abundant calcareous microfossil in lacustrine environments, and often the only verifiable source of primary carbonate. Preliminary investigations strongly suggest that freshwater ostracode carapaces are precipitated in isotopic equilibrium with the ambient dissolved carbonate species (Durazzi 1977; Gasse et al. 1987; Lister 1988a). In circumstances where ostracode tests precipitate in isotopic equilibrium from a well-mixed reservoir, oxygen isotope variations in biogenic carbonate record temporal changes in ^{18}O composition of the lake water. Such compositional changes may then be related to climatic shifts or hydrologic changes within the basin. The value of ostracode shell carbonate as a source of stable isotope data has been demonstrated in the recent work of Chivas et al. (1986b) and Lister (1988a; 1988b).

The extent to which taxonomic factors influence incorporation of ^{18}O in the ostracode shell is uncertain and should be addressed. Previous studies (Durazzi 1977) have indicated that different ostracode taxa from the same

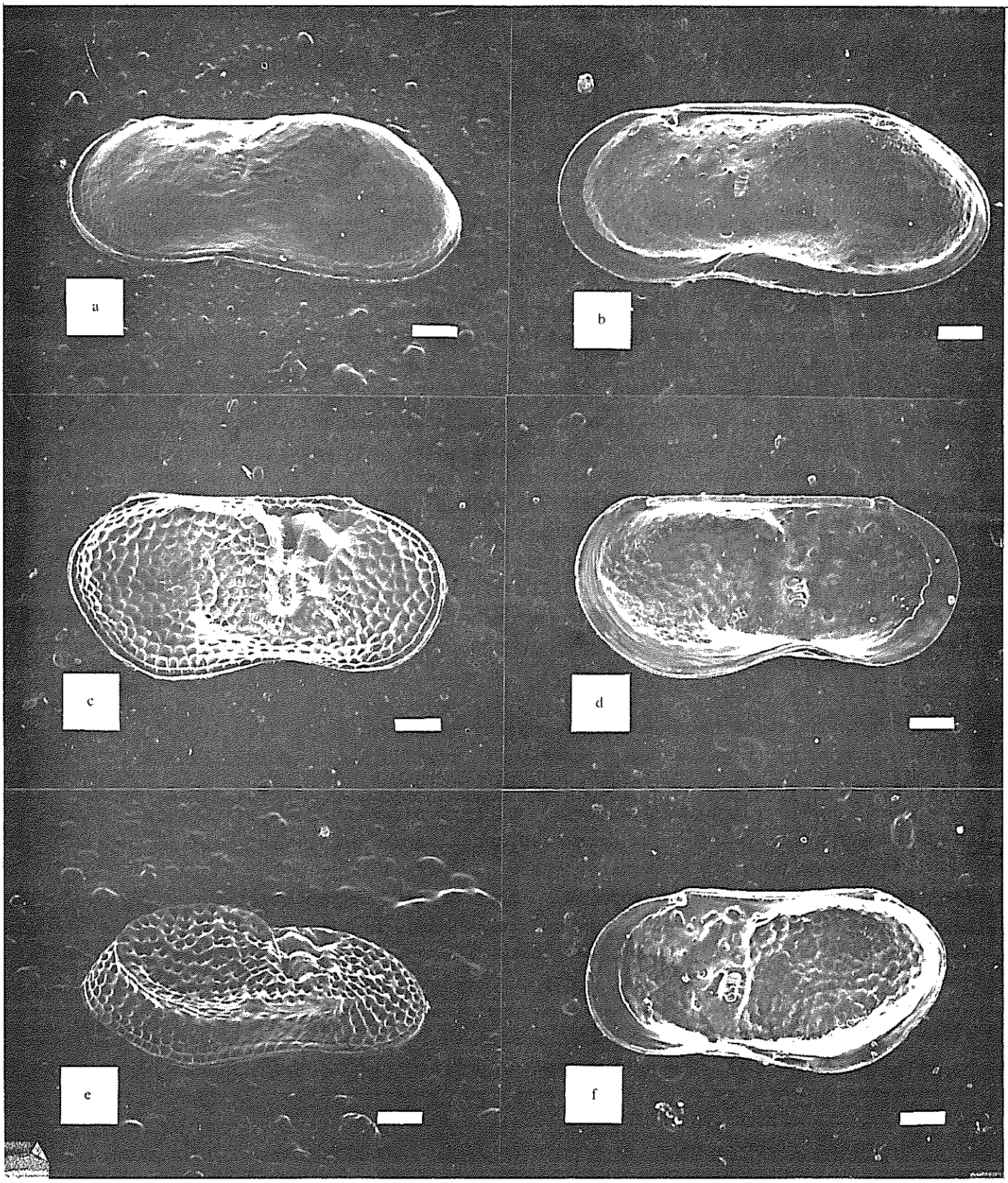

FIGURE 32. Ostracode specimens from Plains of San Agustin. Bar scale is 100 micrometers. (a) Limnocythere bradburyi, lateral view, left valve exterior, male; (b) L. bradburyi, lateral view, right valve interior, male; (c) L. ceriotuberosa, right valve exterior, male; (d) L. ceriotuberosa, left valve interior, male; (e) L. ceriotuberosa, right valve exterior, male; (f) L. platyforma, right valve interior, male

sample show significant differences in ^{18}O composition. Based on recent studies which support equilibrium isotopic fractionation during shell precipitation, the most likely explanation is that such taxonomic variations reflect different seasonal growth preferences or environmental conditions. In any case, problems resulting from such "vital effects" should be avoided by analyzing samples consisting of a single species or an assemblage of closely related species. The influence of taxonomic factors on ^{18}O composition of ostracode shells in this study is discussed later in this report.

Modern Biogeographic Distribution and Occurrence of Ostracode Species.

The geographic and ecologic occurrence of *Limnocythere bradburyi* has been well studied by Forester (1985; 1987). Today, *L. bradburyi* lives in large, shallow, ephemeral lakes in the central Mexican Plateau and in southern New Mexico. It has also been identified in Quaternary sediments from localities in Mexico and the southwest U.S. (Cameron and Lundin 1977; Forester 1985; 1987). *Limnocythere ceriotuberosa* lives in deep and shallow lakes including ephemeral waters. Its modern distribution extends throughout the central Great Basin and from the central prairies north into the interior plains of Canada (Delorme 1971; Forester 1985; 1987). It has been found coexisting with *L. bradburyi* in fossil lake sediments of Lake Cochise in Arizona (Cameron & Lundin 1977).

Forester (1985; 1987) has also made special interpretations of the co-occurrence of *Limnocythere bradburyi* and *L. ceriotuberosa*. Geographic distribution of these two species is separated latitudinally along the frost line; *L. bradburyi* required relatively warm water to hatch, mature and reproduce. *L. bradburyi* can live in water with a greater seasonal temperature range (0^0 to 25 ^0C) than *L. bradburyi*. *L. ceriotuberosa* lives in regions where summer temperatures meet or exceed those of central Mexico, but it does not live in Mexico. Its occurrence there may be precluded by warm winter temperatures. Similarly, absence of *L. bradburyi* in northern latitudes may be due to cold winter temperatures. Coexistence of *L. bradburyi* and *L. ceriotuberosa* at San Agustin implies that winter temperatures were probably warmer than today (above -2^0 to -4 ^0C) but not as warm as currently occur in central Mexico (10 ^0C). Transitions between the two species may then by viewed in terms of relative temperature changes. For example, replacement of *L. ceriotuberosa* by *L. bradburyi* indicates a trend toward warm winter temperatures. Replacement by *L. bradburyi* by *L. ceriotuberosa*, on the other hand, suggests either cooler summers or significantly colder winters, or both.

The modern occurrence of *Limnocythere platyforma* (Delorme 1971) is rare. The species has only been found in a small pond in the central prairies of Canada. *L. platyforma* is viewed as an ecophenotype of *L. ceriotuberosa* (R.M. Forester, written commun., 1987) based on a complete gradational series between the two forms. Morphs generation is not completely understood.

Because *L. platyforma* is more heavily calcified, one possible explanation calls for it living in waters with a higher Ca^{2+} concentration, that is, fresh waters. The occurrence of *L. platyforma* therefore suggests corresponding increase in fresh-water inflow. Its co-occurrence with *L. ceriotuberosa* could be due to sediment averaging or to seasonal variability in water chemistry.

Candona patzcuaro lives in ditches and ponds throughout the semiarid regions of the North American plains and the southwest central position of the Canadian prairies (Delorme 1970). *Candona patzcuaro* and *Heterocypris spA*, collectively separated from the sediment residue, are both characteristic of ephemeral waters and are associated at San Agustin with a shoreline facies. *Heterocypris* spA, a new species recognized by Richard M. Forester (written commun. 1987) is believed to have affinities to *H.incongruens*. The five ostracodes species occurring in San Agustin sediments live in chemically similar waters which are carbonate enriched and dominated by Na^{+}, Mg^{2+}, HCO_3^{-}, CO_3^{2-}, and/or Cl^{-} ions. *Limnocythere ceriotuberosa* lives in fresh to slightly saline waters with a TDS ranging from 500 to 25,000 ppm, with a greater salinity tolerance in Cl^{-} dominated water (Forester, 1987). *L. bradburyi* tolerates a narrower salinity range, from 1,000 to 10,000 ppm (Neale 1988).

Sample Selection, Preparation and Isotopic Analysis

Sample selection. Sample size was primarily governed by a need to obtain sufficient carbonate from one ostracode species for isotopic analysis. A second consideration was to produce a sample interval with a resolution adequate to define short-term climatic fluctuations, that is, about 100 years or less. Sample volume ranged from 90 to 120 cm^3, and sediment samples were processed from one-inch sections of core spaced at two-inch intervals. Based on the chronology discussed below, the average time interval represented in a sample is approximately 110 years.

Sample preparation. The samples were prepared by completely disaggregating sediment grains from the ostracodes, and separating the sand-sized fraction containing mature ostracodes from the silt- and smaller-sized fraction. The preparation technique was modified from U.S.G.S., Technical Detailed Procedure HP-78 discussed below.

Sediment samples were initially sealed in plastic soil bags and frozen. Approximately 30 to 40 cm^3 of frozen sediment was thawed and gently mixed with 500 to 600 ml of boiling, distilled water and one teaspoon sodium bicarbonate. After cooling to room temperature, one teaspoon each of sodium hexametaphosphate (HMP) and sodium triphosphate (TSP) were added as dispersants, and the sample was allowed to stand for 48 hours. The disaggregated sediment was gently washed through a 100-mesh (150 micrometer

openings) sieve. The size fraction remaining in the sieve was washed with distilled water onto a stack of paper towels, sealed in the towels, and dried at room temperature.

Ostracode extraction and identification. Mature ostracode carapaces were separated from the sand- and larger-sized sediment for identification and analysis. The dried sediment residue was gently poured and brushed from the papertowel into a nested set of three-inch sieves containing 20-, 40-, 50-, 60-, and 80-mesh sizes, and a receiver pan. Adult specimens were largely confined to the 40-, 50-, and 60-mesh fractions. These fractions were systematically examined under a binocular microscope with reflected light at 16 to 18X magnification. Adult specimens were removed with a wetted, fine-tip (00) red sable brush and transferred to a standard micropaleontologic slide. The shells were inspected for overgrowth and/or dissolution and separated by species.

Isotopic analysis. *Limnocythere bradburyi*, the dominant specie in the core, was preferentially selected for isotopic analysis to provide the most consistent data set. Where *L. bradburyi* was not present in sufficient numbers for analysis, *L. ceriotuberosa* or a mix of species of the genus *limnocythere* was used. Only four samples consisted of some mixture of *Heterocypris* spA and *Candona patzcuaro*.

One hundred eighty-six samples from 159 intervals was analyzed for oxygen and carbon isotope ratios. Analyses were performed at the Stable Isotope Laboratory, NMIMT, using McCrea's (1950) methods for acid decomposition. About 0.5 to 1.5 mg of shell sample comprised of 40 to 150 individual ostracode valves were reacted under vacuum with 100 percent phosphoric acid at 25^0 C for 10 to 15 hours. The acid reaction produces 2.5 to 15 micromoles of CO_2 gas. $^{13}C/^{12}C$ and $^{18}O/^{16}O$ ratios of the evolved CO_2 gas were determined using a Finnigan MAT Delta E mass spectrometer.

A special technique was developed for mass spectrometric analysis of the small volumes of CO_2 gas produced. For gas samples less than approximately three micromoles, the gas was first frozen into a coldfinger on the mass spectrometer inlet and then released directly into the ion source. For samples larger than three micromoles, the coldfinger was also used. However, the gas was allowed to expand back into the variable volume to protect the source from excessive pressures. The bellows were then used to equalize sample and standard volumes prior to releasing the gas into the source.

Isotopic results are presented using standard (δ) notation (Craig 1957) as the per mil ($^{0}/_{00}$) deviation of the sample carbonate from PDB Standard for $^{13}C/^{12}C$, or from SMOW Standard for $^{18}O/^{16}O$.

Reproducibility of the isotopic composition of normal volumes (i.e., 100 micromoles) of duplicate CO_2 gas samples is 0.05 per mil for both carbon and oxygen. Due to the small volumes of gas generated in this study, these specification values could not be verified by duplicate analyses of the same gas sample.

A standard deviation for extraction and isotopic analysis of the CO_2 gas was determined by analyzing six separate samples of *Limnocythere bradburyi* from each of two different depths. Intervals where this species of ostracode was especially abundant (9.12 feet and 19.54 feet) were used and all samples sizes were of equal. The standard deviations in ^{18}O were determined to be ± 0.425 per mil and ± 0.504 per mil for the upper and lower sample intervals, respectively; deviations in ^{13}C were ± 0.160 per mil and ± 0.264 per mil.

Chronology

Radiocarbon dating of three fiberous plant material samples and two ostracode samples was attempted by accelerator mass spectrometry. However, the plant fiber samples yielded anomalous ages. The results are displayed in Table 4 and evaluated below. The plant fragments have ^{14}C ages ranging from 160 to 410 yr B.P., and are apparently root remains of former vegetation whose root system penetrated to depth from the surface. (Today the only vegetation at the drill site is bunch grass, whose roots could not penetrate to depths of 5 m.) This plant material was common throughout the core from a depth of 4.0 feet (1.22 meters), just below the modern root zone, to 19.0 feet (5.79 meters).

The chronologic framework (Fig. 33) was established from three ^{14}C dates on organic and biogenic carbonate material from core SAC3-4, and correlation of the ostracode biostratigraphy with a previously developed ^{14}C-dated biostratigraphic record. Radiocarbon dating on core SAC3-4 samples was completed by accelerator mass spectrometry at the National Science Foundation Accelerator Facility for Isotope Dating, University of Arizona. Organic material consisting of two seeds of *Eleocharis sp.*, a specie of spike rush (Betancourt, J., personal communication, 1989), yielded a ^{14}C date of 19,720 ±210 yr. B.P. (AA-4711) at 3.04 m (9.96 ft). Two samples consisting of ostracode shell material from depths of 3.01 m (9.88 ft) and 12.36 m (40.54 ft), provided respective ^{14}C dates of 22,400 ±210 yr B.P. (AA-3965) and 37,700 ±1100 yr B.P. (AA-3962). Comparison of ^{14}C dates from the seed material at 3.04 m (19,720 yr B.P.) and the shell material at a similar depth

TABLE 4. Results of ^{14}C analysis of organic material and ostracodes from core SAC 3-4 by accelerator mass spectrometry

Sample No.	Depth (ft)	Depth (m)	Material	^{14}C Age (yr B.P.)	^{14}C Analysis Number
SA4-6-2-2	6.21	1.89	Plant fragments	410 ± 60	AA-3963
SA4-9-10-11A	9.88	3.01	Plant fragments	160 ± 65	AA-3964
SA4-9-10-11B	9.88	3.01	ostracodes	22,400 ± 210	AA-3965
SA4-9-11-12	9.96	3.04	*Eleocharis* seed	19,720 ± 210	AA-4711
SA4-18-9-10	18.79	5.73	Plant fragments	350 ± 55	AA-3966
SA3-40-6-7	40.54	12.34	ostracodes	37,700 ± 1,100	AA-3962

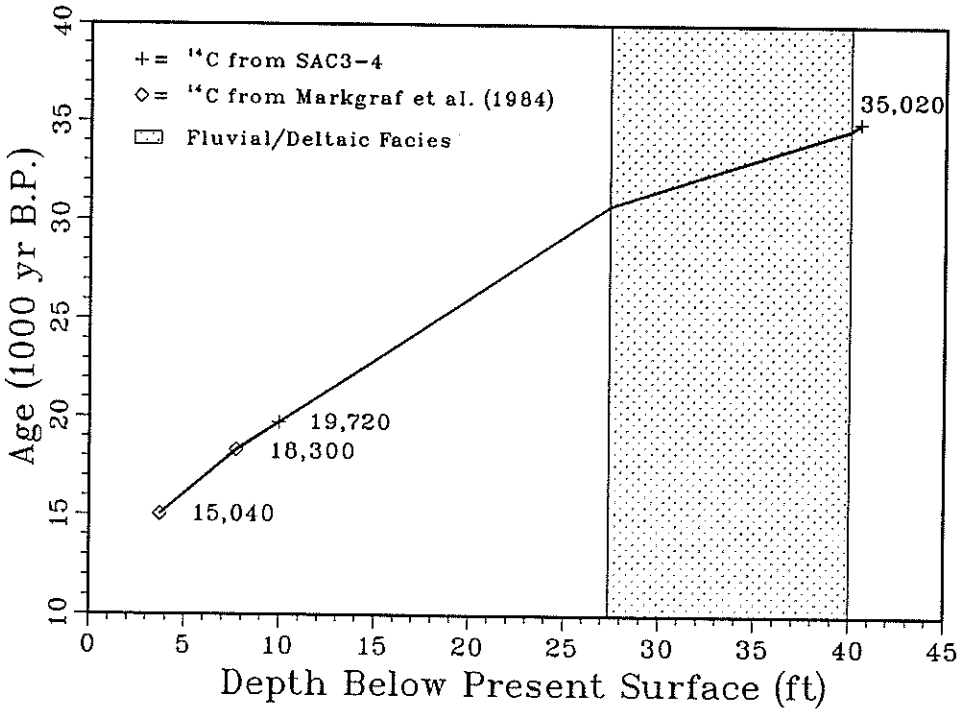

FIGURE 33. Age versus depth plot for core SAC 3-4 from ostracode stratigraphy correlations and ^{14}C dates

of 3.01 m (22,400 yr B.P.) indicates that the $^{14}C/^{12}C$ ratio in the biogenic carbonate sample is anomalously low. This is probably due to dilution by a source of dead carbon, or the "hard-water effect". The ^{14}C date for the shell sample at 12.36 m was also assumed to be too old by a margin of 2680 years and the age of this sample was corrected to 35,020 ±1100 yr B.P. The chronology was further constrained by correlation of the ostracode biostratigraphy (Fig. 3) with an ostracode record developed by Markgraf et al. (1984) and Forester (1987). Two dated biostratigraphic markers in the record reported by Markgraf et al. (1984) were correlated to the SAC3-4 core: (1) replacement of *Limnocythere bradburyi* with predominantly *L. ceriotuberosa* at a depth of 2.35 m (7.71 ft) in core SAC3-4 and an age of 18,300 ±300 yr B.P. in the core described by Markgraf et al. (1984); and (2) the transition point at 1.14 m (3.73 ft) in core SAC3-4 where the ostracode distribution reflects approximately 75% *L. bradburyi*, *25%* *L. ceriotuberosa* and *0%* *Heterocypris* spA/*Candona patzcuaro*, and which corresponds to an age of 15,040 ±200 yr B.P. in the record of Markgraf et al. (1984). The age-depth relationship was also adjusted for a faster deposition rate assumed to be associated with the fluvial/deltaic sands and gravels deposited in the depth interval 8.35 m (27.4 ft) to 12.19 m (40.0 ft). The resulting chronology indicates that the ostracode and isotope samples span the period from approximately 35,370 to 15,360 yr B.P. with an average sampling interval of 110 years.

RESULTS

Ostracode Stratigraphy

The relative abundance and stratigraphic distribution of ostracode species in core SAC-3/4 is displayed in Figure 34; the raw data are summarized in Appendix K. *Limnocythere bradburyi* and *L. ceriotuberosa* occur in greatest abundance and alternately dominate the core. *L. bradburyi* dominates intervals from 15 to 16.2 ka, 18.4 to 19.7 ka, and 21.8 to 28.7 ka. *Limnocythere ceriotuberosa* dominates a short section from 18.0 to 18.5 ka and intervals 19.5 to 22.0 ka, and 28.0 to 31.0 ka. *L. platyforma* occurs sporadically in low numbers throughout the stratigraphic column from approximately 20 to 29 ka, with significant spikes centered at 22.6, 25.1, and 26.5 ka. The two species, *Candona patzcuaro* and *Heterocypris* spA, are rare and collectively dominate only the interval from 15 to 18 ka.

Oxygen and Carbon Isotopes.

The oxygen- and carbon-isotope curves for Lake San Agustin as determined from ostracode shell carbonate are shown in Figure 35; raw data from isotopic analyses are presented in Appendix L. $\delta^{18}O$ values vary over a range of 6.15 per mil and ^{13}C values over a range of 6.05 per mil. Assuming isotopic equilibrium, negligible interference from taxonomic effects, and a well-mixed reservoir, deviation in ^{18}O and ^{13}C content of the biogenic carbonate will

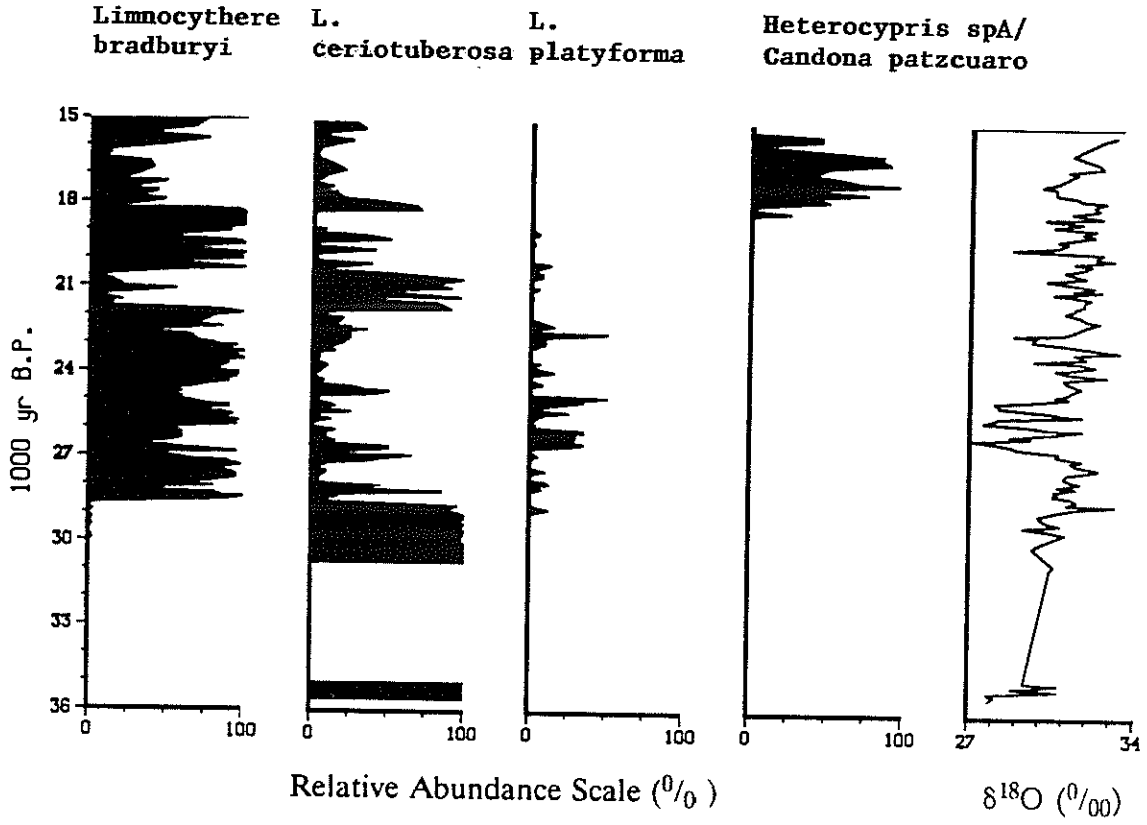

FIGURE 34. Relative abundance of ostracode species (as percent) and $\delta^{18}O$ as a function of age for core SAC 3-4

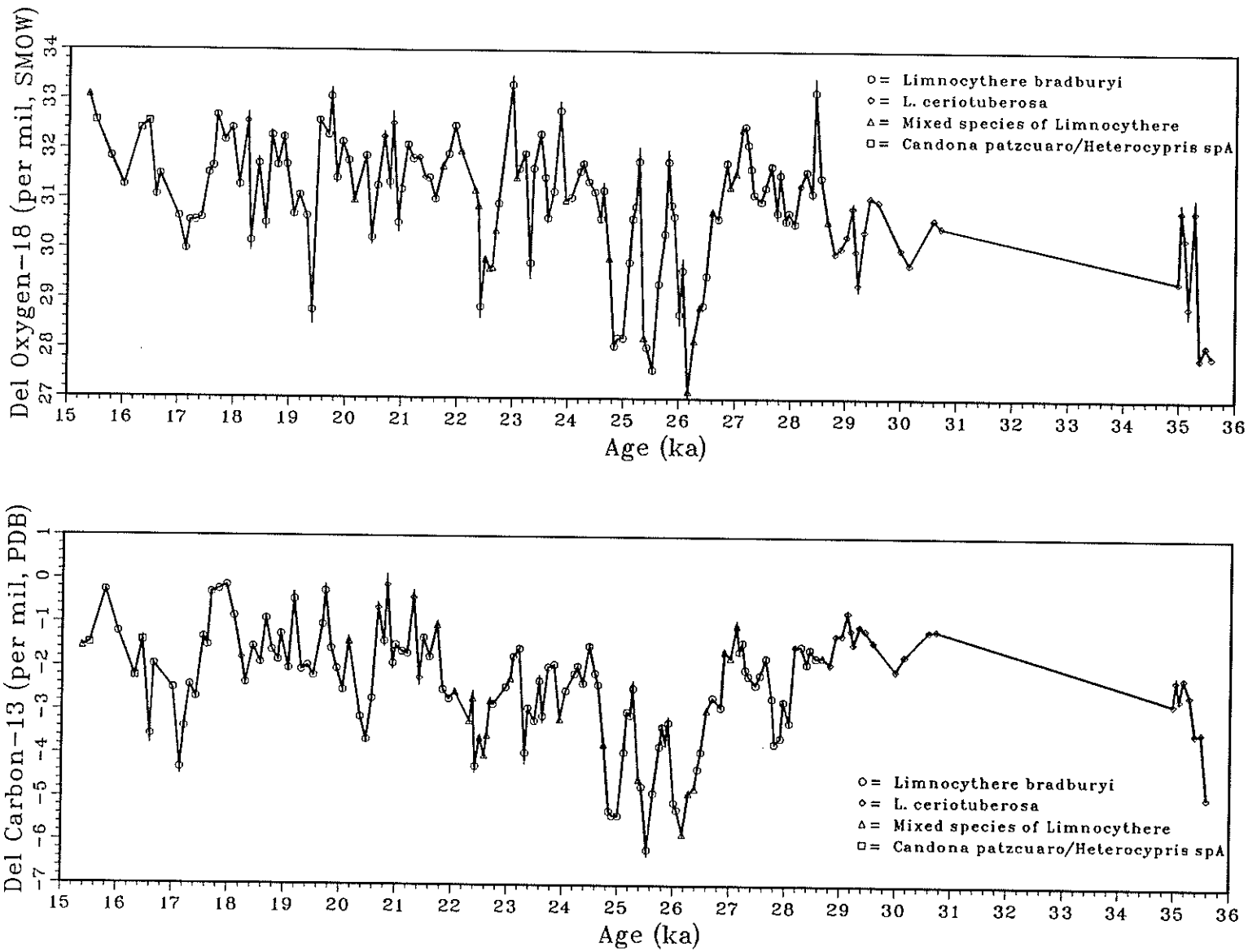

FIGURE 35. $\delta^{13}C$ and $\delta^{18}O$ as a function of age for core SAC 3-4

reflect temporal changes in isotopic composition of the lake water and can be used to infer a history of lake-level fluctuations.

Nine samples included in the raw data shown in Appendix L have been deleted from the isotopic curves. Two samples at the top of core SA4 (LHMX3-1-2 and LB3-8-9.5) appeared to consist of reworked shell material. The ostracode tests in these samples were typically broken and etched and remained coated with clay and other material even after preparation with dispersants. Two samples at the bottom of core SA4 (C-26-0-2 and C-26-2-4) and five samples in core SA3 (C-26-6-8, C-26-8-10, C-26-10-12, C-33-8-10, and C-34-0-2) were further excluded because of alteration. The appearance of these seven samples suggested that the original shell material had been completely replaced. All the valves were articulate, opaque and filled with a crystalline carbonate material. In addition, the anomalously enriched ^{13}C content of these samples provides further support for post-depositional alteration.

To address the issue of taxonomic factor influence on the isotopic composition of shell carbonate, the three species of the genus *Limnocythere* were evaluated for variability of ^{18}O and ^{13}C content. The samples from which the ostracodes were separated for comparison represent approximately 100 years of sedimentation each. *L. ceriotuberosa* and *L. platyforma* are collectively plotted against *L. bradburyi* for both ^{18}O and ^{13}C in Figure 36. *L. ceriotuberosa* and *L. platyforma* are treated as a single population because the wo forms are most likely a response to water chemistry variation, rather than truly distinct species. Both species apparently occur under similar temperature constraints, and it is therefore appropriate to group them for statistical evaluation of isotopic composition. The sample regression line (solid line) displays good correlation in both plots with a hypothetical one-to-one regression line (dashed line). The hypothetical regression line represents the ideal circumstance in which *L. bradburyi* incorporates ^{18}O and ^{13}C in the same ratio as the other species of *Limnocythere*. The correlation between the sample regression line and the ideal is admittedly not exact; however, it does not indicate any systematic taxonomic effects.

All species of the genus *Limnocythere* live in bottom-water conditions. *Heterocypris spA* and *Candona patzcuaro* are characteristic of shoreline facies and will presumably produce isotopic data unique to that environment. If San Agustin Lake did not have a history of stratification, such distinctions would be unnecessary. Covariance of the oxygen- and carbon-isotope curves suggests that during the last 25,000 years, stratification did not occur. Further, lake waters were likely shallow enough that bottom waters were thermally coupled with the atmosphere, and relative changes in water temperature recorded by ostracode distribution reflect a response to changing air temperature.

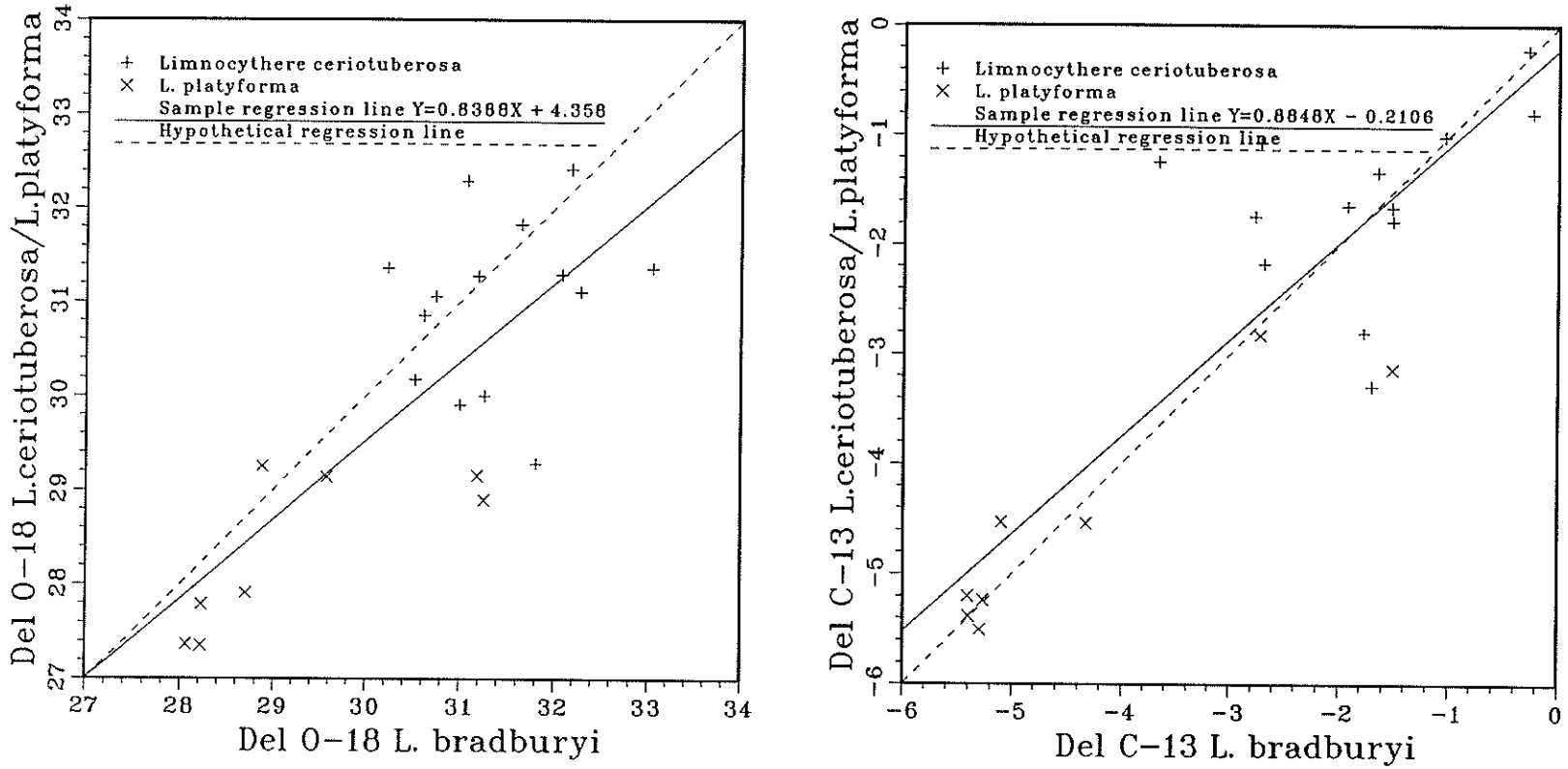

FIGURE 36. $\delta^{18}O$ and $\delta^{13}C$ for L. ceriotuberosa, and L. platyforma plotted against $\delta^{18}O$ and $\delta^{13}C$ for L. bradburi

Correlation and Interpretation of Ostracode Stratigraphy and Oxygen Isotopes.

Oxygen isotope data from biogenic carbonate for the period 35 ka to 15 ka are displayed together with the ostracode stratigraphy in Figure 34. By inferring lake level fluctuations from the ^{18}O curve and correlating this lake level record with the ostracode distribution, a qualitative history of relative changes in temperature, inflow and lake size can be developed for the San Agustin Basin.

A significant event is recorded at 28.6 ka where *Limnocythere ceriotuberosa* was abruptly replaced by *L. bradburyi*, and a corresponding sharp positive shift of 3.2 per mil in ^{18}O occurred over a time span of approximately 360 years. Prior to 28.6 ka when *L. ceriotuberosa* was dominant, lake levels were relatively high and stable. Temperatures were either cooler in summer, or significantly colder in winter than present, or both. This interval coincides with the classic period of maximum advance of continental glaciers during late Wisconsin. The species transition was preceded by an increase in inflow, as suggested by the appearance of *L. platyforma* between 29.0 and 28.6 ka. An abrupt summer warming trend began at 28.6 ka and is represented by the sudden dominance of *L. bradburyi*. The magnitude of abruptness of the ^{18}O shift between 29.0 and 28.6 ka further suggests an increase in the mean annual temperature and increase evaporative enrichment. Subsequent to 28.6 ka, lake levels gradually declined and an interval of low to intermediate lake stage with minor fluctuations was maintained until about 26.4 ka. Temperatures remained relatively stable, with warm summers and temperate winters.

At 26.4 ka Lake San Agustin was apparently at a relatively low level. Spikes of *Limnocythere ceriotuberosa* which occur from 27.3 to 26.9 ka and 25.0 to 24.8 ka indicate the onset of relatively cooler temperatures. A broad band of *L. platyforma* from 26.7 to 26.0 ka, and a negative shift in ^{18}O of 4.59 per mil over the same interval strongly suggest filling in response to a long period of sustained inflow and reduced evaporation. The span between 26.5 and 24.5 ka experienced with a series of extreme lake level fluctuations. Inflow intervals are delineated with bands of *L. platyforma* and high stages in lake level are defined by large negative deviations in ^{18}O on the order of 4.2 to 4.6 per mil. Cyclic fluctuations in relative abundance of *L. bradburyi* suggest a variable temperature regime with relatively warm, temperatures accompanying low lake levels, and intermediate temperatures occurring during inflow intervals. This period ended with an interval of abnormally cool temperatures, defined by a peak in *L. ceriotuberosa* at 25.0 ka.

The interval from 25.0 to 23.5 ka marked a period of relatively stable, intermediate lake levels in the San Agustin basin. Temperatures were similarly stable and quite warm; relative absence of *Limnocythere*

ceriotuberosa suggests temperate winters. The next major event was a very low stand at 23.0 ka, which was immediately followed by an interval of gradual lake level rise, culminating in a high stand at 22.8 ka. This rise in stage was most likely a response to a sustained increase in inflow (defined by occurrence of *L. platyforma* at 22.7 ka combined with cooler temperatures (indicated by an increase in *L. ceriotuberosa*).

Cold temperatures are indicated from 22.2 to 19.2 ka (indicated by a clear dominance of *Limnocythere ceriotuberosa*), but were replaced by a relatively warmer, more variable temperature regime beginning 19.2 ka. Several small inflow events, defined by the presence of *L. platyforma* and negative deviations in ^{18}O, occurred during this period. Low to intermediate stages prevailed after 18.5 ka with relatively minor fluctuations. Temperatures during this interval remained quite warm and stable.

A significant transition in the ostracode distribution occurred at 18.5 ka with the appearance and relative dominance of *Heterocypris* spA and *candona patzcuaro*. This transition clearly defines the onset of generally low lake levels. However, persistence of species of the genus *Limnocythere* indicates some degree of lake stability. Relative absence of species of *Limnocythere* at 17.2 and 16.2 ka suggest playa rather than lacustrine conditions prevailed at these times. Temperatures after 18.5 ka appear to be characterized by marked seasonality.

NUMERICAL MODELING

INTRODUCTION

One goal of this project was to reconstruct quantitatively the lake surface-area histories for the paleo-Owens River system and San Agustin Lake using the stable isotope records. Examples of lake-level and stable isotope evolution models were presented earlier using simple analytic solutions to simulate the histories. Continuous variations in model input parameters cannot readily be incorporated into analytical solutions. Therefore we have constructed several numerical models for this purpose.

The main tool for the lake-level reconstructions is a transient numerical model called TRANSISO. The complete program is listed in Appendix M. The equations used were initially presented by Gonfiantini (1965). The model is based on one described in Phillips et al. (1986), but differs from that model in being formulated on a time-derivative basis rather than a volume-derivative basis. The model consists of linked water mass balance and isotope mass balance equations. To compute the mass balance, the model requires history of temperature, humidity, precipitation rate, evaporation rate, isotopic composition of inflow water, isotopic composition of precipitation on the lake surface, and isotopic composition of the atmospheric humidity. The independent parameter that "drives" the model is the inflow to the lake or lakes. The dependent variables calculated by the

model are the surface area of the lake(s) and the isotopic composition of the lake water. For cases (such as the paleo-Owens River system) in which a series of lakes are involved, the model sequentially calculates the lake history for each lake individually, then uses the outflow from that lake as the inflow to the next lake in the chain.

The basic approach used in implementing the transient numerical model was to vary the inflow history so as to match the isotopic history. Based on the linked water/isotope mass balance, the model then calculates the lake surface area as a function of time. To avoid a long and tedious matching procedure, the initial "guess" for the influence history of the lake was taken from the output of a steady-state lake simulation model. The steady-state model back-calculated the lake inflow at each ^{18}O data point based on the much simpler steady-state equations. This steady-state approximation was then entered into the transient model and used as the input for the initial simulation. The inflow was then varied to better match the ^{18}O data for intervals where transient effects were important. This approach proved to be much more efficient than intuitive guessing of an initial inflow history.

In addition to calculating an isotopic history of the lake water, the model also produces a history of chloride accumulation in the lake sediments. It performs this using a constant chloride influx and mass-balance equations and assuming the chloride is conservative in the lake water unless its concentration exceeds that for solubility of halite. Although variations in soluble salts accumulation at Searles Lake have sometimes previously been explained by long-term variations in the influx (e.g., Smith 1979), we have found that the chloride accumulation history can largely be explained simply by climatically controlled variations in the inflow of water. We believe accumulation of many other solutes can be explained similarly. There is some evidence for relative constancy of the average chloride influx over long time periods (Jannik, 1989), and explaining the chloride deposition using only climatically-controlled water inflow changes is more parsimonious than arbitrary variations in chloride influx.

MODEL FORMULATION

The model is a transient numerical lumped-parameter model simulating surface area and isotopic evolution of five lakes in the paleo-Owens River system. This includes Owens Lake, China Lake, Searles Lake, Panamint Lake and Lake Manly (Death Valley). Water mass balance for each lake is given by:

$$\frac{dV_L}{dt} = Q_I + Q_P + Q_C - Q_O - Q_E \qquad (9)$$

where V_L is the lake volume, Q_I is the inflow flux (from the Owens River or the preceding lake), Q_P is the flux of precipitation onto the lake, Q_C is the back-condensation flux, Q_O is the overflow flux, Q_E is the gross evaporative flux, and t is time. The isotopic mass balance is described by:

$$\frac{d(V_L \delta_L)}{dt} = \delta_I Q_I + \delta_P Q_P + \delta_C Q_C - \delta_O Q_O - \delta_E Q_E \qquad (10)$$

where δ is the relative isotopic enrichment of the reservoirs and fluxes indicated by the subscripts. Applying the chain rule to (10) we have:

$$V_L \frac{d\delta_L}{dt} + \delta_L \frac{dV_L}{dt} = \delta_I Q_I + \delta_P Q_P + \delta_C Q_C - \delta_O Q_O - \delta_E Q_E \qquad (11)$$

Letting $B = \delta_I Q_I + \delta_P Q_P + \delta_C Q_C - \delta_O Q_O - \delta_E Q_E$ and solving (11) for $\frac{d\delta_L}{dt}$ gives:

$$\frac{d\delta_L}{dt} = (B - \delta_L \frac{dV_L}{dt})/V_L \qquad (12)$$

(9) and (12) are solved for each time step of the numerical simulation using the Runge-Kutta-Fehlberg difference-equation method. Because calculations in the modeling involved numbers which differ by many orders of magnitude, all variables in the FORTRAN code were declared as double precision to minimize rounding errors. The accuracy of the numerical solution was verified by comparison with an analytical solution.

Bathymetric data for each of the lake basins (Appendix P) were used to convert the volumes calculated by the model to surface areas. Data for Owens and Searles Lakes are from G.I. Smith (1979); for China Lake from N.O. Jannik (1989); for Panimint Lake from R.S.U. Smith (1976); and for Lake Manly from N.O. Jannik (1989); and for Panamint Lake from R.S.U. Smith (1976). Salinity strongly affects both evaporation and isotopic fractionation and must therefore be taken into account by the model. The model calculated changes in salinity with time for Owens, China, Searles, and Panamint Lake using a simple mass balance approach. Specifically calculated is the concentration of chloride ions. The starting point for the mass balance is a constant input of chloride. Several studies have concluded that the chloride load of the Owens River has been at least roughly constant with time (Jannik 1989; Smith 1976) and approximately equal to 5.9×10^6 kg yr^{-1} (Smith 1976). For a given time step of the model, the mass (kg) of chloride entering Owens Lake is simply:

$$Cl = \Delta t \frac{5.9 \times 10^6 kg}{yr} \quad (13)$$

where Δt is the size (yr) of the current time step. To determine whether chloride will be precipitated, the model then calculates the chloride concentration (moles ℓ^{-1}) at the end of the time step as:

$$Conc_{Cl} = Cl \frac{10^3 g}{kg} \frac{mole}{35.453 g} VOL^{-1} \frac{m^3}{10^3 \ell} \quad (14)$$

where VOL is the volume (m^3) of the lake at the end of the current time step. If $Conc_{Cl}$ is greater than 6.1 moles ℓ^{-1}, the solubility of halite, the mass (kg) of chloride precipitated in the lake is given by:

$$Cl_{dep} = (Conc_{Cl} - 6.1) \frac{35.453 \times 10^{-3}}{mole} VOL \frac{10^3 \ell}{m^3} \quad (15)$$

For a lake at overflow, $dV_L/dt = 0$ and from (9), we see that the flux out of the lake is:

$$Q_O = Q_I + Q_P + Q_C - Q_E \quad (16)$$

The chloride flux (moles yr^{-1}) out of one lake and into the next is then:

$$Q_{Cl} = Q_O \frac{10^3 \ell}{m^3} Conc_{Cl} \quad (17)$$

The gross evaporative flux is given by:

$$Q_E = q_E a_w A \quad (18)$$

where q_E is the evaon rate for pure water, a_w is the chemical activity of the lake water, and A is the lake surface area. The back-condensation flux, Q_C, can be related to the gross evaporative flux, the relative humidity, h, and the activity of water by:

$$Q_C = \frac{h Q_E}{a_w} \quad (19)$$

The activity of water is given by (Graf, 1982):

$$a_w = \exp\ (-M_w\ \Phi\ \Sigma\ m_i)\ 10^{-3} \qquad (20)$$

where M_w is the molecular weight of water (g $mole^{-1}$), Φ is the osmotic coefficient for water in the solution, and $\Sigma\ m_i$ is the sum of the molal electrolyte concentrations in the solution. These concentrations were obtained for each time step from the chloride mass-balance subprogram described above. The osmotic coefficient was calculated using a simplified form of equation (11) in Pitzer and Kim (1974).

The isotopic composition of the back-condensation flux can be determined from the equilibrium isotopic enrichment factor (ϵ_v) for the liquid/vapor phase change and the isotopic composition of the atmospheric water vapor (δ_a):

$$\delta_C = \epsilon_v\left(1 + \frac{\delta_a}{10^3}\right) + \delta_A \qquad (21)$$

The equilibrium enrichment factor is a function of temperature alone and was calculated according to Friedman and O'Neil (1977):

$$\epsilon_v = \left\{\exp\left[\left[1.534\ (10^6 T^{-2}) - 3.206\ (10^3 T^{-1}) + 2.644\right]/10^3\right] - 1\right\} 10^3 \qquad (22)$$

Because the degree of fractionation during evaporation is determined by the kinetics of vapor diffusion away from the liquid surface, the ^{18}O of the gross vapor flux (δ_E) is a function of humidity, wind speed, and temperature (Craig and Gordon, 1965). Modification of an expression from Merlivat and Jouzel (1979) was used in the model to take these factors into account:

$$\delta_E = \left[\frac{(1 + 10^{-3}\ \delta_L)(1 - k)}{(1 + 10^{-3}\epsilon_v)\ (1 - kh)} - 1\right] 10^3 \qquad (23)$$

where k is a variable which accounts for both diffusive and turbulent transport of the isotopic species away from the water surface. For the range of wind speeds expected in most continental settings, k may be treated as a constant having the value of 6.8×10^{-3} for $H_2{}^{18}O$ (Merlivat and Jouzel, 1979).

The model solves (9) and then uses the necessary values along with the other calculated parameters to solve (12). It should be noted that $\delta_L = \delta_O$ in the model, based on the assumption that each lake can be treated as a well-mixed system over each time step. The $\delta^{18}O$ value calculated by the model from (12) is the relative isotopic enrichment of the water. Because the isotopic history the model is attempting to match is given as $\delta_{dolomite}$ the water values are converted by first calculating the equilibrium isotopic enrichment factor for water/dolomite:

$$\epsilon_{H_2O,dol} = \left\{ \exp \left[\left((3.2\ (10^6\ T^{-2}) - 4.3)/10^3 \right) - 1 \right] \right\} 10^3 \qquad (24)$$

and then calculating the relative isotopic enrichment of the dolomite:

$$\delta_{dol} = \epsilon_{H_2O,dol} + \delta_{H_2O} \left(\frac{\epsilon_{H_2O,dol}}{10^3} + 1 \right) \qquad (25)$$

MODEL PARAMETERIZATION

Paleo-Owens River System

To calculate lake surface areas, the numerical model requires histories of $\delta^{18}O$ of the inflow, $\delta^{18}O$ of atmospheric humidity, temperature, evaporation rate, precipitation on the lake surfaces, and relative humidity. Obviously, there are no independent histories covering the past 1.2 Myr for each of these parameters in the study area. Consequently, histories for the independent parameters must be estimated by correlation to existing paleoclimatic parameter histories that cover the time period. We know of only two such histories. One is the $\delta^{18}O$ measurements at Searles Lake, and the other is the marine $\delta^{18}O$ record.

Fortunately, an independent basis exists for choosing the appropriate history with which to link the various independent parameters. Winograd et al. (1988) have published a U/Th dated chronology of $\delta^{18}O$ variations in vein calcite from Devils Hole, Nevada. The $\delta^{18}O$ of the calcite reflects ^{18}O variations in the groundwater from which the calcite was precipitated, and thus ultimately the $\delta^{18}O$ of precipitation, probably mostly on the Spring Mountains of Nevada. The most notable feature of this ^{18}O record is the remarkable fidelity with which it mimics the marine ^{18}O record. (We note that Winograd et al. (1988) observed dating discrepancies between their record and the marine one. We assume the discrepancies are due to errors in one or both of the chronologies, but since the differences are within the uncertainties of our chronology, we have not attempted to

resolve them.) The primary control on $\delta^{18}O$ of precipitation is temperature (Dansgaard, 1964) and we take the strong similarity of the Devil's Hole and marine $\delta^{18}O$ records as evidence that the marine $\delta^{18}O$ is a good proxy for temperature in the study area. The similarity is certainly evidence that the $\delta^{18}O$ of precipitation (and thus also the $\delta^{18}O$ of atmospheric moisture) can be reconstructed on the basis of the marine $\delta^{18}O$ record.

In this model, evaporation is parameterized as the difference of the gross evaporation flux and the atmospheric back-condensation flux. The gross evaporation is thus independent of atmospheric humidity and is presumably largely a function of temperature (although the results of Benson (1986) indicate that factors we have not incorporated into the model, such as the cloudiness, also play a significant role). We have therefore linked the (gross) evaporation to the temperature record.

The remaining independent parameter of major significance is the relative humidity. Sensitivity analyses showed that wide variations in humidity are necessary to explain the lacustrine $\delta^{18}O$ data. High humidities were required for the model to produce the observed light $\delta^{18}O$ values, even if all other parameters were favorable. Conversely, low humidities were required to match the observed heavy $\delta^{18}O$ values. We therefore considered that the Searles $\delta^{18}O$ record itself was the best guide to the relative humidity history. This approach is consistent with the basic assumption that lighter $\delta^{18}O$ periods represent favorable water balance (and thus presumably higher humidity) while periods of heavy $\delta^{18}O$ represent unfavorable water balances, and thus lower humidity.

The histories were constructed for all the independent parameters (except humidity) by first establishing a correlation between temperature and the marine $\delta^{18}O$ record, then correlating the other parameters to the temperature history. A linear relation between temperature and $\delta^{18}O$ was assumed and was calibrated by matching the modern mean annual temperature of 19.1^{0}C at Searles to the modern $\delta^{18}O$ of 3.51 per mil, and the late Wisconsin minimum assumed temperature of 12.1^{0}C at 13.6 ka to the corresponding $\delta^{18}O$. The 12.1^{0}C temperature at 13.6 ka is based on a temperature reduction estimate of about 7^{0}C at the late Wisconsin glacial maximum by Dohrenwend (1984), Spaulding et al. (1983), and Phillips et al. (1986).

The correlations of climatic parameters to temperature were obtained by assuming that the ancient correlations of these parameters with temperature correspond to the modern correlation with elevation. Climatic data for stations at different elevations in the region were assembled from Smith (1979), Smith and Street-Perrott (1983), Ruffner (1985), NOAA (1982) University of California (1988) and Meyers (1962). Temperature and the

other climatic parameters were regressed against elevation. The regressions showed good correlations with elevation. The regression "r^2" values ranged from 0.94 to 0.99. The regression plots and equations can be found in Appendix I. The temperature versus elevation, and other climatic parameters versus elevation regressions were then combined to regress the other climatic parameters against temperature.

The assumption that the ancient relationship of temperature with the other climatic parameters, as a function of time, mimics the modern relationship with elevation is obviously at best an approximation. However, it does provide an internally consistent basis for reconstructing the covariation of all climatic parameters. The effect of inadequacies in the reconstruction was assessed by means of a sensitivity analysis, described below.

The calibration of relative humidity to Searles $\delta^{18}O$ was performed using the other parameters obtained as described above. The calibration was accomplished by matching lake surface areas from the model with estimates from times for which there is independent evidence of lake level. The most important calibration points were: 12 to 11 ka, when the lake volume had declined until the lake water was near saturation with halite and the isotopic composition showed evidence of equilibrium; a similar period during the interval 810 to 800 ka; and, the period 15 to 13 ka, when varnish radiocarbon dates show that Searles was overflowing (Dorn et al. 1990) but geological evidence from Panamint Valley indicates only a small lake resulting from that overflow (Smith 1976). The calibration exercise yielded the following relation of humidity to $\delta^{18}O$:

$$h = 135 - 2.2\ \delta^{18}O_{dol} \qquad (15)$$

A sensitivity analysis was performed by varying the slope and intercept of the humidity/$\delta^{18}O$ equation and substituting them into the steady-state lake model. In general, the resultant steady-state lake levels were quite insensitive to the slope and intercept parameters used, so long as the high and low humidities were within certain ranges. Humidities above 50% were required to keep lake levels within reasonable bounds during light isotopic episodes. If humidities fell below 30 percent, the model was unable to yield low levels, even during times when geological evidence showed that desiccation was imminent. However, given that the maximum and minimum humidities were above 50 percent and 30 percent, respectively, additional changes in the humidity/$\delta^{18}O$ relationship produced only small variations in the simulated lake surface areas. The humidity parameterization thus appears to be quite robust.

Lake San Agustin.

Unlike Searles Lake, no good proxy record for continental paleotemperatures exists for west central New Mexico. Without local corroboration, marine ^{18}O records were so geographically distant from the Plains of San Agustin as to render a good correlation problematical. An internally consistent alternative is provided by the ostracode stratigraphy of San Agustin, with the assumption that changes in the proportion of *Limnocythere bradburyi* to the other species of the genus *Limnocythere* are a sensitive reflection of relative changes in temperature (Forester 1985; 1987). Because the modern geographic distribution of *L. bradburyi* and *L. ceriotuberosa* appears to be principally controlled by seasonal variations in water temperature (discussed above), we feel the ostracode biostratigraphy is itself the best available indicator of historic temperature changes.

The temperature history was developed by applying the same 7^0C temperature differential as used at Searles, between the modern mean annual temperature and that from the late Wisconsin glacial maximum. A current mean annual temperature of 9.42^0C was determined using the longest available (9- to 17-year) temperature records compiled by Gabin and Lesperance (1977) for two sites (the Birmingham ranch and the Danley ranch) in the southwestern Lake San Agustin subbasin. By linearly interpolating proportions of *Limnocythere bradburyi* to both *L. ceriotuberosa* and *L. platyforma* over the temperature range of 2.42 to 9.42^0C (that is, 100 percent *L. bradburyi* corresponds to 9.42^0C and 100 percent *L. ceriotuberosa* plus *L. platyforma* to 2.42^0C), a history of estimated mean ostracode life cycle temperature was created for the lower elevations of the Plains of San Agustin basin. A 500-year moving average of the temperature data is illustrated in Figure 37. This chronology was developed principally to incorporate a temperature-dependent fractionation factor into the numerical model, and is not intended to stand on its own merit as a definitive record of absolute paleotemperature. Although we do feel the chronology is a good representation of temperature trends, ambiguities inherent in the data limit its use as an independent proxy for continental paleotemperatures.

In the San Agustin model, as with Searles Lake, gross evaporation is linked to the temperature record. It was necessary to make a similar assumption that a correlation between ancient temperature and evaporation rate with changing climate can be approximated by a modern temperature and pan evaporation rates for altitudinally-varied sites across western New Mexico. Applying a pan coefficient of 0.70 to convert to lake evaporation, the following regression relationship was established between lake evaporation and temperature:

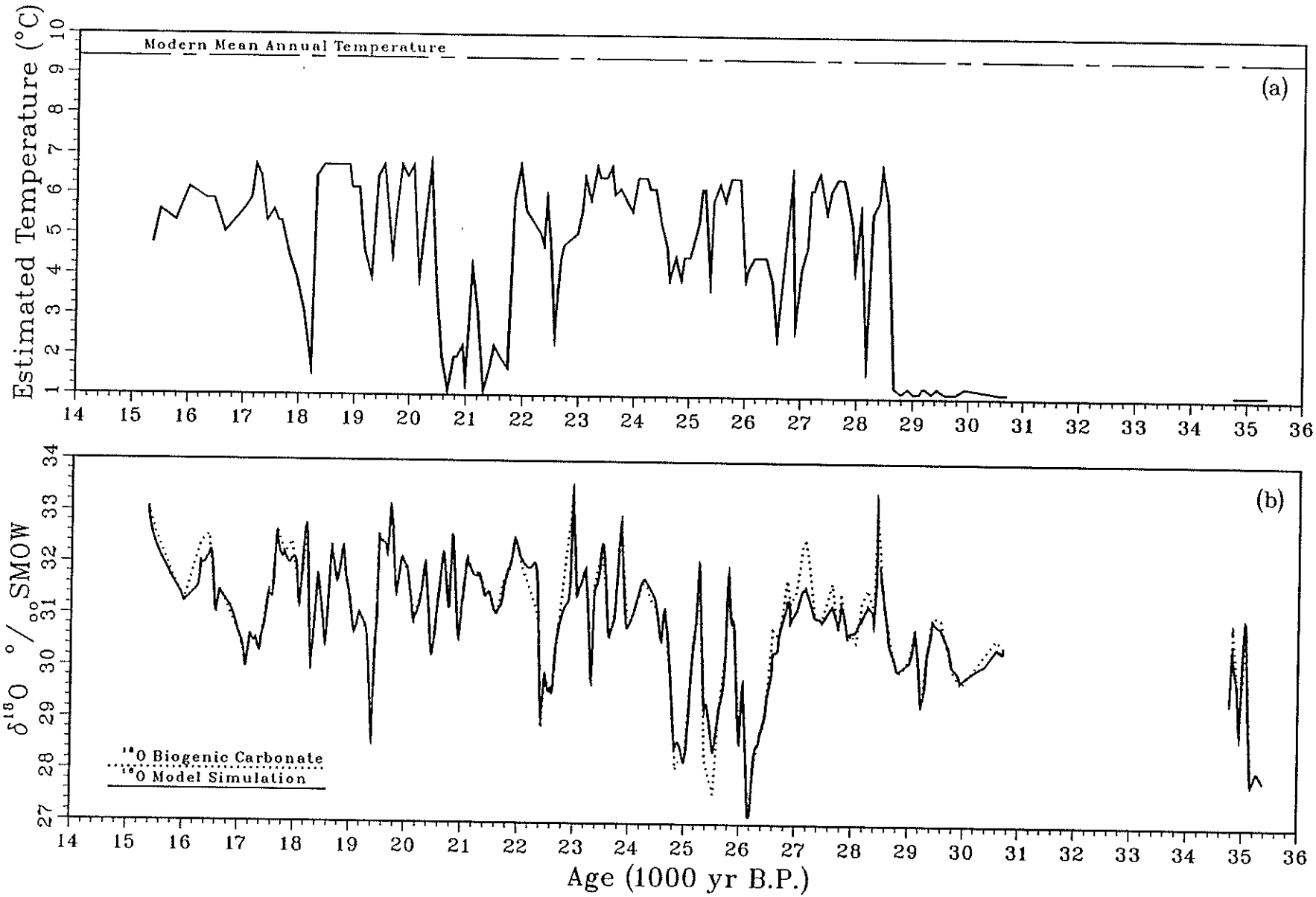

FIGURE 37. (a) Chronology of estimated mean annual temperature for the plains of San Agustin developed from the ostracode biostratigraphy and plotted as a 500-year moving average (b) comparison of measured $\delta^{18}O$ of ostracode carbonate as a function of time with $\delta^{18}O$ simulated by numerical model

$$q_E = 0.06567\ T + 0.65924 \qquad (26)$$

The equation has a squared correlation coefficient of 0.60458. The regression plot and equation data can be found in Appendix R.

As with the Searles Lake model, the most accurate reflection of the humidity record in the San Agustin basin was the ^{18}O record itself. By applying a similar calibration technique of varying the slope and intercept of a humidity/$\delta^{18}O$ regression equation, and substituting the relationship into an analytical steady-state model, it was discovered that both high lake levels (light isotopic episodes) and low lake levels (heavy isotopic episodes) could be matched with the following relation of humidity (in percent) to $\delta^{18}O$:

$$h = 262 - 7\ \delta^{18}O_{cal} \qquad (27)$$

This regression relationship yields maximum and minimum humidities of 72 percent and 30 percent.

In modeling the water balance for the San Agustin basin, we have lumped all inflow parameters into one inflow flux, which is the independent parameter for the model. Because lake/groundwater interactions are a major control on lake level, groundwater inflow is a significant component of the inflow flux, with precipitation on the lake surface and direct runoff constituting short-term inflow components. Variation of the ^{18}O composition of this inflow water with time is a required input for the model. An estimate of the variation in $\delta^{18}O$ of precipitation and groundwater recharge in the San Juan Basin (northwest New Mexico) over the last 35,000 years has been developed by Phillips et al. (1986b). This $\delta^{18}O$ history should also be a reasonably accurate representation of the ^{18}O composition of precipitation- and runoff-derived inflow, as well as groundwater inflow, for the San Agustin basin a short distance to the south of the San Juan Basin.

The remaining parameter (not incorporated in the Owens River system model) is the groundwater outflow flux. The paleohydrologic environment in the San Agustin basin, as discussed earlier, is known to include a substantial component of groundwater seepage from the basin. This outflow component must be incorporated into the model.

First, to determine the importance of transient effects in lake/aquifer interactions, the analytical solution to the one-dimensional hydraulic diffusion equation, with a sinusoidally fluctuating boundary condition, was evaluated using aquifer parameters estimated for the regional flow system. Mathematical manipulation of the solution yields an expression

for the time lag between a lake-level fluctuation and the aquifer response given by:

$$t_L = x\ ((t_0 S/4\ T)^{\frac{1}{2}}) \qquad (28)$$

where x is the distance into the aquifer at which the response is evaluated (1 km in this case); t_0 is the period of the sinusoidal lake fluctuation in years; S is aquifer storativity; and T is aquifer transmissivity. For a 200-year period sinusoidal input function, a range of storativities of 10^{-1} to 10^{-4}, and a range of hydraulic conductivities of 10^{-4} to 10^{-8} m/s, the time lags of the aquifer response at 1 km vary from about 0.045 years to 142 years. Because the estimated values for this "time constant" fall below or near the average time span of our sampling interval (105 years), we have considered the regional transient effects associated with lake/groundwater interactions to be negligible.

The problem remaining is to develop a steady-state relationship which will describe the groundwater seepage from the lake basin. By using the modern regional hydraulic gradient of 0.0054 (Blodgett and Titus, 1973), assuming this gradient remains constant (i.e., that fluctuations in lake level have a negligible effect on the regional gradient), and applying an estimated hydraulic conductivity of 10^{-6} m/s (an average value for fractured volcanics and silty sand), Darcy's law gives a volumetric outflow flux which is linearly related to lake area: $Q_{GW} = 0.17A$. Although this relationship provided a reasonable "first guess," we discovered that the model simulations were heavier isotopically than the measured data by an average 1.5 $^{0}/_{00}$. Considering the uncertainty in estimating the aquifer parameters vis-a-vis the climatic parameters, it was reasonable to calibrate the model by varying the groundwater outflow function.

Lake surface area fluctuations developed numerically from the ^{18}O chronology were constrained by geologic data from San Agustin shoreline and sediment records. The highest shoreline mapped by Powers (1939), located at 2115 m (6940 ft), is generally accepted as the highest lake stage during mid-to-late-Wisconsin. This lake level, corresponding to a lake surface area of 780 km^2, provided the approximate upper limit for lake levels simulated by the model. A shoreline located at 2110 m (6920 ft) with a ^{14}C date (on tufa) of 21,400 ±300 yr B.P. (Markgraf, V., personal communication, 1989) further constrained the lake surface area to 700 km^2. The sediment

record from core SAC3-4 provided additional constraints in the time interval from 35,000 to 25,000 yr B.P. In addition, the groundwater outflow flux was used as an internal calibration factor to help simulate transient effects. Because the outflow flux will increase with lake level and higher hydraulic heads, the flux was varied between 0.34*Area and 0.15*Area, depending on simulated lake levels.

The actual groundwater outflow flux is clearly a nonlinear function of lake level which cannot be accurately determined without a transient, distributed parameter lake-aquifer model. Our approach is a simplistic attempt to simulate this nonlinearity and we believe it to be the most reasonable alternative available. The technique cannot, however, fully accommodate local transient effects manifested in bank storage. Storage of water in, and release of water from, sediments peripheral to the shoreline constitute a major component in lake/groundwater interactions. This bank-storage effect further complicates the groundwater outflow flux by making it a function of the rate of lake level change in addition to absolute lake level. Accordingly, the solutions obtained by our model for lake surface area and inflow are not unique. The solutions are probably good approximations as the bank-storage effect is significant only during episodes of rapid lake level fluctuations.

MODEL IMPLEMENTATION

The initial inflow history used to "drive" the transient model was derived using a FORTRAN code, SS.FOR (Appendix O). In the main routine, this steady-state model sequentially calculated the surface area of $\delta^{18}O$ for each lake in the system. Using nested DO loops to iterate selected input variables, specifically inflow (Q_i), temperature (T), and humidity (h), $\delta^{18}O$ and surface area were calculated as function of these "possible solutions" as a 3-D array and a search through the array was implemented to back-calculate Q_I. Simulations were performed using variable temperatures and also constant high and low temperatures to provide sensitivity analysis.

Three parameters were entered at the start of the program: the chemical activity of the water (a_W), a starting value for Q_I, and an ending value for Q_I. a_W was assigned a value of 1.0, the activity of pure water, to simulate non-saline conditions, and a value of 0.761, the activity of halite saturated water, to simulate saline conditions. It should be noted that the variable a_W was used only in the Searles Lake calculations. The implicit assumption was, therefore, that a_W was a constant with a value of 1.0 for all other lakes in the system. For the variable temperature steady-state simulations, the starting and ending values for Q_I were 4.0×10^7 and

5.0×10^9 m^3 yr^{-1}, respectively. These values were increased by approximately half an order of magnitude for the constant high-temperature simulations and decreased by the same amount for the constant low-temperature simulations. Diagnostics written to files along with the output aided in calibrating the inflow ranges. If the range of input values used for Q_I was such that the steady-state model could not match the simulated possible solutions to the actual Searles Lake histories, error messages were obtained.

The outermost FORTRAN DO loop iterated temperature. For the variable temperature simulations, the temperature at Owens Lake was varied from 6.5°C. The corresponding temperature for both China and Searles lakes was 3.6°C higher. The temperature at Panamint Lake was calculated by adding 2.35°C to the Searles Lake temperature and the temperature at Lake Manly was 4.08°C higher than at Panamint Lake. For the constant low and high temperature simulations, the temperatures at Owens Lake were 7.7 and 15.2°C, respectively. Temperature variations between lakes were the same as those given above. The next DO loop nested within the temperature loop incremented Q_I. For the range of Q_I entered at the beginning of the program, this loop divided that range into 100 equal increments. The innermost DO loop was used to increment humidity from 30 percent to 90 percent in 1 percent steps. For a given interaction, the humidity values for all the lakes were the same.

The first parameter calculated in the steady-state model were those assumed to be a function of temperature. These included the isotopic compositions of the inflow (δ_I), the atmospheric water vapor (δ_A), and the precipitation (δ_p), as well as the precipitation (q_p) and evaporation (q_E) rates. q_E for all lakes was not allowed to be less than 1.35 yr^{-1}. All parameters were calculated as linear functions of temperature using regressions described in the MODEL PARAMETERIZATION section above.

The isotopic composition of the back-condensation flux (δ) was then determined from (21), and the equilibrium enrichment factor was calculated using (22). The kinetic isotopic enrichment factor was calculated as:

$$\epsilon_k = \left[\left(\frac{\alpha_v(1-kh)}{1-k}\right) - 1\right] \quad 10^3 \qquad (29)$$

where α_v, the isotope enrichment factor, is related to ϵ_v by:

$$\alpha_v = 1 + \frac{\epsilon_v}{10^3} \qquad (30)$$

Surface area was given by:

$$A = Q_I \left[q_E \left(\frac{1-h}{a_W} \right) - q_P \right]^{-1} \quad (31)$$

The steady-state model then determined fluxes for the different parameters. Gross evaporation flux was given by:

$$Q_E = q_E \quad A \quad a_W \quad (32)$$

the precipitation flux was given by:

$$Q_P = q_P \quad A \quad (33)$$

and the back-condensation flux was:

$$Q_C = Q_E \quad \frac{h}{a_W} \quad (34)$$

When the steady-state model was run, the range of inflow values were adjusted so that the first two lakes in the system, Owens Lake and China Lake, were always at overflow. The lakes were determined to be at overflow when the calculated surface area was greater than the maximum surface area as determined by the bathymetric data. The relative isotopic enrichment of the lakes at overflow was calculated as:

$$\delta_{H_2O} = \frac{Q_I \delta_I + Q_P \delta_P + Q_E \ (h\delta_c + a_w + \epsilon_k)}{Q_I + hQ_E + Q_P} \quad (35)$$

Searles Lake, however, was not always overflowing. For non-overflow conditions, the $\delta^{18}O$ of the lake was given by:

$$\delta_{H_2O} = \frac{Q_I \ \delta_I}{Q_E} + \epsilon_k + h \ \frac{\delta_C}{a_W} + \frac{Q_P \ \delta_P}{Q_E} \quad (36)$$

These $\delta^{18}O$ values were the relative isotopic enrichment of the water. Because isotopic water values were converted by first calculating the equilibrium isotopic enrichment factor for water/dolomite using (24) and

then calculating the relative isotopic enrichment of the dolomite from (25). The flux out of one lake into the next was calculated using (16). At various times during the modeled history, Searles Lake would exceed a critical volume (65.87×10^9 m^3) and couple with China Lake, forming one lake. During these periods the outflow from Owens Lake became the inflow for Searles Lake and there was essentially no China Lake.

The above equations were used to calculate $\delta^{18}O$ and surface area for each lake in the system for each iteration, I, of the temperature DO loop, J, of the Q_I DO loop, and k, of the humidity Do loop. At the end of each interaction, the $\delta^{18}O$ of Searles Lake and total surface area of the system were saved in 3-D FORTRAN arrays as functions of these variables, that is $A(Q_I(I), T(J), h(K))$, and $\delta(Q_I(I),T(J),h(k))$. After this process was completed, the steady-state model read the data files containing the temperature ($T_{Searles}$), humidity ($h_{Searles}$), and $\delta^{18}O$ ($\delta_{Searles}$) histories for Searles Lake. For a specific point in time, $h_{Searles}$ was compared with each h(K) until a match was found and likewise with $T_{Searles}$ matched $\delta(T(I),Q_I(J),h(K))$. $Q_I(J)$ was then saved as the inflow value for that time. The corresponding surface area for the system was given by $A(T(I),Q_I(J),h(K))$.

This process was used to generate three inflow histories for input for the transient model; a variable temperature history, a constant high temperature history, and a constant low temperature history. The variable temperature inflow history was used as the initial "guess" for the actual transient modeling. The constant temperature histories were used for sensitivity analysis. When the steady-state model was run with a constant temperature, all the parameters assumed to be a function of temperature, also became constants, that is, δ_I, δ_A, δ_P, q_P, and q_E. This enabled testing the sensitivity of the model to the assumed histories for the above parameters.

Each of the three histories was generated in two parts. By varying a_W, the steady-state model could be used to simulate both low lake levels (saline conditions) and high lake levels (non-saline conditions). For each of the temperature histories, the model was run once with $a_W = 1$, the activity of pure water, and once with $a_W = 0.761$, the activity of water at halite saturation. The final history was constructed by substituting Q_I values from the saline history into the non-saline history when geologic evidence showed that Searles Lake was at or near chloride saturation.

The transient modeling was performed using a numerical lumped-parameter code, TRANSISO, written in FORTRAN (Appendix M). The code solves (9) and (12) for each time step of the stimulation using the Runge-Kutta-Fehlberg (RKF) difference-equation method (Burden and Faires 1985). Results of the simulation are displayed along with the actual histories in graph form for visual evaluation.

The main program first reads three files, OWENS.IMP, C_S.IMP, and P_D.INP. These files contain initial values for parameters necessary to begin and control the simulation. The file OWENS.INP contains the Owens Lake parameters, China Lake and Searles Lake parameters are contained inC_S.INP, and Panamint and Lake Manly (Death Valley) parameters are found in P_D.INP. Contained in these files are values for maximum reactions, lake volume (m^3), $\delta^{18}O_{Dolomite}$, maximum time step, minimum time step, lake volume tolerance, $\delta^{18}O$ tolerance,and chloride concentrations (moles ℓ^{-1}).

Maximum iterations refers to the number iterations the RKF subroutine is allowed to use while solving (9) and (12) over the designated simulation period. The RFK subroutine calculates and constantly changes the step size used by the program while solving the differential equations. The number of interactions necessary to simulate a designated block of time is therefore not known in advance. To prevent overflow of the solution arrays, the maximum number of iterations must be limited. Values used have been 6,000 for Owens Lake and 25,000 for China Lake and Searles Lake. The logic used in assigning these values involves an "optimization process," that is, allowing enough iterations of the RKF algorithm to simulate the entire designated time period but not allowing so many as to allow overflow of the solution arrays. Both array sizes and number of iterations must be limited to maintain a reasonable file.

Lake volume is entered in units of m^3. Particular care should be taken when entering the interpreting volumes for China Lake and Searles Lake. A zero volume for China Lake may mean that China Lake is dry, or the volume for Searles Lake is greater than or equal to 65.87 m^3 and the two lakes have coupled. If the Searles volume at the start of the simulation is greater than or equal to 65.87 m^3, the model will automatically assign a volume of zero to China Lake regardless of the number that is entered. $\delta^{18}O$ values should be entered as $\delta_{Dolomite}$. All of the modeling calculations, however, use δ_{H_2O}. The final values are then converted to output as $\delta_{Dolomite}$ to allow comparison to the Searles $\delta^{18}O$ history.

Maximum and minimum time step are the limits imposed on the RKF step-size calculations. If the maximum step size is too large, the program may use a large number of iterations reducing the step size to control the

error in the calculated derivative. The minimum step size need not be unreasonably smaller or again iterations may be wasted. It must, however, by small enough to allow the RKF algorithm to iterate to a solution when the derivative is changing rapidly. The maximum and minimum time steps used when modeling Owens Lake were 250 and 10 years, respectively. The corresponding values for the China Lake and Searles Lake system were 100 to 0.1 years. These smaller values were used because, given its "pancake" bathymetry, China Lake tended to experience relatively rapid volume and $\delta^{18}O$ fluctuations.

Lake volume tolerance and $\delta^{18}O$ tolerance are the maximum error size allowed in the calculation of the corresponding derivative. If these limits are too restrictive, the simulation will be solved in an unreasonably small time step. The RKF algorithm will not iterate to a solution, however, if these limits are restrictive enough. When the calculated error exceeds the tolerance, the RKF routine decreases the step size to reduce the error. Values for these parameters were determined by observing the errors calculated by the model during actual simulations. The lake volume tolerance was set at $5x10^{3}$ and the $\delta^{18}O$ tolerance was set at $1x10^{-3}$. Chloride concentration is the concentration entered as moles per liter at the beginning of the simulation.

At the start of each simulation, the default value for each of these eight parameters is the value assigned in the previous simulation. The model then prompts the user, asking if changes are to be made. Final values for each parameter are displayed at the end of the simulation. These values should then be input at the start of the next simulation if the modeling is to continue from that point.

To match the chloride deposition history at Searles Lake, a beginning value for the mass of chloride deposited per square meter at KM-3 must be entered at the start of each simulation. This value is usually taken from the output of the previous simulation or from the actual depositional history, depending on the particular simulation. All the chloride deposited over the course of the simulation is then added to this initial value. The default value for this parameter is zero.

The model allows the user to choose from a variety of inflow functions. Possible choices include the following simple functions; linear, exponential, logarithmic, power, sinusoidal, step, and zero inflow. The user may also choose from among three steady-state derived histories. These include a variable temperature history. Constant high temperature history was derived using a steady-state model (SS.FOR) and has been previously described in this section. The constant temperature histories are to be used in conjunction with the constant parameter option. If one of the

constant temperature histories is chosen, the constant parameter option should be used. Three constant parameter options are available and are prompted for in the model: UPPER LIMIT, to be used with the constant low temperature history; and CUSTOM, which may be used with either. The UPPER LIMIT and LOWER LIMIT options read values for temperature, precipitation, gross evaporation, and δ_A, δ_I, and δ_P from existing data files. Derivation of the values in the LOWER LIMIT and UPPER LIMIT files was described in the steady-state modeling section. The CUSTOM option allows the user to input the values for these parameters from the terminal. If the variable temperature inflow history is chosen, the values for the corresponding parameters are read from the data files. Unique data files exist for Owens Lake, Panamint Lake, and Lake Manly. Searles Lake and China Lake, however, share history files. Sensitivity analysis show that wide variations in relative humidity are necessary for the model to match the Searles $\delta^{18}O$ data. For this reason, humidity is not treated as a constant during the constant temperature simulations. A single humidity history is used for all lakes.

Values for parameters necessary to restart the modeling process may be saved at any point during a simulation. The model prompts for this option, asking for the number of restart points desired and corresponding times. This feature is useful for "fine tuning" the end of a simulation without having to rerun the entire simulation.

The remaining parameters necessary to begin a simulation are a beginning and an ending time. These should define a continuous block of time over which the simulation is to proceed. Present day is designated as time 0 and any positive number represents a corresponding number of years in the past. For example, to model from ten thousand years in the past to the present, 1×10^4 would be entered for the beginning time and 0 would be entered for the ending time.

To proceed with the modeling, the main program first calls the RFK subroutine. The subroutine solves (9) and then (12) for Owens Lake for each time step of the numerical simulation. Intermediate values for (9) and (12) are calculated at six different points within a given time step in a function subprogram, F(t). Each derivative is calculated first at the beginning of the time step, then at points 1/4, 3/8, 12/13, at the end, and 1/2 of the way through the time step. Using these intermediate values, the RFK subroutine determines whether calculating dV/dt and $d\delta/dt$ over the current step size will result in a unacceptably large error. If the calculated error is greater than the designated tolerance, the RKF subroutine incrementally decreases the step size within the given limits. If after the step size is decreased the error becomes less than than the

tolerance, the results are written to any array and the process moves forward. At the end of a successful iteration, the subroutine will increase the step size, attempting to speed the simulation process.

The RFK algorithm assumes the function to be differentiated is continuous. Unfortunately, volume calculated as a function of time, VOL, contains two singularities. These occur at the points where the lake desiccates or exceeds maximum volume and begins to overflow. To avoid simulating across these singularities, a logical variable, ZEROCHK, is used to detect their approach and allow the model to "step across" the singularity. If the calculated volume at any of the six intermediate points within the time step is zero and the step size is the minimum allowable step size, ZEROCHK is set to TRUE. When ZEROCHK is TRUE, the model sets the volume to zero without calculating an error and comparing it to the tolerance as would normally be done. In this way, the solving routine comes as close to the singularity as the minimum step size will allow while preventing the model from "crashing" at the singularity.

When the calculated lake volume exceeds maximum volume as determined by bathymetric data, dV/dt is zero and the lake begins to overflow. At this point, however, potions of the model are "lied to", that is, dV/dt is not allowed to equal zero. The RFK subroutine solves (9) and from that result, calculates a new volume. Because dV/dt is not set to zero, this volume grows beyond the known maximum volume as long as the derivative is positive. The volume written to the solution array, however, is the known maximum volume. When the calculated derivative becomes negative, the lake volume is reduced. By doing this, the part of the model that solves (9) "sees" the function as continuous. The excess volume at the end of each time step is the amount of water that flows into the next lake over that time step. In reality, dV/dt would be zero when the lake begins to overflow. Because the term dV/dt is found in (12), the portion of the model that calculated (12) is "told" that dV/dt is zero as long as the calculated volume indicates that the lake is at overflow. This continues until the calculated volume is less than the maximum volume.

The parameters necessary to solve (9) and (12) at the intermediate points within the time step are calculated in the function subprogram F(t). This function first determines values for δ_I, δ_P, δ_A, temperature, evaporation, and precipitation at a designated point in time, t. If the simulation is being run with constant parameters, these values have already been assigned in the main program. For variable temperature simulations, these values are calculated by interpolating linearly between data points in the histories read in the main program. These histories are read as 1-D arrays, and each value of a particular parameter has a corresponding time

array element, (for example, $\delta_p(40)$ corresponds to time(40)). The subroutine FINDT is used to determine where the current time, t, lies in relation to the time array elements. Using a binary search routine, the subroutine may find, for example, that t is between time(40) and time(41). This in turn means that the current value of δ_p is between $\delta_p(40)$ and $\delta_p(41)$ and likewise for the other parameters. The values for these parameters are then calculated by linear interpolation in the subroutine OINTERP. Because the humidity history and inflow history have unique chronologies, this process is repeated using two subroutines, FINDHT and HUMTERP, for humidity, and two subroutines, FINDQT and QINTERP, for inflow. The current surface area of Owens Lake is calculated in the subroutine OAREA, which uses bathymetric data to convert a given volume to surface area. As explained above, this volume (VOL) may exceed the known maximum volume (VOLMAX), indicating that the lake is overflowing. The volume of water (m^3) that flows out of Owens Lake during the time step is: V_{out} = VOL-VOLMAX. The precipitation flux, Q_p, is given by (33).

The next parameters calculated relate to the chloride mass balance. The total moles of chloride (CL) in Owens Lake at the start of a time step is either given at the beginning of the simulation (for the first time step) or known from the last point solved in the RKF subroutine. The model must then calculate the total moles of chloride (TCL) at points 1/4, 3/8, 12/13, at the end, and 1/2 of the way through the time step. The total moles of chloride at each of these points is given by:

$$TCL = (OTIME-t)\ QCL + CL - V_{out}\ \frac{10^3 \ell}{m^3}\ CONC_{CL} \qquad (37)$$

where OTIME is the time at the beginning of the time step, t is the time at each intermediate point, QCL is the chloride flux (1.67×10^8 moles yr^{-1}) into Owens Lake, and $CONC_{CL}$ is the chloride concentration (moles ℓ^{-1}) at the beginning of the time step. If the chloride concentration at any time t within the time step exceeds 6.1 moles ℓ^{-1}, the model sets the concentration at 6.1 moles ℓ^{-1}. This would indicate that halite precipitated at that time. Geological evidence indicates that no halite was precipitated in Owens Lake during the time period covered by the modeling. Chloride saturation in Owens Lake should therefore not exceed 6.1 moles ℓ^{-1} during a successful simulation.

The chemical activity of water is given by (20). The function subprogram FPHI, which calculates Φ, the osmotic coefficient for water, was adapted from Pitzer and Kim (1974). It should be noted that this routine

has been modified to work with only sodium chloride. Q_E is given by (18) and Q_C is given by (19). The isotopic enrichment factor, ϵ_v, is calculated in the function subprogram FEPS using (22). The del of the back-condensation is given by (21). The del of the evaporation is calculated in the function subprogram DELE using (23). Equations (9) and (12) are then solved and these values are returned to the RKF subroutine.

Once the Owens Lake simulation is complete, the process is repeated for China Lake and Searles Lake using the subroutine RKF_CS and the function subprogram F_CS. Because these lakes couple and decouple over time, they must be simulated simultaneously. If China Lake and Searles Lake are coupled, the flux out of Owens Lake is the flux to Searles Lake. Inflow into China/Searles is calculated by linearly interpolating between outflow data points saved as an array, OQO, during the Owens simulation. This linear interpolation process is the same as that previously described. The chloride flux out of Owens is saved in the array TIMECL_IN. Chloride flux into China/Searles is also calculated using linear interpolation.

The transient model was not used to simulate periods of chloride deposition at Searles Lake, but it does contain a correction factor which aids in this process. The chloride deposition history for Searles Lake was derived from analysis of the KM-3 core. After developing a chronology for the core, chloride analysis was used to produce a table of cumulative chloride versus age/depth (Jannik 1989). A small part of this chloride can be attributed to brine which soaked the core during drilling. This chloride was therefore not actually precipitated as halite from Searles Lake, but it does appear in the history. To account for this added chloride in the history, the model deposits a small amount of chloride over each time step regardless of the chloride saturation in Searles Lake. The calculated correction factor, SLTCONST, is 1.27×10^{-2} kg m^{-2} yr^{-1}. The actual chloride history-matching process is described later in this section.

Equation (10) and (12) are not used in the Panamint Lake and Lake Manly simulations. $\delta^{18}O$ histories are not simulated for Panamint Lake or Lake Manly. These lake areas are calculated in the subroutine RKF_CS in the following manner. PDINTERP is a linear interpolation subroutine used to calculate evaporation rates from histories read in the main program. When the evaporation rate is determined, the surface area for each lake is given by:

$$A = \frac{Q_I}{q_E} \tag{38}$$

The final calculation in the transient model is the calculation of total surface area for the paleo-Owens River system. This is done by finding the change in surface area over the current time step for each lake. This change is added to the previous surface area and the surface areas are then summed.

The transient modeling using the variable temperature history was begun at 1.18 Ma. Because the model is not sensitive to initial conditions, the starting parameters were chosen arbitrarily. Owens Lake and China Lake were both at overflow and the δ values were 25 $^{0}/_{00}$ and 32 $^{0}/_{00}$, respectively. The starting volume for Searles Lake was 65 x 10^{9} m^{3}, and the δ value was 32 $^{0}/_{00}$. Chloride concentration for each of the three lakes was set at 2.0 x 10^{-4} moles/liter. Both Panamint Lake and Lake Manly were dry at the start of the simulation.

To guide the modeling process, a table detailing the salt deposition history at Searles Lake was used (Appendix 7 in Jannik 1989). The transient modeling was performed in discrete blocks, simulating intervals between these tabulated periods of salt deposition, that is, intervals during which the model could match the Searles isotopic history. Starting with the "initial guess" inflow values, adjustments were made until the transient model output matched Searles ^{18}O values and the modeled lake was at or very near halite saturation (6.1 moles/liter) immediately preceding a known period of salt deposition. If Searles Lake was not quite at saturation at the end of the simulation period, the volume at saturation was calculated by:

$$VOL_{SAT} = VOL_{END} \times \frac{CONC_{END}}{6.1 \frac{MOLE}{\ell}} \qquad (39)$$

where VOL_{END} and $CONC_{END}$ were the volume and chloride concentration output by the transient model at the end of a simulation period.

Periods of salt deposition were not modeled with the transient code. Simple mass balance calculations were done by hand and the volume of Searles Lake was adjusted accordingly, giving the starting parameters for the next non-depositional period. The tabulation of salt deposition history gave the observed salt deposition ($SALT_{OBS}$) at the KM-3 core site in Searles Lake and also the length of the depositional episode (Δt). The mass of salt per square meter that flowed in during the depositional period was calculated by:

$$SALT_{INFLOW} = \Delta t \times 0.19 \frac{kg}{m^2 yr} \quad (40)$$

where 0.19 kg m^{-2} yr^{-1} was the average chloride accumulation rate at KM-3 (Jannik 1989). The additional mass of salt per square meter necessary to match the observed salt deposition at KM-3 was given by:

$$SALT_{ADD} = SALT_{OBS} - SALT_{INFLOW} \quad (41)$$

If $SALT_{ADD}$ had a positive value, VOL_{SAT} was decreased by the amount necessary to precipitate the mass of salt per square meter equal to $SALT_{ADD}$. If $SALT_{ADD}$ had a negative value, VOL_{SAT} was increased by the amount necessary to accommodate the mass of salt equal to $SALT_{ADD}$ and remain at halite saturation. Because salt was not deposited evenly over the Searles playa, an additional conversion was necessary to determine the mass of salt that would be deposited per square meter at KM-3 for a given volume of Searles Lake at halite saturation. This conversion was calculated by:

$$SALT_{CORR} = \frac{\frac{0.19 \text{ kg}}{m^2 \text{ yr}}}{\frac{6.7 \times 10^6 \text{ kg}}{\text{yr}}} = 3.22 \times 10^{-8} m^{-2} \quad (42)$$

where 6.7×10^6 kg yr^{-1} was the approximate chloride load of the Owens River over the past 20 kyr (Smith 1976). The new volume (m^3) was given by:

$$VOL_{NEW} = \frac{SALT_{ADD}}{\frac{1000 \ell}{m^3} \frac{6.1 \text{ moles}}{\ell} \frac{35.435 \text{ g}}{\text{mole}} \frac{1 \text{ kg}}{1000 \text{ g}} SALT_{CORR}} \quad (43)$$

VOL_{SAT} was changed linearly over Δt such that VOL_{SAT} equaled VOL_{NEW} at the end of the depositional period.

To start the transient model at the beginning of the next simulation period, it was necessary to input values for volume, chloride concentration, and δ_{WATER} for Owens, China, and Searles lakes. These values for Owens and China lakes were taken from the final output for the previous simulation period. The starting volume for Searles Lake was VOL_{NEW}, chloride

concentration was set at 6.1 moles/liter, and δ_{WATER} was the final value from the previous simulation. Searles Lakes surface area was calculated from VOL_{NEW} using bathymetric data. A simplified version of the steady-state model was used to calculate a value for Q_I that was in equilibrium with VOL_{NEW}, allowing the simulation to begin under stable conditions.

In addition to the modeling described above, the transient model was also used to investigate the system response to variations in the inflow frequency. To ensure that the observed responses were due only to variations in the inflow, the model was run with constant parameters until equilibrium was achieved. Starting with a constant inflow (B) of 9.43×10^7 m^3 yr^{-1}, the change in inflow with time was given by:

$$Q_I = B + A \text{ SIN } (C\ t) \qquad (44)$$

where A, the amplitude, was 2.82×10^7 m^3 yr^{-1}, C was the designated frequency, and t was time. Analysis of the signal response showed that the lag time for the $\delta^{18}O$ response increased from 24 to 70 years as the inflow period ($2\pi/C$) increased from 90 to 675 years. As the period increased from 675 to 9000 years, the $\delta^{18}O$ lag time decreased linearly from 70 to -565 years. The negative lag time indicated that the $\delta^{18}O$ equilibrated prior to the lake volume equilibration.

The amplitude of $\delta^{18}O$ response increased from 0.125 to 0.85 $^0/_{00}$ as the inflow period increased from 90 to 1575 years. As the inflow period increased from 1575 to 9000 years, the amplitude of the $\delta^{18}O$ response decreased from 0.85 to 0.5 $^0/_{00}$. Dependence of the lag and amplitude on frequency is shown in figure 38a.

The system response to a step change in inflow is shown in figure 38b. The calculated response time was approximately 900 years, which is greater than the average spacing of the data points in the Searles $\delta^{18}O$ history. This would indicate that all major changes in the stage of the system would be represented in the present $\delta^{18}O$ history.

SENSITIVITY ANALYSIS

One goal of this study was to compare the lake surface-area history of Searles Lake with the marine ^{18}O record. Use of the marine ^{18}O record itself to parameterize the temperature history of the model (and, through regression equations, most of the other environmental parameters of the model) introduces a serious concern of biasing the model output in the direction of forcing it to mimic the marine record. To quantify the degree to which the assumed temperature history influenced the model output, we

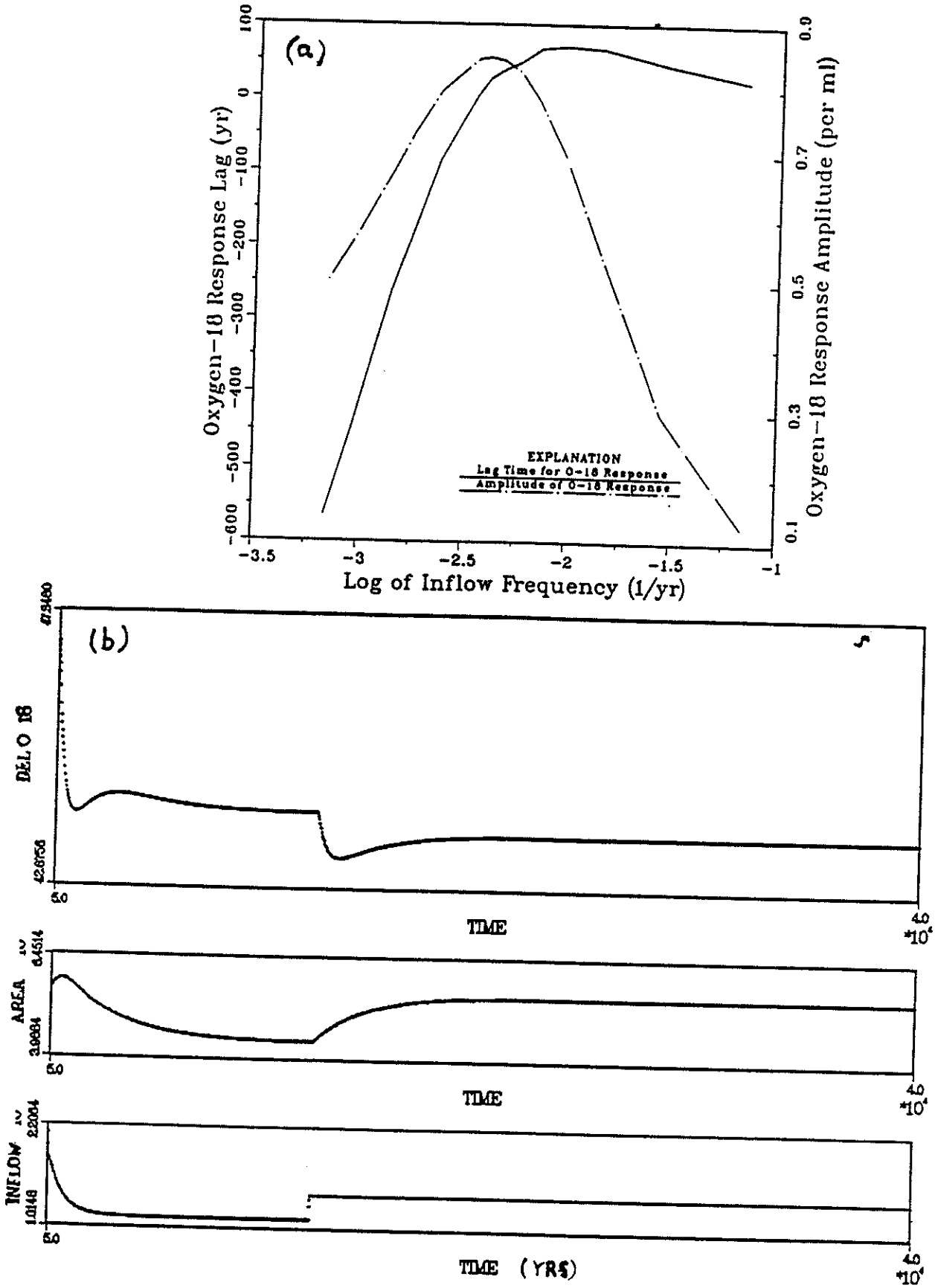

FIGURE 38. (a) Variation in time lag of $\delta^{18}O$ response, and response amplitude, for sinusoidal inflow variations (b) Illustration of Searles Lake volume and lake $\delta^{18}O$ response for a step-function change in inflow

conducted a sensitivity analysis for the interval 0.97 to 1.13 Ma. This interval was selected because it was one of the longest in the lake record without evaporite precipitation, and thus over which the surface area history could be considered only by the $\delta^{18}O$ data.

Over this interval the $\delta^{18}O$ data were matched by simulated values using three different temperature histories: a constant value of 19.1^0 C (high temp), variable temperatures linked to the Williams et al. (1988) stacked marine ^{18}O record (variable temp simulation), and a constant value of 12.1^0C (low temp). The high temp and low temp values correspond approximately to the extreme maximum and minimum temperatures calculated by the variable temp equation over the lake history. The match of the three simulated ^{18}O histories to the data are illustrated in Figure 39. The model lake surface area outputs for the three histories are shown in Figure 40. Given that the temperature histories represent the extremes actually expected over the lake history, the variation between the three simulations is remarkably small. The standard deviation of the lake surface areas produced by the variable temp simulation is 255 km^2, while the standard deviation of the residuals of the high temp and low temp simulations (relative to the variable temp) are 82 and 81 km^2, respectively. In other words, the residuals average only about 32 percent of the simulated lake area variation, and 5.1 percent of the mean simulated lake area.

In addition to the sensitivity magnitude of the simulations to the temperature history, we were also concerned about the timing of the residuals. In figure 41 we show a spectral analysis of the coherency of residuals (between the two constant temp simulations and the variable) and the Williams et al. (1988) marine ^{18}O record used to generate the variable temp history. Significant coherency between the two would demonstrate that the input history was biasing the mode output. As figure 41 shows, there is no coherency at significant levels.

Analysis of the magnitude and the timing of the residuals indicates that the numerical model is surprisingly robust with respect to the input temperature history. On the other hand, examination of the inflow histories for the different temperature scenarios (not illustrated in this report) shows that the inflow estimation is not similarly robust. The reason for the robust surface area estimation can be seen by comparing the governing differential equations for isotope mass balance and water mass balance (1 and 2). The surface area and the δ_L terms occupy analogous positions in the two equations and thus simulations calibrated to the isotope history will tend to compensate for differing temperature histories by requiring

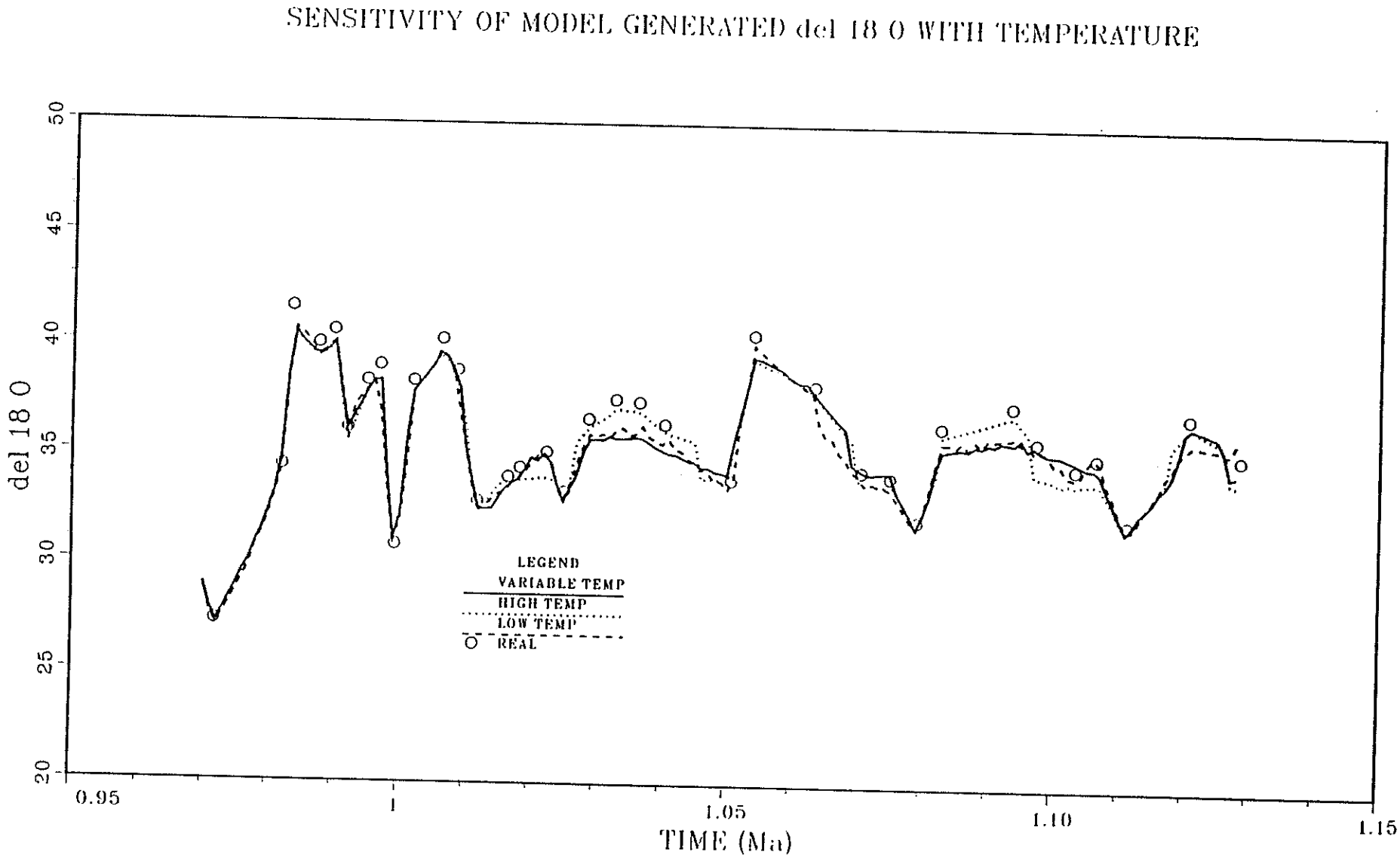

FIGURE 39. Comparison of constant high temperature (19.1°C), constant low temperature (12.1°C, and variable temperature simulations of $\delta^{18}O$ history for temperature sensitivity analysis

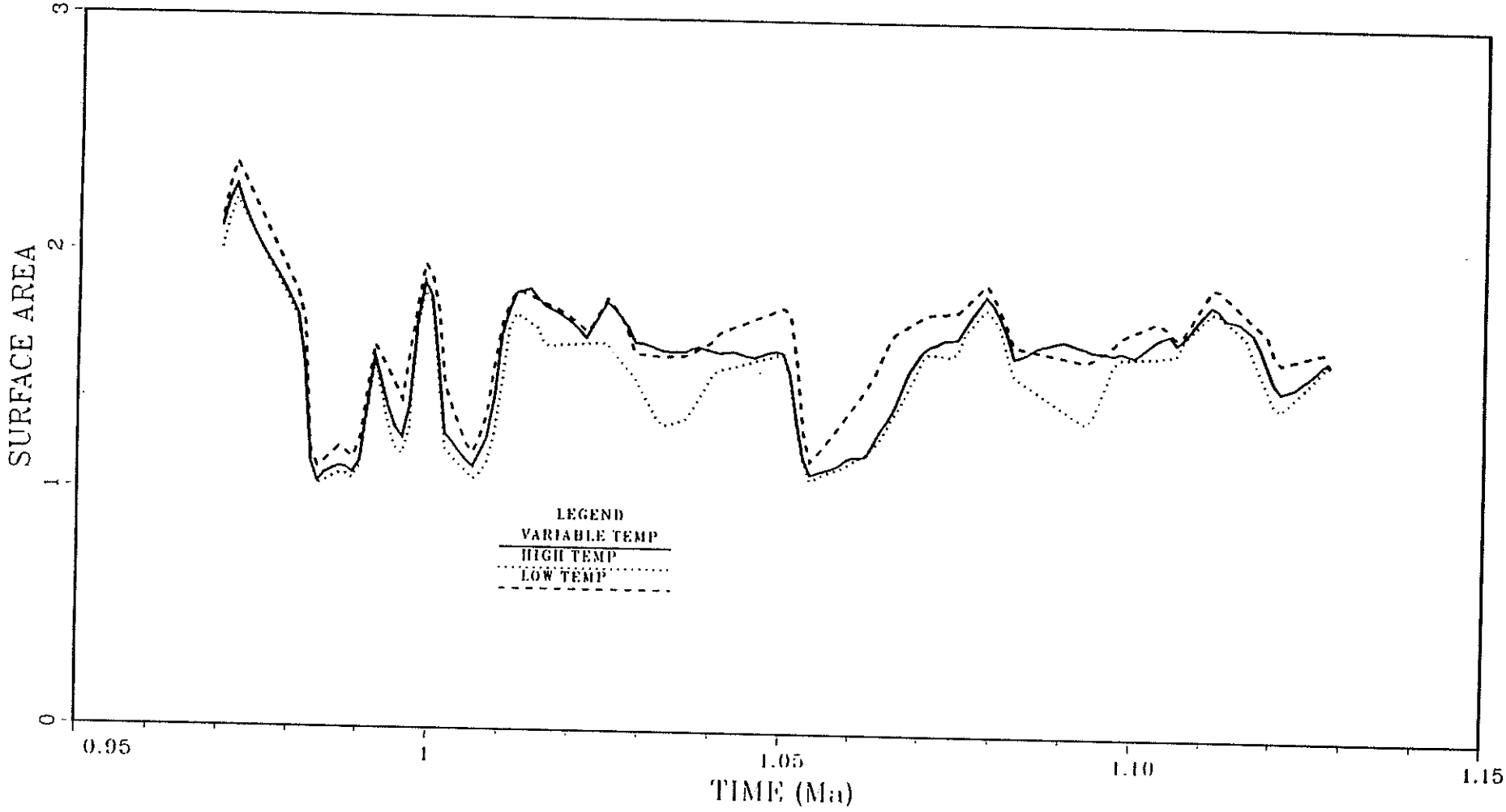

FIGURE 40. Comparison of lake surface areas simulated using constant high and low temperature histories and variable temperature history

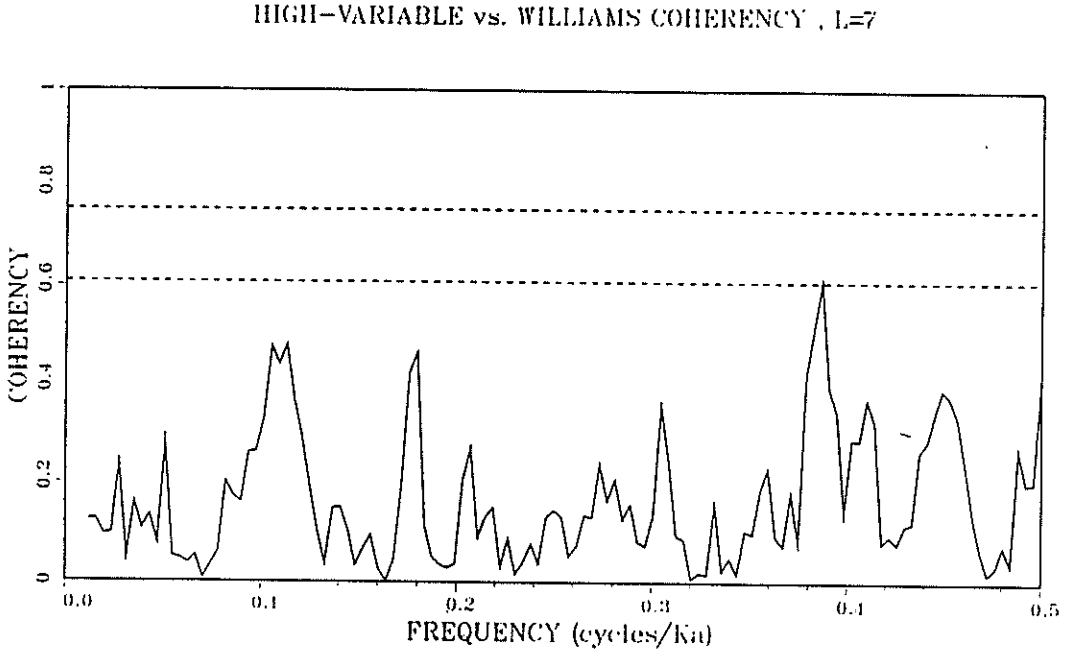

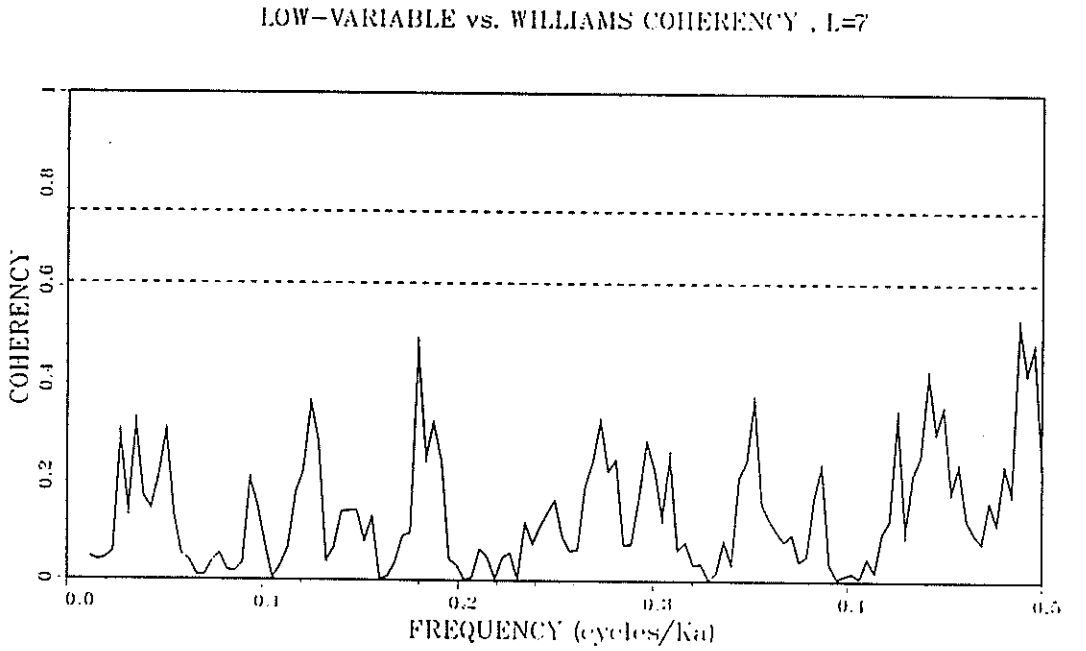

FIGURE 41. (a) Coherency (as a function of frequency) between residuals of high temperature minus variable temperature sensitivity run surface areas with Williams et al. (1988) marine $\delta^{18}O$ record used to generate variable temperature history (b) Coherency (as a function of frequency) between residuals of low temperature minus variable temperature sensitivity run surface areas with Williams et al. (1988) marine $\delta^{18}O$ record used to generate variable temperature history

differing inflows rather than by producing differing surface areas. This robustness of the surface area simulation leads confidence to model application.

MODEL RESULTS

Paleo-Owens River System

Numerical model results for Searles Lake simulations are listed in Appendix R. The match of the simulated $\delta^{18}O$ and chloride deposition to the data is shown in figure 42. The lake surface area history produced by the simulation is illustrated in figures 43 through 49. In these figures, the solid lines indicate intervals of the lake history in which the surface area is simulated by the numerical model and constrained by both the $\delta^{18}O$ record and the chloride deposition. Dashed lines correspond to intervals of evaporite deposition in which the main constraint is chloride mass balance from the numerical model. Dotted lines represent intervals for which the lake surface area was reconstructed using qualitative interpretation of stable isotope data, chloride deposition, and independent geological data.

The lacustrine isotope evolution model was able to simulate the entire lake history, with the exceptions noted below. The halite bed deposited at 1.145 Ma is unusually thick, but the model "dumped" most of the chloride in Searles Lake into Panamint Valley during the preceding overflow, leaving an insufficient amount in the lake water to match the observed deposition. Therefore we assumed that the lake remained density stratified during the overflow (in contradiction to the "well-mixed lake" model assumption) and thus retained sufficient chloride below the chemocline to supply the observed halite deposition at 1.145 Ma. A similar problem was encountered in the interval 355 to 300 ka, in which the modeled chloride deposition was insufficient to match the observed. Again, the lake was assumed to be stratified during the preceding overflow episode, thus retaining chloride that would otherwise have been flushed into Panamint Valley.

The modeling process itself was not successful for the interval 300 to 150 ka. During most of this interval, the sediments deposited consisted of mud thinly interbedded with trona, nahcolite, and halite, clearly indicating that the lake was shallow to moderate depth, fluctuated rapidly, and was usually saline. In contrast, the $\delta^{18}O$ of the carbonate sediments is generally very light, but also quite variable. This apparent conflict is easily resolved. During intervals when the lake water is saline for long periods, the chemical activity of the lake water is reduced, and with it, the evaporation rate. However, the atmospheric back-condensation is not affected. Thus, the isotopic composition of the lake water is strongly affected by light atmospheric water vapor.

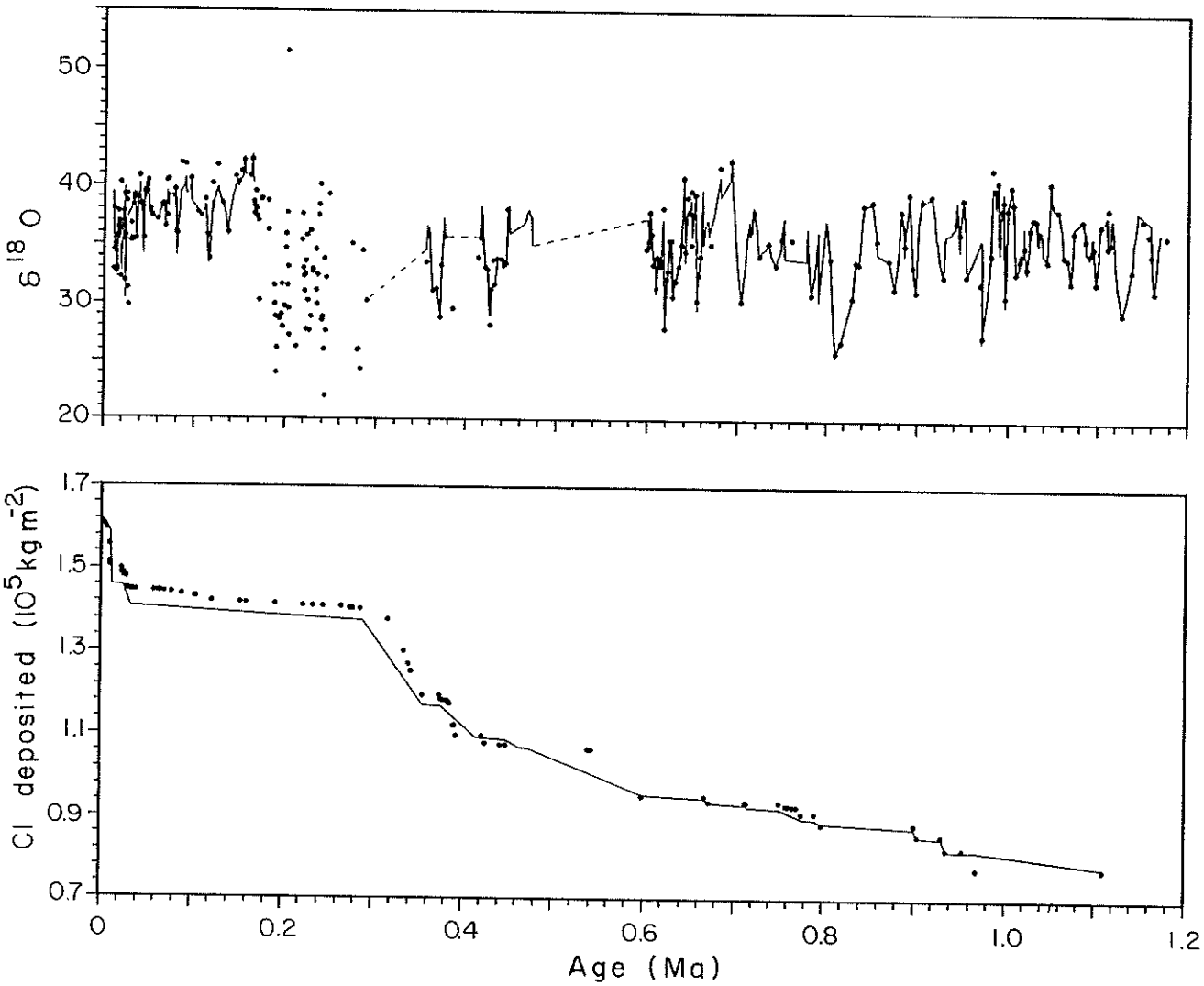

FIGURE 42. (a) Match of simulated $\delta^{18}O$ (solid line), used to constrain lake history, with $\delta^{18}O$ data (open circles) (b) Match of simulated chloride deposition (solid line), used to constrain lake history, with chloride deposition data (open squares)

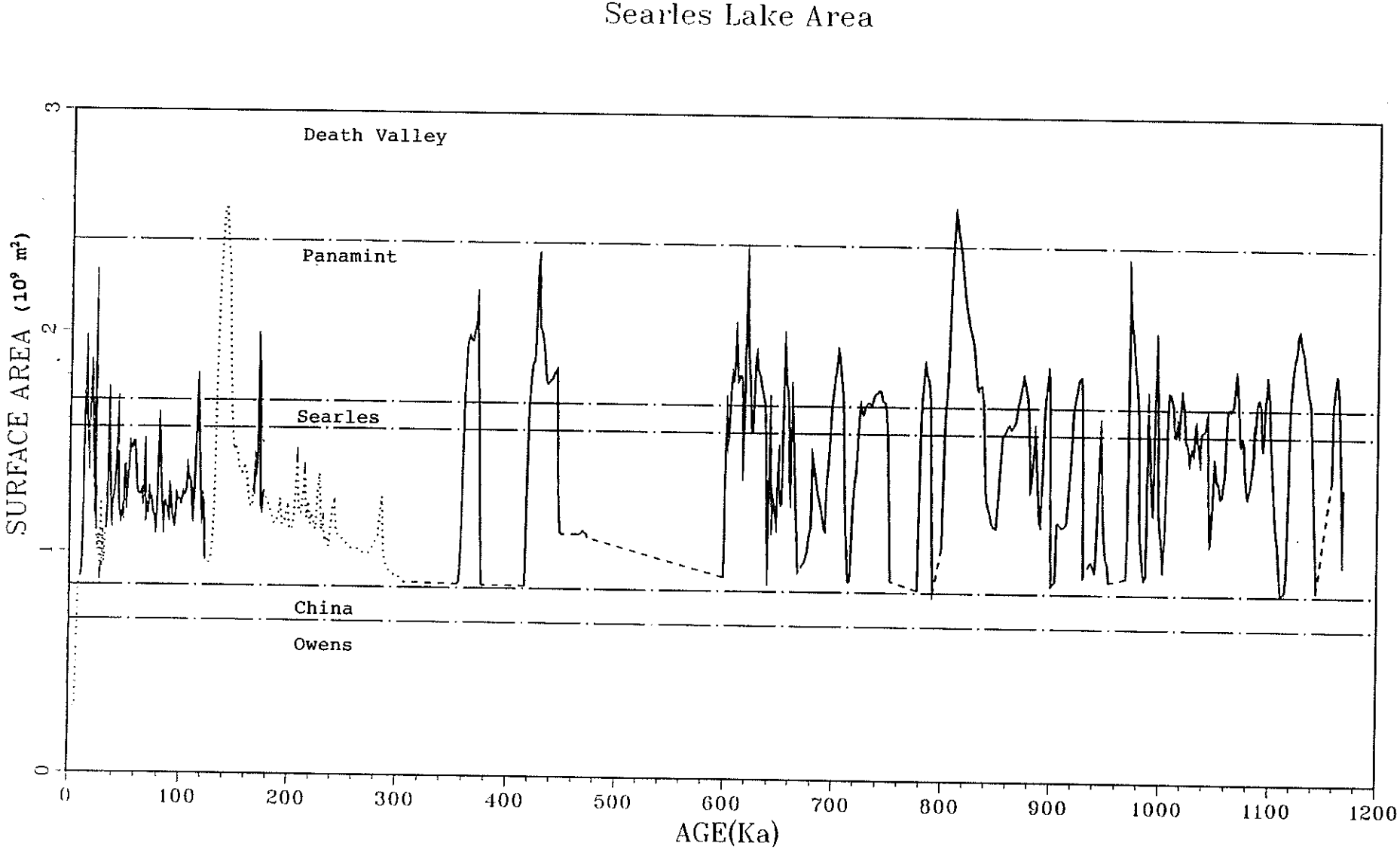

FIGURE 43. Simulated paleo-Owens River lake surface area from 1.18 Ma to the present. Solid lines represent intervals constrained by $\delta^{18}O$ data and chloride mass balance, dashed lines intervals constrained by only chloride mass balance, dotted lines constrained by semi-quantitative interpretation of isotopic, chloride balance, and independent geological data

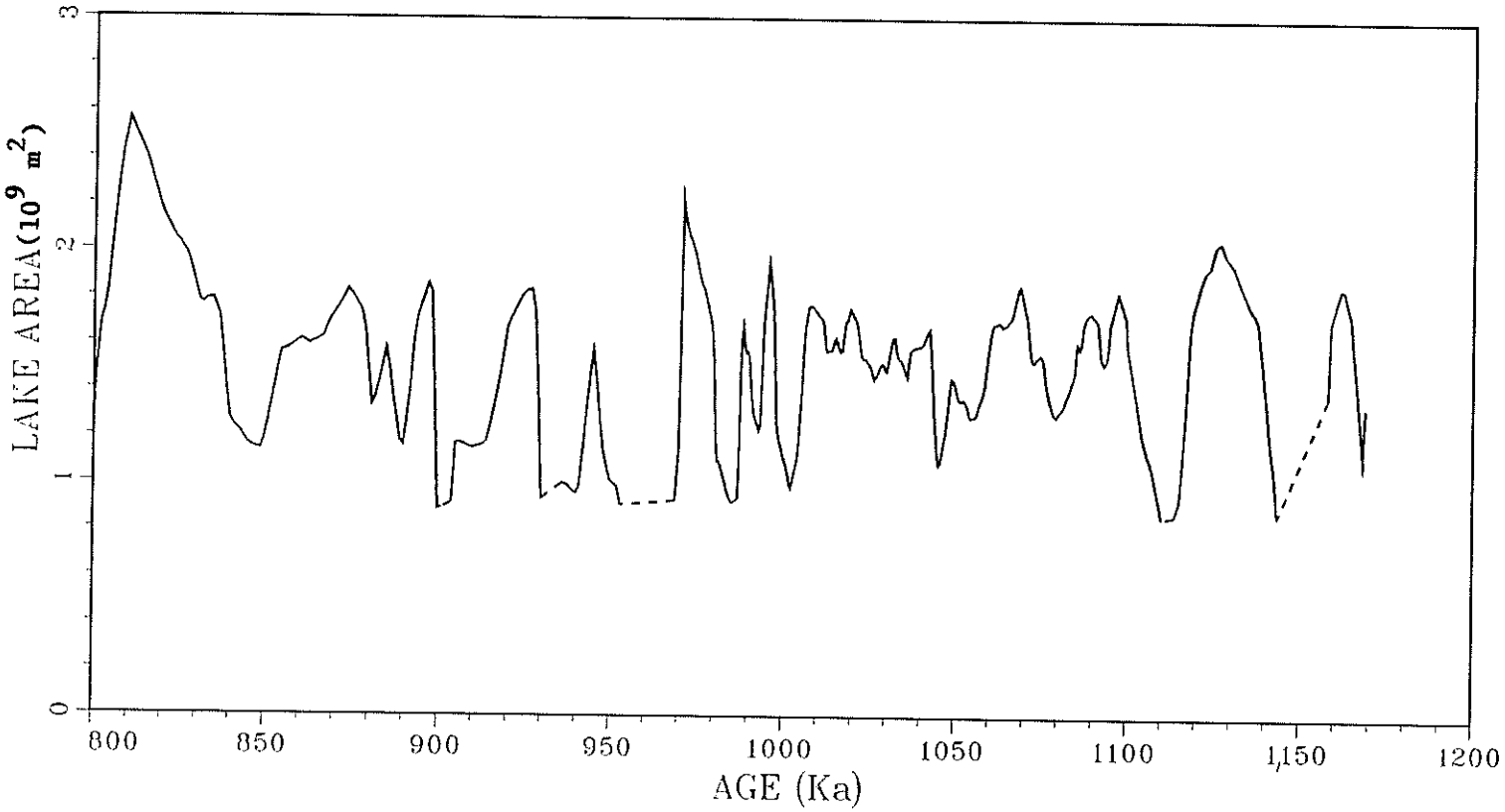

FIGURE 44. Simulated paleo-Owens River lake surface area from 1.180 Ma to 0.800 Ma. Symbols as in Figure 43

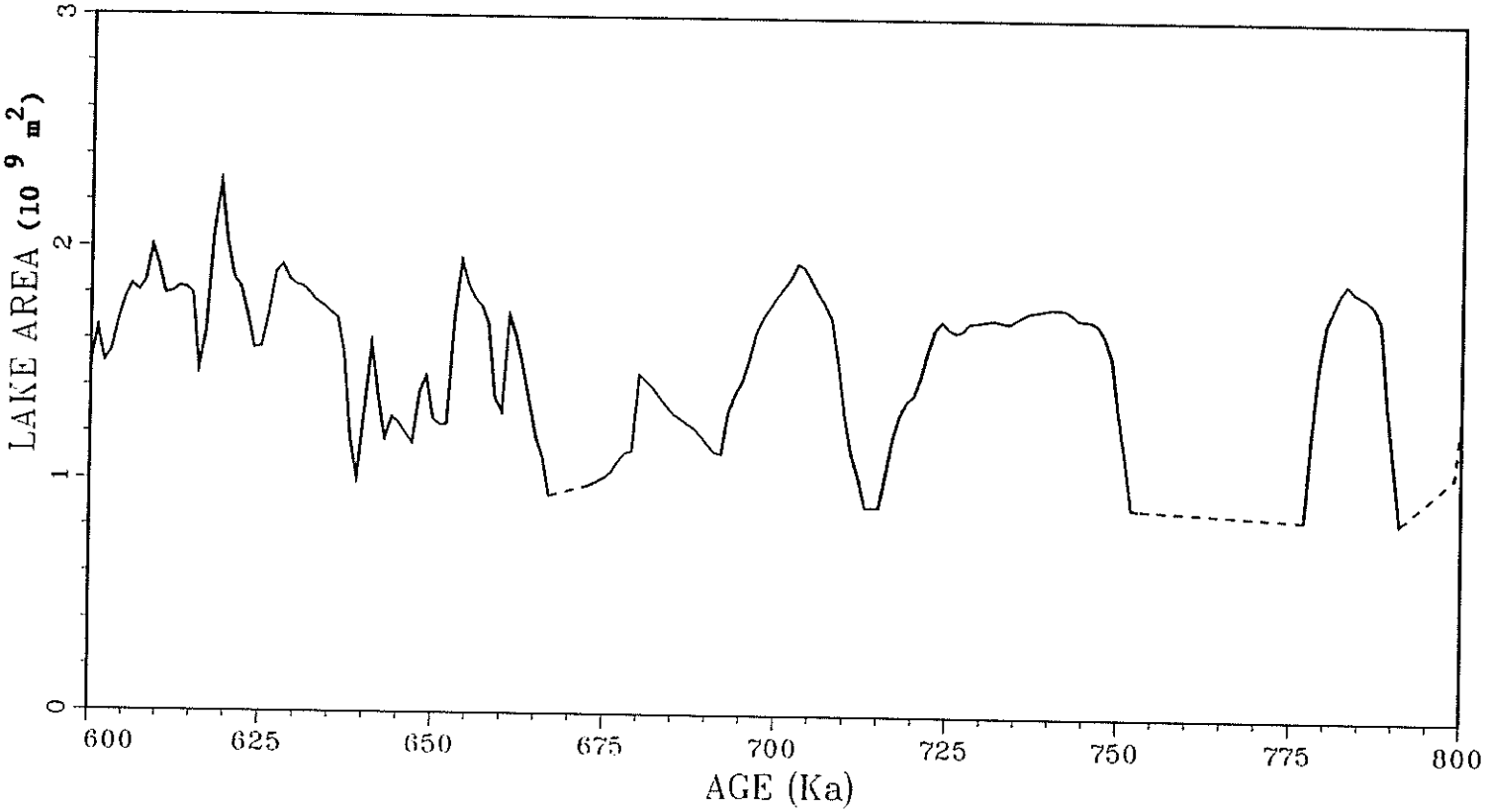

FIGURE 45. Simulated paleo-Owens River lake surface area from 0.800 Ma to 0.600 Ma. Symbols as in Figure 43

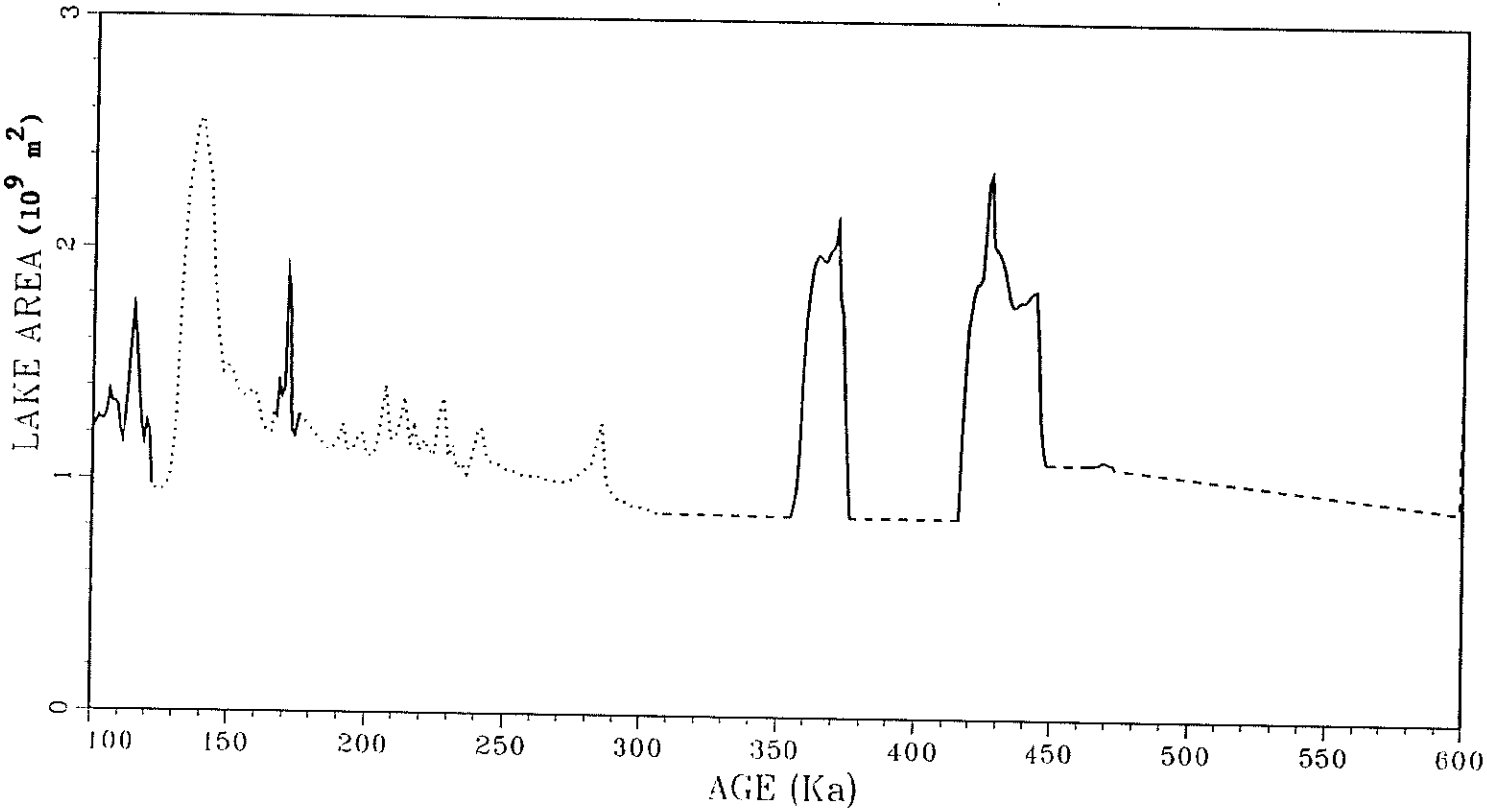

FIGURE 46. Simulated paleo-Owens River lake surface area from 0.600 Ma to 0.100 Ma. Symbols as in Figure 43

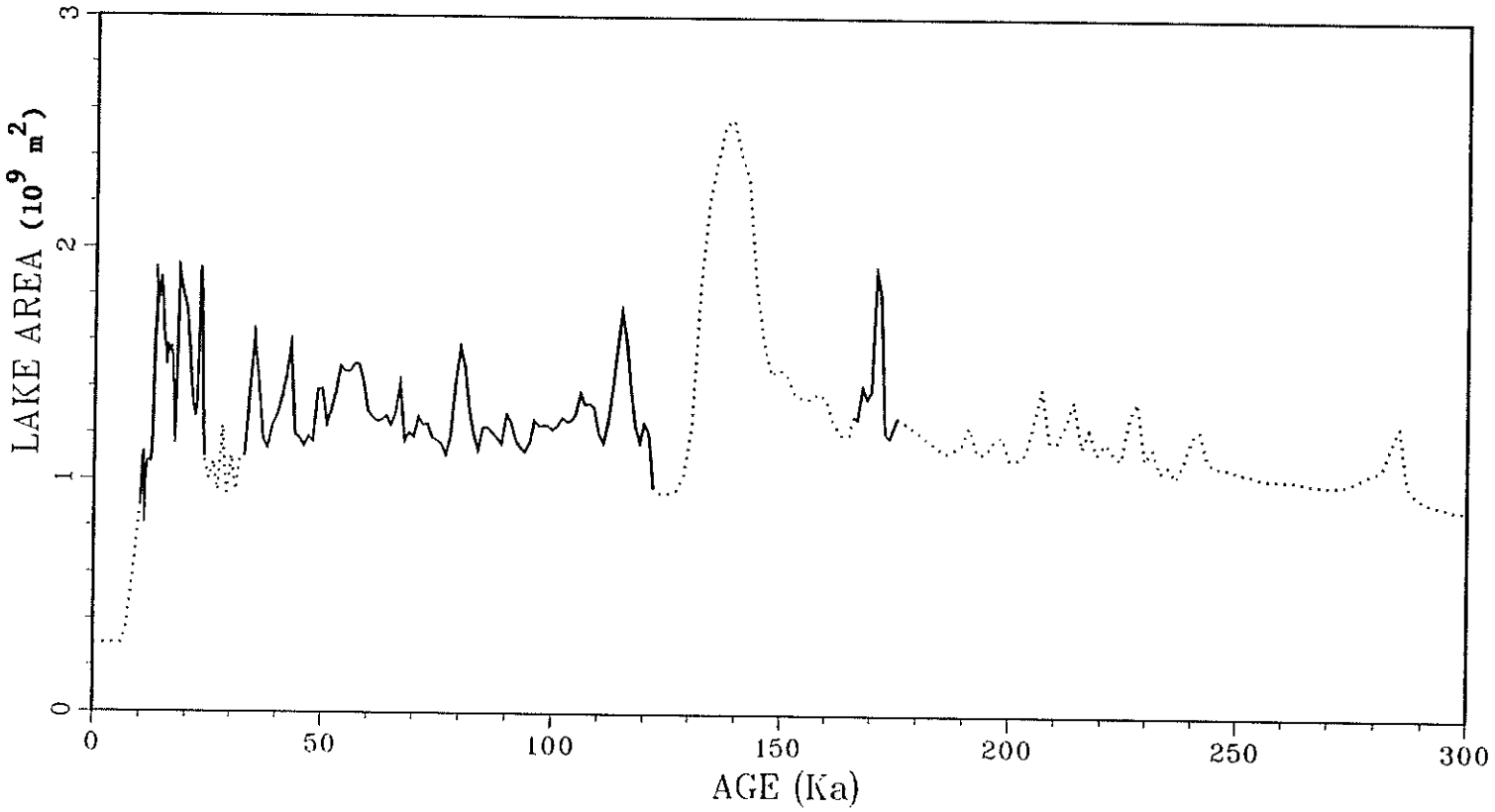

FIGURE 47. Simulated paleo-Owens River lake surface area from 0.300 Ma to 0.000 Ma. Symbols as in Figure 43

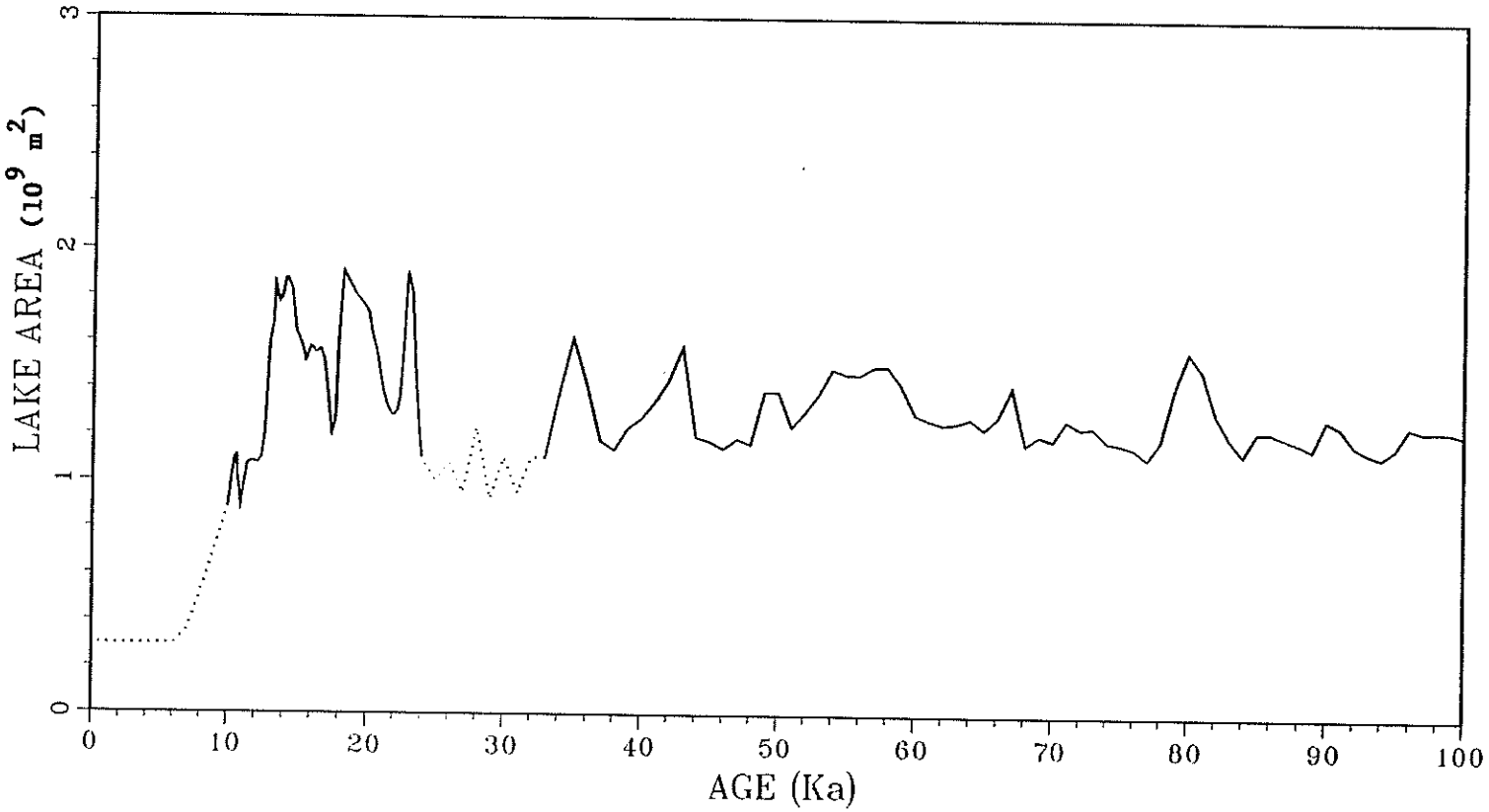

FIGURE 48. Simulated paleo-Owens River lake surface area from 0.100 Ma to 0.000 Ma. Symbols as in Figure 43

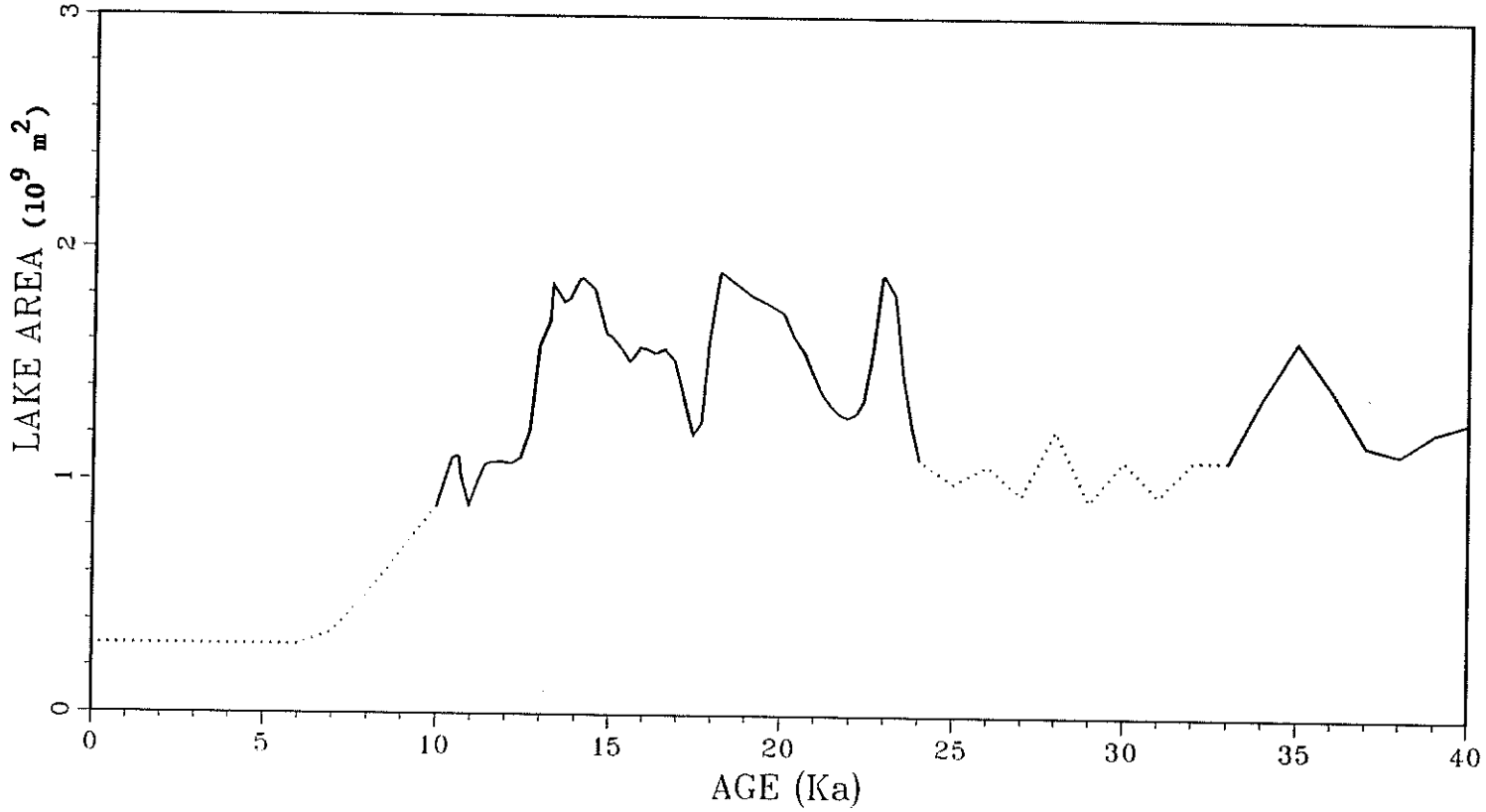

FIGURE 49. Simulated paleo-Owens River lake surface area from 0.040 Ma to 0.000 Ma. Symbols as in figure 43

The model was capable of simulating the light isotopic values for this interval, given appropriate (low) values for the water activity. However, sensitivity analyses showed that the model became very responsive to the poorly constrained histories of humidity and $\delta^{18}O$ of atmospheric water vapor. The model was also difficult to match to the data because, at the low water volumes that prevailed for most of the interval, the model output was hypersensitive to small changes in the specified inflow. Given these difficulties, we decided that numerical simulation of this interval was not reliable. Instead, we estimated lake surface areas in a qualitative fashion, based on the ^{18}O data, the sediment mineralogy, and sedimentological evidence from the basins upstream and downstream of Searles (Jannik 1989). In addition to the data in Jannik (1989), we also used unpublished ^{36}Cl buildup dates on incised shorelines in Panamint Valley that indicate the last overflow of Panamint Valley into Death Valley occurred at about 140 ka.

Our sample spacing was not close enough to resolve adequately the rapid lake fluctuations during the interval 32 to 24 ka (the Lower Salt). Therefore, we supplemented the simulation with a geologically based interpretation provided by G.I. Smith (Personal communication, 1990). In the numerical simulation, the modeled lake did not contain sufficient chloride at 10 ka to match the halite deposition observed in the Upper Salt, due to chloride flushing during the overflow episodes between 24 and 18 ka. Although geological evidence from Panamint Valley does demonstrate that a small lake was created in that valley by overflow from Searles, it also indicates that no thick halite was precipitated when the lake desiccated. We again assumed that the chloride was retained in Searles by chemical stratification. Finally, since Searles Valley has been desiccated for most of the Holocene, we used the historical surface area of Owens Lake as representative of this interval.

Lake San Agustin.

The $\delta^{18}O$ history calculated by the transient model for Lake San Agustin is shown in figure 50, together with the measured ^{18}O data. The input data for the model are listed in Appendix Q and the model outputs in Appendix S. The ^{18}O record was closely simulated with the exception of two time intervals, 28,400 to 26,600, and 25,600 to 25,400 yr B.P., in which the lake surface area was constrained by geologic evidence rather than isotopic simulation. Fine sands and silts with periodic occurrence of gypsum indicate that very low lake stands bordering on the playa level were

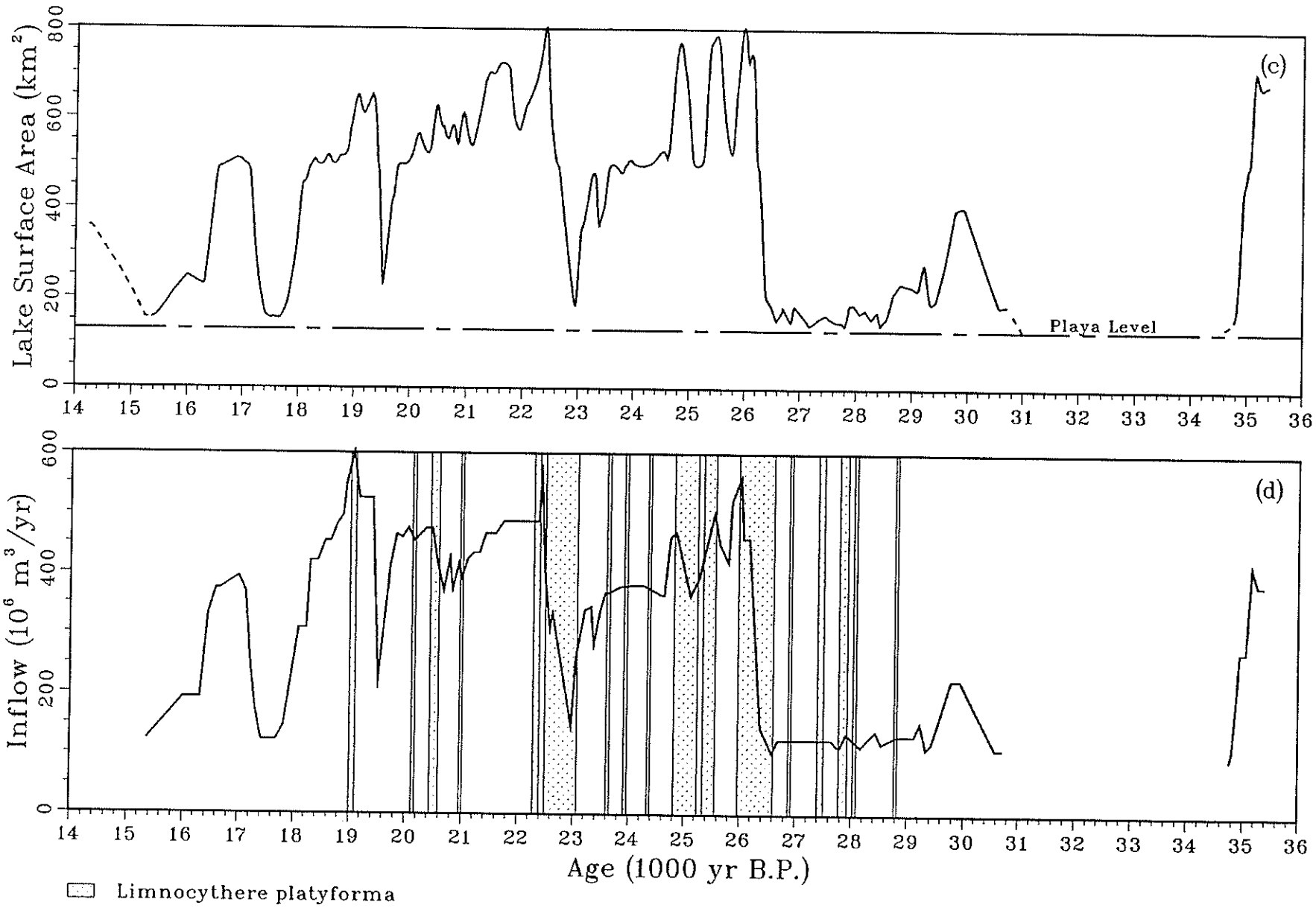

FIGURE 50. Results of numerical modeling for Lake San Agustin: (a) simulated surface area history and (b) inflow history and L. platyforma biostratigraphy

maintained from about 28,500 to 26,600 yr B.P. The lake level during the interval 25,600 to 25,400 yr B.P. was limited to the Powers shoreline.

The lake surface area history calculated by the model, and the inflow chronology which produced the model simulations, are shown in figure 50. The surface area curve mimics the inflow curve with minor deviations produced by temporal variation in temperature and, accordingly, evaporation, thus indicating that precipitation rather than temperature fluctuations exert the dominant control on lake level variations. Dashed portions of the lake surface area curve were developed solely on the basis of geologic evidence. Sand and gravel intervals in core SAC3-4 indicate that lake levels dropped below the modern drill core elevation from 34,700 to 34,300, and from 33,700 to 31,500 yr B.P. Fine sand and silt with gypsum indicate a very low lake level was maintained from 31,500 to 31,200 yr B.P., and clays logged from drill cuttings suggest brief low stands occurred during the intervening periods, 34,300 to 33,700 and 31,200 to 30,800 yr B.P. Silt and very fine sand with iron-coated grains occurred in the interval from 25,300 to 24,800 yr B.P., and imply that decreases in lake surface area simulated at 25,700 and 25,100 yr B.P. were probably much more dramatic than model results indicate. This anomaly is probably due to the humidity feedback problem discussed above. Lake surface area between 15,000 and 14,000 yr B.P. was estimated based on a shoreline at 2085 m and ^{14}C dated at 14,200 ± 140 (Markgraf, V., personal communication, 1989).

The inflow history correlates closely with occurrence of *Limnocythere platyforma* shown by patterned boxes in figure 51. The association between intervals of high or increasing inflow and *L. platyforma* provides sound support for the proposal that this ostracode specie is principally associated with fresh water lake phases (Forester, R.M., personal communication, 1971). The geologic constraints and biostratigraphic correlation also establish a high level of confidence in the modeling results; however, uncertainties inherent in model input parameters and the problem of nonunique solutions introduce some uncertainty in the lake surface area simulation and much uncertainty into the inflow simulation. Values for surface area and inflow should be considered reasonable approximations. The lake level chronology developed numerically is well constrained by the known geologic record and is consistent with sediment and shoreline records, the biostratigraphy, and qualitative lake level reconstructions proposed by Forester (1987) and Markgraf et al. (1984).

Paleoclimatic and Paleohydrologic Reconstruction. The late Wisconsin full-glacial climate between 35,000 and 26,400 yr B.P. in the San Agustin record was a dry period with low basin inflow and relatively stable low lake levels. Interpretation of the thermal regime during this interval from the ostracode record alone is problematic because dominance of *Limnocythere ceriotuberosa* and absence of *L. bradburyi* may be due to either increased salinity accompanying low lake levels, or to cold temperatures. The ^{18}O record, however, indicates that salinity levels were

normal, and supports the interpretation of a cold thermal regime. An abrupt warming event is recorded at 28,600 yr B.P. by total replacement of *Limnocythere ceriotuberosa* with *L. bradburyi*, and a positive shift in ^{18}O of $3.2^{0}/_{00}$. The ostracode replacement occurred very rapidly over approximately 50 years. The less sensitive ^{18}O record, which reflects the lake level response, did not peak until 28,400 yr B.P. The temperature shift forced only about a 30 percent decrease in lake surface area, while the basin inflow remained essentially constant. Warmer temperatures continued until 21,800 yr B.P. interrupted by only short term cold pulses.

The time interval from approximately 26,400 to 24,600 yr B.P. is represented in the San Augustin record by a dramatic increase and cyclic oscillations in inflow and lake surface area. Extreme, rhythmic fluctuations in the ^{18}O curve suggest that both lake inflow and surface area varied between near-extreme late Wisconsin levels with a periodicity of about 600 years. Temperature fluctuations during this interval appear to have been minor. The correlation between *Limnocythere platyforma*, which is associated with large influxes of fresh water, and periods of high or rising lake level during this interval provides good support for the contention that the dominant driving mechanism for these climate oscillations was increased moisture input and not reduced temperature. The integrated data from this study -- the surface area simulation, inflow history, ^{18}O history, and ostracode biostratigraphy -- all support the hypothesis that extreme changes in lake level were driven more by variation in inflow than by changes in evaporative outflow.

The late Wisconsin thermal minimum was initiated at San Agustin by a cold and wet period between 21,800 and 20,600 yr B.P. During this interval, *Limnocythere ceriotuberosa* comprised 80 to 100 percent of the ostracodes in the record, suggesting a prolonged, intense cold period. Cold temperatures resulted in a very favorable water balance reflected by high, stable, lake levels which were maintained through a period of moderately decreased inflow. A rapid warming trend at 20,600 yr B.P., substantially before estimates for the close of the late Wisconsin glacial maximum, is suggested by replacement of *L. ceriotuberosa* by *L. bradburyi*.

This reconstruction is supported by local paleoclimate indicators. Based on ^{18}O data from groundwater in the San Juan basin in northwest New Mexico, Phillips et al., (1986) proposed a cold, wet period before about 20,000 yr B.P., followed by an interval of relatively high temperature and low effective precipitation between 20,000 and 17,000 yr B.P., and a brief episode of moist conditions around 17,000 yr B.P. Based on the San Agustin record, and support from independent, regional, paleoclimate indicators, we

propose that the period of late Wisconsin glacial maximum in the American Southwest extended from about 21,800 to 20,600 yr B.P., and was characterized by a long (1200-year) period of climatic stability, with cold temperature and a moisture influx at least four times that of the modern-day water balance. Retreat of the glacial maximum was initiated about 20,600 yr B.P. by a period of relative climatic instability characterized by rapid, dissynchronous fluctuations in temperature and moisture influx.

DISCUSSION AND CONCLUSIONS

SEARLES LAKE

Sources of Uncertainty

Our final best estimate of the Owens River system lake level history has been presented above in Figures 43 through 49. The reconstructions in these figures have been based on proxy paleohydrologic data, largely chemical sediment mineralogy and ^{18}O measurements on lacustrine carbonates. These data were interpreted with the aid of a numerical model.

Like all paleoenvironmental reconstructions, the estimated history depends on assumptions regarding the materials examined, the behavior of the system and the history of extrinsic processes that have influenced the system. One important assumption in this study is that the carbonate minerals analyzed for ^{18}O were primary precipitates from the lake waters that preserve the isotopic signature of the original water. Unaltered primary character is difficult to petrologically and geochemically "prove" for even a single intensively studied sample, and would require an immense effort for the hundreds of samples that were processed from Searles Lake. Such detailed characterization would be highly desirable and should be a priority for future research, but was not within the scope of this project. Instead, we must rely on two main lines of evidence. The first is the independent evidence for the primary nature of gaylussite and dolomite that has been adduced by previous investigators and summarized on pages 17 through 24. The second is the way in which the large number of ^{18}O and ^{13}C data are consistent with the expected isotopic systematics of primary carbonates, but inconsistent with a diagenetic origin. The ^{18}O values are consistent with primary precipitate compositions predicted from a simple analytical model of the Owens River system. Both the ^{18}O and ^{13}C are comparable to values measured in unquestionably primary modern gaylussite from Mono Lake. The $\delta^{13}C$ does not show the extreme enrichment (often greater than $+20^{0}/_{00}$) that characterizes diagenetic dolomite created in lacustrine sediments as a result of methanogenesis (Irwin et al. 1977, Talbot and Kelts, 1986). Nor does it exhibit the consistent $\delta^{18}O$ enrichment

that would be expected of diagenetic dolomite precipitation from downward-percolating evaporative brines. In contrast the analyses show the strong $\delta^{18}O$ - $\delta^{13}C$ covariance that is a diagnostic feature of primary lacustrine carbonates in closed-basin lakes (Stuiver 1970, Talbot 1990).

The pattern of $\delta^{18}O$ within individual lake cycles is also consistent with the hydrologic pattern of the cycles. A typical sediment cycle begins with a massive halite. Above an often-abrupt contact the halite is overlain by lacustrine "mud", the top of which grades into moderately soluble evaporite carbonates (nahcolite and trona), which in turn is overlain by massive halite. The hydrological interpretation of this sequence is an initial shallow halite-saturated brine pool that is diluted by fresh inflow at the beginning of a humid cycle. After rising to some high (and dilute) lake level, diminishment of inflow causes shrinkage of the lake volume until soluble salt saturation is reached, with the most soluble salts precipitated last. Typical $\delta^{18}O$ patterns (figures 24 to 29) over these sediment cycles show initial moderate to enriched $\delta^{18}O$ values that progressively decrease to a depleted plateau or peak near the end of the cycle. Just below the terminating evaporitic salt bed the $\delta^{18}O$ values usually show a pronounced enrichment. This is exactly the pattern expected from the hydrological cycle inferred above. Although any one of these lines of evidence is not conclusive, taken together they present a strong case that the isotopic measurements have indeed been performed on materials representative of the primary carbonate precipitates.

Another important assumption is that the numerical model used to reconstruct the lake levels mainly responds to the $\delta^{18}O$ input. This assumption is important because any reconstructions of environmental parameters entered into the model are necessarily highly uncertain, and thus if the model output depends strongly on these parameters it will also be very uncertain. This issue was addressed by means of the sensitivity analyses, which demonstrated that the simulated lake levels were quite insensitive to the assumed temperature history. Therefore, uncertainties in any of the parameters assumed dependent on temperature (e.g., evaporation rate, isotopic composition of precipitation) will not contribute large degrees of uncertainty to the lake-level reconstruction. The only remaining potentially independent input variable is humidity. This was linked to the ^{18}O data record itself. The humidity parameterization thus serves as an "amplification factor" for the amplitude of the lake cycles, rather than being treated as an external input. Given that under even the most elementary qualitative interpretation, light $\delta^{18}O$ would be considered

indicative of humid conditions and heavy $\delta^{18}O$ of arid ones, the humidity parameterization seems to be a relatively reliable approach.

A further indication of the relative conservativeness of the modeling approach can be obtained by comparing the raw $\delta^{18}O$ data for the period 700 to 600 ka with the modeled lake levels in figure 51. For the most part, the lake surface-area reconstruction constitutes a rough linear inversion of the isotope data. This generally linear correspondence is an indication that the data have not been overinterpreted, and that the $\delta^{18}O$ data themselves are a good proxy for the water balance. In this sense, the main function of the model is to provide a "conversion factor" between $\delta^{18}O$ deviations and water balance fluctuations.

A final assumption in the interpretation of the isotope data is that the ancient hydraulics of the Paleo-Owens River system are adequately described by changes in discharge of the basin in its present configuration. There are only two likely violations of this assumption. One is discharge contributions by overflow of Lake Russell (Mono Basin). Although Lake Russell clearly did overflow and discharge into the Owens System (Putnam 1950) the very small ratio of basin area to lake surface area at overflow indicates that the overflow volumes are likely to have been insignificant in comparison to Owens River discharges under the same pluvial maximum conditions.

The other violation of the assumption is potentially more significant. During portions of the Pleistocene, Long Valley (near the headwaters of the Owens River) was occupied by a large lake (Mayo 1934). Evaporation rates at the approximately 2,500 m elevation of Long Valley are undoubtedly much less than at the 500 m elevation of Searles Lake, but the lake may nevertheless have made an appreciable contribution to the evaporation balance of the river system. Unfortunately, the history of the lake, and in particular the date of its draining, are very poorly constrained. At present it is thus not possible to include the effects of the lake in our simulations, but should chronological data ever become available it would be desirable to do so.

In summary, we wish to emphasize that our lake surface-area reconstructions depend on a wide range of assumptions which should be considered when evaluating the reconstructions. We have attempted, insofar as is feasible, to test these assumptions and uncertainties using sensitivity analyses and statistical tests. We believe that additional testing should be an important part of any future extensions of this work. We point out that any paleoenvironmental reconstructions from proxy records (e.g., paleotemperatures from pollen data or ice volumes from marine $\delta^{18}O$)

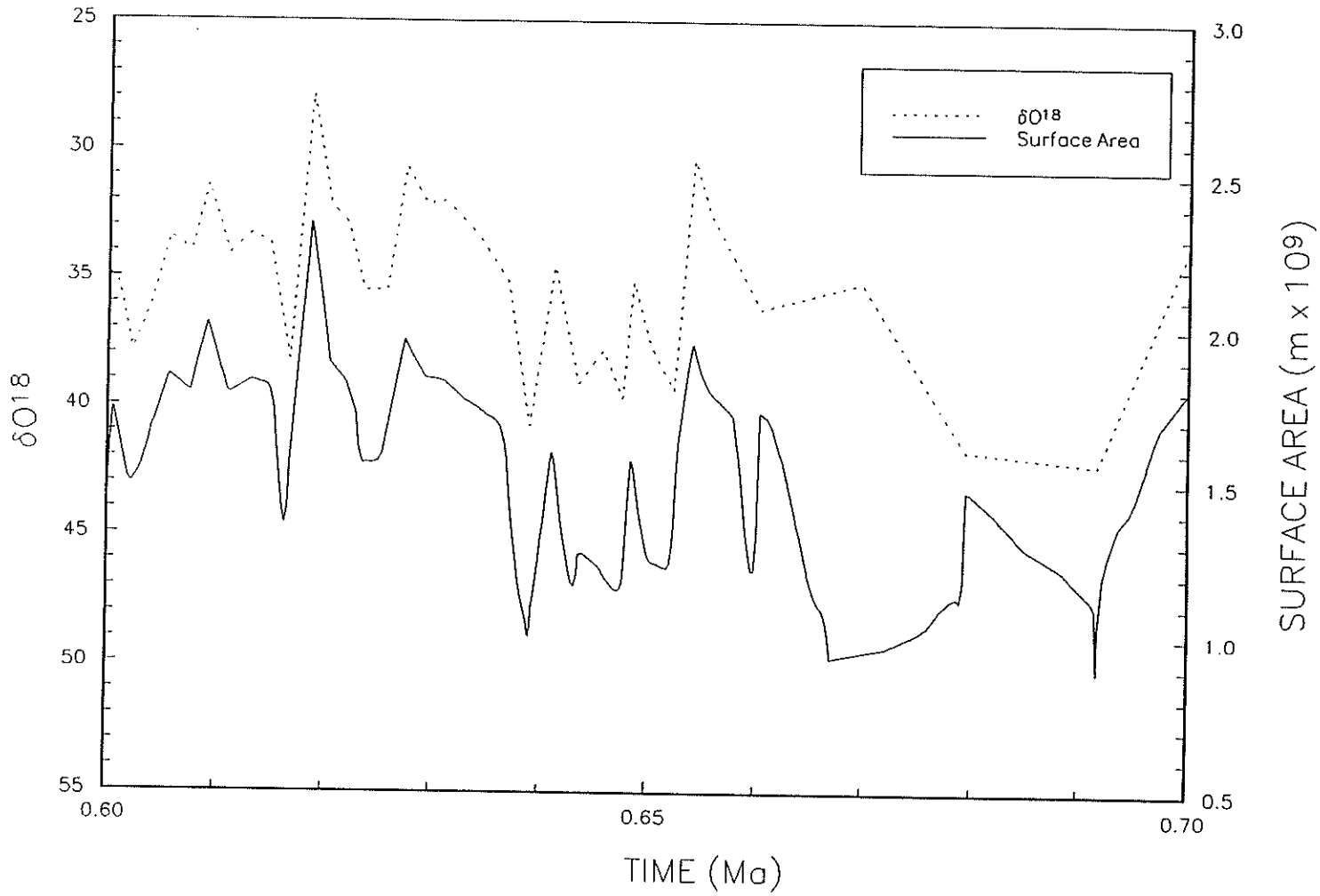

FIGURE 51. Comparison of $\delta^{18}O$ data for interval 0.7 Ma to 0.6 Ma with modeled lake surface area for the same time interval

are subject to similar assumptions. Although the degree of uncertainty in our reconstructions is difficult to quantitatively assess (in part because the methods we used have not been previously employed), we believe that the degree is generally commensurate with those of other accepted approaches to paleoenvironmental reconstruction, and that the reconstructions should be tentatively accepted, subject to future confirmation. We therefore proceed to comparisons with some of these other paleoenvironmental proxy records.

Comparisons With Other Records

In Figure 52 our simulation of the Searles lake surface-area history is compared to other long records of Quaternary climate change. The three records selected were the "stacked" marine ^{18}O curve of Williams et al. (1988), the mid-North Atlantic (site 607) percent $CaCO_3$ record of Ruddiman et al. (1989), and the magnetic susceptibility record from the Xifeng loess profile in central China published by Kukla (1987). The Williams et al. (1988) marine ^{18}O curve was selected because, as a composite of several cores, it should be representative of global trends in the same way as the well-known SPECMAP stacked curve (Imbrie et al. (1984), but because it is not "orbitally tuned" it offers the opportunity to compare independent radiometrically based chronologies. In contrast, the Ruddiman et al. (1989) percent $CaCO_3$ curve does follow the conventional orbital tuning. The Kukla (1987) loess profile is included because it represents one of the few continental paleoclimatic records of comparable length to the Searles reconstruction. It should be noted that absolute dating of the Xifeng profile is limited to correlation with paleomagnetic boundaries. Using these records for comparison, we can address the questions raised in the first section.

The first two questions originally stated on pages 4 and 5, dealt with whether the Searles Lake record could be directly correlated with the marine ^{18}O history. The answer is a qualified "yes." Suggested correlations are shown in figure 52. The numbers assigned to the Searles "lake cycles" have been chosen to match with the correlative Williams isotope stage numbers. The absolute chronologies for both records have uncertainties estimated to range from plus or minus 10 kyr to 30 kyr, depending on core location. Given this uncertainty, the discrepancies in the timing of the correlative peaks are probably due to chronological error rather than any real leads or lags. (The chronological inconsistencies are certainly no greater than those between the untuned Williams and tuned Ruddiman curves (figures 52 (b and c), which are unquestionably correlative.) This inference is supported by the marked similarity in the shape of many of the peaks, especially in the interval of cycles 24 through 16. Although it is not apparent in the smoothed Williams curve (due to the

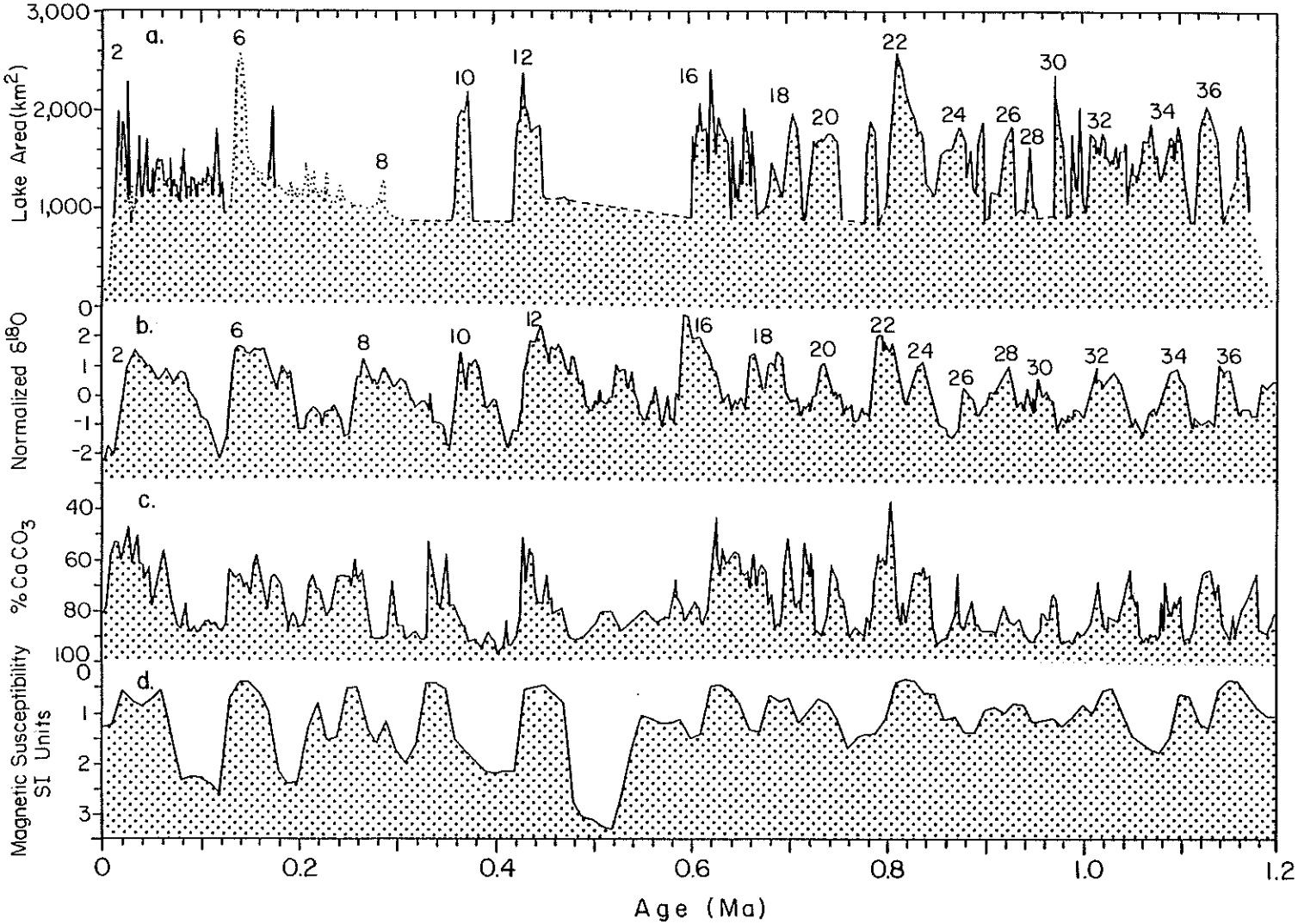

FIGURE 52. Lake surface area reconstruction and comparison to other paleoclimatic records. All records are plotted so that glacial stages correspond to the top of the graph.
(a) Simulated surface area of ancient Owens River terminal lakes
(b) Stacked marine $\delta^{18}O$ (Williams et al. 1988)
(c) Percent calcium carbonate at North Atlantic site 607 (Ruddiman et al. 1989)
(d) Magnetic susceptibility of the Xifeng loess profile (Kukla 1987)
Numbers identify glacial marine oxygen isotope stages, according to Williams et al. (1988)

effect of the stacking procedure), the inception of lake cycle 24 is remarkably similar in its high-frequency oscillation to the corresponding isotope stage 24 in the site 607 isotope record (Ruddiman et al. 1989). Although difficult to quantify, this similarity in form can leave little doubt that the approximate correspondence of the timing of the peaks does indeed represent a valid correlation.

This conclusion can be further supported by comparing the Searles and marine records in the spectral domain. Figure 53 is a contour plot of spectral density calculated through moving windows using the Lomb periodiogram method (Lomb 1976). Prior to 900 ka the plot shows dominant periodicities close to 23 kyr, 31 kyr, 41 kyr, and 54 kyr. These are all periodicities that have been noted in untuned marine ^{18}O curves from the same general time interval (Ruddiman et al. 1988; Joyce et al. 1990). The 23 kyr and 41 kyr periodicities correspond to the precession and obliquity frequencies of Milankovitch forcing (Berger 1988). In oceanographic studies, the standard procedure is to suppress the non-Milankovitch frequencies (and correspondingly enhance the Milankovitch ones) through orbital tuning, and we are confident that within the constraints of our absolute chronology (generally superior to that of marine cores), we could accomplish the same result. However, this procedure does not address the fundamental question of the extent to which this assemblage of dominant frequencies is a result of non-Milankovitch forcing versus simple errors in chronology or lake surface-area reconstruction. This fundamental chronological problem is illustrated by the generally poor coherency between the Searles curve and the Williams et al. (1988) marne ^{18}O curve, shown in figure 54. Except for near the 100 kyr period, between 600 and 100 ka, the coherency is not statistically significant. This is not surprising, considering that the chronological uncertainties of the two records are on the same order as the periodicities identified.

After about 800 ka figure 53 shows the development of strong 100 kyr power. Power in this frequency range continues throughout the lake history, but shifts toward 80 kyr at about 400 ka and weakens toward the end. The shift is due to the close temporal spacing (about 80 kyr) of the cycle 12 and 10 peaks, but the timing of these events is relatively loosely constrained by ^{36}Cl dates with large analytical uncertainties and thus the shift may be spurious. In any case, the general pattern of strong spectral power close to 40 kr prior to the Brunhes/Matuyama reversal (with very little 100 kyr power) followed by strong power close to 100 kyr (and little close to 40 kyr) is so similar to spectral analysis of the marine isotope record (Joyce et al. 1990) that is strongly supports the correlations made above.

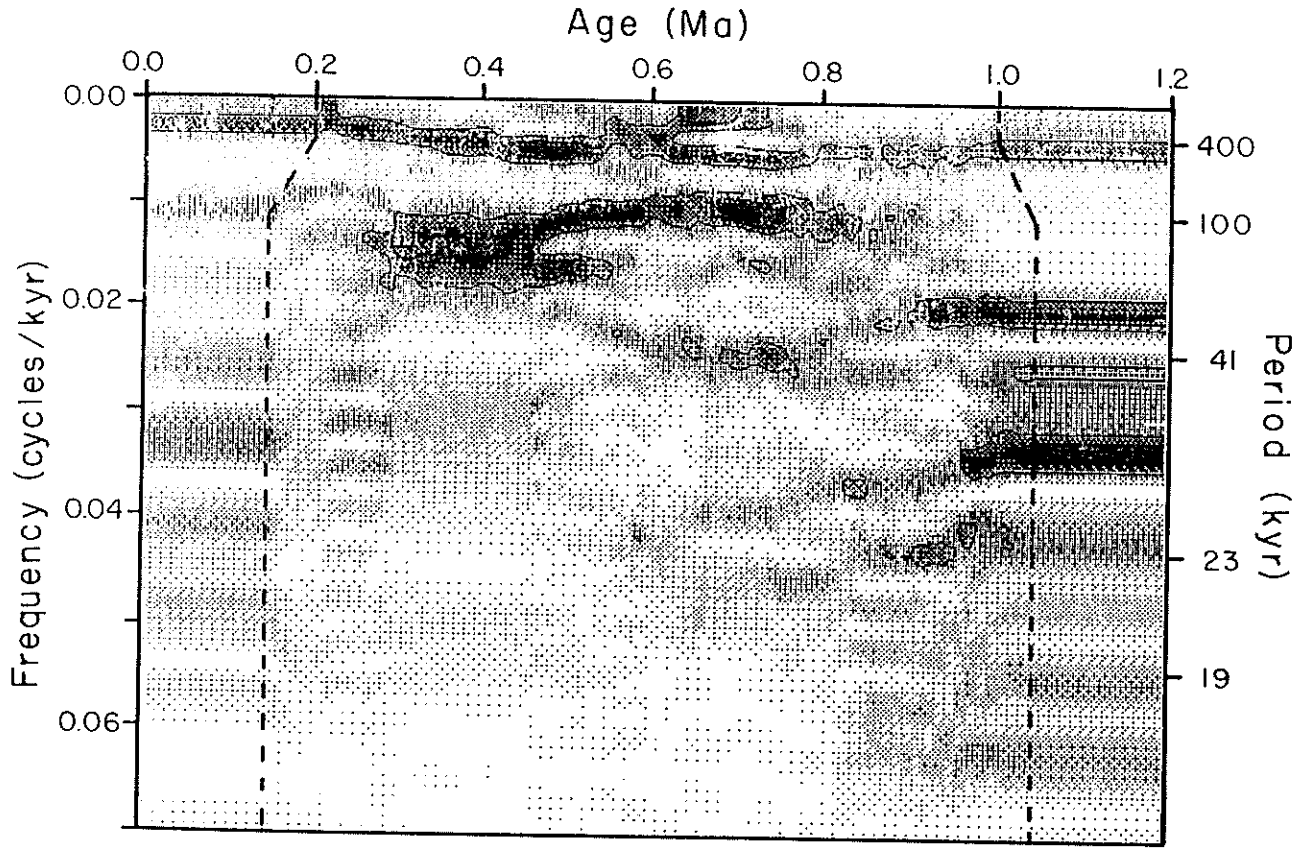

FIGURE 53. Spectral analysis of Searles Lake surface area reconstruction. Spectral density is contoured for spectral analyses at intervals through a moving, frequency-dependent window. Window half-width is indicated by dashed lines on either side of graph.

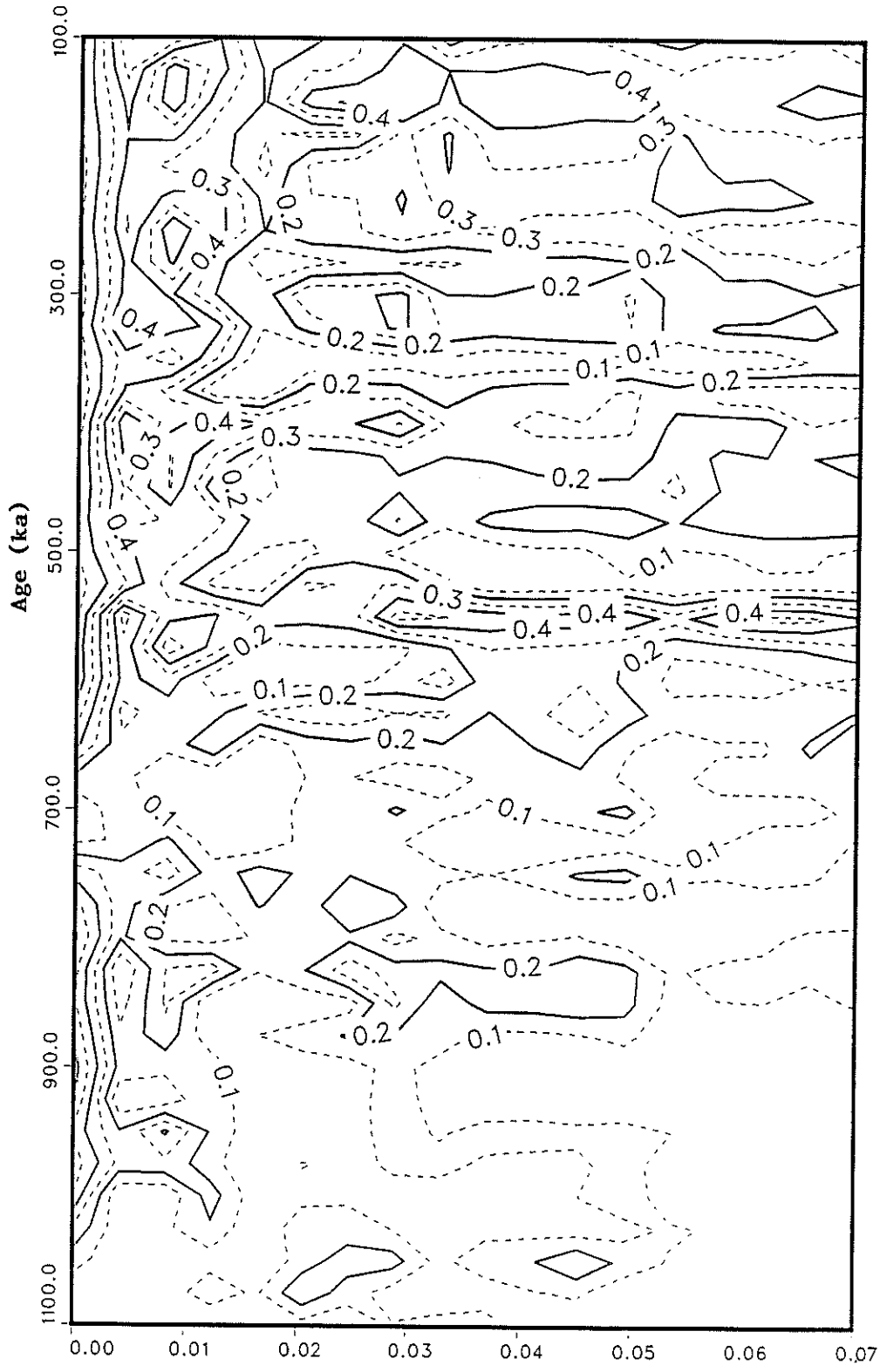

FIGURE 54. Coherency between Searles lake-surface-area reconstruction and stacked marine $\delta^{18}O$ (Williams et al. 1988). Coherency is contoured for analysis at 25 kyr intervals through a moving, frequency-dependent window

The third and four questions raised in the first section dealt with systematic differences between the lacustrine and marine records, and possible explanations for any differences. We do indeed see systematic differences in two characteristics. The first is long-term periodicity. Figure 53 shows significant power in the Searles time series close to the 400 kyr period. Similar conclusions were previously obtained by Smith (1984) based on a qualitative analysis. Low-frequency power with magnitude comparable to the 40 and 100 kyr periods is rare or absent in the marine records (Ruddiman et al. 1989). At Searles Lake, the source of this low-frequency power is clearly the long interval of predominantly low lake surface area centered around 450 ka, but matched before and after by long intervals of predominantly high lake surface area. Although this pattern is not reflected in the marine ^{18}O record (figure 52(b)), some long records strongly affected by mid-latitude climate do show similarities. The variations in the percent $CaCO_3$ data from core 607 (illustrated in figure 52(c)) reflect mainly dilution of the $CaCO_3$ by ice rafted debris (Ruddiman and McIntyre 1976; Ruddiman 1977). Periods characterized by low percent $CaCO_3$ presumably represent times when continental glaciers penetrated to sufficiently southerly latitudes to release icebergs across much of the North Atlantic. The percent $CaCO_3$ for the period 600 to 300 ka resembles the Searles surface-area history much more than does the ^{8}O pattern in figure 52(b). Similarly, the Xifeng loess magnetic susceptibility curve in figure 52(d) (Kukla 1987) shows prolonged episodes of high susceptibility (indicative of warm, humid climate) during the same time interval.

In summary, the Searles Lake surface areas show long-term trends of predominantly large surface area (from 1.1 to 1.0 Ma, 850 to 600 ka, and 200 ka to the present) and small surface area (from 1.0 Ma to 850 ka and from 600 to 300 ka). These trends are at best weakly reflected in the marine ^{18}O, but are more clear in records that reflect mid-latitude continental climate. We postulate that one possible reconciliation of the differing characteristics would be that the marine ^{18}O is an accurate indication of global ice volume, but that the locus of continental glaciation has shifted between more southern positions (e.g., from 850 to 600 ka), deflecting continental climate belts south of the ice sheets at the same time. This hypothesis is clearly testable. If verified, it would indicate that some as-yet unidentified process is exerting long-term control over global climate.

Another systematic difference between the Searles record and the marine ^{18}O is the nature of the climatic transitions. The marine ^{18}O (e.g., figure 52(b)) is characterized by brief interglacial episodes, generally

gradual progressions toward full glacial state, and abrupt terminations. In contrast, the Searles Lake area show in many cases longer interglacials followed by abrupt transitions to lake level highs and abrupt terminations. The impression is one of relatively stable humid (i.e., glacial) climate and stable arid (interglacial) climate with rapid switches between these modes. This impression can be supported quantitatively by comparison of the frequency distributions of the Searles lake levels with the Williams et al. (1988) stacked marine ^{18}O record (figure 55). The Searles histogram shows a much more pronounced bimodal distribution than the marine ^{18}O data. This tends to support a model of bimodal interglacial/glacial climate, with sudden switches between modes, such as has been presented by Birchfield et al. (1990). We suggest that the gradual interglacial to glacial transitions in the marine ^{18}O record may be more a reflection of kinetic factors in the growth of continental-scale ice sheets than of the nature of the climate impulses driving the transitions.

LAKE SAN AGUSTIN

The paleohydrologic reconstruction of Lake San Agustin over the period 36,000 to 15,000 yr B.P. is of particular interest because there are few detailed lake level histories for the southwestern United States older than 20,000 yr B.P. The relatively sparse data from this period for the Great Basin, summarized in Benson et al. (1990), uniformly indicates a prolonged period of low lake levels during the interval around 30,000 yr B.P., in excellent agreement with the San Agustin reconstruction. Searles Lake, in eastern California, is the only other basin for which detailed reconstructions have been presented (Smith 1987; Benson et al. 1990; Phillips et al. 1991). Searles Lake data indicate that the lake underwent a series of high amplitude oscillations with approximately a 1000-year periodicity between 32,000 and 25,000 yr B.P. This pattern is very similar to that modeled for San Agustin during the latter part of the same period, except that the periodicity of the fluctuations at San Agustin appears to be close to 600 years. The chronology in this interval of SAC3-4 is not well constrained, however, and additional dating will be necessary to resolve this discrepancy.

The period of the lake cycles is of special interest because Birchfield and Broecker (1990) have proposed that during glacial periods the circulation of the North Atlantic Ocean was controlled by a "salt oscillator" with a period of about 1000 years. Broecker et al. (1990) have shown that the interval from about 35,000 to 25,000 yr B.P. in Greenland ice cores and North Atlantic sediment cores was characterized by much stronger oscillations in climate-related parameters than the preceding and following ones. Similar-period oscillations in southwestern U.S. lakes might indicate that these oscillations influenced a much larger area.

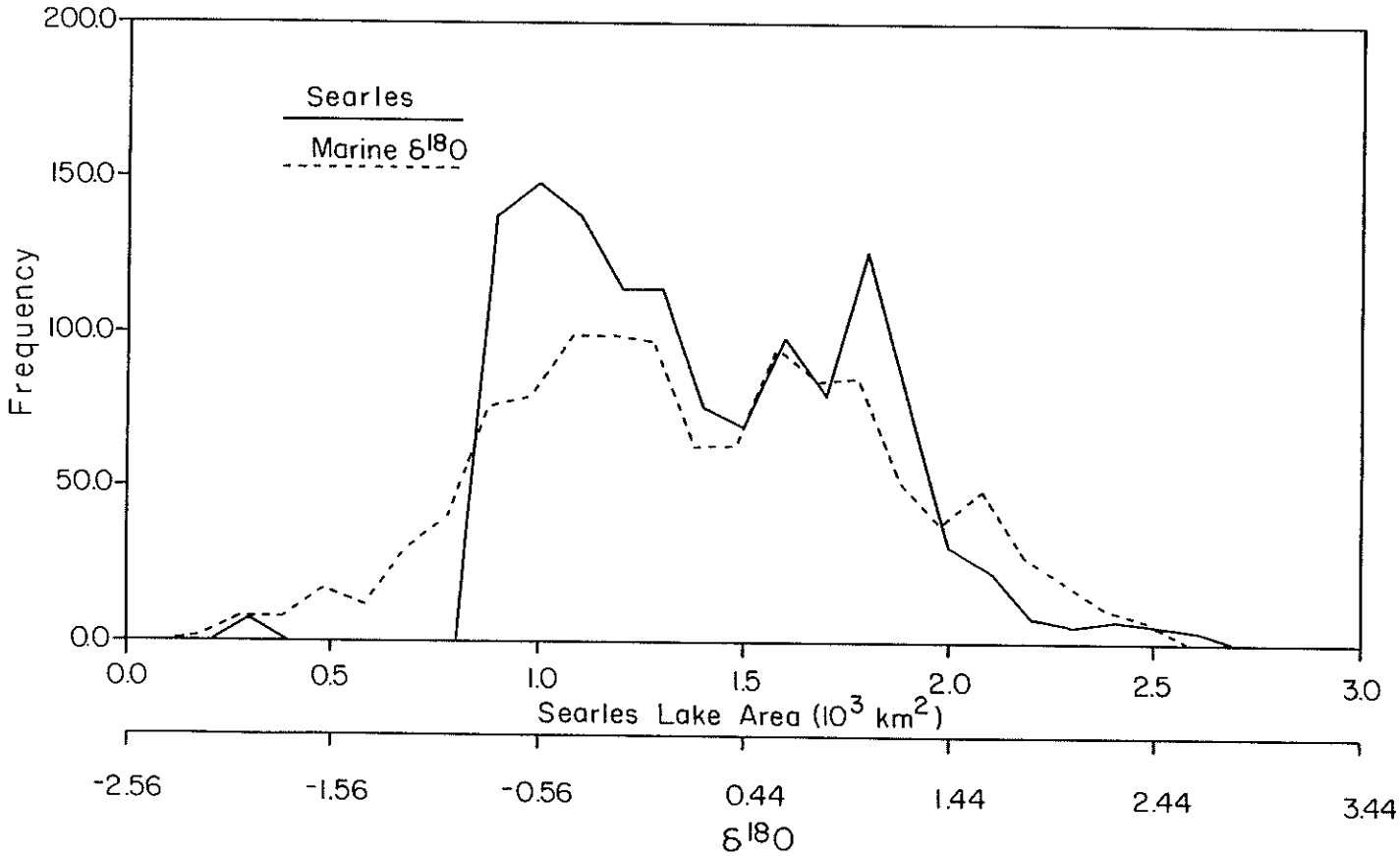

FIGURE 55. Normalized relative frequency distributions of Searles Lake surface areas and stacked marine $\delta^{18}O$ values (Williams et al. 1988) for past 1.2 Myr

The reconstruction from San Agustin indicates that "full glacial" (here defined as combined high inflow and relatively low temperature) began about 26,000 yr B.P. and ended about 20,600 yr B.P. Although this may appear to be in conflict with standard definitions of the full glacial lasting until the initiation of continental deglaciation at c.a. 15,000 (radiocarbon) yr B.P., it is in very good agreement with the regional glacial evidence. Summarizing a large body of data, Richmond (1986) placed the age of the maximum Late Wisconsin ice advance at about 22,000 yr B.P. He estimates that over a wide region of the Rocky Mountains the glaciers had undergone major recession by 17,000 yr B.P.

Our San Agustin reconstruction is in good agreement with histories inferred for nearby lake basins, but shows major discrepancies with more northern basins. Waters (1989) found that a moderate high-stand existed in Lake Cochise (southeastern Arizona) at about 13,500 yr B.P., and evidence for at least two significantly higher stands prior to that time. Allen (1991) reconstructed a lake level history for the period 20,000 to 10,000 yr B.P. at Lake Estancia (central New Mexico) that is very similar to ours for the same interval. However, in contrast to our results that show a series of lake cycles with progressively lower peaks at 22,000, 19,000, 17,000 and 14,000 yr B.P., histories from Lakes Bonneville and Lahonton (Benson et al. 1990) in the northern Great Basin show a pattern of increasing lake level until about 13,500 yr B.P., followed by abrupt decline. Interestingly, the reconstruction in this report from Searles Lake, which is intermediate in latitude, shows peaks with approximately equal surface areas at 22,000, 17,000 and 13,000 yr B.P. Taken together, these data support a model of synchronous fluctuations in the water balance over the entire region, but overlain by a progressive south-to-north shift in latitude of maximum precipitation.

IMPLICATIONS FOR WATER RESOURCES

This study was partly motivated by societal concern over the possible ramifications of human-induced global climate change. The release of anthropogenic "green-house" gases, among other human alternations of the global environment, is virtually certain to produce measurable modifications in the climate system, presumably in the direction of global warming. However, the chain of interrelated climatic consequences of these modifications cannot currently by predicted reliably.

Although global warming has received most of the popular attention, it will probably be one of the less important direct effects. Humans and most food plants are tolerant of a fairly wide temperature range. The most significant effects will likely relate to soil moisture availability, water supply, and sea level changes. All are directly linked to the water balance

(sea level changes being a result of water-balance changes in ice sheets) and thus the water-balance reconstructions we have developed for the southwestern U.S. should be useful for predicting the impacts of global climate change. This does not mean that we maintain these reconstructions are directly useful in an "analog" fashion; since the exact combination of circumstances that are going to force global climate change in the near future have not been duplicated in the past, we cannot expect to see the effects duplicated in the past either. However, the basin water-balance reconstructions can contribute to fundamental understanding of the hydroclimatic processes involved in future water-balance changes. We note the following specific points:

1) Magnitude of Water Balance Fluctuations. The reconstructions at both Searles Lake and San Agustin indicate that over the periods of record the water balance (measured by the ratio of basin runoff to lake evaporation) at both sites has fluctuated by roughly one order of magnitude. Clearly, this degree of variability is sufficient to cause major human disruptions, were it to occur over a short-time scale. The data support the hypothesis that water-balance fluctuations should be a matter of major concern in global change studies.

2) Nature of Hydroclimatic Regimes. In contrast to the marine ^{18}O record, the lake-level records show a strongly bimodal frequency distribution. This suggests that the continental-scale climate system tends to operate in certain stable "modes," with brief transitions between them. Most current detailed climate models do not seem to account adequately for this type of behavior. This behavior raises several questions: What regimes characterize these modes? What forcing drives transitions between modes? Might the global climate system find a completely new (and possibly radically different) mode in response to unprecedented anthropogenic forcing?

3) Rates of Climate Transition. The data from Searles Lake give the impression of relatively rapid transition between stable climate modes. The high-temporal-resolution data from San Agustin confirm this inference. This record, with an average resolution on the order of one hundred years, shows transitions between very positive and very negative water balances over time spans of less than 500 years. It is quite possible that even higher resolution records would show the transitions to be more abrupt. These data imply that future climate changes could also result in rapid water-balance changes. Since the rate of change of the generally accepted climatic forcing (astronomically driven changes in insolation) is slow, but the water-balance shifts are rapid, these paleohydrologic reconstructions also show that we need a better understanding of the mechanism of such rapid shifts.

4) Hydroclimatic Instability. The high-resolution record from San Agustin shows that about 25,000 years ago the hydrologic balance went through a series of remarkable oscillations. These oscillations imply that the climate can undergo periods of instability. What is the origin of this instability? It is possible that future climate changes could also generate such instabilities?

5) Long-Term Nonlinearity. One of the study's most intriguing results is the finding that there apparently exist long-term nonlinearities in the response of the water balance at Searles Lake to global climate forcing. This is not apparent when comparing the Searles surface area curve for the interval 600 to 300 ka to the marine ^{18}O record for the same period.

Although the global climate fluctuations (and also the presumed Milankovitch forcing) appear to be relatively stationary for the period 700 to 200 ka, the water-balance response at Searles is markedly different from 600 to 300 ka than for the beginning and end of the period. This unexplained nonlinear response should serve as a warning when attempting to use present climatic processes as a basic for predicting future ones.

6) Climate Model Verification. To have confidence in climate model predictions (under unprecedented boundary conditions), they should at least be demonstrated capable of "postdicting" past conditions. This postdiction should include not only quasi-steady state episodes such as the last glacial maximum, but more importantly, highly transient phenomena such as the San Agustin oscillations. This study has provided the climate modeling community with 1.2 Myr of water-balance fluctuations against which to test and refine their simulators.

REFERENCES

Abdel-Monem, A., Watkins, N.D., Gast, P.W., 1972, Potassium-argon ages, volcanic stratigraphy, and geomagnetic polarity history of the Canary Islands: Tenerife, La Palma, and Hierro: *American Journal of Science*, v. 272, pp. 805-825.

Abell, P.I., 1982, Paleoclimate at Lake Turkana, Kenya, from oxygen isotope ratios of gastropod shells: *Nature*, v. 297, pp. 321-323.

Allen, B.D., 1991, Effect of climate change on Estancia Valley, New Mexico: Sedimentation and landscape evolution in a closed-drainage basin, in *Field Guide to Geologic Excursions in New Mexico and Adjacent Areas of Texas and Colorado, New Mexico Bureau of Mines and Min. Resour. Bull.* 137, Socorro, pp. 166-170.

Bachhuber, F.W., 1989, The occurrence and paleolimnologic significance of cutthroat trout (*Oncorhynchus clarki*) in pluvial lakes of the Estancia Valley, central New Mexico: *Geological Society of American Bulletin*, v. 101, no. 12, pp. 1543-1551.

Bailey, G.E., 1902, The Saline Deposits of California: *California State Mining Bureau Bulletin*, v. 24, 216p.

Barkov, N.I., Korotkevich, E.S., Gordienko, F.G., Kotlyakov, V.M., 1977, The isotope analysis of ice cores from Vostok station (Antarctica) to the depth of 950 m, pp. 382-387, in Isotopes and impurities in snow and ice; *International Association of Hydrological Sciences Publication* 118.

Benson, L.V., 1986, The sensitivity of evaporation rate on climate change; results of an energy-balance approach: *U.S. Geological Survey Water Resources Investigation Report* 86-4148, 40 p.

Benson, L.V., Curry, D.R., Dorn, R.I., Lajoie, K.R., Oviatt, C.G., Robinson, S.W., Smith, G.I., Stine, S. 1990. Chronology of expansion and contraction of four Great Basin lake systems during the past 35,000 years: *Palaeogeography, Palaeoclimatology, Palaeoecology*, v. 78, pp. 241-286.

Benson, L.V., Paillet, F.L., 1989, The use of total lake surface area as an indicator of climatic change: Examples from the Lahonton Basin: *Quaternary Research*, v. 32 pp. 262-275.

Benson, L.V., Thompson, R.S., 1987, The physical record of lakes in the Great Basin, chap. 11 in Ruddiman, W.F., Wright, H.E., Jr. (eds.), North America and adjacent oceans during the last deglaciation: *The Geology of North America*, v. K-3, Geological Society of America, Boulder, pp. 241-260.

Bentley, H.W., Phillips, F.M., Davis, S.N., 1984, Chlorine-36 in the terrestrial environment, pp. 427-480 in Fontes, J.C., Fritz, P. (eds.), 1984, *Handbook of Environmental Isotope Geochemistry*, vol 2B: Elsevier, Amsterdam, 556 p.

Berger, A., 1988, Milankovitch theory and climate: *Reviews of Geophysics*, v. 26, pp. 624-657.

Birchfield, G.E., Wang, H., Wyant, M., 1990, A bimodal climate response controlled by water vapor transport in a coupled ocean-atmosphere box model: *Paleoceanography*, v. 5, pp. 383-396.

Birchfield, G.E., Broecker, W.S. (1990), A salt oscillator in the glacial Atlantic? 2. A "scale analysis" model: *Paleoceanography*, v. 5, pp. 835-843.

Bischoff, J.L., Herbst, D.B., Rosenbauer, R.J., 1991, Gaylussite formation at Mono Lake, California: *Geochimica Cosmochimica Acta*, v. 55, pp. 1743-1747.

Bischoff, J.L. Rosenbauer, R.J. Smith, G.I., 1985, Uranium-series dating of sediments from Searles Lake: differences between continental and marine climate records: *Science*, v. 227, pp. 1222-1224.

Blodgett, D.D., Titus, F.B., 1983, Hydrogeology of the San Augustin Plains, New Mexico: *New Mexico Bureau of Mines and Mineral Resources, Open-file Report* 51, 55p.

Bodine, M.W., Jr., Fernalld, T.H., 1973, EDTA dissolution of gypsum, anhydrite, and Ca-Mg carbonates: *Journal of Sedimentary Petrology*, v. 43, pp. 1152-1156.

Bottinga, Y. Craig, H., 1968, High temperature liquid-vapor fractionation factors for H_2O-HDO-$H_2{}^{18}O$: *Eos (Am. Geophysical Union Trans.)*, v. 49, pp. 353.

Briden, J.C., Rex, D.C., Faller, A.M., Tomlin, J.F., 1979, K-Ar geochronology and paleomagnetism of volcanic rocks in the Lesser Antilles island are: *Philosophical Transactions of the Royal Society of London*, v, 291, pp. 485-528.

Broecker, W. 1965, The geochemistry of ^{14}C in fresh-water systems: *Geochimica et Cosmochimica Acta*, v. 16, pp. 15-38.

Broecker, W.S., Andree, M., Wolfli, W., Oeschger, H., Bonani, G., Kennett, J., Peteet, D.M., 1988, The chronology of the last deglaciation: implications to the cause of the Younger Dryas event: *Paleoceanography*, v. 3, pp. 1-19.

Broecker, W.S., Denton, G.H., 1989, The role of ocean-atmosphere reorganizations in glacial cycles: *Geochimica et Cosmochimica Acta*, v. 53, pp. 2465-2501.

Broecker, W.S., Walton, A.F., 1969, Re-evaluation of the salt chronology of several Great Basin lakes: *Geological Society of America Bulletin*, v. 70, pp. 601-618.

Brocker, W.S., Bond, G., Klas, M., Bonani, G., Wolfli, W., 1990, A salt oscillator in the glacial Atlantic? 1. The concept: *Paleoceanography*, v. 5, pp. 469-477

Burden, R.L., Faires, J.D., 1985, *Numerical Analysis (3rd Ed.)*: Prindle, Weber, and Schmidt, Boston, pp. 234-235, 264-265.

Cameron, S.P., Lundin, R.F., 1977, Environmental interpretation of the ostracode succession in late Quaternary sediments of pluvial Lake Cochise, southeastern Arizona, pp. 335-357, in Loffler,H., Danielopol, D. (eds.), *Proceedings of the 6th International symposium on Ostracodes, Saalfelden (Salzburg) Aspects of Ecology and Zoogeography of Recent and Fosssil Ostracoda*, Dr. W. Junk, b.v., The Hague.

Carbonel, P., Colin, J.-P., Danielopol, D., Loffler, H., Neustrueva, I., 1988, Paleoecology of limnic ostracodes: a review of some major topics: *Palaeogrography, Palaeoclimatology, Palaeoecology*, v. 62, pp. 413-461.

Carrara, P.E., Mode, W.N., Rubin, M., Robinson, S.W., 1984, Deglaciation and postglacial timberline in the San Juan Mountains, Colorado: *Quaternary Research*, v. 21, pp. 42-55.

Chapin, C.E., Seager, W.R., 1975, Evolution of the Rio grande Rift in the Socorro, and Las Cruces area, pp. 297-321, in *New Mexico Geol. Soc. Guidebook, 26th Field Conf.*, Las Cruces Region.

Chappell, J., Shackleton, J.J., 1986, Oxygen isotopes and sea level: *Nature*, v. 324, pp. 337-340.

Chivas, A.R., De Deckker, P., Shelley, J.M.G., 1986b, Magnesium and strontium in non-marine ostracod shells as indicators of palaeosalinity and palaeotemperature: *Hydrobiologoca*, v. 143, pp. 135-142.

Chivas, A.R., De Dekker, P., Michael, A.J., Shelley, G., 1985, Strontium content of ostracods indicates lacustrine palaeosalinity: *Nature*, v. 316, pp. 251-253.

Chivas, A.R., De Dekker, P., Shelly, J.M.G., 1986b, Magnesium content of non-marine ostracode shells: a new palaeosalinometer and palaeothermometer: *Palaeogeography, Palaeoclimatology, Palaeoecology*, v. 54, pp. 43-61.

Christiansen, R.L. Blank, H.R., Jr., 1972, Volcanic stratigraphy of the Quaternary rhyolite plateau in Yellowstone National Park: *US Geological Survey Professional Paper* 729-B, 18p.

Clayton, R.N., Jones, B.F., Berner, R.A., 1968, Isotope studies of dolomite formation under sedimentary conditions: *Geochimica et Cosmochimica Acta*, v. 32, pp. 415-432.

Clisby, K.H., Sears, P.B., 1956, San Augustin Plains-Pleistocene climatic changes: *Science*, v. 124, pp. 537-539.

Craig, H., 1957, Isotopic standards for carbon and oxygen and correction factors for mass spectrometric analysis of carbon dioxide: *Geochimica et Cosmochimica Acta*, v. 12, pp. 133-149.

Craig, H., 1961, Isotopic variations in meteoric waters: *Science*, v. 133, pp. 1702-1703.

Craig, H., Gordon, L.I., 1965, Deuterium and oxygen-18 variations in the ocean and marine atmosphere, pp. 9-130, in *Stable Isotopes in Oceanographic Studies and Paleotemperatures*: Lishi, Pisa.

Dalrymple, G.B., 1964, Cenozoic chronology of the Sierra Nevada, California: *University of California Publications in Geological Sciences*, v. 47, 41p.

Dansgaard, W., 1964, Stable isotopes in precipitation: *Tellus*, v. 4, pp. 436-467.

Dansgaard, W., 1969, One thousand centuries of climatic record from Camp Centruy on the Greenland ice sheet: *Science*, v. 166, pp. 377-381.

De Dekker, P., Last, M.W., 1988, Modern dolomite deposition in continental, saline lakes, western Victoria, Australia: *Geology*, v. 16, pp. 29-32.

De Dekker, P., Forester, R.M., 1988, the use of ostracodes to reconstruct continental paleoenvironmental records, pp. 175-199, in De Deckker, P., Colin, J.P., Peypouqet, J.P. (eds.), 1988, *Ostracoda in the Earth Sciences*: Elsevier, Amsterdam.

Degens, E.T., Epstein, S., 1964, Oxygen and carbon isotope ratios in coexisting calcites and dolomites from recent and ancient sediments: *Geochimica et Cosmochimica Acta*, v. 28, pp. 23-44.

Delorme, L.D., 1969, Ostracodes as Quaternary paleoecological indicators: *Canadian Journal of Earth Sciences*, v. 6, pp. 1471-1476.

Delorme, L.D., 1970, Freshwater ostracodes of Canada. Part III. Family Candonidae: *Canadian Journal of Zoology*, v. 48, pp. 1099-1127.

Delorme, L.D., 1971, Freshwater ostracodes of Canada. Part V. Families Limnocytheridae, Loxoconchidae: *Canadian Journal of Zoology*, v. 49, pp. 43-64.

Dincer, T., 1968, The use of ^{18}O and deuterium concentrations in the water balance of lakes: *Water Resources Research*, v. 4, pp. 1289-1306.

Dohrenwend, J.C., 1984, Nivation landforms in the western Great Basin and their paleoclimatic significance: *Quaternary Research*, v. 22, pp. 275-288.

Dorn, R.I., Jull, A.J.T., Donahue, D.J., Linick, T.W., Toolin, L.J., 1990 Latest Pleistocene lake shorelines and glacial chronology in the Western Basin and Range Province, U.S.A.: Insights from AMS radiocarbon dating of rock varnish and paleoclimatic implications: *Palaeogeography, Palaeoclimatology, Palaeoecology*, v. 78, pp. 315-331.

Dorn, R.I., Turrin, B.D., Jull, A.J.T., Linick, T.W., Donahue, D.J., 1987, Radiocarbon and cation-ratio ages for rock varnish on Tioga and Tahoe morainal boulders of Pine Creek, eastern Sierra Nevada, California, and their paleoclimatic implications: *Quaternary Research*, v. 28, pp. 38-49.

Droste, J.B., 1961, Clay minerals in sediments of Owens, China, Searles, Panamint, Bristol, Cadiz, and Danby lake basins, California: *Geological Society of America Bulletin*, v. 72, pp. 1713-1722.

Durazzi, J.T., 1977, Stable isotopes in the ostracode shell: a preliminary study: *Geochimica et Cosmochimica Acta*, v. 41, pp. 1168-1170.

Ehhalt, D.H., 1974, Vertical profiles of HTO, HDO and H20 in the troposphere: *United States NTIS, PB Report* 245731, 136 pp.

Elias, S.A., Toolin, L.J., 1990, Accelerator dating of a mixed assemblage of late Pleistocene insect fossils from the Lamb Spring site, Colorado: *Quaternary Research*, v. 33, pp. 122-126.

Elliott-Fisk, D.L., 1987, Glacial geomorphology of the White Mountains, California and Nevada: establishment of a glacial chronology: *Physical Geography*, v. 8, pp. 299-323.

Epstein, S., Graf, D., Degens, E., 1962, Oxygen isotope studies on the origin of dolomites in Craig, H., Miller, S., Wasserburg, G., (eds.) *Isotope and cosmic chemistry*: Amsterdam, North-Holland, pp. 169-180.

Eugster, H.P., Hardie, L.A., 1978, Saline Lakes, Chapter 8, pp. 237-293, in Lerman, A., ed., 1978, *Lakes-Chemistry, Geology, Physics*: Springer-Verlag, New York.

Eugster, H.P., Smith, G.I., 1965, Mineral equilibria in the Searles Lake evaporites, California: *Journal of Petrology*, v. 6, pp. 473-522.

Fairbanks, R.G., 1989, A 17,000-year glacio-eustatic sea level record: influence of glacial melting rates on the Younger Dryas event and deep-ocean circulation: *Nature*, v. 342, pp. 637-642.

Flint, R.F., Gale, W.A., 1958, Stratigraphy and radiocarbon dates at Searles Lake, Calfiornia: *American Journal of Science*, v. 256, pp. 589-714.

Fontes, J. Ch., Gonfiantini, R., 1967, Comportment isopotique ,occurs de l'evaporation de deux bassins Sahariens: *Earth and Planetary Science Letters.*, v. 3, pp. 258-266.

Foreman, F., Clisby, K.H., Sears, P.B., and Stearns, C.E., 1959, Plio-Pleistocene sediments and climates of the San Augustin Plains, New Mexico, pp. 117-120, in *New Mexico Geol. Soc. Guidebook, Tenth Field Conference.*

Forester, R.M., 1983, Relationship of two lacustrine ostracode species to solute composition and salinity: Implications for paleohydrochemistry: *Geology*, v. 11, pp. 435-438.

Forester, R.M., 1985, *Limnocythere bradburyi* n.sp.: a modern ostracode from Central Mexico and a possible Quaternary paleoclimatic indicator: *Journal of Paleontology*, v. 59, pp. 8-20.

Forester, R.M., 1986, Determination of the dissolved anion composition of ancient lakes from fossil ostracodes: *Geology*, v. 14, 796-798.

Forester, R.M., 1987, Late Quaternary paleoclimatic records from lacustrine ostracodes, Chap. 12 pp. 261-276, in, Ruddiman, W.F., Wright, H.E., Jr. (eds.), 1987, North America and adjacent oceans during the last deglaciation: *The Geology of North America, v. K-3*, Geological Society of America, Boulder.

Friedman, G.M., 1980, Dolomite is an evaporite mineral: evidence from the rock record and from sea-marginal ponds of the Red Sea: *Society of Economic Paleontologists and Mineralogists Special Publications* No. 28, pp. 69-80.

Friedman, I., O'Neill, J.R., 1977, compilation of stable isotope fractionation factors of geochemical interest, chap. KK in Fleischer, M. (ed.), Data of Geochemistry, Sixth Edition: *U.S. Geological Survey Professional Paper* 440, pp. 1-12.

Friedman, I., Smith, G.I.; and Matsuo, S., 1982, Economic implications of the deuterium anomaly in the brine and salts in Searles Lake, California: *Economic Geology*, v. 77, pp. 694-702.

Fullerton, D.S., and Richmond, G.M. 1986, Comparison of the marine oxygen isotope record, the eustatic sea level record, and the chronology of glaciation in the United States of America, pp. 197-200, in Sibrava, V., Bowen, D.Q., Richmond, G.M. (eds.), 1986, Quaternary Glaciations in the Northern Hemisphere, *Quaternary Science Reviews*, v. 5, 513 p.

Gabin, V.L., Lesperance, L.E., 1977, New Mexico climatological data -- precipitation, temperature, evaporation, and wind -- monthly and annual means 1850-1975: W.K. Summers and Assoc., Socorro, New Mexico, 436 pp.

Gale, H.S., 1914, Salines in the Owens, Searles and Panamint Basins, southeastern California: U.S. *Geological Survey Bulletin* 580-L, pp. 251-323.

Gasse, F., Fontes, J.C., Plaziat, J.C., Carbonel, P., Kaczmarska, I., De Deckker, P., Souline-Marsche, I., Callot, Y., Dupeuble, P.A., 1987, Biological remains, geochemistry and stable isotope for the reconstruction of environmental and hydrological changes in the Holocene lakes from North Sahara: *Palaeogeography, Palaeoclimatology, Palaeocecology*, v. 60, pp. 1-46.

Geyh, M.A., Krumbein, W.E., Kudrass, H. -R., 1974, Unreliable ^{14}C dating of long-stored deep-sea sediments due to bacterial activity: *Marine Geology*, v. 17, pp. 5-50.

Glover, E.D., 1961, Method of solution of calcareous materials using the complexing agent EDTA: *Journal of Sedimentary Petrology*, v. 31, pp. 622-626.

Gonfiantini, R., 1965, Effetti isotopici nell'evaporazine di ague salati: *Att. Cos. Tosiana Nat. Sci. Pisa*, v. 72, pp. 135-150.

Gonfiantini, R., 1978, Standards for stable isotope measurements in natural compounds: *Nature*, v. 271, pp. 534-536.

Graf, D.L., 1982, Chemical osmosis, reverse chemical osmosis, and the origin of subsurface brines: *Geochimica Cosmochimica Acta*, v. 46, pp. 1431-1448.

Guldman, S.G.P., 1984, Silicate diagenesis in core KM-3 from Searles (Dry) Lake, California: *M.S. Thesis, Geology*, Univ. of California, Berkeley, 61 p.

Haines, D.V., 1959, Core logs from Searles Lake, San Bernardino County, California: *U.S. Geological Survey Bulletin*, 1045-E, pp. 139-317.

Haynes, C.V., Jr. 1990, Archaeological and paleohydrological evidence for a terminal Pleistocene drought in North America and its bearing on Pleistocene extinction [abs.] Abstracts with Programs 86th Annual Meeting Cordilleran Section Geological Society of America, pp. 29.

Hallberg, G.R., 1986, Pre-Wisconsin glacial stratigraphy of the central plains region in Iowa, Nebraska, Kansas, and Missouri, pp. 11-15, in Sibrava, V., Bowen, D.Q., Richmond, G.M.. (eds.), 1986, Quaternary Glaciations in the Northern Hemisphere, *Quaternary Science Reviews*, v. 5, 514 p.

Halley, E., 1715, On the cause of the saltiness of the ocean and the several lakes that emit no rivers, with a proposal, by help thereof, to discover the age of the world: *Philosophical Transactions of the Royal Society of London*, v. 29, pp. 296-300.

Hardt, W.E., Moyle, R.W., Jr., Dutcher, L.C., 1972, Proposed water-resources study of Searles Valley, Calif., *U.S. Geological Survey Open-file Report* OF 72-0158, 69 p.

Hay, R.L., Guldman, S.G., 1987, Diagenetic alteration of silicic ash in Searles Lake, California: *Clays and Clay Mineralogy*, v. 35, pp. 449-457.

Hay, R.L. Moiola, R.J., 1963, Authigenic silicate minerals in Searles Lake, California: *Sedimentology*, v. 2, pp. 312-332.

Hays, J.D., Imbrie, J., Shackleton, N.J., 1976, Variations in the earth's orbit: pacemaker of the ice ages: *Science*, v. 194, p. 1121-1131.

Horita, J., 1987, Stable isotope study on brines and evaporites: Ph.D. Dissertation, Dept. of Chemistry, Tokyo Institute of Technology, Japan, 193. p.

Horita, J., 1990, Stable isotope paleoclimatology of brine inclusions in halite: Modeling and application to Searles Lake, California: *Geochimica et Cosmochimica Acta*, v. 54, pp. 2059-2073.

Huber, N.F., 1981, Amount and timing of Late Cenozoic uplift and tilt of the central Sierra Nevada, California-evidence from the upper San Joaquin River Basin, *U.S. Geological Survey Professional Paper* 1197, 28 p.

Imbrie, J., Hays, J.D., Martinson, D.G., McIntyre, A., Mix, A.C., Morley, J.J. Pisias, N.G., Prell, W.L., Shackelton, N.J., 1984, The orbital theory of Pleistocene climate: support from a revised chronology of the marine ^{18}O record, pp. 269-305. in Berger, A., Imbrie, J., Hays, J., Kukla G., Saltzman, B. eds., *Milankovitch and Climate-Understanding the Response to Astronomical Forcing*: D. Reidel Publishing Co., Dordrecht.

Irwin, H., Curtis, C.D., Colman, M.L., 1977, Isotopic evidence for source of diagenetic carbonate formed during burial of organic-rich sediment: *Nature*, v. 269, pp. 209-213.

Izett, G.A., 1981, Volcanic ash beds: recorders of upper Cenozoic silicic pyroclastic volcanism in the western United States: *Journal of Geophysical Research*, v. 86, pp. 10200-10222.

Izett, G.A., Obradovich, J.D., Mehnert, H.H., 1988, The Bishop Ash bed (middle Pleistocene) and some older (Pliocene and Pleistocene) chemically and mineralogically similar ash beds in California, Nevada and Utah: *U.S. Geoligical Survey Bulletin* 1676, 37 p.

Jannik, N.O., 1989, Lake history in the paleo-Owens River system, CA, for the past 2.0 myr, based on ^{36}Cl dating of evaporites from Searles Lake: *Ph.D. dissertation*, New Mexico Institute of Mining and Technology, Socorro, NM, 190 p.

Jannik, N.O., Phillips, F.M., Smith, G.I. Elmore, D., 1991, A ^{36}Cl chronology for lacustrine sedimentation in Searles Lake, California: *Geological Society of America Bulletin*, v. 103, pp. 1146-1159.

Jennings, C.W., Burnett, J.L., Troxel, B.W., compilers, 1962, Geologic map of California, Olaf P. Jenkins edition, Trona sheet: California Division of Mines and Geology, scale 1:250,000.

Jones, B.F., 1965, The hydrology and mineralogy of Deep Springs Lake, Inyo County, California: *U.S. Geological Survey Professional Paper* 502-A, 56 p.

Joyce, E.J., Tjalsma, L.R.CC., Prutzman, J.M., 1990, High-resolution planktic stable isotope record and spectral analysis for the last 5.35 M.Y.: Ocean Drilling Program Site 625 Northeast Gulf of Mexico: *Paleoceanography*, v. 5, pp. 507-530.

Keigwin, L.D., 1990, Deglacial climatic oscillations in the Gulf of California [abs.]: *Abstracts with Programs 86th Annual Meeting Cordilleran Section Geological Society of America*, pp. 34.

Ku, T.L., Liang, Z.C., 1984, The dating of impure carbonates with decay-series isotopes: *Nuclear Instruments and Methods in Physics Research*, v. 223, pp. 563-571.

Kukla, G., 1987, Loess stratigraphy in central China: *Quaternary Science Reviews*, v. 6, pp. 191-219.

Kutzbach, J.E., Street-Perrott, F.A., 1985, Milankovitch forcing of fluctuations in the level of tropical lakes from 18 to 0 kyr BP: *Nature*, v. 317, pp. 130-134.

Land, L.S., 1980, The isotopic and trace element geochemistry of dolomite: the state of the art: *Society of Economic Paleontologists and Mineralogists Special Publication* No. 28, pp. 87-110.

Last, W.M., 1990, Lacustrine dolomite - an overview of modern Holocene, and Pleistecene occurrences: *Earth-Science Reviews*, v. 27, pp. 221-263.

Lee, C.H., 1912, An intensive study of the water resources of a part of Owens Valley, California: *U.S. Geological Survey Water-Supply Paper* 294, 135 p.

Li, C.C., 1964, Introduction to experimental statistics: McGraw-Hill, New York, pp. 75-78.

Liddicoat, J.C., Opdyke, N.D., Smith, G.I., 1980, Paleomagnetic polarity in a 930-m core from Searles Valley, California: *Nature*, v. 286, pp. 22-25.

Lister, G.S., 1988a, Stable isotopes from lacustrine Ostracoda as tracers for continental palaeoenvironments, pp. 201-218, in De Dekker, P., Colin, J.P., Peypouqet, J.P. (eds.), 1988, *Ostracoda in the earth sciences*: Elsevier, Amsterdam.

Lister, G.S., 1988b, A 15,000-year isotopic record from Lake Zurich of deglaciation and climatic change in Switzerland: *Quaternary Research*, v. 29, pp. 129-141.

Lomb, N., 1976, Least-squares frequency analysis of unequally spaced data: *Astrophysics and Space Science*, v. 39, pp. 447-462.

Lorius, C., Jouzel, J., Ritz, C., Merlivat, L., Barkov, N.I., Korotkevich, Y.S., Kotlyakov, V.M., 1985, A 150,000-year climatic record from Antarctic ice: *Nature*, v. 316, pp. 591-596.

McCrea, J.M., 1950, On the isotopic chemistry of carbonates and a paleotemperature scale: *Journal of Chemical Physics*, v. 18, pp. 849-858.

McKenzie, J.H., 1984, Carbon isotopes and productivity in the lacustrine and marine environment in Stumm, W. (ed.), 1984, *Chemical Processes in Lakes*: Wiley Interscience, New York.

Madole, R.F., 1986, Lake Devlin and Pinedale glacial history, Front Range, Colorado: *Quaternary Research*, v. 25, pp. 43-54.

Madsen, D.B., Currey, D.R., 1979, Late Quaternary glacial and vegetation changes, Little Cottonwood Canyon area, Wasatch Mountains, Utah: *Quaternary Research*, v. 12, pp. 254-270.

Mankinen, E.A., Dalrymple, G.B., 1979, Revised geomagnetic polarity time scale for the interval 0-5 m.y. B.P.: *Journal Geophysical Research*, v. 84, pp. 615-626.

Mankinen, E.A., Donnelly, J.M., Gromme', C.S., 1978, Geomagnetic polarity event recorded at 1.1 m.y. on Cobb Mountain, Clear Lake volcanic field, California: *Geology*, v. 6, pp. 653-656.

Mankinen, E.A., Gromme', C.S., 1982, Paleomagnetic data for the Coso Range, California, and current status of the Cobb Mountain geomagnetic polarity event: *Geophysical Research Letters*, v. 9, pp. 1279-1282.

Markgraf, V., Bradbury, J.P., Forester, R.M., McCoy, W., Singh, G., Sternberg, R., 1983, Paleoenvironmental reassessment of the 1.6-million-year-old record from San Agustin Basin, New Mexico, pp. 291-297, in *New Mexico Geological Society Guidebook, 34th Field Conf.*, Socorro Region II.

Markgraf, V., Bradbury, J.P., Forester, R.M., Singh, G., Sternberg, R.S., 1984, San Agustin Plains, New Mexico: Age and paleoenvironmental potential reassessed: *Quaternary Research*, v., 22, pp. 335-343.

Mayo, E.B., 1934, The Pleistocene Long Valley Lake in eastern California: *Science*, v. 80, pp. 95-96.

Martinson, D.G., Pisias, N.G., Hays, J.D., 1987, Age dating and the orbital theory of the ice ages: Development of a high - resolution 0 to 300,000 yr chronostratigraphy: *Quaternary Research*, v. 27, pp. 1-27.

Meinzer, O.E., 1922, Map of the Pleistocene lakes of the Basin and Range Province and its significance: *Geological Society of America Bulletin*, v. 33, pp. 541-552.

Merlivat, L., Jouzel, J., 1979, Global climatic interpretation of the deuterium - ^{18}O relationship for precipitation: *Journal of Geophysical Research*, v. 84, pp. 5029-5033.

Meyers, J.S., 1962, Evaporation from the surface of lakes in 17 western states: *U.S. Geological Survey Professional Paper* 272-D.

Mifflin, M., Wheat, M. 1979, Pluvial lakes and estimated pluvial climates of Nevada: *Nevada Bureau of Mines and Geology Bulletin* 94, 57 p.

Milankovitch, M.M., 1941, Canon of insolation and the ice-age problem: Koniglich Serbische Akademic, Boegrad, (English translation by the Israel program for Scientific Translations: published by the U.S. Department of commerce and the National Science Foundation, Washington, D.C.).

Morrison, R.B., 1964, Lake Lahontan: Geology of southern Carson Desert, Nevada: *U.S. Geological Survey Professional Paper* 401, 156 p.

Morrison, R.B., and Davis, J.O., 1984, Quaternary stratigraphy and archeology of the Lake Lahonton area: A re-assessment in Lintz, J., Jr. (ed.), Western geological excursions (fieldtrip guidebook, 1984 *Geological Society of America Annual Meeting, Reno*), v. 1, Mackay School of Mines, Reno, pp. 252-281.

Muller, G. (1970), High magnesian calcite and protodolomite in Lake Balaton (Hungry) sediments: *Nature*, v. 226, pp. 749-750.

Naeser, C.W., Izett, G.A., Wilcox, R.E., 1973, Zircon fission-track ages of Pearlette family ash beds in Meade County, Kansas: *Geology*, v. 1, pp. 187-189.

Neale, J.W., 1988, Ostracods and palaeosalinity reconstruction,pp. 125-155, in De Dekker, P., Coling J.P., Prypovqet N.P. (eds.), *1988, Ostracoda in the Earth Sciences*; Elsevier, Amsterdam.

NOAA, 1982, Monthly normals of temperature, precipitation, and heating and cooling degree days 1951-1980, no. 81 (California): *National Climatic Data Center*, Asheville, North Carolina.

Northrop, D.A., Clayton, R.N., 1966, Oxygen isotope fractionation in systems containing dolomite: *Journal of Geology*, v. 74, pp. 174-196.

Oana, S., Deevey, E.S., 1960, ^{13}C in lake waters and its possible bearing on paleolimnology: *American Journal of Science*, Bradley Volume, v. 258-A, pp. 253-272.

Osborn, G., 1990, Late Wisconsin deglaciation in the Great Basin: a review [abs]: *Abstracts with Programs 86th Annual Meeting Cordilleran Section Geological Society of America*, pp. 73.

Oviatt, C.G., 1990, Evidence for an overflowing lake in the Sevier Lake Basin, Utah, from about 12,000 to 10,000 yr B.P. [abs.]: *Abstracts with Programs 86th Annual Meeting Cordilleran Section Geological Society of America*, pp. 74.

Pearson, F.J., Coplen, T.B., Jr., 1978, Stable isotope studies of lakes, pp. 35-339, in Lerman, A. (ed.), 1978, *Lakes-Chemistry, Geology, Physics*: Springer-Verlag, New York.

Peng, T.-H., Goddard, J.G., Broecker, W.S., 1978, A direct comparison of ^{14}C and ^{230}Th ages at Searles Lake, California: *Quaternary Research*, v. 9, pp. 319-329.

Phillips, F.M., Smith, G.I., Bentley, H.W., Elmore, D., Gove, H.E., 1983, Chlorine-36 dating of saline sediments: Preliminary results from Searles Lake, California: *Science*, v. 222, pp. 925-927.

Phillips, F.M., Person, M.A., Muller, A.B., 1986a, A numerical lumped-parameter model for simulating the isotopic evolution of closed-basin lakes: *Journal of Hydrology*, v. 85, pp. 73-86.

Phillips, F.M., Peeters, L.A., Tansey, M.K., Davis, S.N., 1986b, Paleoclimatic inferences from an isotopic investigation of groundwater in the central San Juan basin, New Mexico: *Quaternary Research*, v. 26, pp. 179-193.

Pitzer, K.S., and Kim, J.J., 1974, Thermodynamics of electrolytes: IV. Activity and osmotic coefficients for mixed electrolytes: *Journal of the American Chemical Society*, v. 96, pp. 5701-5707.

Potter, L.D., 1957, Phytosociological study of San Agustin Plains, New Mexico: *Ecological Monographs*, v. 27, pp. 113-136.

Powers, W.E., 1939, Basin and shore features of the extinct Lake San Augustin, New Mexico: *Journal of Geomorphology*, v. 2, pp. 345-356.

Putnam, W.C., 1950, Moraine and shoreline relationships at Mono Lake, California: *Geological Society of America Bulletin*, v. 61, pp. 115-122.

Rind, D., Peteet, D., Broecker, W., McIntyre, A., Ruddiman, W., 1986, The impact of cold North Atlantic sea surface temperatures on climate: implications for the Younger Dryas cooling (11-10): *Climate Dynamics*, v. 1, pp. 3-33.

Ruddiman, W.F. Wright, H.E., Jr. 1987, Introduction, pp. 1-12, in Ruddiman, W.F., Wright, H.E., Jr. (eds.), North America and adjacent oceans during the last deglaciation, *The Geology of North America*, v. K-3, Geological Society of America, Boulder,.

Ruddiman, W.F., Raymo, M.E., Martinson, D.G., Clement, B.M., Backman, J., 1989, Pleistocent evolution: Northern Hemisphere ice sheets and North Atlantic Ocean: *Paleoceanography*, v. 4, pp. 353-412.

Ruffner, J.A., (ed.), 1985, Climates of the States v. 1,: Gale Research Company, Detroit, Michigan.

Russell, I.C., 1885, Geological history of Lake Lahonton, a Quaternary lake of northwestern Nevada: *U.S. Geological Survey Survey Monograph* 11, 287 p.

Shacklton, N.J., 1987, Oxygen isotopes, ice volume, and sea level: *Quaternary Science Reviews*, v. 6, pp. 183-190.

Shackleton, N.J., Imbrie, J., Hall, M.A., 1983, Oxygen and carbon isotope record of east Pacific core V19-30: implications for the formation deep water in the late Pleistocene North Atlantic: *Earth and Planetary Science Letters*, v. 65, pp. 233-244.

Shackleton, N.J., Opdyke, N.D., 1973, Oxygen isotope and paleomagnetic stratigraphy of Equitorial Pacific core V28-283: Oxygen isotope temperatures and ice volumes on a 10^5 and 10^6 year scale: *Quaternary Research*, v. 3, pp. 39-55.

Sharma, T. Clayton, R.N., 1965, Measurement of $^{18}O/^{16}O$ ratios of total oxygen from carbonates: *Geochimica et Cosmochimica Acta*, v. 29, pp. 1347-1353.

Smith, G.I., 1962, Subsurface stratigraphy of late Quaternary deposits, Searles Lake, California-A summary, article 82 of Short Papers in Geology and Hydrology: *U.S. Geological Survey Professional Paper 450-C*, pp. C65-C69.

Smith, G.I., 1968, Lake Quaternary geologic and climatic history of Searles Lake, California pp. 293-310, in Morrison, R.B., Wright, H.E., Jr. (eds.), *Means of Correlation of Quaternary Successions*, v. 8: University of Utah Press, Salt Lake City, Utah.

Smith, G.I., 1979, Subsurface stratigraphy and geochemistry of late Quaternary evaporites, Searles Lake, California: *U.S. Geological Survey Professional Paper 1043*, 130 p.

Smith, G.I., 1984, Paleohydrologic regimes in the southwestern Great Basin, 0-3.2 my ago, compared with other long records of "global" climate: *Quaternary Research*, v. 22, pp. 1-7.

Smith, G.I., 1987, Searles Valley, California: Outcrop evidence of a Pleisotcene lake and its fluctuations, limnology, and climatic significance: *Geological Society of America Centennial Field Guide - Cordilleran Section*, pp. 137-142.

Smith, G.I., Barczak, V.I., Moulton, G.F., Liddicoat, J.C., 1983, Core KM-3, a surface-to-bedrock record of late Cenozoic sedimentation in Searles Valley, California: *U.S. Geological Survey Professional Paper 1245*, 27 p.

Smith, G.I., Friedman, I., McLaughlin, R.J., 1987, Studies of Quaternary saline lakes-III. Mineral, chemical, and isotopic evidence of salt solution and crystallization processes in Owens Lake, California, 1969-1971: *Geochimica et Cosmochimica Acta*, v. 51, pp. 811-827.

Smith, G.I., Haines, D.V., 1964, Character and distribution of nonclastic minerals in the Searles Lake evaporite deposit California: *U.S. Geological Survey Bulletin* 1181-P, 58 p.

Smith, G.I., Pratt, W.P., 1957, Core logs from Owens, China, Searles, and Panamint basins, California: *U.S. Geological Survey Bulletin 1045-A*, pp. 1-62.

Smith, G.I., Street-Perrott, F.A., 1983, Pluvial Lakes of the western U.S., pp. 190-212, in Porter, S.C. (ed.), *Late Quaternary Environments of the United States*, Volume 1, The Late Pleistocene, University of Minnesota Press, Minneapolis, 407p.

Smith, R.S.U., 1976, Late-Quaternary pluvial and tectonic history of Panamint Valley, Inyo and San Bernadino Counties, California: *Ph.D. dissertation*, California Institute of Technology, Pasadena, California, 300 p.

Sofer, Z., Gat, J.R., 1972, Activities and concentrations of oxygen-18 in concentrated aqueous salt solutions: analytical and geophysical implications: *Earth and Planetary Science Letters*, v. 15, p. 232-238.

Sofer, Z., Gat, J.R., 1975, Isotope composition of evaporating brines: Effect of the isotope activity ratio in saline solutions: *Earth and Planetary Science Letters*, v. 26, pp. 179-186.

Spaulding, W.G., 1990, Packrat midden evidence of environmental conditions at 10,680 ±160 yr B.P.: southern Great Basin and northern Sonoran Desert [abs.]: *Abstracts with Programs 86th Annual Meeting Cordilleran Section Geological Society of America*, pp. 85.

Spaulding, W.G., Grumlich, L.J., 1986, The last pluvial climatic episodes in the deserts of southwestern North America: *Nature*, v. 320, pp. 442-444.

Spaulding, W.G., Leopold, E.B., Van Devender, T.R., 1983, Late Wisconsin paleoecology of the American Southwest, chap. 14 in Porter, S.C. (ed.), *Late Quaternary environments of the United States*. Volume 1, The Late Pleistocene: University of Minnesota Press, Minneapolis, pp. 259-293.

Spencer, R.J., Baedecker, M.S., Eugster, H.P., Forester, R.M., Goldhaber, M.B., Jones, B.F., Kelts, K., McKenzie, J., Madson, D.B., Retting, S.L., Rubin, M., and Bower, C.J. 1984. Great Salt Lake and precursors, Utah: The last 30,000 years: *Contributions to Mineralogy and Petrology*, v. 86, pp. 321-334.

Spencer, R.J., Eugster, H.P., and Jones, B.F. 1985. Geochemistry of Great Salt Lake, Utah, II. Pleistocene-Holocene evolution: *Geochimica et Cosmochimica Acta*, v. 49, pp. 739-748.

Sterns, C.E., 1962, Geology of the north half of the Pelona quadrangle, Catron County, *New Mexico Bureau of Mines and Mineral Resources Bulletin* 78, 46 p.

Stiller, M., Rounick, J.S., Shasha, S., 1985, Extreme carbon-isotope enrichments in evaporating brines: *Nature*, v. 316, pp. 434-435.

Street, F.A., Grove, A.T., 1979, Global maps of lake-level fluctuations since 30,000 B.P.: *Quaternary Research*, v. 12, pp. 83-118.

Street-Perrott, F.A., Harrison, S.P., 1985, Lake levels and climate reconstruction, pp. 291-341, in Hecht, A.D. (ed.), 1985, *Paleoclimate Analysis and Modeling*: Wiley, New York.

Street-Perrott, F.A., Roberts, N., 1983, Fluctuations in closed-basin lakes as an indicator of past atmospheric ciruclation patterns, pp. 331-345, in Street-Perrott, F.A., Beran, M., Ratcliffe, R. (eds.), 1983, *Variations in the Global Water Budget*: D. Reidel, Boston, 518 p.

Stuiver, M., 1964, Carbon isotopic distribution and correlated chronology of Searles Lake sediments: *American Journal of Science*, v. 262, pp. 377-392.

Stuiver, M., Smith, G.I., 1979, Radiocarbon ages of stratigraphic units, pp. 68-73, in Smith, G.I., 1979, Subsurface stratigraphy and geochemistry of late Quaternary evaporities, Searles Lake, California: *U.S. Geological Survey Professional Paper 1043*.

Szestay, K., 1974, Water balance and water level fluctuations of lakes: *Hydrological Science Bulletin*, v. 19, pp. 73-84.

Talbot, M.R., 1986, Primary and diagenetic carbonates in the anoxic sediments of Lake Bosumtwi, Ghana: *Geology*, v. 14, pp. 912-916.

Talbot, M.R., 1990, A review of the paleohydrological interpretation of carbon and oxygen isotopic ratios in primary lacustrine carbonates: *Chemical Geology (Isotope Geoscience Section)*, v. 80, pp. 261-279.

U.S. Geological Survey, 1985, Ostracode sample preparation and data acquisition procedures: *Technical Detailed Procedure HP-78*, 12 p.

University of California - Davis, 1988, Climatic data summary for the White Mountains research stations (1 and 2): (unpublished).

Van Devender, T.R., Spaulding, W.G., 1979, Development of vegetation and climate in the southwestern United States: *Science*, v. 204, pp. 701-710.

Van Devender, T.R., Thompson, R.S., Betancourt, J.L., 1987, Vegetation history of the deserts of southwestern North America; the nature and timing of the late Wisconsin-Holocene transition, chap. 15 in Ruddiman, W.F., Wright, H.E., Jr. (eds.), North America and adjacent oceans during the last deglaciation: *The Geology of North America*, v. K-3, Geological Society of America, Boulder, pp. 323-352.

Walters, L.J., Jr., Claypool, G.E., Choquette, P.W., 1972, Reaction rates and ^{18}O variation for the carbonate phosphoric acid preparation method: *Geochimica et Cosmochimica Acta*, v. 36, pp. 129-140.

Waters, M.R., 1989, Late Quaternary lacustrine history and paleoclimatic significance of pluvial Lake Cochise, southestern Arizona: *Quatenary Research*, v. 32, pp. 1-11.

Weber, R.H., 1980, Geology of the Ake site, appendix A in Beckett, P.H. (ed.), 1980, The Ake site: *Department of Anthropology and Sociology, Report No. 357*, New Mexico State University, Las Cruces, pp. 223-238.

Welcher, F.J., 1958, The analytical uses of ethyleldiaminetetraacedi acid: D. van Nostrand Company, Princeton, New Jersey, 366 p.

Williams, D.F., Thunell, R.C., Tappa, E., Rio, D., Raffi, Il, 1988, Chronology of the Pleistocene oxygen isotope record: 0-1.88 m.y. B.P.: *Palaeogeography, Palaeoclimatology, Palaeoecology*, v. 64, pp. 221-240.

Winograd, I.J., Szabo, B.J. Coplen, T.B., Riggs, A.C., Kolesar, P.T., 1985, Two-million-year record of deuterium depletion in Great Basin ground waters: *Science*, v. 227, pp. 519-521.

Winograd, I.J., Szabo, B.J., Coplen, T.B., Riggs, A.C., 1988, A 250,000-year climatic record from Great Basin vein calcite: implications for Milankovitch theory: *Science*, v. 242, pp. 1275-1280.

Zuber, A., 1983, On the environmental isotope method for determining the water balance components of some lakes: *Journal of Hydrology*, v. 61, pp. 409-427.